A study of turbulent diffusion in the lower atmosphere using artificially produced electric space charge

C. D. Jones

A STUDY OF TURBULENT DIFFUSION IN THE LOWER ATMOSPHERE USING ARTIFICIALLY PRODUCED ELECTRIC SPACE CHARGE

by

C. D. JONES, M. Inst. P., F.R. Met. Soc., of
the Graduate Society of the University of Durham

Presented in candidature for the degree of Doctor of Philosophy in the University of Durham

January 1974

ABSTRACT

An investigation into the behaviour of artificially produced ions, released from a point source a few metres above the Earth's surface, is presented. It is shown both experimentally and theoretically that the ions form a plume downwind of the ion source and, moreover, that the nature of this plume is rather similar to that of a smoke plume. Electric field and ion concentration measurements have been used to deduce certain features about ion plumes and distinct connexions between ion plume behaviour and the local meteorological conditions have been observed. In particular, the use of bidirectional vane techniques has indicated that ions can be used quite successfully as a tracer in short range atmospheric diffusion experiments. The technique does, however, possess certain limitations, the details of which are included in the text.

FOREWORD

In accordance with modern practice, I have used the rationalized MKS system of units throughout this thesis. Apart from any adherence to convention, the employment of this system is both convenient and simple and thus the choice seemed obvious.

Considerable confusion has arisen in Atmospheric Electricity when discussing electric fields and potential gradients. Unfortunately, quite often, the term 'field' has been used to denote dV/dz and not, as the definition strictly requires $-dV/dz$. Here z is the height, measured vertically upward. In this work both the terms potential gradient and electric field have been used, but great care has been taken to employ these correctly. When discussing experimental results the numerical observations are, where appropriate, expressed in terms of potential gradient to facilitate comparisons with other work.

The descriptions ion plume and space charge plume are used virtually synonomously in the text. Strictly speaking, the term space charge plume is more accurate because the artificial ions, on leaving the generator, become mixed with natural ions of both signs. In cases where it is necessary to distinguish between the two concepts this has been done.

ACKNOWLEDGEMENTS

I would like to offer my sincere thanks to my supervisor, Dr. W. C. A. HUTCHINSON, who has always maintained a keen interest in the progress of this project and made many helpful suggestions. I wish also to express my appreciation to Mr. T. J. MORALEE for both his help in constructing the apparatus, and during the later stages of the work, for his assistance with experiments in the field. I am indebted to Mr. E. W. LINCOLN for his valuable advice on the design of certain of the electronic systems and also to his staff for the construction of much of the electrical equipment used in this investigation.

Messrs. A. T. E. MUNRO and K. M. DAILY willingly offered valuable assistance in the writing of certain computer programmes and this is much appreciated. I wish also to thank the entire staff at the Durham University Computer Unit for their good-natured tolerance of my considerable data processing requirements! In particular, I am most grateful to Mrs. J. ELVES and her staff for punching out many thousands of data cards for my benefit.

Thanks are also due to Mr. D. SMITH, Greenfields Farm, Oxen Law, Nr. Consett, who offered me, without hesitation, the use of his land for the experimental work. I am also much indebted to Mr. A. HENDERSON, Superintendent, Maiden Castle Sports Centre, for permission to use the facilities there.

I wish also to express my gratitude to the National Environment Research Council for financial support throughout this research project. In addition, I wish to record my thanks both to the American Geophysical Union and the Royal Meteorological Society who generously provided funds for me to attend the recent conference on 'Turbulent Diffusion and Environmental Pollution' at Charlottesville, Va., U.S.A.

I am grateful to Professor G. D. ROCHESTER for the use of the excellent facilities at Durham and would like to express

my appreciation to the entire staff of the Physics Department.

I would like to express my gratitude to my wife, whose understanding, tolerance and encouragement have been of inestimable value in the last three years.

Finally, thanks are due to Mrs. Diana MUNRO for the speed and efficiency with which she typed this thesis.

The author would also to express his gratitude to the Ordnance Survey, Southampton for permission to include copies of maps in this thesis. The copies are extracts from Ordnance Survey sheets NZ 24/34 and NZ 04.

LIST OF SECTION HEADINGS

Chapter 1: INTRODUCTION

1.1 General Background

The lower atmosphere consists of a uniform mixture of gases, the chief of these being nitrogen, oxygen, argon and carbon dioxide. In addition, there is always present a relatively small, but nonetheless highly significant, proportion of water vapour. Unlike the gases, the concentration of this vapour varies both from time to time and from place to place. It is, in fact, these constant variations of water vapour content which are, to a great extent, responsible for the various types of weather.

As well as the substances referred to above, the atmosphere, and particularly the lower atmosphere, always contains suspended particulate matter in considerable amounts. In times past, the origins of such matter were almost exclusively natural and arose from activities such as volcanic eruptions and the evaporation of sea-spray. However, in the last century or so, and particularly in industrial or urban environments, man's activities have resulted in very considerable increases in the concentrations of particulate, and other, materials.

In addition to the substances above, there are varying concentrations of ions present in the lower atmosphere. The existence of such entities was recognized as early as 1899 by ELSTER and GEITEL, but at that time their origin was obscure. Later EBERT (1904) found that air diffusing from

the ground contained ions, the ionization resulting presumably from radioactivity in the earth's crust. HESS (1911) discovered that ions were more plentiful at higher levels in the atmosphere. This was later attributed to an effect of cosmic rays.

A most important property of ions, particularly insofar as this project is concerned, is their ability to persist for periods of up to several minutes (or even longer) in the lower atmosphere. CHALMERS (1967) gives values of 20 - 300 s for the lifetime of a small ion (see *Sec.* 3.2), depending on the locality. Any ion, being electrically charged, will, of course, move in an electric field. It has been known since 1752 (LEMONNIER) that such a field exists near the earth's surface. However, the magnitude of this field is such that, except perhaps in stormy conditions, resulting ion motions are only in the order of a few centimetres per second. Consequently, the movement of ions, at least in the lower atmosphere, is often largely determined by the wind.

The actual concentration of ions near the surface is small, only about one molecule in 10^{17} being ionized at any one time. This implies that there are in the order of 10^{9} ions of each sign in a cubic metre of air.

1.2 Artificially produced ions and the concept of a space charge plume

We can readily envisage the existence of a cloud of ions in the atmosphere, such an entity being, in all probability, rather similar in nature to a puff of smoke. The origin of the ion cloud could be either natural or artificial, but in both cases the cloud will be blown along with the wind. Like a smoke puff, the ion cloud will become more dilute as it moves downwind. If the numbers of ions of each sign (assuming they are singly charged) within the cloud are equal, then the total net charge will be zero. However, if ions of one sign are in the majority, the cloud will possess a net space charge. Elementary electrostatic theory predicts that there will be an electric field in the vicinity of all space charges and consequently electric field observation may be a useful technique for the *detection* and measurement of such charges.

KELVIN (1860) was the first to recognize the effects of man-made space charges. He measured the electrical disturbances due to locomotive steam and concluded that it was always positively charged. Much later, WHITLOCK and CHALMERS (1956) observed that these space charge "packets" from steam locomotives were detectable as far as 1 km from their source. In fact, many combustion processes produce space charge. MUEHLEISEN (1953) found large positive charges in diesel exhaust gases and negative charges in the effluents of chemical factories and gasworks. OGDEN (1967) has also reported positive charges near diesel engines.

The high electric fields during showers and thunderstorms often result in copious ion production by point discharge processes. In this case, the ionization results from electron-molecule and ion-molecule collision phenomena in the high field region near the point. The ions, once produced, are blown away from the point by the wind. In many respects this is a very similar situation to that of smoke being blown from a chimney stack, it being a matter of familiar experience that, usually, a long plume is formed downwind of the source. Observations show that the size of a smoke plume steadily increases as it moves downwind, this diffusion process being intimately connected with the gusty, or turbulent, character of the wind. Similarly, when point discharge occurs, we might reasonably expect that an ion plume will be formed downwind of the point. As in the case of the smoke plume, the dimensions of the ion plume will increase at greater distances from the ion source.

MAUND (1958) has shown that, at horizontal distances less than about twice the height of a discharging point, the ion or space charge plume may be regarded as a line charge. That is, the effects of turbulent diffusion can be ignored relatively near the source. MAUND, in fact, wanted to estimate the current flowing through the point by comparing the upwind and downwind electric fields. Considering the ion plume as a line charge, therefore, greatly facilitated his theoretical calculations of electric field.

CHALMERS (1967) suggested that if space charge could be generated artificially, then measurements of charge density downwind of an ion source might provide useful information on atmospheric diffusion. In fact, CRAMER, GILL and RECORD (1954) had already used an electrically charged smoke, rather than ions, to conduct just such an investigation into the effects of turbulent diffusion. However, experiments involving the use of ions, although also suggested by LARGE and PIERCE (1957) and OGDEN (1967), do not appear to have ever been carried out. Techniques involving ions would in many ways be closely analogous to more familiar methods using such substances as sulphur dioxide. Space charge density measurements in ion plumes have their counterpart in SO_2 concentration measurements in those plumes, but electric field measurements offer a unique tool for the investigation of ion plumes, no analogous measurement being possible with uncharged plumes. The value of the electric field at a particular point is determined by both the total charge present and its distribution in space relative to that point. Therefore, electric field measurements near ion plumes might provide useful, certainly interesting, information regarding the behaviour of plumes in general.

Point discharge currents depend, to a considerable extent, on the wind speed as well as the prevailing electric field. Consequently, a discharging point, being therefore a variable-output ion source, would hardly be suitable for an investigation of turbulent diffusion. In order to minimize the effects of the earth's potential gradient, LARGE and PIERCE (1957) connected a raised point to a high voltage supply in their

studies of point discharge. These workers were interested in the effects of wind on point discharge currents and therefore the point was left exposed. However, if a discharging point were shielded from both the wind and external electric fields, it might be possible to construct a constant-output ion source suitable for use in diffusion studies.

DAYARATNA (1969) investigated the behaviour of artificially produced ions in a wind tunnel. However, his design of ion generator, being specifically intended for work in wind tunnel environments, could not readily be adapted to the needs of the current project. Details of the constant-output ion generator specially developed for use in the diffusion studies conducted here can be found in *Sec.* 4.4.

1.3 The nature of the proposed investigation and the choice of experimental sites

The basis of the proposed investigation has already been intimated in the previous section. Considerable interest has always been centred on the dispersal of atmospheric pollutants, usually produced by point sources, and thus it was thought that an analogous study, involving the use of a point source of ions, might be very worthwhile.

Much previous work on turbulent diffusion has required the expenditure of considerable resources, both in terms of man-hours and equipment. Many research programmes have been really ambitious, notably the Project Prairie Grass in 1956. In this study several hundred sampling stations were placed in a series of arcs downwind of a point source of sulphur dioxide. However, as the present investigation had to be conducted virtually single-handed, relatively modest goals were set.

It was proposed to design and construct a constant output ion source capable of producing either negative or positive ions, the choice being that of the experimenter. This ion source was to be mounted on a mast, and, at various distances downwind, the electric field and ion concentration were to be measured. It was hoped that measurements would be feasible up to about 500 m. from the ion source.

At this stage, it was clear that certain meteorological observations would be necessary in order to make the best use of the electrical measurements. The wind speed and

direction both have a considerable effect on any plume and, initially, it was proposed that just these quantities be measured. Later, it was expected that, as experimental work advanced, more sophisticated meteorological data would be required.

The experimental technique was entirely novel and therefore, to some extent, the investigation was open-ended, that is, no precise objectives were defined. The aim of the project was to investigate the behaviour of ion plumes in as much detail as possible, and then to try to draw comparisons between these and plumes of uncharged material.

Clearly, an investigation of the type proposed demands the use of a site where pollution levels are low, otherwise the effects mentioned in sec. 1.2 might produce erroneous results.

Previous workers at Durham, e.g. SHARPLESS (1968), have conducted extensive investigations at Lanehead, which is situated high in the Pennine hills in West County Durham. SHARPLESS concluded, from his electrical measurements, that atmospheric pollution levels were minimal in this area and consequently it appeared suitable for the current project. In particular, the existence of a large, and substantially level area near the top of the hill, 1 km NNW of the centre seemed an ideal location for the experimental work. In fact, initial work was carried out at this site, but owing to the altitude (600 m), severe weather was often experienced, even in Summer, and efforts were therefore made to seek a more congenial environment in which to conduct the experiments.

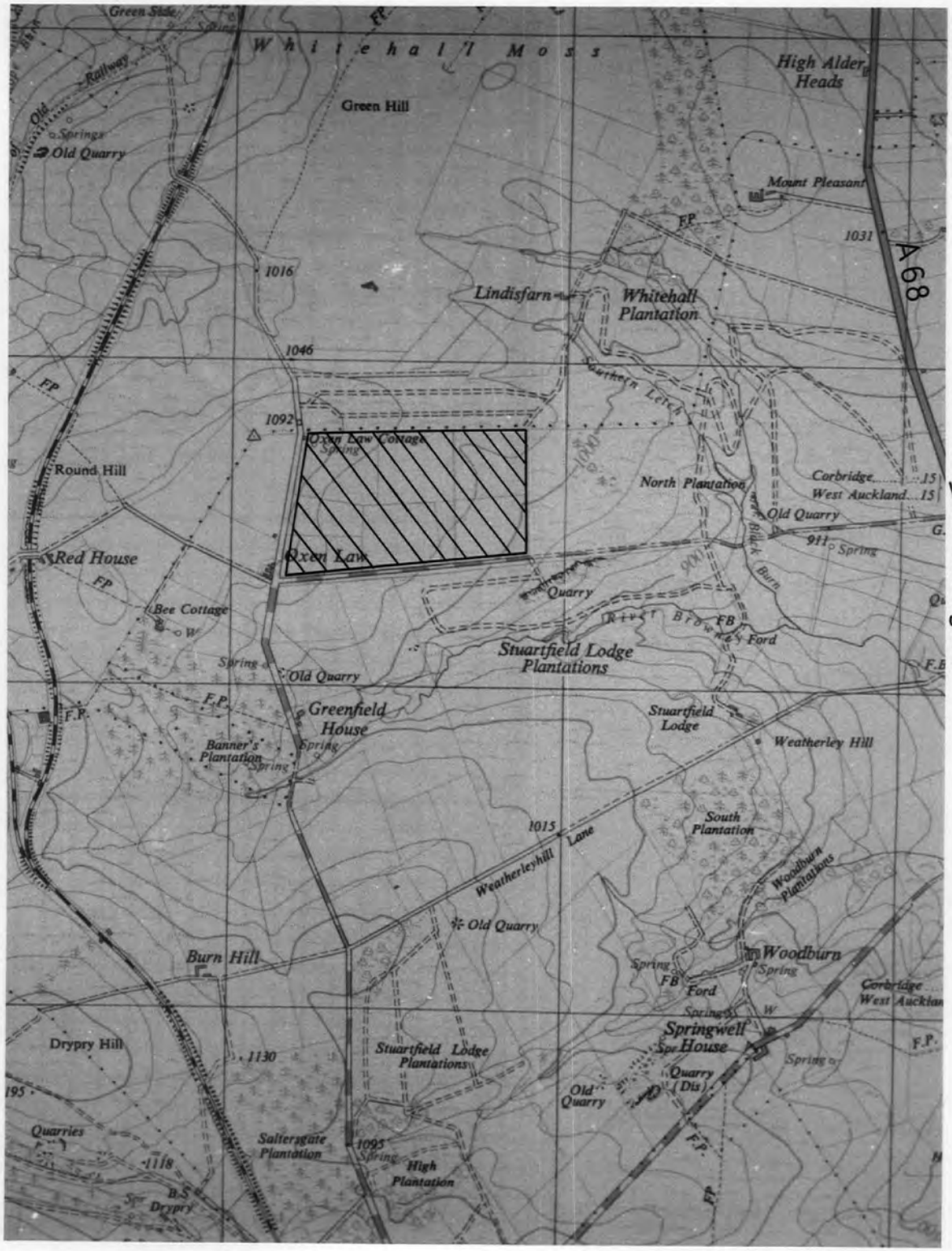

THE OXEN LAW SITE

1km

THE MAIDEN CASTLE SITE

1km

The use of a site at Oxen Law, about 6 km SW of Consett, was obtained. The terrain in this locality consists of gently rolling grass and moorland, with relatively few trees or other projections likely to disturb the air flow. The elevation of this site is only 300 m. and, together with the fact that it is only half the distance from the University (30 km) as is Lanehead, made it an attractive proposition for experimental work. The details of this site are shown in Fig. *P1* .

Some investigations were also carried out in a large field at the University Sports Centre, Maiden Castle, Durham. Details are shown in Fig. *P2* . The Centre, which is located in a very shallow region of the Wear Valley, is only 1 km from the University, thus making it a very convenient field work site.

Despite the proximity of Consett in the case of the Oxen Law site, and Durham in that of the Maiden Castle site, surprisingly little trouble was experienced from air pollution. Occasionally difficulties did arise, however, and these are discussed further in *Sec.* 3.2.

Chapter 2: THE DISPERSAL OF IONS BY TURBULENT DIFFUSION

2.1 Purpose of the Chapter

It soon became obvious that the behaviour of the ion plume, in common with that of smoke plumes, was largely determined by the local air motion. It is my intention in this chapter to present first a brief account of the general nature of winds and secondly to examine in detail features of turbulent flow relevant to this project. A steady state plume model, based on traditional methods, is first presented and then, in view of the statistical nature of turbulence, more realistic "fluctuating plume" models are proposed. The electric fields due to the ion plume may then be computed by applying an appropriate model.

Certain electrostatic effects are also capable of influencing the behaviour of the ion plume. These will be discussed in the following chapter.

22 Initial Considerations

REYNOLDS (1883) showed that two distinct types of flow exist; at relatively low velocities the fluid moves in a steady, quiet manner - laminar flow, whilst at higher velocities the flow becomes irregular and unpredictable - turbulent flow. It has been found in the lower atmosphere that winds are nearly always turbulent, observation of a smoke plume readily confirming this.

Any flow requires a continuous input of energy to maintain it, otherwise its kinetic energy would decrease, being ultimately dissipated by viscosity as heat. Solar radiation is the driving force as far as the earth's winds are concerned. The sun's heat produces large-scale convective systems which are modified by the Coriolis force into the extensive vortices known in our latitude as depressions and anticyclones.

At heights above 500 m., it is possible to neglect the frictional effect of the earth's surface on the air flow. At these levels the flow is the result of a balance between the pressure gradient and Coriolis forces and is referred to as the geostrophic wind. Further details on this and other aspects of synoptic scale meteorology can be found in BRUNT (1939) and are therefore not discussed here.

The increasing effect of friction at the lower levels causes the relatively steady geostrophic flow to be broken down into a series of irregular vortices near the ground. The mean velocity of the air gradually reduces until at the surface it

is close to zero. This layer between the surface and the geostrophic flow region is known as the planetary boundary or friction layer. It is the physics of this layer which is of most interest to us in this project.

2.3 The Transport of Material and Momentum in the Earth's Boundary Layer

This is a region in which momentum from the geostrophic layer is continually transferred downward towards the earth's surface. The flow is turbulent and thus the momentum flux takes the form of eddies.

Let us now examine mathematically some of the consequences of the velocity fluctuations which occur in all turbulent flows. It is customary, both in the measurement and analysis of atmospheric turbulence, to choose the co-ordinate directions (x, y and z) so that the mean velocity ($\bar{u}$) lies along the x-axis, thus making the y and z directions those of the lateral and vertical components respectively. This is represented in Fig. 2.1(a). It is also conventional to regard an instantaneous value of velocity at a particular point as being the sum of a mean and a fluctuating component (see Fig. 2.1(b).). It is, of course, perfectly feasible to consider other varying quantities in a similar manner; this approach being used extensively later.

In the case of the longitudinal velocity component , we may write its mean value $\bar{u}$ as,

$$\bar{u} = \frac{1}{T}\int_0^T u \, dt \qquad (2.1)$$

by definition, similar relations holding for the other two components v and w.

Suppose we were measuring the concentration χ of a pollutant as a function of time. Then, by employing the above method, we can write:

$$\chi(t) = \bar{\chi} + \chi'(t) \qquad (2.2)$$

where the overbar and prime refer to the mean and fluctuating components as before.

Consider now the effect of a turbulent flow on the distribution of material, the system being assumed horizontally homogeneous for the sake of simplicity. This implies that χ is function of the height, z, only. The amount of material crossing a small horizontal surface in the upward direction is given by:

$$\boxed{M_z = \chi w} \qquad (2.3)$$

that is, the flux is equal to the instantaneous concentration multiplied by the vertical velocity.

Expanding 2.3, we obtain:

$$M_z = (\bar{\chi} + \chi')(\bar{w} + w')$$

and upon multiplying out and taking the time mean value, we find:

$$\boxed{\overline{M_z} = \overline{\bar{\chi}\bar{w}} + \overline{\bar{\chi}w'} + \overline{\chi'\bar{w}} + \overline{\chi'w'}} \qquad (2.4)$$

Certain of the terms in 2.4 can be shown to be zero. In the calculation of the product $\overline{\chi'\bar{w}}$, for instance, it is clear that:

$$\overline{\chi'\bar{w}} = \bar{\chi}'\bar{w}$$

since the quantity $\bar{w}$ acts only as a constant coefficient for the fluctuating portion χ'. Further, the mean value of χ' is zero by definition. In view of this, equation 2.4 simplifies to:

$$\boxed{\overline{M_z} = \bar{\chi}\bar{w} + \overline{\chi'w'}} \qquad (2.5)$$

Conventions used in studies of atmospheric turbulence

(a) Choice of co-ordinate system

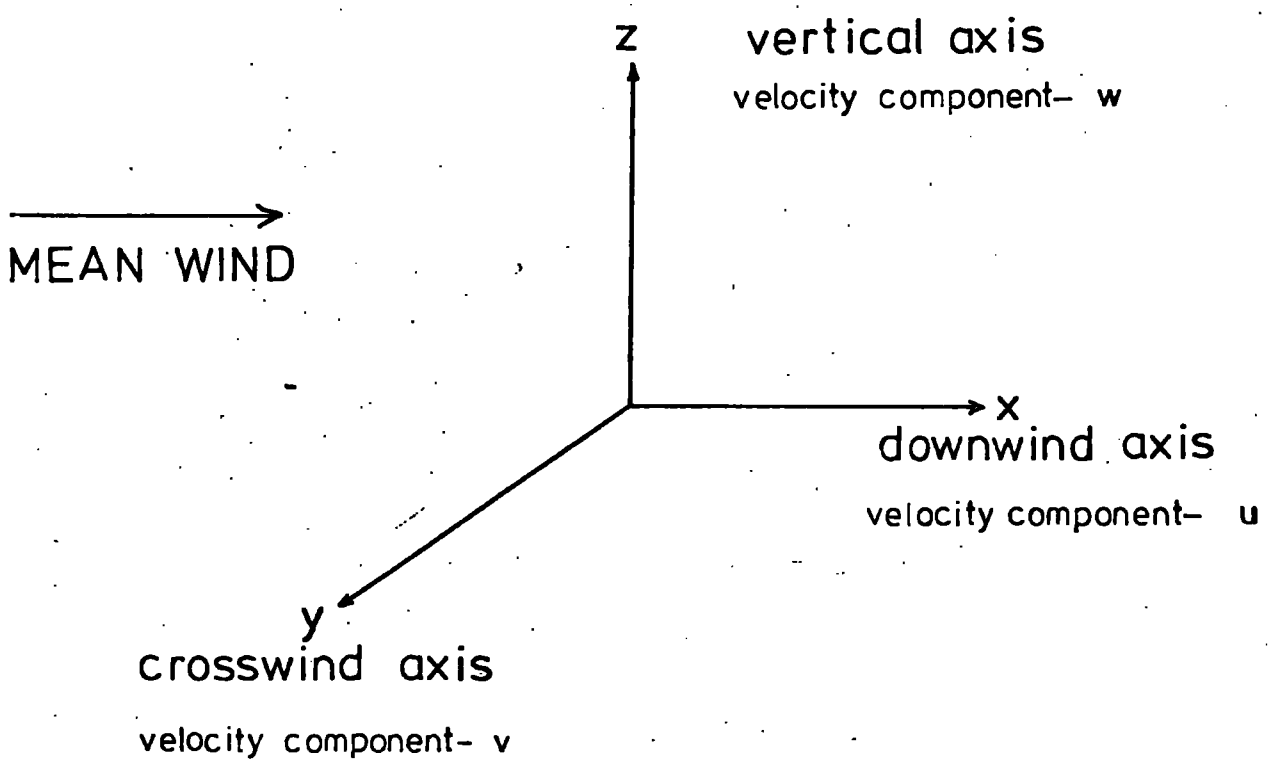

(b) Mean and fluctuating values

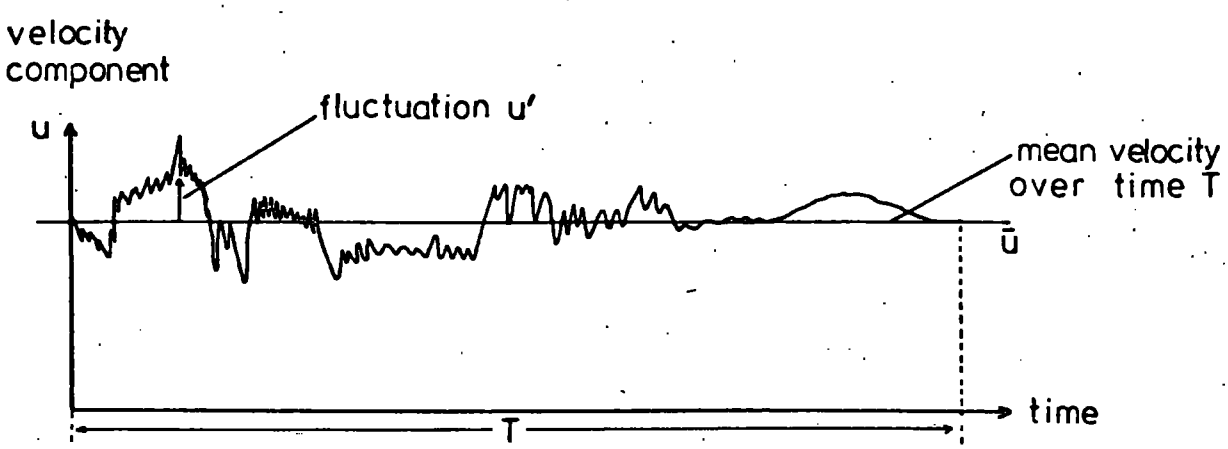

$$U(t) = \bar{U} + U'(t)$$

actual value = mean value + fluctuation

The first term represents the flux to be associated with the mean vertical motion and would have appeared even if the flow had been laminar. The second term, which is not necessarily zero, is apparently a transfer caused by the fluctuations themselves.

In the lower atmosphere, the mean vertical velocity $\bar{w}$ is usually small and can normally be ignored in comparison with w'. Hence, 2.5 reduces to:

$$\boxed{\bar{M}_z = \overline{\chi' w'}} \qquad (2.6)$$

We may generalize equation 2.6 to represent the transport of other entities by turbulence. In particular, we could write:

$$\boxed{\tau = d\overline{u'w'}} \qquad (2.7)$$

to represent the transfer of momentum in the boundary layer. The density, d, appears because the instantaneous momentum is du per unit volume, this, therefore, replacing χ in 2.6. The quantity τ refers to the amount of momentum crossing a unit horizontal surface and is known as the turbulent or Reynolds stress.

The viscous stress is, as usual, given by an expression of the type:

$$\boxed{\tau_v = \eta \frac{du}{dz}} \qquad (2.8)$$

where η is the coefficient of viscosity.

There is no physical reason why viscous and turbulent effects cannot occur together. However, it so happens in the atmosphere that the Reynolds stress is much larger than any viscous

stresses. Thus, in most cases, it is quite satisfactory to consider the Reynolds stress as if it were acting alone.

2.4 The Concepts of Eddy Diffusivity and Viscosity

In the previous section, we established a simple relation for the flux of material that is transferred by the turbulent eddies. Naturally, our main interest here is the transport and diffusion of space charge, rather than these more familiar entities.

Apart from certain electrostatic factors to be discussed later, there would seem to be no reason why equation 2.6 cannot be generalized to include space charge transfer. Hence we may write:

$$\boxed{\bar{S}_z = \overline{\rho' w'}} \qquad (2.9)$$

where ρ is the instantaneous space charge concentration at a particular point and S_z the space charge flux (equivalent to current per unit area). We now recall the relationship between flux and concentration for a simple molecular diffusion process. Fick's first law states that the flux of material is proportional to the concentration gradient, thus:

$$\boxed{m_z = -D_m \frac{dx}{dz}} \qquad (2.10)$$

where m_z is the upward flux of material due to molecular diffusion and D_m the appropriate coefficient. Similarly, in the special case of space charge, we can write, by analogy, that:

$$\boxed{s_z = -D_s \frac{d\rho}{dz}} \qquad (2.11).$$

Early workers, notably SCHIMDT (1918), explored the possibility of representing the turbulent fluxes in a way mathematically similar to their molecular counterparts. This is, of

course, largely just a mathematical artifice because the mechanisms of molecular and turbulent transfer are so different.

On this basis, we can rewrite equation 2.6 in the form:

$$\overline{M_z} = - K_m \frac{d\bar{\chi}}{dz} \qquad (2.12)$$

where K_m is a turbulent diffusion coefficient for the material and $d\bar{\chi}/dz$ the gradient of mean concentration.

A cautionary note should be sounded here regarding the nature of K_m. The reader is probably aware that a molecular diffusion coefficient is essentially a property of the fluid and diffusing species. This is not, however, the case with turbulent diffusion coefficients as their values depend on the nature of the flow rather than on that of the fluid itself. We shall see that in the lower atmosphere K_m can vary by as much as two orders of magnitude as the conditions change.

We may extend the exchange coefficient hypothesis, as it is known, to include the transfer of momentum and presumably ions. In the case of momentum we write:

$$\overline{\tau} = - K_v \frac{d\bar{u}}{dz} \qquad (2.13)$$

where K_v is referred to as the eddy viscosity. Similarly, for the turbulent transfer of space charge we obtain:

$$\overline{S_z} = - K_s \frac{d\bar{\rho}}{dz} \qquad (2.14)$$

Provided that the ions are in low concentration, so that the electrostatic effects are small, we may assume that there will be no difference between the transfer mechanisms of ions and those of any other material. This implies that:

$$K_s = K_m.$$

KAWANO (1957) has determined a value for K_s indirectly by measurements of electric field, conductivity and space-charge, whilst HOPPEL and GATHMAN (1972) performed a similar measurement by a slightly different method. All three workers find values of K_s not far removed from those of K_m and we may assume that the similarity in transfer mechanisms is experimentally established.

2.5 Some Important Cases of Turbulent Diffusion in the Lower Atmosphere

2.5.1 The Basic Equations

It is the purpose of this section to apply the results obtained previously to describe the behaviour of space charge clouds. As a point source of ions was employed, it is obvious that diffusion will proceed in all three co-ordinate directions and, therefore, we must generalize the transfer relations to include those cases. Hence we write:

$$\boxed{\begin{aligned} \bar{S}_x &= -K_x \frac{\partial \bar{\rho}}{\partial x} \\ \bar{S}_y &= -K_y \frac{\partial \bar{\rho}}{\partial y} \\ \bar{S}_z &= -K_z \frac{\partial \bar{\rho}}{\partial z} \end{aligned}} \qquad (2.15)$$

The subscript s has been omitted from the diffusivity because, in future, we shall only be concerned with the diffusion of space charge. The possibility of non-isotropic diffusion has, however, been allowed for by inclusion of the directional subscripts x, y, and z. In practice, atmospheric diffusion processes are rarely isotropic, particularly in the boundary layer.

Equations of the type 2.15, whilst being mathematically simple, are not, from our point of view, in a very helpful form. We wish to know, if possible, how the space charge concentration varies downwind of the source. Suppose we consider the flux of space charge through a small volume and at the same time, apply the principle of conservation of charge. It is found that:

$$\boxed{\frac{d\bar{\rho}}{dt} = \frac{\partial}{\partial x}\left(K_x \frac{\partial \bar{\rho}}{\partial x}\right) + \frac{\partial}{\partial y}\left(K_y \frac{\partial \bar{\rho}}{\partial y}\right) + \frac{\partial}{\partial z}\left(K_z \frac{\partial \bar{\rho}}{\partial z}\right)} \qquad (2.16)$$

the details of a similar derivation being given by SUTTON (1953). If K_x, K_y and K_z are independent of position, we may simplify 2.16 to:

$$\boxed{\frac{d\bar{\rho}}{dt} = K_x \frac{\partial^2 \bar{\rho}}{\partial x^2} + K_y \frac{\partial^2 \bar{\rho}}{\partial y^2} + K_z \frac{\partial^2 \bar{\rho}}{\partial z^2}} \qquad (2.17)$$

and, if the diffusion process if also isotropic, that is $K_x = K_y = K_z = K$ say, then:

$$\boxed{\frac{d\bar{\rho}}{dt} = K \nabla^2 \bar{\rho}} \qquad (2.18)$$

where ∇^2 is the Laplacian Operator.

We now consider some relevant solutions of these equations.

2.5.2 Diffusion from an Instantaneous Point Source

This type of source is exemplified in practice by a smoke bomb or shell burst. We imagine a source that suddenly releases a quantity Q of space charge and thereafter ceases to produce ions. We further assume, for mathematical simplicity, that the ion source is far above ground. The boundary conditions in this case are:

$$\rho \longrightarrow 0 \text{ as } t \longrightarrow 0 \text{ at } r > 0,$$

$$\rho \longrightarrow 0 \text{ as } t \longrightarrow \infty,$$

r being the radial distance from the source.

If we assume that the total space charge is conserved, we may write:

$$\int_V \rho dV = Q \qquad (2.19)$$

where the integral is with respect to volume.

We also assume the diffusion process is isotropic, and, bearing in mind the symmetry of the system, we can rewrite equation 2.18 in the form:

$$\frac{\partial \bar{\rho}}{\partial t} = \frac{K}{r^2} \frac{\partial}{\partial r} \left(r^2 \frac{\partial \bar{\rho}}{\partial r} \right) \qquad (2.20)$$

The solution of 2.20 was first given by ROBERTS (1923) and is

$$\bar{\rho}(x,y,z,t) = \frac{Q}{8(\pi K t)^{3/2}} \exp\left(-\frac{r^2}{4Kt}\right) \qquad (2.21)$$

We observe that the concentration, at any particular time, is a gaussian function of the radial distance, a feature which is invariably present in the solutions of diffusion equations of this type.

A situation of more interest to ourselves is the dispersal of a puff of ions in a wind. ROBERTS assumed that the diffusion process continues in this case as before, the diffusing puff being merely carried bodily forward by the wind.

In certain circumstances, it might be possible for small portions of a plume to become virtually detached from the main system. Equation 2.21 may therefore be of assistance when discussing the behaviour of these separated elements.

2.5.3 Diffusion from a Continuous Point Source

2.5.3.1 Ion Source in Calm Conditions for Above Ground

We can find the solution quite simply in this case by integrating 2.21 with respect to time. This is equivalent to considering a continuous ion source as being the sum of an infinite number of instantaneous sources. (More details of this technique can be found in works on the conduction of heat, e.g. CARSLAW and JAEGER, 1959). We rewrite the integral in the form:

$$\bar{\rho}(x,y,z,t) = \frac{Q}{8(\pi K)^{3/2}} \int_0^t t^{-3/2} \exp\left(\frac{-r^2}{4Kt}\right) dt,$$

which has the solution:

$$\bar{\rho}(x,y,z,t) = \frac{i}{4\pi K r} \operatorname{erfc}\left(\frac{r}{(4Kt)^{1/2}}\right) \qquad (2.22)$$

where *erfc* denotes the complementary error function and i is the net current output of the ion generator.

The behaviour of 2.22 is illustrated in Fig. 2.2(a) and this shows clearly how the charge builds up around the source. At large values of time expression 2.22 takes the form:

$$\bar{\rho}(r) \longrightarrow \frac{i}{4\pi K r} \qquad (2.23)$$

This case of diffusion in calm conditions is, although of interest, rather unlikely to happen in practice. Occasionally, the wind speed may be low enough for the process to commence but it is thought that certain electrostatic factors would intervene, and as a result, prevent such a build-up of charge actually occurring. This point is discussed further in the next chapter.

2.5.3.2 Continuous Ion Source in a Wind

We turn now to a much more familiar situation - that of a continuous source in a wind. It is a matter of common experience that in these circumstances, a long plume of material is formed downwind of the source, see Fig. 2.2(b). We assume, as before, that we can describe the diffusion process in terms of equation 2.18. However, in this case we must also allow for the advection of ions by the wind. Making this adjustment we find that:

$$\frac{\partial \bar{\rho}}{\partial t} + u\frac{\partial \bar{\rho}}{\partial x} = K\nabla^2\bar{\rho} \qquad (2.24)$$

where u is the wind velocity, assumed constant.

Equation 2.24 is difficult to solve as it stands and therefore we shall only consider the steady state solution obtained by setting $\partial\bar{\rho}/\partial t$ equal to zero. Any solution can only give <u>mean</u> values of the concentration, and it should be clearly appreciated that, in reality, the concentration fluctuates in the vicinity of all sources. (The diffusion theory employed cannot possibly predict the fluctuations because, at the outset, we deliberately expressed the instantaneous fluxes in terms of the gradients of mean concentration).

The steady state solution, first given by ROBERTS (1923) is:

$$\bar{\rho}(x,y,z) = \frac{i}{4\pi K x}\exp\left[-\frac{u(y^2+z^2)}{4Kx}\right] \qquad (2.25)$$

Equation 2.25, which expresses the concentration downwind of an isolated point source, can be readily adapted to the case where the source is near the ground, a situation which is, of course, of particular importance here. The details of the modification are not discussed as a full account is given

The ion concentration due to a continuous point source

(a) conditions:- zero wind, far above ground, electrostatic effects negligible

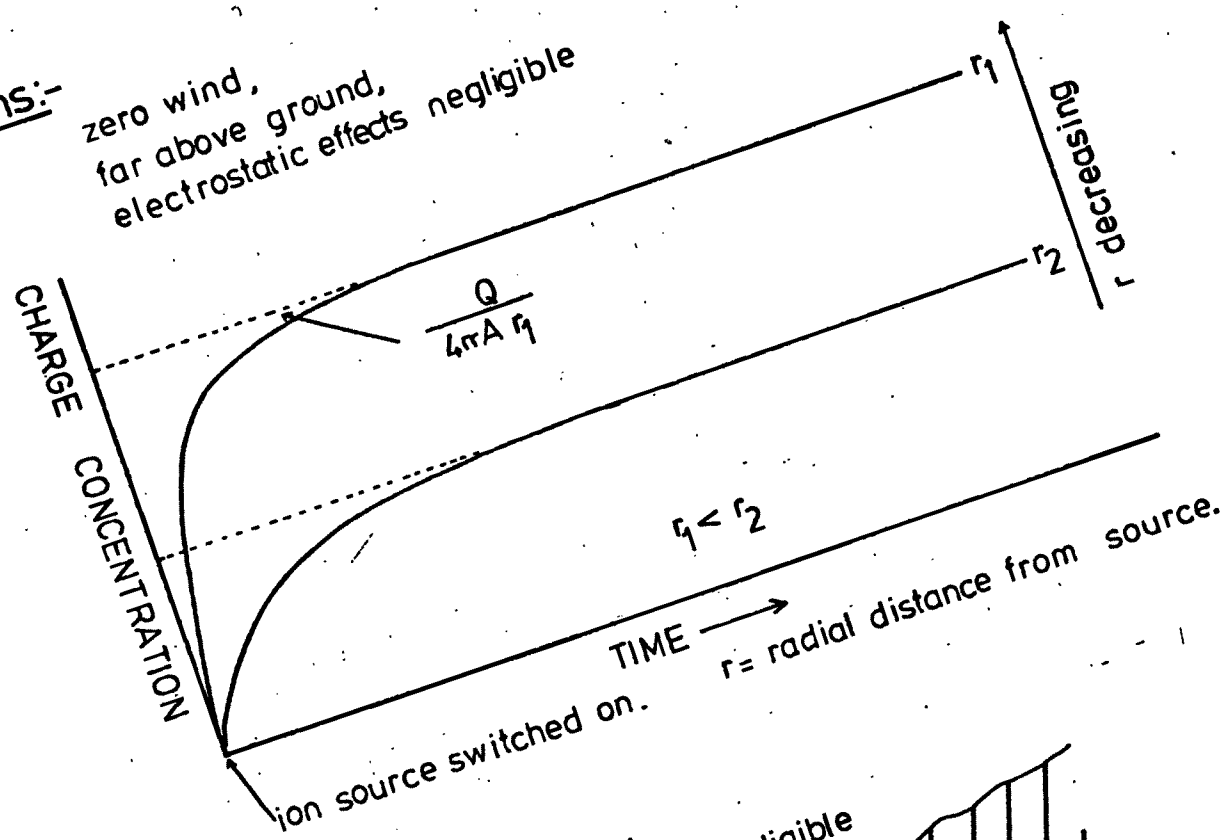

(b) conditions:- wind speed u, electrostatic effects negligible

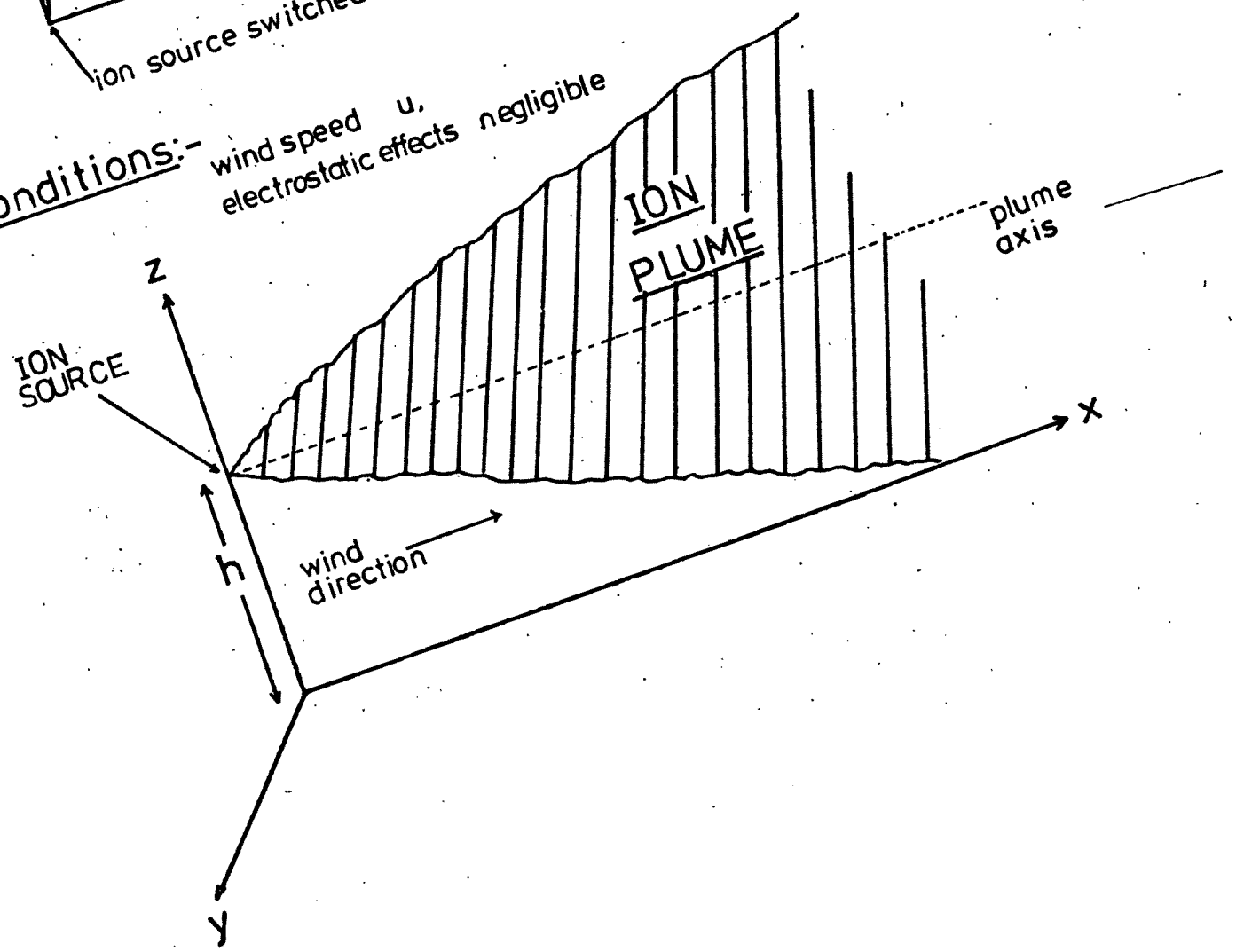

by SUTTON (1953). It is found that:

$$\bar{\rho}(x,y,z) = \frac{i}{4\pi Kx} \exp\left[\frac{-uy^2}{4Kx}\right]\left[\exp\left[\frac{-u(z-h)^2}{4Kx}\right] + \exp\left[\frac{-u(z+h)^2}{4Kx}\right]\right] \quad (2.26)$$

where h is the source height.

MAUND (1958) used an equation similar to 2.26 to estimate the electric field under an ion plume. In his case, the ions were produced by a point discharging during stormy conditions, his requirement being to estimate the point discharge current by making electric field measurements under the plume.

The implications of equation 2.26 are difficult to visualize. As it stands, however, it is clear that both the crosswind and vertical concentration profiles are gaussian. As a simplification, consider the variation of concentration directly under the plume axis, this being obtained by setting y and z equal to zero. Thus:

$$\bar{\rho}(x,0,0) = \frac{i}{2\pi Kx} \exp\left[\frac{-uh^2}{4Kx}\right] \quad (2.27)$$

It is found that in all cases, equation 2.27 predicts that the concentration attains a maximum value at a certain distance downwind. This feature is found in practice although not necessarily at the distance predicted by the equation.

Equation 2.26 forms the basis of the steady state plume model and its application to electric field calculations is discussed in the next chapter. We shall now consider certain

statistical features of turbulence before proceeding with the development of the "fluctuating plume models".

Fuller details of diffusion theory and comparison with experimental results can be found in PASQUILL (1962)

2.6
The Statistics of Atmosphere Turbulence and the Complicating Effects of Radiation and Topography

2.6.1
Preliminary Remarks

The smoke from a chimney changes its direction and inclination in response to the varying wind. Observation reveals that these motions are random in nature and occupy time scales from a fraction of a second to many minutes. The ion plume was expected to behave similarly in the turbulent wind.

Previously, we absorbed the dispersing effect of the fluctuations into an eddy diffusion coefficient. However, the use of this technique can only provide mean concentration values. It is my intention now to develop more sophisticated plume models which can predict the fluctuating values of space charge concentration downwind of source. We shall first digress a little to discuss the topic of atmospheric stability.

2.6.2
A brief note on Atmospheric Stability

During the daytime, particularly if the sky is clear, incoming solar radiation warms the ground. Air is virtually transparent to the radiation and thus the ground temperature rises more rapidly than that of the air. Close to the surface, however, the air is warmed in addition by the proximity of the hot ground. The effect is, of course, largest at the lowest levels and we therefore would expect the air temperature to fall rapidly with increasing height in these circumstances. Conversely, at night, under a clear sky, the earth radiates heat and the ground cools more quickly than the air. If the

radiation effect is strong enough, the temperature of the air may even increase with height for a short distance above the surface.

When the sky is clouded and the net radiation reduced to low levels, the vertical temperature gradient assumes a small negative value - the dry adiabatic lapse rate. This lapse rate is, in fact, determined solely by thermodynamic processes and is numerically about 1^{o} C. per 100 m.

The three cases above are those of unstable, stable and neutral conditions respectively.

It is felt that the majority of readers will be familiar with these effects hence the brevity of this discussion. Further details are to be found in SUTTON (1953).

2.6.3 Fundamental Characteristics of the Velocity Fluctuations

The mean and standard deviation are of fundamental importance in a statistical description of turbulence. We denote the mean by an overbar as before, the standard deviation being represented by the symbol σ . A quantity which is of considerable interest is the gustiness (g). It is defined by the relations:

$$g_x = \frac{\sigma_u}{\bar{u}}$$

$$g_y = \frac{\sigma_v}{\bar{u}} \qquad (2.28)$$

$$g_z = \frac{\sigma_w}{\bar{u}}$$

and is a measure of the intensity of turbulence in the three co-ordinate directions.

In the lower atmosphere it is normally found that gustiness values lie between 0.1 and 0.2 for the g_x and g_y components, while g_z tends to be more variable. Early researchers, notably SCRASE (1930) and BEST (1935), soon discovered that, near the ground, g_y was usually larger than g_z, the difference becoming more accentuated at lower levels. This was attributed to the presence of the ground inhibiting vertical motion, and thus, near the surface, the turbulence is anisotropic.

At higher levels within the boundary layer it was discovered that the turbulent energy was more equally distributed among its components. In practice, this equipartition is only attained at heights above 50 m or so and thus all the experimental work in this project was conducted in the lower, anisotropic region.

In unstable conditions we would expect the vertical velocity component, in particular, to be enhanced by convective effects and the level of turbulence to be augmented generally. Conversely, in stable conditions, the vertical motions tend to be suppressed and thus turbulent activity diminishes. It was mentioned that turbulence arose as a result of the frictional effects of the earth's surface, and in neutral and stable conditions this is undoubtedly true. In unstable conditions convective effects also contribute to the turbulent energy and thus, in this case, our original statement needs modification.

A very useful parameter, introduced by RICHARDSON (1925) enables one to compare the relative importance of the thermal and mechanical parts of the turbulence. Richardson, in his analysis, compares the dissipation (or production) of energy by mechanical and thermal processes and concludes that the quantity:

$$Ri = \frac{g}{\bar{T}} \frac{\frac{\partial \bar{T}}{\partial z} + \Gamma}{\left(\frac{\partial \bar{u}}{\partial z} \right)^2} \qquad (2.29)$$

is of considerable importance.

In the above T is the absolute temperature,

$\partial \bar{T}/\partial z$ the mean temperature gradient,

$\partial \bar{u}/\partial z$ the mean wind speed gradient,

Γ the dry adiabatic lapse rate,

and g the acceleration due to gravity.

He suggested if Ri were less than unity, the flow would remain turbulent, but that if Ri were greater than unity, the flow would become laminar. This criterion, although slightly incorrect numerically, does provide a valuable indication of the atmospheric stability and has been used extensively in this investigation.

It is possible, by appropriate mathematical techniques, to present a velocity fluctuation record in the form of a spectrum, this approach being used widely in practice. Spectral analysis has been a very effective probe with which to uncover the mechanisms of turbulence and we now consider a result of direct relevance to this project. Analysis of the velocity variations has revealed that the thermal (i.e. convective)

processes are responsible for variations of frequency lower than those caused by mechanical (i.e. frictional) effects. Typical spectra illustrating this point are shown in Fig.2.3. Generally speaking, "convective" eddies have periodicities of a few minutes whilst those of "mechanical" eddies are measured in tens of seconds. This implies that the convective systems, as we might expect, are rather larger than those of mechanical origin. The reader is referred to PRIESTLEY (1959) for a fuller discussion of this topic.

2.6.4 Topographic and other effects

The majority of theoretical work on the turbulent boundary layer has assumed the system to be horizontally uniform. Further, most of the experimental work has, until recently, been conducted at locations where there was a considerable expanse of flat ground. The implications are that, strictly, the results discussed above should only be applied to large flat areas. Although this is apparently a severe limitation, fortunately the essential features of turbulence are retained even over quite undulating terrain.

One must bear in mind that topographic effects will superimpose themselves on the turbulent variations in a complex way. Consequently, the observer must be able to recognise the presence of orographic, anabatic and katabatic effects on his data. Additionally, if the site is near the coast, then sea breezes may alter the conditions further.

The proximity of local obstructions had also to be considered when choosing a site. Clearly siting instruments too near

trees or houses is most undesirable because of the disturbance such objects would have on the local air flow. In both sites chosen for this project (see Sec.1.3) it is not thought that this effect has caused any trouble.

Finally, the fact that meteorological conditions are never steady for long, at least in this country, must also be taken into consideration. The wind, for example, may be veering or backing quite systematically during an experiment, or perhaps periods of sunshine and cloudiness are alternating with each other.

Unfortunately, as it is virtually impossible to quantify any of the highly variable factors mentioned above, the onus rests very much on the observer to assess the prevailing conditions. However, by choosing one or two sites and working frequently at them, the author suggests that it is possible to become familiar with a location and thus know in a rough, but useful, way what is likely to happen.

Showing the effect of atmospheric stability on the velocity component spectra

(a) u spectra

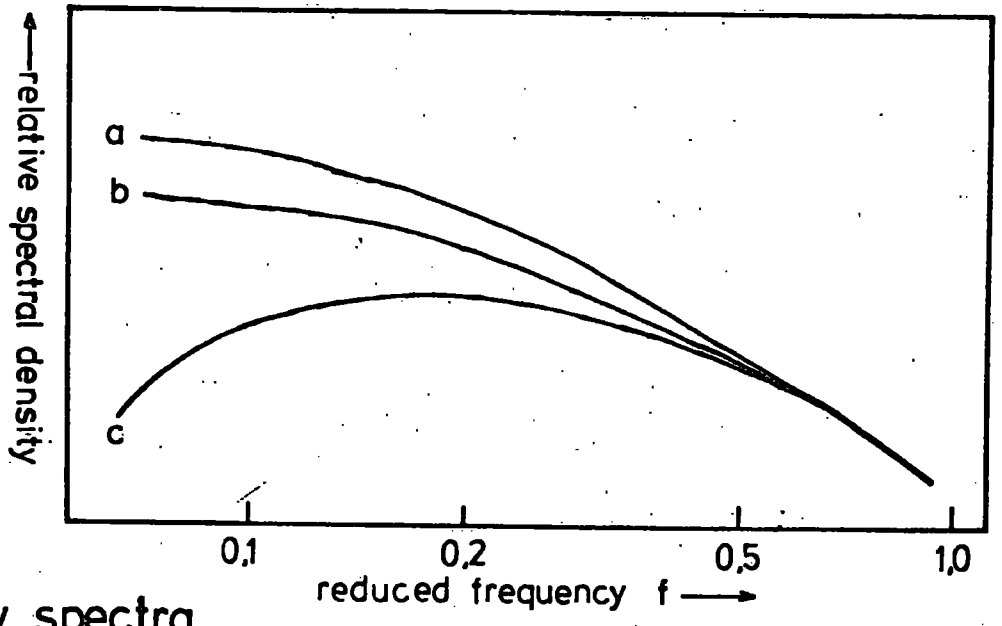

(b) w spectra

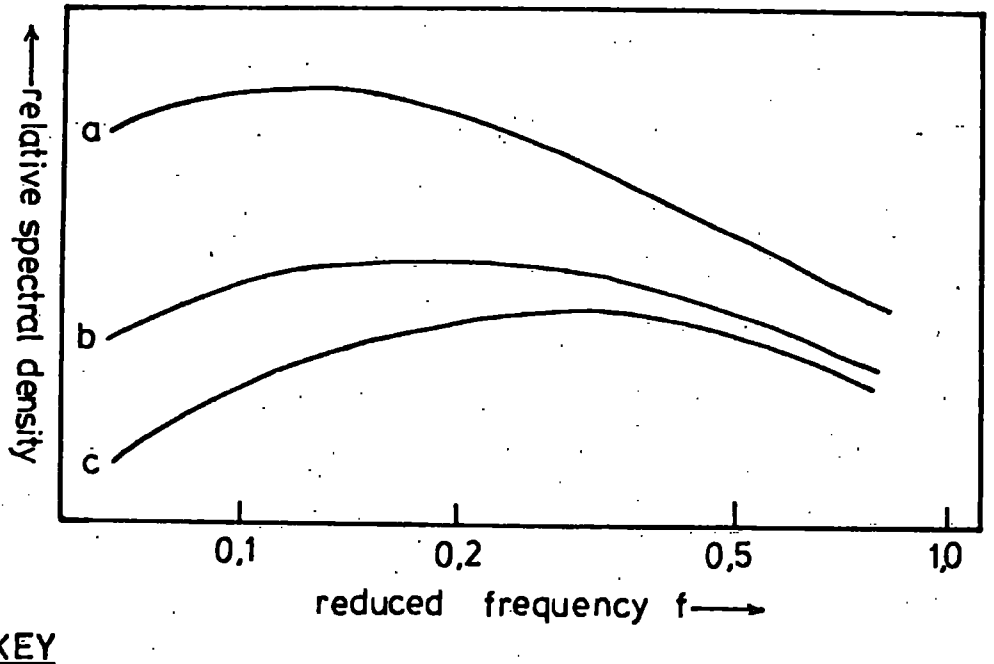

KEY

a strong instability
b moderate instability
c weak instability

where $f = \frac{nz}{\bar{u}}$.

n measured frequency
z height of measurement
$\bar{u}$ mean wind speed

2.7 The Influence of Atmospheric Stability on the Form of Plumes

Systematic observation of smoke plumes indicates that their behaviour depends on the nature of the turbulence and consequently on the atmospheric stability. The three types of plume behaviour, shown in Fig. 2.4., are known as looping, *coning* and fanning, and can be associated with unstable, neutral and stable conditions respectively.

In unstable conditions, the vertical movements are strongly accentuated by convective effects. There is more turbulent energy present generally, particularly at low frequencies. These large low frequency variations displace the plume bodily, forming the loops. The higher frequency components, which are responsible for the smaller scale diffusive effects, produce a progressive increase in width as the plume is blown downwind.

During neutral conditions, the mechanically produced turbulence is neither suppressed nor augmented because thermal effects are absent. Large, low frequency eddies are absent and therefore the plume shows little tendency to loop. The neutral stability encourages the variations to become isotropic because the distinction between vertical and horizontal motion is, effectively, removed. These factors result in the material spreading away from the source in the form of a cone.

The onset of stable conditions results in turbulent activity being suppressed, particularly the vertical component fluctuations. Horizontal eddies still exist, to a limited extent,

but very little energy is available for vertical movement. The plume, almost unable to diffuse vertically, takes the form of a thin "fan" lying horizontally downwind of the source.

It should be mentioned that the distinction between these types of behaviour is not always as marked as indicated above, and therefore caution must be exercised in applying these conclusions to the analysis of experimental situations. Nevertheless, the concepts described here have been of considerable assistance in understanding the ion plume behaviour.

The influence of stability on the form of a plume

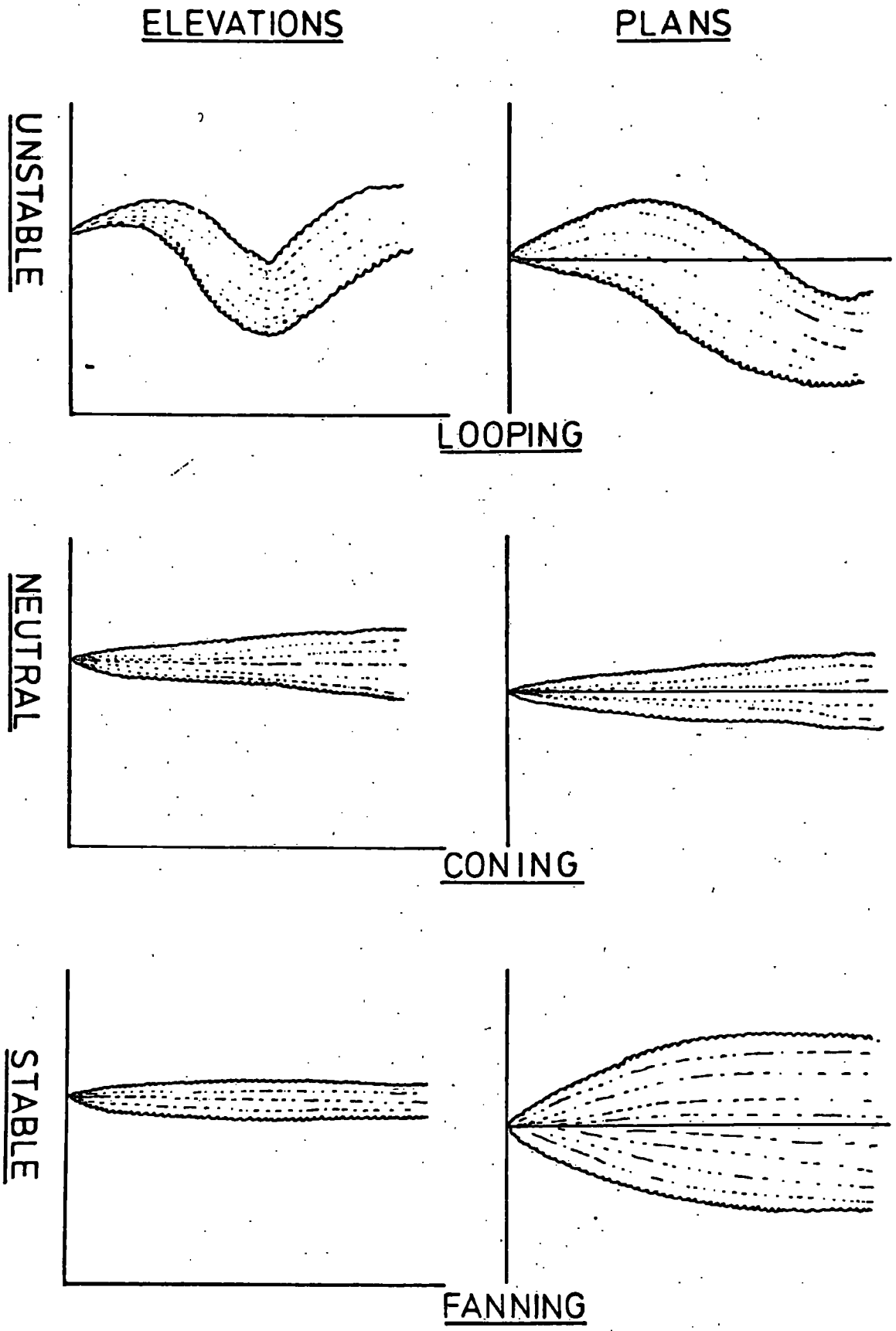

2.8 The Evolvement of Plume Models

2.8.1 The Rôle of Plume Models

The principal object of this project was to assess the feasibility of using ions, rather than more conventional materials, in small-scale atmospheric diffusion experiments. It was found that, whilst the ion plume behaviour could be roughly correlated with the atmospheric stability, a more precise knowledge of the changing plume configuration would have been very useful. These requirements prompted the development of plume models which, when supplied with the necessary meteorological data, would realistically simulate the ion plume behaviour.

2.8.2 The BIVANE Data Model

DAVIDSON and HALITSKY (1957) discovered that, if smoke plumes were photographed on cine film and the film then wound backwards, an interesting feature became apparent. Portions of the plume which were identifiable appeared to travel back to the source in straight lines. As the author's experiments were conducted at much lower levels than those of Davidson and Halitsky, it was necessary to establish whether this "straight line effect" still occurred nearer the ground. Some field tests were conducted and it was found that the effect was maintained with source heights down to about 5 m., but, below this the presence of the ground caused a plume to depart radically from the straight line behaviour.

It was Davidson and Halitsky's intention to reconstruct the plume configuration with the aid of bidirectional vane (bivane) data. A bivane, in conjunction with a suitable anenometer, measures the instantaneous values of the three velocity components, thus making it possible to predict the direction of the plume as it leaves the source. By invoking the straight line hypothesis, we may then predict the trajectory of the plume element as it moves away downwind. The technique can be extended by computing the paths of the succession of elements which comprise the plume. This is the basis of the bivane data model.

The approach is shown in Fig. 2.5(a), where only the X—Z plane is shown for reasons of clarity. Let us suppose we have u, v and w data from a bivane near the ion source, and that the values of these components are averages over the sampling interval s. We list these values below:

Time	Velocity Components			Plume Element just leaving Source
$-4s$	u_4	v_4	w_4	P_4
$-3s$	u_3	v_3	w_3	P_3
$-2s$	u_2	v_2	w_2	P_2
$-s$	u_1	v_1	w_1	P_1
0	u_0	v_0	w_0	P_0

Consider the situation at $-s$ when the plume element P_1 was just leaving the source. From the velocity component values we may write down the co-ordinates of P_1 when the time is zero. These are:

$$x_1 = u_1 . s$$
$$y_1 = v_1 . s$$
$$z_1 = w_1 . s$$

At time $-2s$ the plume element P_2 was leaving the source and hence at zero time the co-ordinates of P_2 are:

PLUME MODELS USED TO SIMULATE ION PLUME BEHAVIOUR

(a) Bivane data model

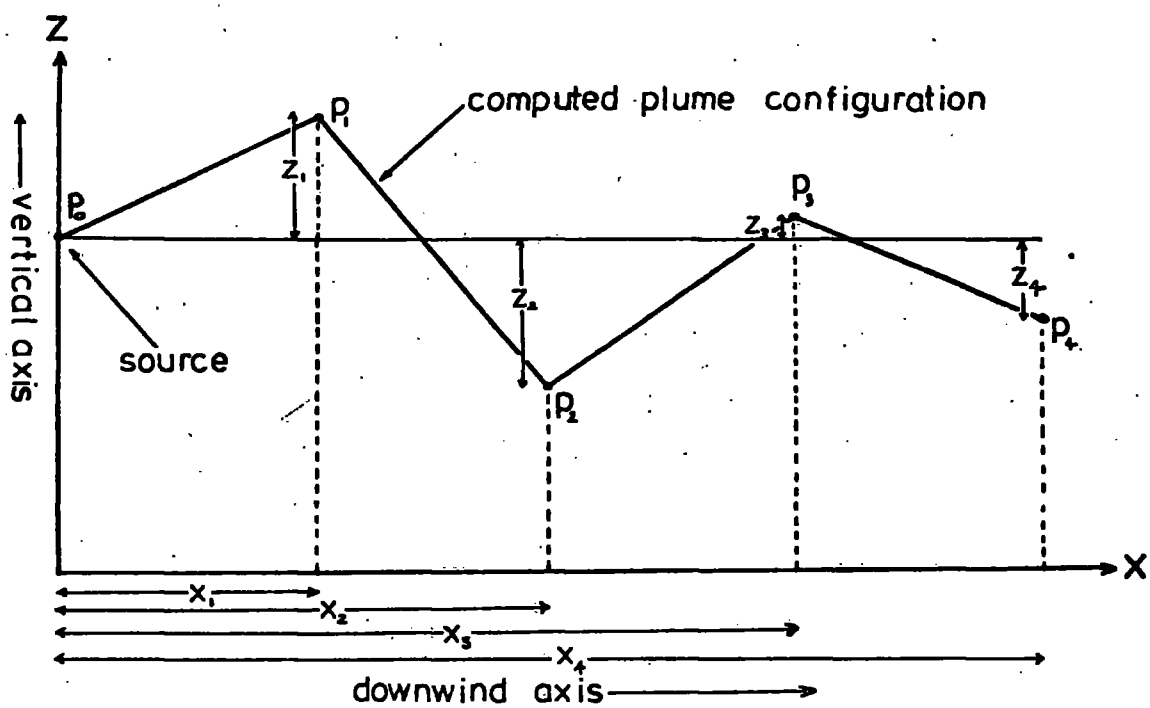

(b) Oscillating plume model

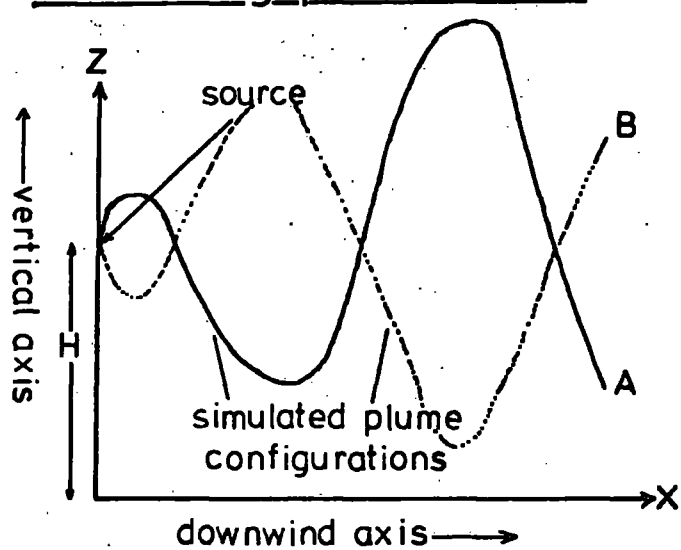

relations used to depict plume co-ordinates

$X = U.P$

$Y = A_y.P.\sin(2\pi.F_y.(P+T))$

$Z = H + A_z.P.\sin(2\pi.F_z.(P+T))$

A_y, A_z	horizontal and vertical amplitude factors.
F_y, F_z	frequency factors.
U	wind speed.
P	parameter having the dimensions of time.
T	time.
H	source height

$$x_2 = u_2 .2s$$
$$y_2 = v_2 .2s$$
$$z_2 = w_2 .2s$$

We may extend the process to compute the co-ordinates of P_3, P_4..... at this time.

The above method thus allowes us to calculate the position of the plume elements, and from this we can assemble a picture of the plume as it was at any particular time. After this, we may, by advancing the entire calculating process by one sampling interval at a time, produce a sequence of computed plume configurations.

In later experimental work, once the bivane was serviceable, the above technique was adopted and proved very helpful in understanding the electric field variations measured under plumes. A discussion of the application of this model will be found in Chapter 3.

2.8.3 The Oscillating Plume Model

It was originally hoped that the steady state model described in *Sec.* 2.5 would be capable of providing realistic electric field values downwind of ion sources in neutral and stable conditions. No steady-state model could possibly give usable information to assist in the analysis of data obtained in unstable conditions, the oscillating plume model being an attempt to imitate both the shape and the movement of the looping plume of these circumstances.

The basis of the model is illustrated in Fig. 2.5(b). The usual system of axes is employed and three equations set-up to generate a series of co-ordinates appropriate to a looping

plume. These are shown in the figure. The model was designed to be used on a digital computer, a special programme (OSCPLMPROG - see Chapter 6) being written for the purpose. It was necessary to specify six variables in order to characterize the plume completely, these being the amplitude and frequencies of the oscillations in both the horizontal and vertical, requiring four constants A_y, A_z, F_y, F_z , the source height, H , and the wind speed, U . In use the arbitrary parameter P (having the dimensions of time) was increased from zero up to a sufficiently large value to generate enough plume for the particular application in view. Usually P was increased until the x co-ordinate of the simulated plume attained 50 m. During this process, the y and z co-ordinates would vary as required by the equations; typically the z values behaved as shown by Plume A.

It was also possible, by varying T , the time, in the equations, to make plumes undergo oscillations in terms of time as well as space, and, for example, with an appropriate value of T , the configuration B would be produced.

The model was not used as much as the bivane data model, mainly due to lack of adequate data needed to set realistic values for the amplitude and frequency constants. The effects of crosswind and vertical diffusion were not incorporated in the model and this detracted from the validity of predicted electric field values. The application of the model is discussed in Chapter 3, whilst results obtained with it are considered in Chapter 6.

Chapter 3: ELECTRICAL ASPECTS OF ION PLUMES

3.1 Introduction

The previous chapter was concerned only with those features of ion plume behaviour which were determined by turbulent diffusion processes. However, it is fairly obvious, particularly with the relatively high ion concentrations used in this project, that electrostatic forces may be sufficiently large to substantially modify the form of the plume. Before embarking on a discussion of this topic, we must first consider certain fundamental features of ions and space charges in general. In addition, we cannot afford to ignore the effect of the Earth's natural electric field, both on the plume itself and on the electrical measurements to be made near the plume.

3.2 Basic Principles

3.2.1 Forces and Fields

We begin by quoting Coulomb's law, which expresses the force between two point charges of magnitude q_1 and q_2 as a function of r their distance apart. Mathematically, we can write,

$$F = \frac{q_1 q_2}{4\pi \epsilon_0 \epsilon_r r^2} \qquad (3.1)$$

where F is the force between the charges,

ϵ_0 the *permittivity of* free space,

and ϵ_r the relative *permittivity*

(The relative *permittivity* of air is very close to unity and for our purposes any small difference can be safely ignored.)

The electric field vector, $\underline{E}$, due to a charge q is given by the expression,

$$\underline{E} = \frac{q}{4\pi\epsilon_0 r^3}\,\underline{r} \qquad (3.2)$$

where $\underline{r}$ is directed away from the charge if it is positive and vice-versa.

According to an earlier convention, the atmospheric electric field at the Earth's surface was directed oppositely to that used in electrostatic theory. To avoid this ambiguity it is often better not to use the term "field" but instead to refer to the potential gradient dV/dr . These quantities are related by the expression,

$$\underline{E} = -\,dV/d\underline{r} \qquad (3.3)$$

The electric field and the potential gradient possess both magnitude and direction and are, of course, vector quantities.

3.2.2 Gauss's Theorem

This theorem is often of considerable assistance when we try to understand the nature of electrical effects in the atmosphere. The theorem can be stated in the form that the total integrated normal component of flux over a closed surface is equal to the total charge contained in the volume bounded by that surface. The reasoning upon which this conclusion depends will not be discussed here as it has been widely treated in the literature, an excellent paper on the subject being given by CHALMERS (1963). The theorem can be expressed mathematically in the form,

$$\int_V \rho\, dV = \epsilon_0 \int_S \underline{E}.d\underline{s} \qquad (3.4)$$

where ρ is the space charge density,

$d\underline{s}$ an element of area, the direction being that of the outward normal,

and dV an element of volume.

Further, it can be shown that,

$$\boxed{\frac{\rho}{\epsilon_0} = div\underline{E}} \qquad (3.5)$$

where

$$div\underline{E} = \frac{\partial E_x}{\partial x} + \frac{\partial E_y}{\partial y} + \frac{\partial E_z}{\partial z}$$

A further and very useful implication of Gauss's theorem, admittedly not obvious from the above, is that it allows us to consider certain charge distributions as if they were, at least in some respects, line or point charges. As a consequence of this, we could for example, compute the electric field due to a uniformly concentrated spherical cloud of ions by assuming that the total charge in the system resided entirely at the cloud centre. Clearly this is an important and useful simplification in the treatment of electrical phenomena and the approach has been employed extensively in the theoretical work associated with this project.

3.2.3
The Effect of Boundaries and the Method of Images

Until now we have considered ions and charges as being completely isolated and far away from any boundaries. This state of affairs is clearly unrealistic insofar as this project is concerned and therefore we must consider the implications of the plume being within a few metres of the Earth's surface. In electrostatic terms the earth is a good conductor and although it is, of course, spherical, we may, because of the relatively small scale of this field work investigation, consider its conducting surface to be planar. It is a familiar boundary condition of electrostatic theory that a parallel component of electric field cannot exist at a conducting boundary.

In atmospheric electric terms, this means that, at the Earth's surface, the electric field is entirely vertical. Of course, above the surface there is no reason why horizontal components of electric field cannot exist and, although these have not been measured, the existence of very large horizontal fields in the vicinity of ion plumes has been demonstrated theoretically.

The method of images enables one to incorporate, in a simple way, the effect of the presence of boundaries near to arrangements of charges. In essence, the conducting surface is considered as if it were a mirror, an image charge of the opposite sign to the real charge then being placed at the appropriate point on the other side of this mirror. The use of such an approach is illustrated in Fig.3.1(a). It should be noted that the presence of this oppositely charged image associated with the real charge implies the existence of an attractive force towards the boundary. This actually occurs in practice and thus in this sense (and only this sense) the image charge is very "real". More details of the method of images as applied to the solution of electrostatic problems can be found in BLEANEY & BLEANEY (1965).

3.2.4
The Movement of Ions in Electric Fields - Mobility

The presence of an electric field exerts a force on an ion. In a gas, however, an ion is not able to accelerate continuously under the influence of the field because of the incessant collisions it makes with the molecules comprising the gas. These collisions result in the ion, after a very short time, attaining a terminal velocity, v_t, say. It has been found

experimentally that v_i is proportional to E, the applied electric field, for any particular ion and gas combination. Hence we may write that,

$$\boxed{v_i = \mu E} \qquad (3.6)$$

where μ is a constant known as the mobility. This relationship is of considerable importance, because we can, knowing E and μ, compute the velocities of ions in or near the plume.

3.2.5
The Nature and Concentration of Natural Ions and Nuclei

ELSTER & GEITEL (1899) and WILSON (1900) discovered the existence of atmospheric ions but it was not until some years later that the distinction between ions of various mobilities was appreciated.

Small ions, as they are known, are believed to consist of a few neutral molecules clustered around a singly charged molecule. Such a system was kept together by its charge polarizing the surrounding molecules, thus producing the necessary attractive forces. WRIGHT (1936) considered the mass of a small ion to be equal to about that of ten water molecules, while TORREDON (1939) estimated an ion to be about the size of four oxygen molecules. The mobility of small ions lies between 1×10^{-4} and 2×10^{-4} MKS units. There are, in fact, about 7×10^8 of each sign in a cubic metre of air at an "average land station", (CHALMERS 1967).

The "large" ions were discovered by LANGEVIN (1905) and have mobilities about 0.002 that of the small ions. These ions are considerably larger than the small ions and are charge-

bearing particles of the same type as condensation nuclei. It is probable that they are comprised of such substances as evaporated sea-salt or residues from industrial and domestic pollution. Consequently large ions (and uncharged nuclei) are much more abundant in urban than rural areas. CHALMERS (1967) indicates that, at an "average land station", there are approximately 10^9 large ions of each sign and about 4×10^9 uncharged condensation nuclei in a cubic metre of air.

Clearly an ion may remain as such until it is neutralized by an encounter with an ion of the opposite sign. Ions may however combine with each other in various ways for instance, a small ion could combine with a similar ion of opposite sign and the result would be neutral molecules. Alternatively the small ion might interact with a large ion of the opposite sign this process resulting in an uncharged condensation nucleus plus some neutral molecules. A small ion might also become attached to a neutral nucleus and thus become a large ion of the same sign.

We can, in fact, expect the number of interactions that occur in unit time in a given volume to be proportional to the numbers present of both types of particle involved. On this basis we can define a "combination coefficient" for the process in which we are interested. Following CHALMERS (1967) we may write for small positive ions,

$$\frac{dn_1}{dt} = q - \alpha n_1 n_2 - \eta_{12} n_1 N_2 - \eta_{10} n_1 N_0 \qquad (3.7a)$$

and for negative ions,

$$\frac{dn_2}{dt} = q - \alpha n_1 n_2 - \eta_{21} n_2 N_1 - \eta_{20} n_2 N_0 \qquad (3.7b)$$

In the above:

q denotes the rate of production of small ion pairs per unit volume per unit time,

n_1 the positive small ion concentration,

n_2 the negative small ion concentration,

N_1 the positive large ion concentration

N_2 the negative large ion concentration

and N_0 the neutral nucleus concentration.

The small ion recombination coefficient is α, whilst the other coefficients are as follows,

η_{12} combination coefficient for small positive - large negative ions

η_{21} combination coefficient for small negative - large positive ions

The combination coefficients between small ions and neutral nuclei are denoted by,

η_{10} coefficient for small positive ions and nuclei,

η_{20} coefficient for small negative ions and nuclei.

The values of the combination coefficient are not discussed here as details can be found in CHALMERS (1967). Equations *(3.7a)* and *(3.7b)* are of considerable importance because they enable us to make various deductions concerning the behaviour of the artificially produced ions used in this project. A discussion of this topic now follows.

3.2.6
The Nature and Fate of the Artificially Produced Ions

The ions used for the experimental studies in this project were produced by the application of a very large electric field to a current of air. The discharge processes occurring in the ion generator involve ionized gas molecules (general reference LOEB 1965) and consequently only small ions were produced by the ion source. These artificially produced ions will, like their natural counterparts, be subject to all of the combination processes referred to previously. It is, therefore, of considerable importance to estimate, at least approximately, the effectiveness of the various processes in removing these ions as the plume travels downwind.

It seems logical that near the ion source, say within 20 m, where the artificial ion concentration is very high, there will be, relatively speaking, very few natural ions (of oppo-

site sign) and nuclei available for combination processes. Further calculations show that at distances of 50 *m* or greater from the source the artificial ion concentration will have fallen to 10^{-9} Cm^{-3} or less. If these typical figures are then substituted into equation *(3.7a)* or *(3.7b)* whichever is appropriate, together with suitable values for the various combination coefficients, the rate of small ion removal is found to be about 1 per cent per second. Of this 1 per cent approximately 0.7 per cent is absorbed in conversion to new large ions, whilst the remaining 0.3 per cent is destroyed by neutralization. For a typical plume, therefore, travelling downwind at a few metres per second, it appears a reasonable assumption that these depletion processes will not, under most circumstances, remove more than a few per cent of the ions from the plume in its first hundred metres of travel.

One should appreciate that, whilst the artificially produced ions may be slowly removed from the plume, this does not necessarily imply that the total space charge is decreasing. To illustrate this point consider the following situation. In the lower atmosphere ambient ionization levels are very low; however there, unlike the ion plume, there are, to a reasonable approximation, equal numbers of positive and negative ions. (very near the ground the electrode effect can disturb this equality - see CROZIER 1963). An artificially produced ion, travelling downwind, may encounter an oppositely charged *natural* ion and combine with it. However, when this occurs there still must remain somewhere a surplus natural ion of the same sign as the original artificial ion and thus the net space charge of the ion plume would appear to have been maintained.

On this argument it would seem that recombination processes are in themselves incapable of dissipating the space charge of the plume although, of course, the artificial ions are gradually replaced by natural small and large ions. In actual fact, it is thought that a considerable number of ions are removed from the plume by image forces -*see Sec. (3.5.5)*

OGDEN (1967) estimated, using a different method, that the small ions from a $1\mu A$ source will nearly all be converted into large ions within 1 km downwind of that source. In the case of the ion source used in this project, which had an output of about $0.3\mu A$, it can be computed on the basis of OGDEN's formula that most of the conversion to large ions would be achieved within $500m$ of the source.

In practice, electric field measurements were always made within $100m$ of the ion source, and consequently it is reasonably certain that a small-ion plume was being investigated. However, on a few occasions at the Maiden Castle site it was thought that the nucleus concentration might have been rather higher than the figures given by CHALMERS. If this was indeed so, then the conversion rates deduced previously will be underestimates and thus there could be a significant number of large ions nearer the ion source. Unfortunately, no nucleus concentration measurements were made during this project, the high nucleus concentrations being inferred from relatively high natural fields observed on these occasions.

3.3 The Electric Fields Due to Various Space Charge Distributions

3.3.1 Opening Note

In this section we shall consider the electric fields to be expected in the vicinity of simple charge distributions. The results will, of course, be of considerable interest in themselves but moreover they will serve as a useful prelude to the discussions on the estimation of the electric fields due to ion plumes.

3.3.2 Spherical Space Charge Cloud

This is illustrated in Fig. 3.1(a). A spherical space charge, O, of uniform density ρ_s and radius r_s is at a height h above flat ground. The general point M, at which we wish to know the electric field, is situated a horizontal distance x from the space charge centre. The total charge present is, in accordance with Gauss's theorem, considered to act as if it were entirely at the centre point. In the diagram the image charge, i, is also shown together with the various electric field vectors and their components. The vectors from the real and image charges are indicated by E_o and E_i respectively and we observe that the horizontal components of these, i.e. E_{xo} and E_{xi}, are equal and opposite. Hence the horizontal component of field is zero as required by the boundary conditions.

We can write for the vertical component, E_z,

$$E_z = \frac{2q}{4\pi\epsilon_o}\frac{1}{R^2}\sin\alpha \qquad (3.8)$$

However, we can express the total charge q in the form

$$q = \frac{4}{3}\pi r_s^3 \rho_s$$

and R^2 and $\sin\alpha$ in terms of x and h. As a result we find

$$E_z = \frac{2}{3}\frac{r_s^3\rho_s}{\epsilon_o}\frac{h}{(x^2+h^2)^{3/2}} \qquad (3.9)$$

The electric field due to:-

(a) spherical space charge (elevation)

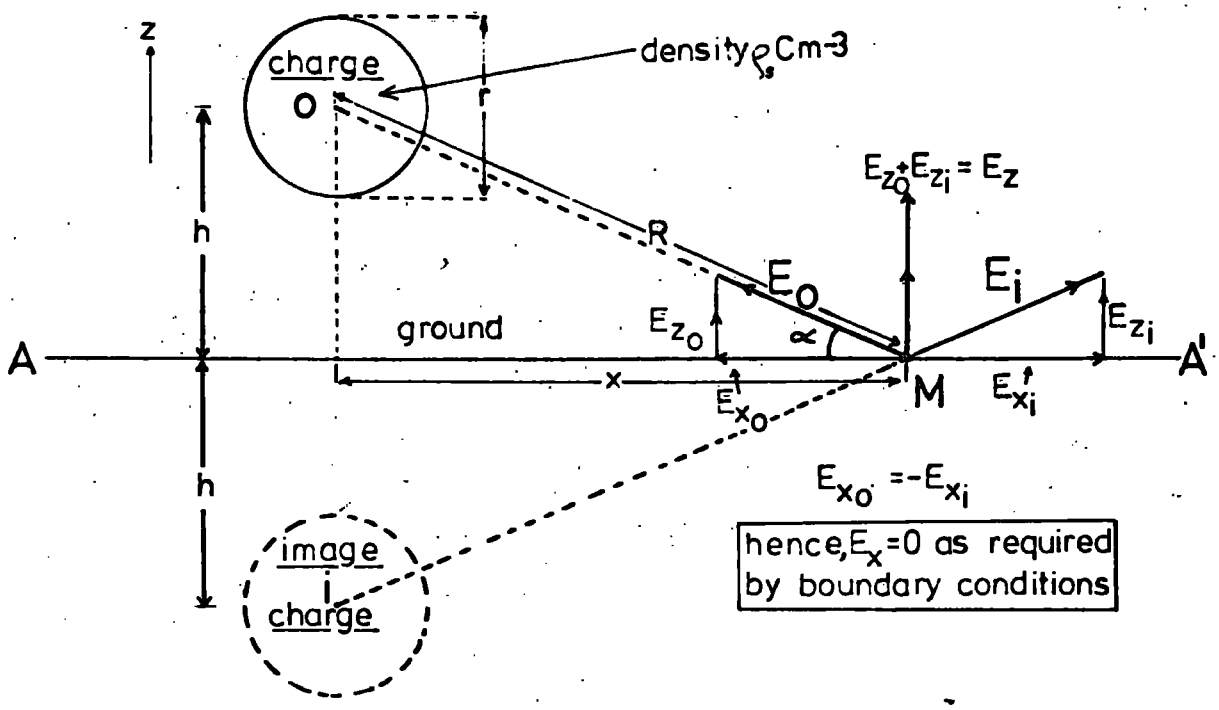

(b) 'infinite' cylindrical space charge (plan)

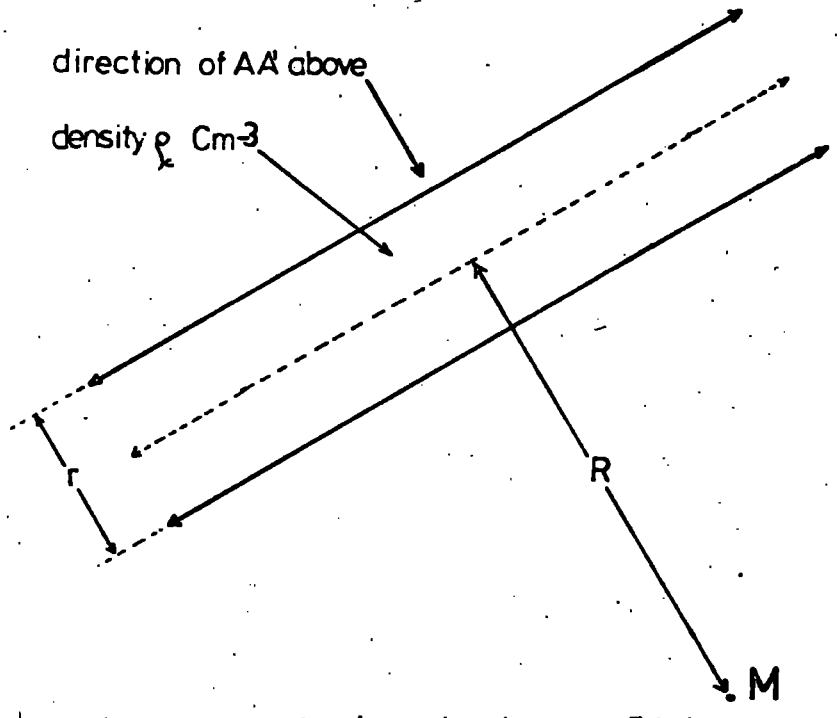

NB. A negative space charge is considered above. This is convenient as the electric field vector is then upward.

Now E_z attains a maximum value when x is zero, i.e. when the charge is overhead, and this is given by

$$E_z\,(max) = \frac{2 r_s^3 \rho_s}{3\epsilon_0 h^2} \qquad (3.10)$$

Let us now consider a numerical example with values appropriate to this *project*. Suppose we set $r_s = 1m$, $\rho_s = 1\mu Cm^{-3}$ and $h = 10m$.

It is found from equation (3.10) that in this case,

$$E_z\,(max) = 750 Vm^{-1}$$

We note immediately that the relatively small space charge, a few micro-coulombs, produces a substantial electric field at the Earth's surface. In fact, it would take the ion generator used in this project about ten seconds to produce this amount of charge.

3.3.3 Cylindrical Space Charge (Infinite Length)

This is illustrated in plan in Fig. 3.1(b). Fig. 3.1(a), although originally drawn to represent a spherical space charge cloud, will also be used to describe the cylindrical charge cloud now under consideration.

In the case of a cylindrical charge cloud, the method used to determine the electric field is essentially no different from the previous one. Hence the derivation of the formulae is not included here, the reader being asked to consult BLEANEY & BLEANEY for the details. The vertical field component at M is given by

$$E_z = \frac{\lambda}{\epsilon_0 \pi R} \sin\alpha \qquad (3.11)$$

where λ is the charge per unit length.

As before we can write

$$\lambda = \frac{\pi r_c^2 \rho_c}{\sin\alpha}$$

and by expressing R and $\sin\alpha$ in terms of x and h we find that

$$E_z = \frac{r_c^2 \rho_c}{\epsilon_0} \frac{h}{(x^2 + h^2)} \qquad (3.12)$$

As in the previous case E_z attains a maximum when the charge is overhead. This is given by

$$E_z(max) = \frac{r_c^2 \rho_c}{\epsilon_0 h} \qquad (3.13)$$

Again we consider a simple numerical example in order to form an idea of the magnitude of the quantities involved. Typical values might be

$$r_c = 1m, \quad \rho_c = 0{,}1\mu Cm^{-3} \quad \text{and} \quad h = 10\,m.$$

Using (3.13) we find that

$$E\ (max) = 1130\ Vm^{-1}$$

In conditions where turbulent diffusion effects are small it may be possible to regard the ion plume as an infinite (or semi-infinite) line-charge. This possibility was recognized by MAUND (1958) in his investigations of point discharge. Clearly our ion plume is not infinitely long but, in practice, provided its length subtends an angle within a few degrees of 180° (or 90°) at the point (M) the assumption can be shown to be acceptable.

3.3.4 Electric Fields Due to Moving Space Charges

A space charge produced in the atmosphere will not, of course, remain stationary but will be blown along by the prevailing wind. Naturally the charge will also be diffused by turbulent

Electric field associated with passing space charges

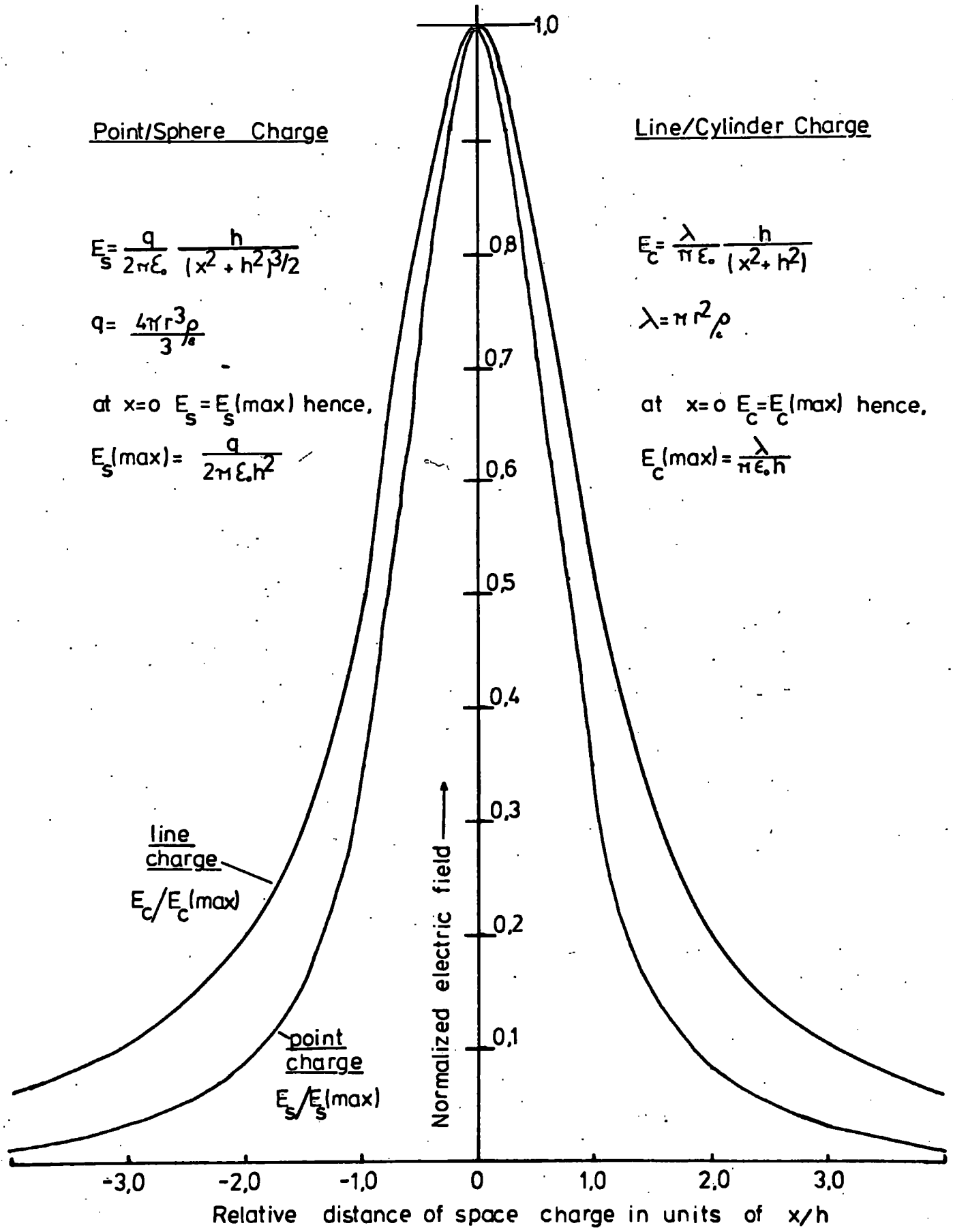

processes but we shall ignore this complication while we are considering the basic principles. It is of great interest to compute the variation of electric field as a space charge cloud passes by. The results of such a calculation, employing equations (3.9) and (3.12) are shown in Fig. 3.2. (In the figure the notation has been changed slightly to emphasize the distinction between the cylindrical case, subscripted c, and the spherical, subscripted s.) We note from the equations that in the case of the spherical charge the shape of the curve in the figure is determined by the quantity

$$h/(x^2+h^2)^{3/2}$$

whilst in the cylindrical system the shape is given by the function

$$h/(x^2+h^2)$$

Accordingly the relationship between the value of the field due to the charge at a distance x and its overhead value depends only on the ratio x/h . This applies in both cases.

We note from the diagram that relatively little effect is felt from the charges until they are within about 2h of the point in question. Thereafter the electric field varies rapidly as the charge system passes overhead. It can be deduced that the variation is most rapid when $x=0,5h$ in the case of the spherical charge and when $x=h/(\sqrt{3})$ for the cylindrical case.

We should also consider the spherical charge cloud that does not pass directly over M . Suppose the perpendicular distance from the projection of the charge trajectory on the ground to the point M were p . Further let us suppose that the projection

of the actual position of the charge is at a distance q from the point where this perpendicular intersects the projected trajectory. Then we may write

$$x = \sqrt{q^2 + p^2}$$

and we may proceed as before and write the electric field as

$$E_z = \frac{2 r_s^3 \rho_s}{3\epsilon_0} \frac{h}{(q^2 + p^2 + h^2)} \qquad (3.14)$$

In practice, the electric field at a particular point would be measured as a function of time, but by employing the transformation $x = ut$, where u is the wind velocity, we can amend our equation accordingly. For example, in the above $q = ut$ and therefore

$$E_z(t) = \frac{r_s^3 \rho_s}{3\epsilon_0} \frac{h}{(u^2t^2 + p^2 + h^2)^{3/2}} \qquad (3.15)$$

3.4 Calculation of Electric Fields Using the Plume Models

3.4.1 Introduction

In the previous section we established, quite simply, the electric field using the plume models described in Secs. 2.5 and 2.8.

In practice the manner of application of all three models is much the same. The electric field due to a plume element is first calculated and then the total field computed by some type of integration or summation process. MAUND (1958) discovered whilst using a similar steady state model to mine that an analytical integration was virtually impossible. MAUND did not have a digital computer at his disposal and was therefore forced

to grossly simplify his equations in order to proceed with an integration. Fortunately, this restriction did not apply as an adequate computer was available to perform the numerical work.

The results obtained with these models are not discussed here. They will be presented immediately before the field data in order to facilitate comparisons.

3.4.2 The Steady State Model

The space charge concentration distribution in this model is based on equation (2.26). The principles of this and the other two models are illustrated in Fig. 3.3.

Consider the plume element $S(p,q,r)$. Suppose its volume were δV and the concentration within the element $\rho(p,q,r)$. The concentration is determined, of course, from equation (2.26) after specifying appropriate values for the ion source strength and height, wind speed and eddy diffusivity. The total charge in the element S is given by

$$\boxed{\delta Q = \rho(p,q,r)\,\delta V} \qquad (3.16)$$

Consequently, the electric field at the general point $M(x,y,z)$ is found to be

$$\boxed{\delta E = \frac{\rho(p,q,r)\delta V}{4\pi\epsilon_0}\,\frac{1}{R^2}} \qquad (3.17)$$

the elemental electric field, δE , being parallel to the line SM in the figure. Let us denote the x, y and z components of this vector by δE_x , δE_y and δE_z respectively. Then, by application of simple trigonomety we can write

$$\boxed{\begin{aligned} \delta E_x &= \delta E \cos\alpha \cos\beta \\ \delta E_y &= \delta E \cos\alpha \sin\beta \\ \delta E_z &= \delta E \sin\alpha \end{aligned}} \qquad (3.18)$$

where α and β are as shown in Fig. 3.3(a), and δE is the magnitude of $\delta \underline{E}$. Now let us derive the field contributions made by the image element at $S'(p,q,r')$. Employing a dashed notation for distances and angles pertaining to the charge image, we can write

$$\boxed{\delta \underline{E}' = \frac{-\rho(p,q,r')\,\delta V}{4\pi\epsilon_0}\,\frac{1}{R'^2}} \qquad (3.19)$$

and here, of course, $r' = -r$ because of the symmetry.

In a similar manner, we may list the components of $\delta \underline{E}'$, these being

$$\boxed{\begin{aligned} \delta E'_x &= \delta E' \cos\alpha' \cos\beta' \\ \delta E'_y &= \delta E' \cos\alpha' \sin\beta' \\ \delta E'_z &= \delta E' \sin\alpha' \end{aligned}} \qquad (3.20)$$

where α' and β' are the angles of elevation and azimuth of the charge element image with respect to the point M. (N.B. $\beta' = \beta$).

It is now possible to determine the field components present at M due to the charge element and its image. Denoting these components by DE_x, DE_y and DE_z we may write,

$$\boxed{\begin{aligned} DE_x &= \delta E_x + \delta E'_x \\ DE_y &= \delta E_y + \delta E'_y \\ DE_z &= \delta E_z + \delta E'_z \end{aligned}} \qquad (3.21)$$

If, and only if, the z coordinate of M is zero the equations reduce to

$$\boxed{\begin{aligned} DE_x &= 0 \\ DE_y &= 0 \\ DE_z &= 2\delta E_z \end{aligned}} \qquad (3.22)$$

We have deduced expressions for the elemental field due to the typical element S and its image S'. Therefore, at least in principle, it should be a straightforward matter to divide the plume into a sufficiently large number of similar elements, usually about 10^4, sum all the field contributions and deduce

Calculation of electric field values from plume models

(a) the steady-state model

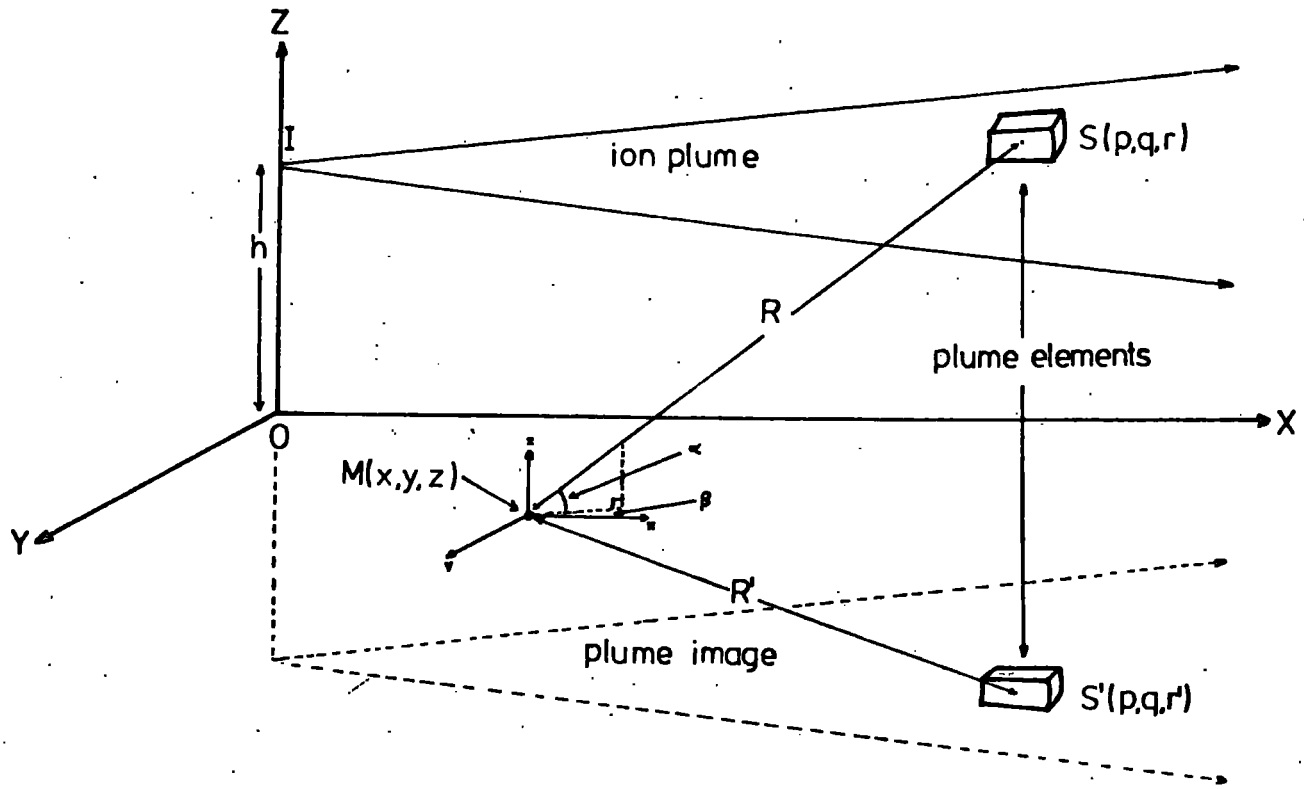

(b) the bivane data model

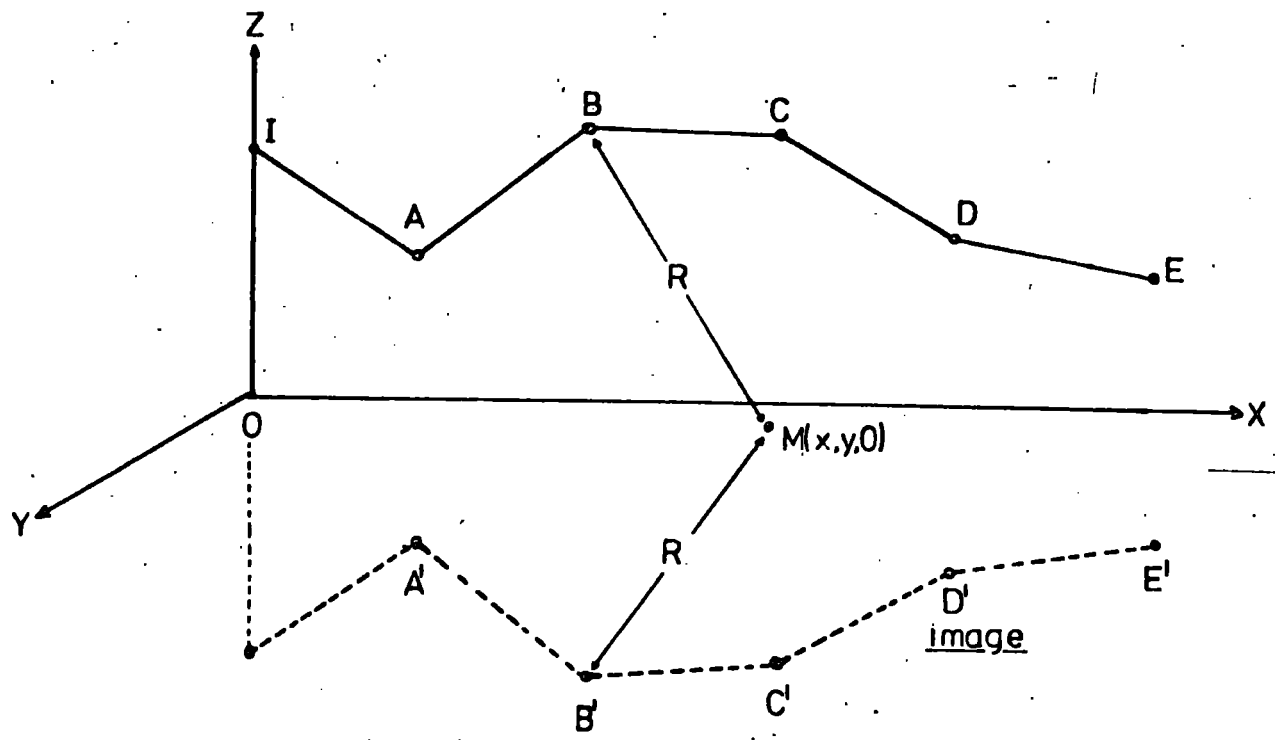

the total field components. A special program (PLMPROG) was written for this purpose. In computing these electric field values the angles of elevation of the real charge and of depression of its image (α and α') together with the azimuth angle (β) were all expressed in terms of the coordinates of M, S and S'. It was also found expedient to express these various coordinates needed in computation on the basis of a spherical polar system, the pole being at M.

A further point was the necessity to "limit" the physical size of the plume in this model. The concentration cross-section implied by equation (2.26) only becomes zero at infinite values of y or z. Thus, in the case of the crosswind and vertical profiles, it was decided that summations should be performed only up to the distance where the concentration had fallen to $0,1$ of its axial value. For similar reasons, the plume in the downwind (x) direction was "stopped" at $300\,m$. The implications of making these somewhat arbitrary truncations were thoroughly investigated and were found to have a negligible effect on the validity of the results obtained.

3.4.3 The Bivane Data Model

The development of this model was described in Sec. 2.8. Its method of use is indicated in Fig. 3.3(b).

It should be borne in mind that this model was devised to directly simulate actual conditions. Consequently, the cooordinates ascribed to M were those of the field mill in the particular run being analysed. These mills were always placed at ground level and therefore we shall only be concerned with the vertical electric field, E_z, here. This is a considerable simplification as compared with the previous model. We now discuss

briefly the method adopted for the electric field calculations.

Ultimately, it was hoped that this model would be used to compute electric field values for entire experimental runs. A typical field run lasted 25 minutes, bivane readings being recorded every 1.5 s throughout the run. Consequently, in the region of 10^3 different plume configurations had to be derived from the data in order to calculate the electric field variations. Even with the very large IBM 360/67 computer at my disposal the computing time required to perform these tasks was rather long. As a result of this the application of the model had to be restricted to some extent. It was not, for instance, possible to incorporate crosswind and vertical diffusion as had been originally intended. In fact, the derived plume was considered to be a series of discrete point charges for the purposes of this model. However, despite all these restrictions quite good results were obtained.

It will be recalled that the points A,B,C, etc. (Fig.3.3(b)) are derived from the bivane readings. These points represent the position of successive plume elements at a particular moment in time. The ion generator used in this project gave a continuous output, but because of the restrictions referred to earlier, it was necessary to assume that the ion plume contained its charge in parcels which resided at the points A, B, C, etc. The magnitude of the charges placed at the points is given directly by the expression $i\,s$, i being the generator output and s the sampling interval. (The alternative procedure, that is to imagine the charge to be uniformly distributed along the lines joining the points, and then to perform a numerical

line integration, unfortunately would have also demanded too much computer time). In many ways the approach used was a rather drastic simplification but it is vindicated, at least to some extent, by the fact that it gave quite good results.

Once the plume configuration had been determined it was a simple matter to evaluate the electric field at any particular point. An image plume was first "constructed", as shown in the figure. Now consider the parcel of charge at the point B, for example. The element of vertical field, DE_z, due to the charge at B and its image at B' is given by

$$DE_z = \frac{is}{2\pi\epsilon_0} \frac{\sin\alpha}{R^2} \qquad (3.23)$$

where α is the angle of elevation of B with respect to the point M. The total electric field can then be determined by adding the contributions from the points A, B, C, etc.

Field mills were never placed at more than $30m$ from the ion source in the experiments which this model was designed to simulate. Thus, in order to consider all the plume segments likely to affect the computed electric field values, the summation process was continued until the simulated plume attained a distance of $50m$ from the source. Computer trials indicated that this was a satisfactory limit.

3.4.4 The Oscillating Plume Model

The basic features of this model were described in Sec.2.8 and are illustrated in Fig. 2.5(b). The method of field computation is indicated in Fig.3.3(c), and is, in fact, very similar to that used for the bivane data model. In

view of this procedure is only noted in outline here.

The oscillating plume is considered as if it were a deformed line charge, crosswind and vertical diffusion having to be excluded for the same reasons as before. In use, the point M, at which the electric field was to be calculated, was always at ground level and thus, as before, we are only dealing with vertical fields. The plume, and its image, were divided into a number of small elements and the field due to a typical element-image pair calculated. We can write:

$$\boxed{DE = \frac{\lambda \delta_s}{2\pi\epsilon_0 R^2} \sin\alpha} \qquad (3.24)$$

where λ is the linear charge density and

δ_s the length of the element.

The quantity λ can be determined from straightforward trigonometry as soon as the various constants for the particular computer run have been specified. The total electric field was found, as usual, by summing the field due to the elements along a sufficient length of plume.

It may be remembered that the configuration of this plume was made to vary with time and thus it was necessary to perform an entirely new summation for each time step. As field work progressed interest was taken in the cross-correlation obtaining between electric field values recorded by various pairs of field mills. In order to investigate these correlations the model was extended to enable calculation of the electric field at three points to proceed simultaneously. (See also Sec. 3.6)

(c) the oscillating plume model

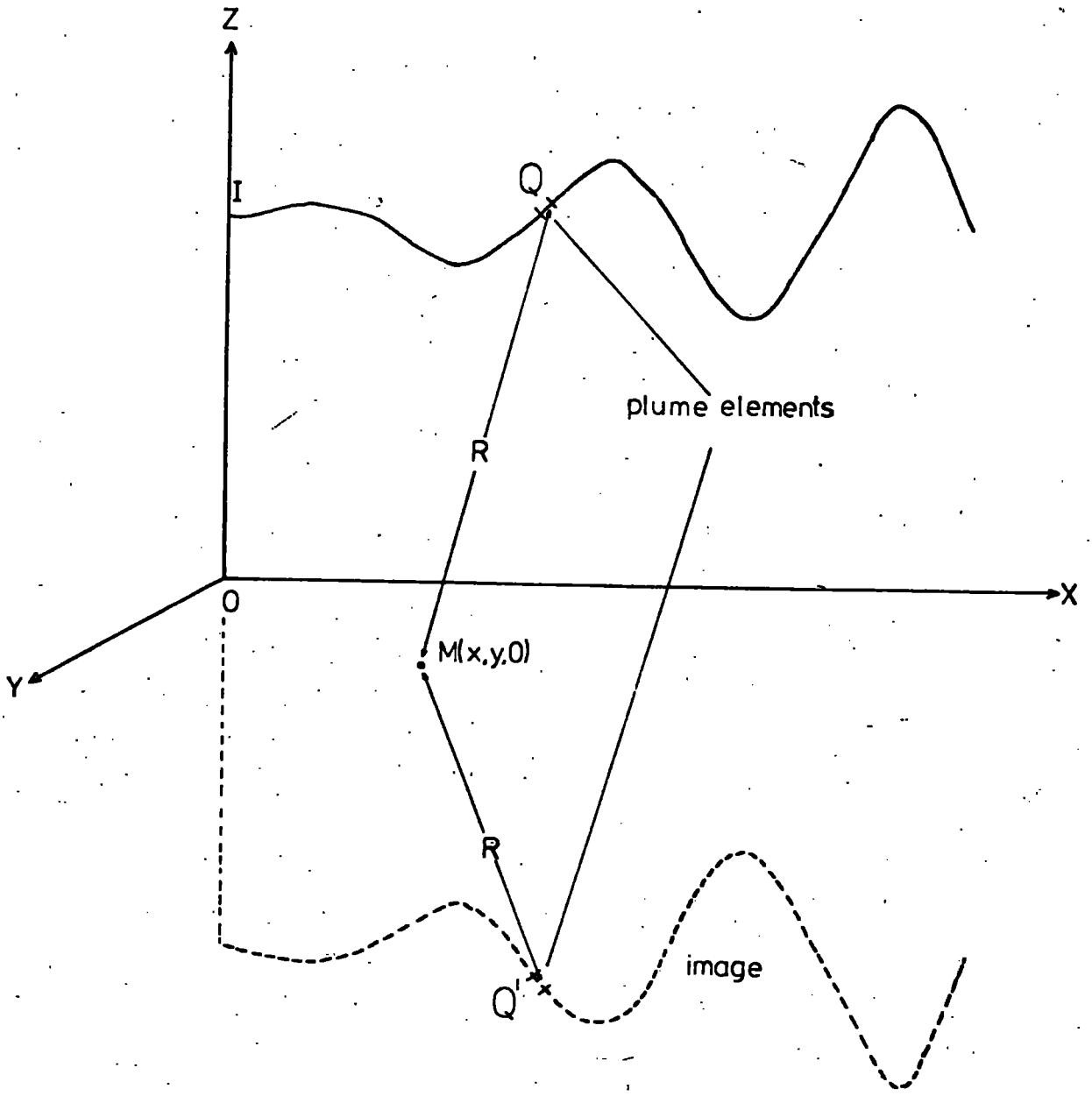

3.5
The Effect of Electrostatic Forces on Simple Charge Systems

3.5.1
Introduction

So far the rôle of electrostatic forces in determining the behaviour of ion plumes, for reasons of simplicity, has been largely suppressed. In the previous chapter the effects of turbulent diffusion were described, and in this chapter we have considered certain fundamentals of electrostatics relevant to ion plumes. As a result, we are now in a position to discuss the effects of these electrostatic forces in some detail. It should be added here, of course, that the turbulent and electrostatic forces do not act separately on the ion plume but together. The plume behaviour is therefore very complex.

The nature of the electrostatic forces is illustrated in Fig.3.4. We note that the ion plume is subjected both to outward radial repulsive forces and to a general downward image force. The origin of these forces was discussed in Sec.3.2 and now we wish to estimate their magnitude and, wherever possible, compare their effects with those of turbulent diffusion.

My early investigations soon revealed that it would be a very complex task to apply equations describing these electrostatic effects directly to a plume. As an alternative, therefore, it was decided to apply such equations to much simpler charge systems, explore their behaviour, and then attempt to interpret the results in terms of ion plumes.

The Electrostatic Expansion of an Instantaneously Produced Spherical Charge Cloud

Let us imagine that such a cloud becomes detached from an ion plume as a result of turbulence and then moves downwind without too much further diffusion occurring. The outward radial electrostatic forces will cause the space charge to expand as it travels downwind and clearly this effect is thus, at least superficially, rather similar to turbulent diffusion (see Sec. 2.5).

In this analysis we shall use the notation that any quantity bearing the subscript 'o' refers to the value of that quantity at time, t, equals zero. Thus, for example, ρ_o indicates the initial charge concentration (supposed uniform) within the charge under consideration. Using this notation we thus refer to the initial radius of the charge cloud as R_o, and consequently the total charge (Q_o) present is

$$\boxed{\frac{4}{3}\pi R_o^3 \rho_o} \qquad (3.25)$$

and we assume, for simplicity, that this is conserved during the process. Let us fix attention (Fig. 3.5) on the sphere A_o, of radius r_o, within the charge cloud, i.e. $r_o < R_o$. We assume that as the expansion proceeds, after a particular time t, A_o will have reached A, a radius r from the charge centre. In a similar way the sphere B_o will expand so as to be at B in the same time. At $t = 0$, the distance A_oB_o is δr_o, whilst at the time t, AB is equal to δr.

Now consider the charge (q_o) enclosed by A_o. We have

$$\boxed{q_o = \frac{4}{3}\pi r_o^3 \rho_o} \qquad (3.26)$$

Electrical forces influencing ion plumes

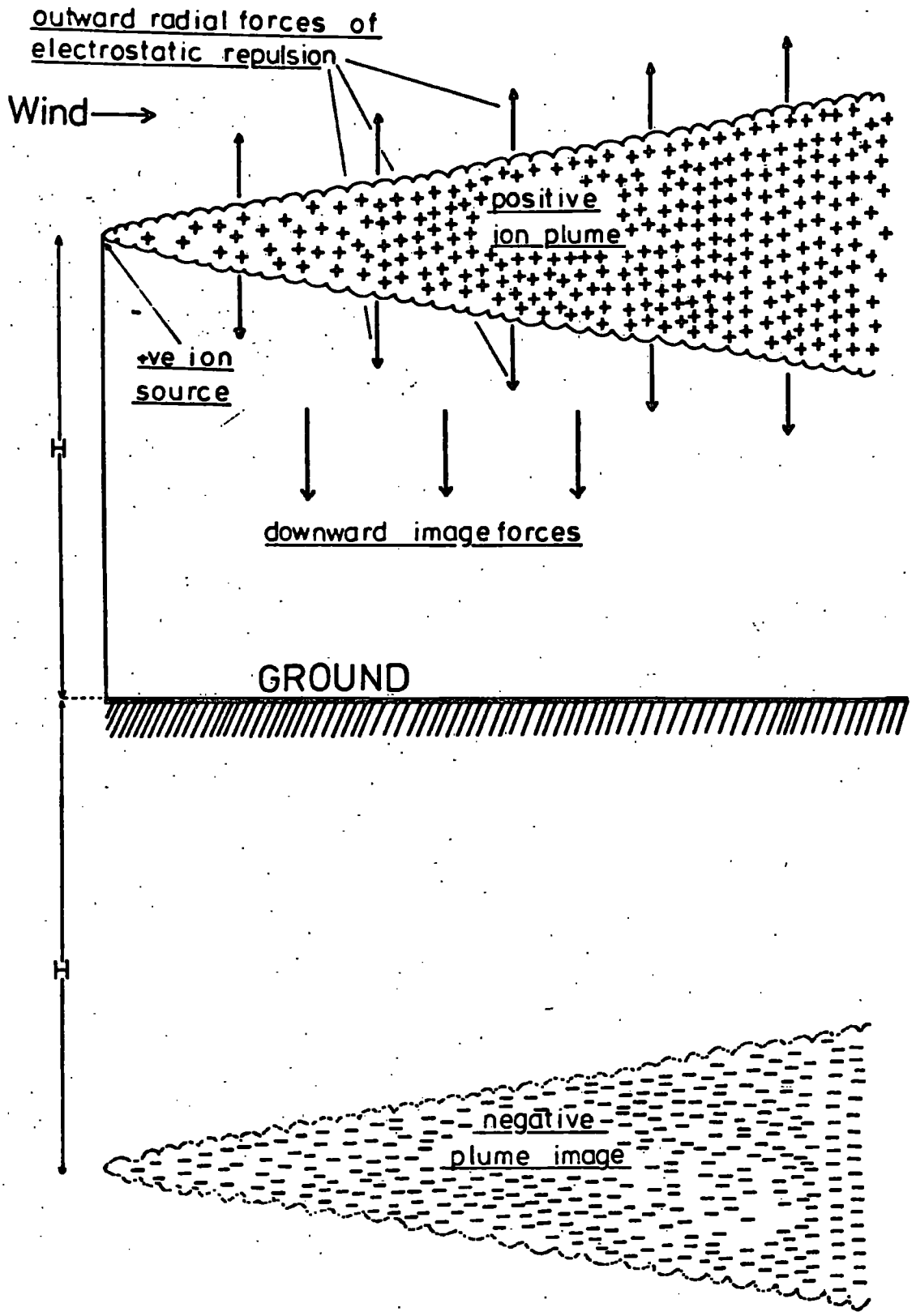

Electrostatic forces acting on simple charge systems

(a) Outward repulsive force

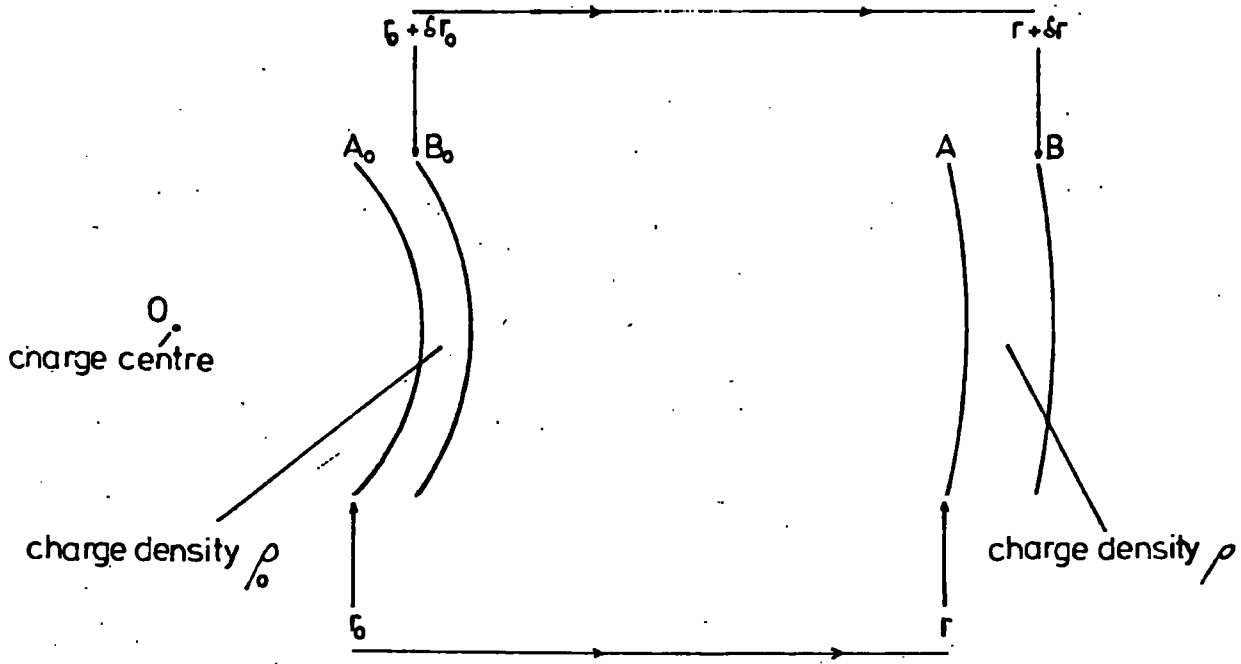

(b) Image force

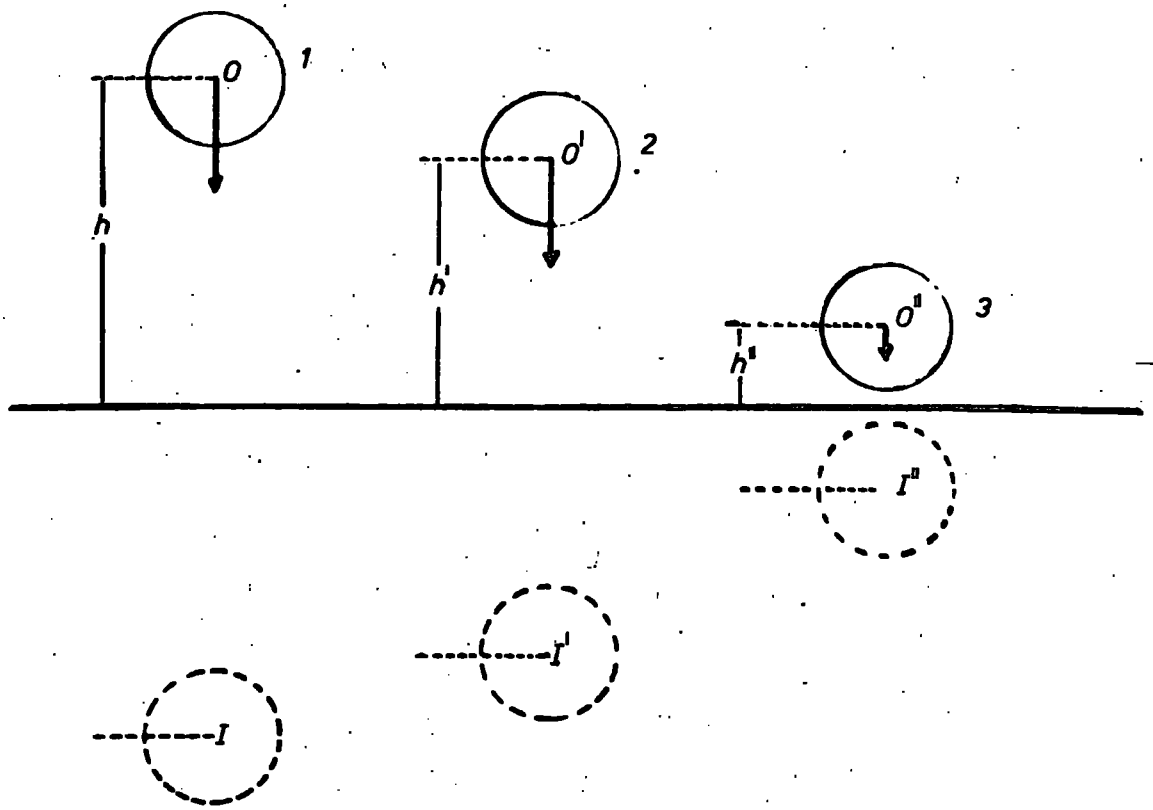

Consider the electric field, E , at the surface of the expanding charge cloud. In time t the cloud has increased its radius from r_0 to r and hence

$$E_r = \frac{q}{4\pi\epsilon_0 r^2} = \frac{r_0^3 \rho}{3\epsilon_0 r^2} \qquad (3.27)$$

If the mobility of the ions is μ then we may write immediately that

$$\frac{dr}{dt} = \mu E_r \qquad (3.28)$$

Using (3.27) and (3.28) we find that

$$\frac{dr}{dt} = \frac{\mu \rho_0 r_0^3}{3\epsilon_0 r^2} \qquad (3.29)$$

and we may integrate this equation, not forgetting that at $t = 0, r = r_0$.

Thus

$$\int r^2 dr = \frac{\mu \rho_0 r_0^3}{3\epsilon_0} \int dt + C$$

which gives after some algebra

$$r = r_0 \left[1 + \frac{\mu \rho_0 t}{\epsilon_0}\right]^{1/3} \qquad (3.30)$$

Equation (3.30) is therefore the relation sought between the charge cloud radius and the time. If now we differentiate (3.30) with respect to r_0 , we find that

$$\frac{dr}{dr_0} = \left[1 + \frac{\mu \rho_0 t}{\epsilon_0}\right]^{1/3} \qquad (3.31)$$

Referring to Fig. 3.5 we note that the quantity of charge contained in the spherical shell A_0B_0 , say q_{r_0} , is given by the expression

$$q_{r_0} = 4\pi r_0^2 \delta r_0 \rho_0 \qquad (3.32)$$

Since charge is conserved in the expansion process, we know that the charge contained in the shell AB must also equal q_{r_0}.

Hence

$$q_{r_0} = 4\pi r^2 \delta r \rho \qquad (3.33)$$

Equating (3.32) and (3.33) we see that in the limit

$$\rho = \frac{r_0^2}{r^2}\frac{dr_0}{dr}\rho_0 \qquad (3.34)$$

Then, from (3.34), (3.30) and (3.31),

$$\rho = \rho_0\left[1 + \frac{\mu\rho_0 t}{\epsilon_0}\right]^{-1} \qquad (3.35)$$

With the aid of equations (3.30) and (3.35) we may now investigate the behaviour of this expanding space charge. However, we have not yet discussed the situation which occurs when the point under consideration is at a distance D, which is greater than R_0, the initial radius of the charge. Under these circumstances the concentration will remain zero until R equals D. Let us suppose that the time taken for R to attain this value is t_1. We can find t_1 by inverting (3.30) and solving for t. Consequently

$$t_1 = \frac{\epsilon_0}{\mu\rho_0}\left[\left[\frac{D}{R_0}\right]^3 - 1\right] \qquad (3.36)$$

At times greater than t_1 the charge density obeys equation (3.35).

The immediate implications of equations (3.30), (3.35) and (3.36) in the context of this project are not easy to visualize. The behaviour of the ratios r/r_0 and ρ/ρ_0 as functions of the relevant parameters is therefore shown in Figs. 3.6 (a) and 3.7. As mentioned in Sec. 3.1 the plume consisted of small ions, at least near the source, and therefore the small ion mobility has been used in the construction of these graphs. The expansion rates with large ion systems are, of course, very much less.

ELECTROSTATIC EXPANSION

(a) 'Instantaneous' spherical space charge cloud

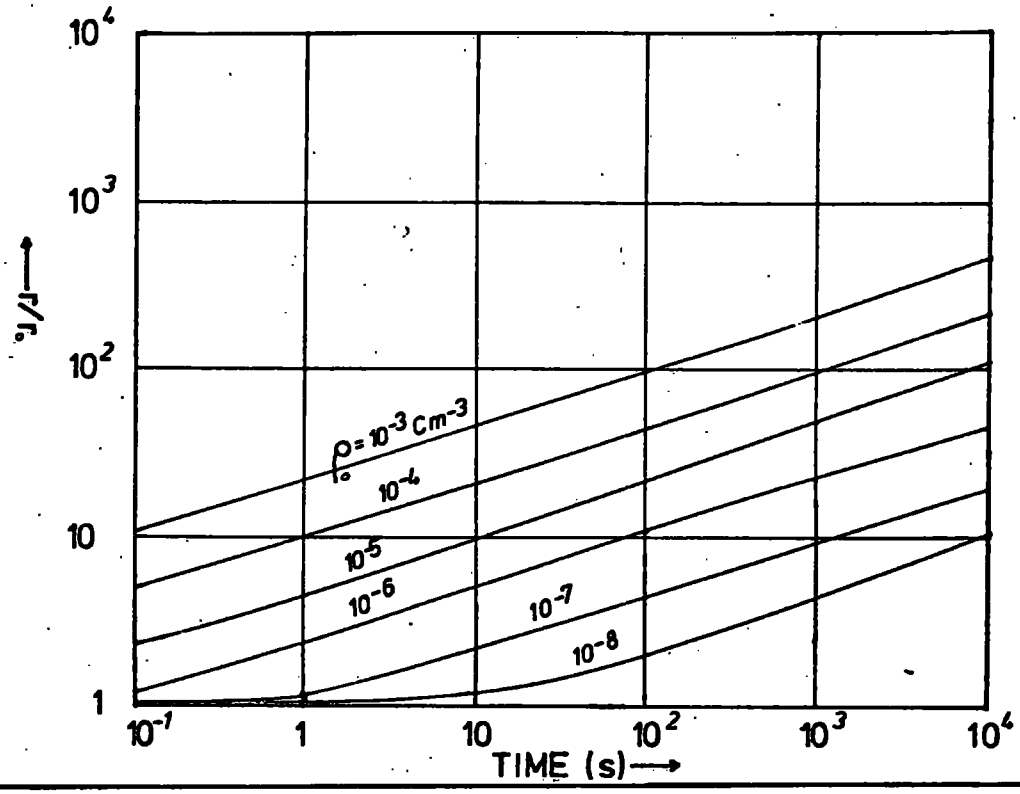

(b) 'Instantaneous' cylindrical space charge cloud

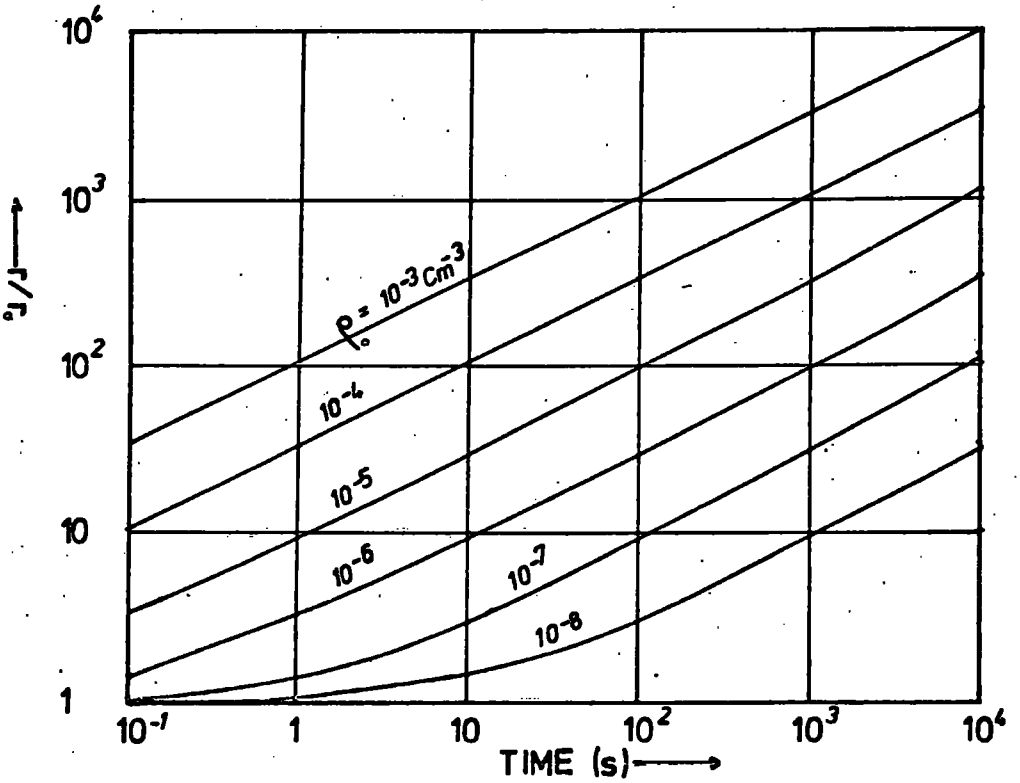

ELECTROSTATIC EXPANSION

'Instantaneous' spherical/cylindrical space charge clouds

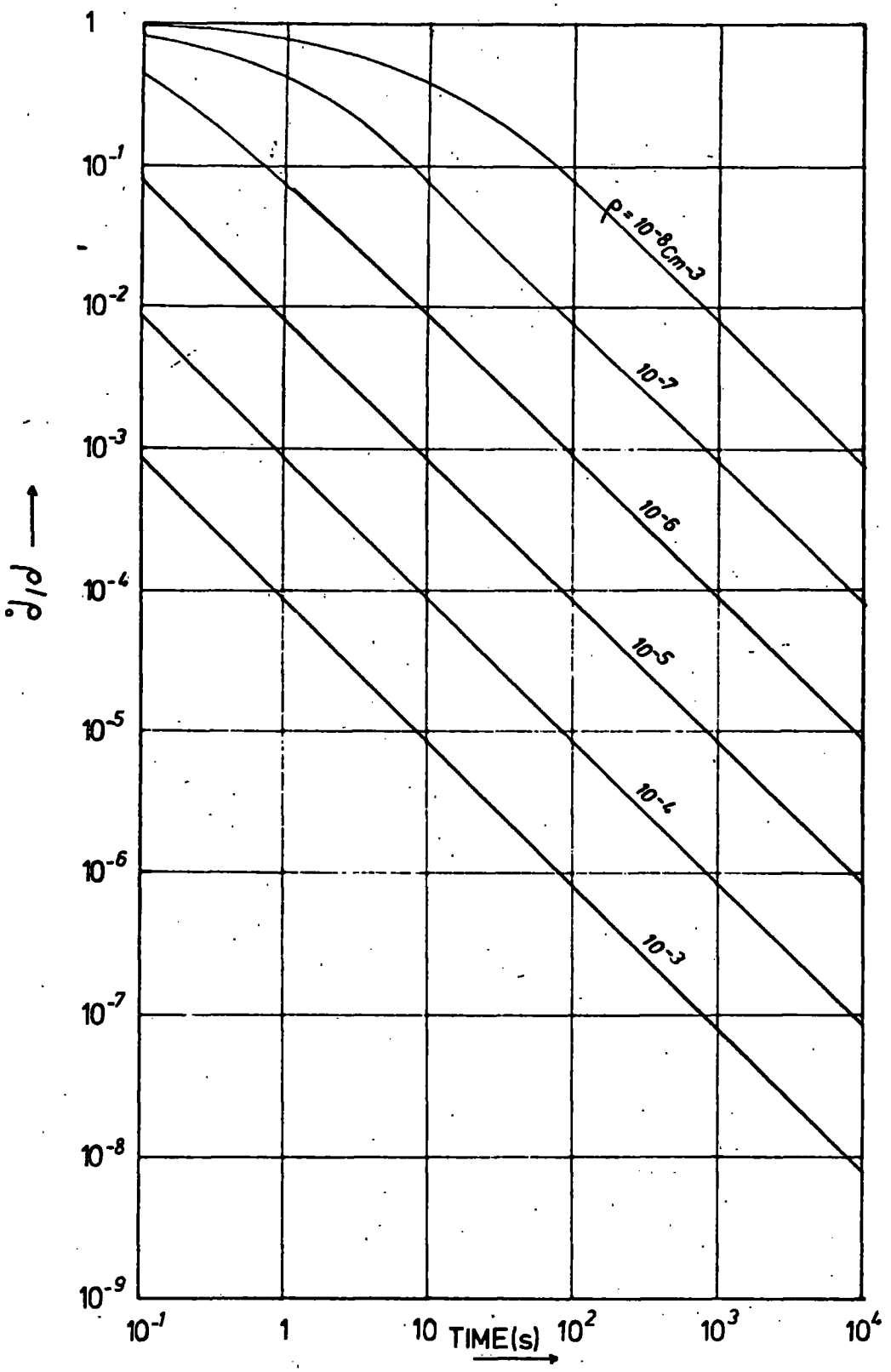

In a typical situation we might consider the expansion of a spherical charge cloud initially of 1 m outer radius and concentration $10^{-8} Cm^{-3}$. Figures of this magnitude have actually been measured in the field work associated with this project. Referring to the 10^{-8} curve on Fig. 3.6(a) we note that, after 100 s for instance, the charge has expanded so that its outermost radius is now 2.3 m. From a knowledge of the increase in radius we can calculate the decrease in concentration directly without reference to Fig. 3.7. It is worth noting also, that during the expansion process the concentration, although falling all the time, remains uniform within the entire sphere at any particular time. (See equation (3.35) which shows that ρ is independent of r).

It is clear then, from this simple example, that the electrostatic expansion effects are substantial, and therefore must be taken into account when estimating the behaviour of an ion plume. Having considered the case of an isolated instantaneous spherical charge cloud we now discuss an isolated instantaneous cylindrical charge cloud.

3.5.3 The Electrostatic Expansion of an Isolated, Instantaneously Produced Cylindrical Space Charge Cloud

We imagine that the charge is brought, somehow, into existence instantaneously and then left to expand under the action of its own electrostatic forces. It will be shown later that the results obtained with this charge configuration can be adapted to indicate, very approximately, the behaviour of an ion plume. Because of the similarity of the analysis with that of the previous case only the results are quoted here.

The radius, as a function of time, of the cylindrical charge is given by the expression

$$r = r_0 \left[1 + \frac{\mu \rho_0 t}{\epsilon_0}\right]^{1/2} \qquad (3.37)$$

and the decrease in charge density with time by

$$\rho = \rho_0 \left[1 + \frac{\mu \rho_0 t}{\epsilon_0}\right]^{-1} \qquad (3.38)$$

In the above r_0 refers to the original radius of a cylindrical shell drawn within the charge cloud, whilst r is the radius of that shell after time t.

These expressions are plotted in Figs. 3.6(b) and 3.7. We note that the radius expansion of the cylindrical charge is more rapid that that of a spherical system having the same initial charge density. It is also worth noting that the expressions describing the expansions in the two cases are very similar, only the indices being different, whilst those describing the behaviour of charge density are identical.

We now rearrange (3.37) and (3.38) in order to discuss the behaviour of a plume. Consider the outermost radius, R, of the expanding cylindrical charge. We may write immediately a similar equation to (3.37) describing the behaviour of R in terms of R_0 and t. If the linear charge density within the cylinder were λ, we could also write.

$$\rho_0 = \lambda / \pi R_0^2 \qquad (3.39)$$

Applying these ideas to equation (3.37) we find that

$$R = \left[R_0^2 + \frac{\mu \lambda t}{\pi \epsilon_0}\right]^{1/2} \qquad (3.40)$$

In the case of an ion plume, the ions are produced at a particular point and are then blown downwind. However, if we were to consider a particular plume segment travelling along we would observe that, once it had been formed, there was no

further charge generation within it. At least in this respect therefore, the portion of plume corresponds quite closely to a segment of an instantaneous cylindrical charge. Consequently it might not be too unreasonable to imagine that the actual electrostatic expansion of an ion plume would be rather similar to that of a cylindrical charge.

Suppose the wind speed is u, then after a time t the plume segment will have travelled a distance ut away from the source. For an ion generator of constant output current i, we can write

$$\lambda = i/u \qquad (3.41)$$

and on substituting the above relations involving t and λ into equation (3.40) we find

$$R = \left[R_0^2 + \frac{\mu i x}{u^2 \pi \epsilon_0}\right]^{1/2} \qquad (3.42)$$

where $x = ut$, the distance downwind.

Equation (3.42) is of great importance as it enables us to compare the electrostatic and turbulent effects directly. In order to facilitate these comparisons both now, and in the analysis of field work, the two effects are contrasted in Figs. 3.8(a) and (b). In Fig. 3.8(a) the curves are appropriate to a source at 10 m above the ground. The turbulent diffusivities associated with the three classes of stability were based on the results of DEACON (1955). (See also PRIESTLEY 1959). Inspection of the curves indicates that on many occasions we might reasonably expect the turbulent and electrostatic effects to be of roughly equal magnitude. In very low wind speeds the electrostatic expansion obviously dominates the turbulent effects whilst at higher wind speeds the converse is true. This interesting feature was actually found in practice and consequently further discussion is postponed until the experimental results are presented in Chs. 7 and 8.

3.5.4 Electrostatic Expansion Effects with a Continuous Point Source of Ions

In the previous chapter we considered the turbulent diffusion of ions from a *continuous* point source in calm conditions. However, in very low wind speeds, turbulent effects tend to be rather small and consequently the validity of the approach in Sec. 2.5 is questionable. As an interesting alternative we shall consider here the effect that the electrostatic forces alone have on such a system and disregard turbulent diffusion effects entirely. In practice, such a situation might arise during a strong inversion with dead calm, any turbulence being virtually eliminated in these circumstances.

It is found, after an analysis rather similar to the previous cases, that once a steady state has been established, the space charge concentration ρ, at a point distance r from the ion source, is given by the expression

$$\rho = \left[\frac{3\epsilon i}{8\pi\mu r^3}\right]^{1/2} \qquad (3.43)$$

where i is the current output of the source. The behaviour of (3.43) is indicated in Fig. 3.9(a). The analysis here has only been concerned with an isolated point source, and thus, in the circumstances of this project, the presence of image forces may seriously disturb the validity of (3.43). Nevertheless, as these results are certainly of relevance to the behaviour of ion clouds at higher levels, where image effects are much smaller, they are included.

It is of interest to calculate the value of the electric field E_r, that would exist at a distance r from the ion source. A simple analysis shows that

$$E_r = \left[\frac{i}{6\pi\mu\epsilon_0 r}\right]^{1/2} \qquad (3.44)$$

ION PLUME EXPANSION

(a) by turbulent diffusion (using steady state model)

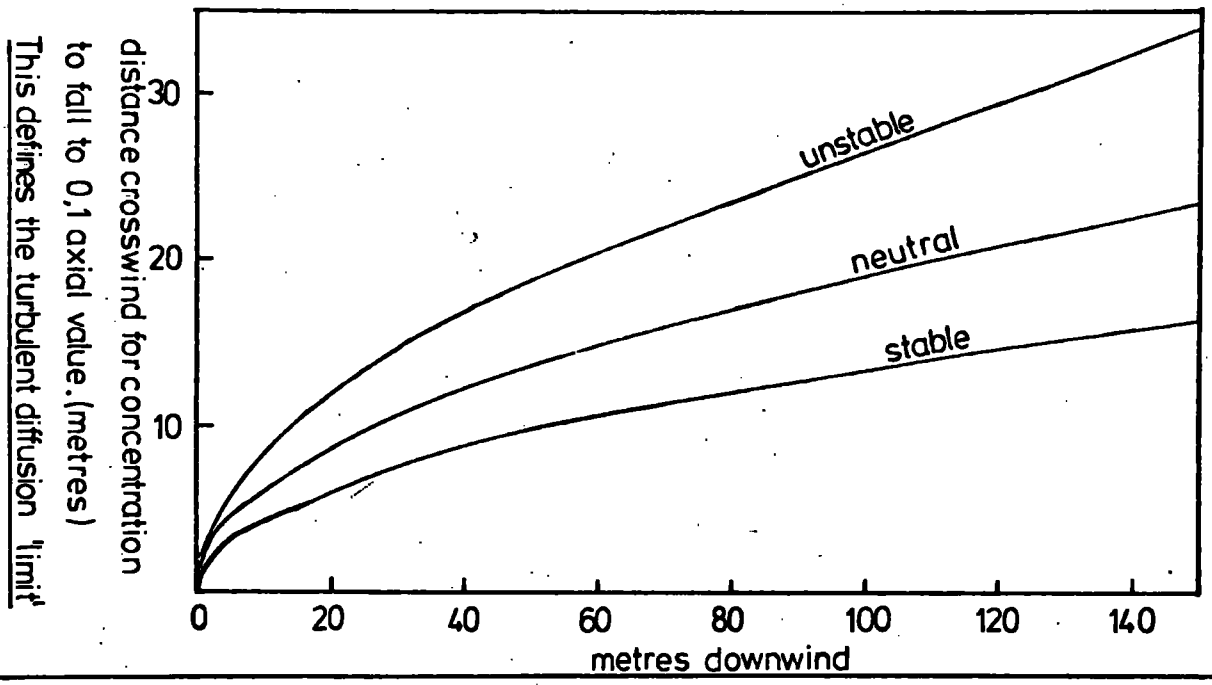

(b) by electrostatic repulsion effect

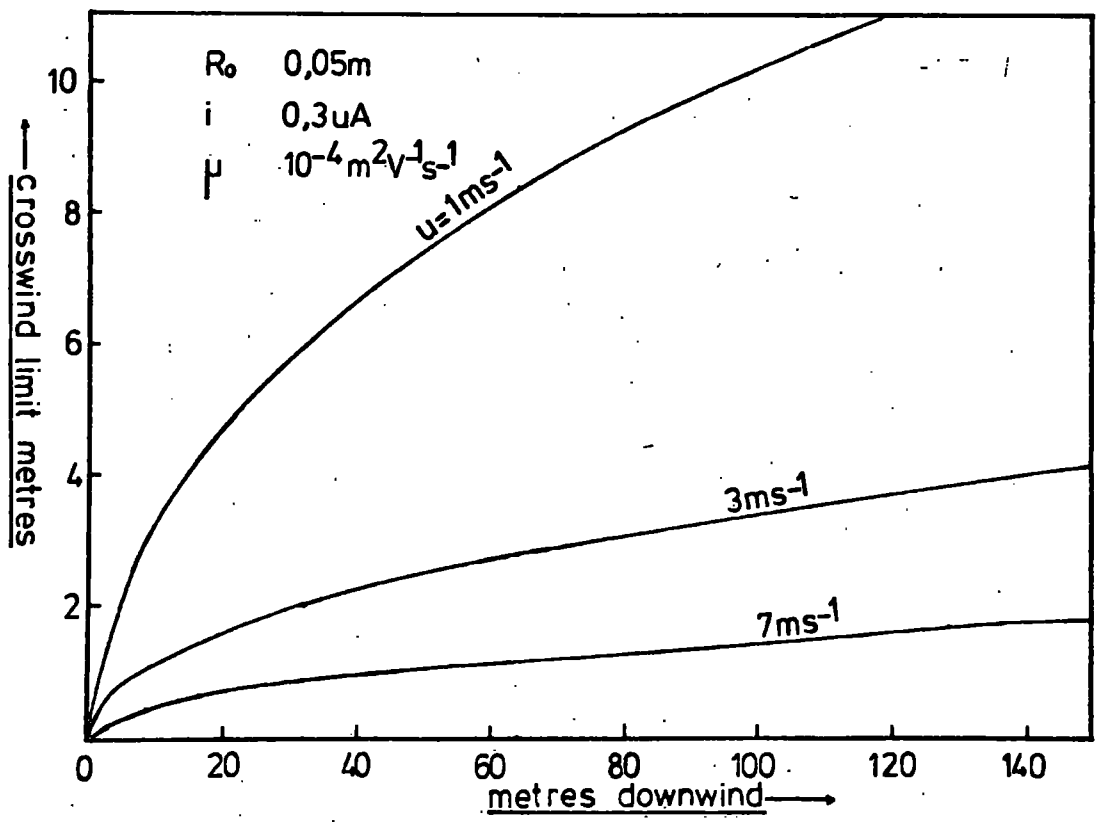

Continuous point source in calm conditions

(a) behaviour of charge concentration

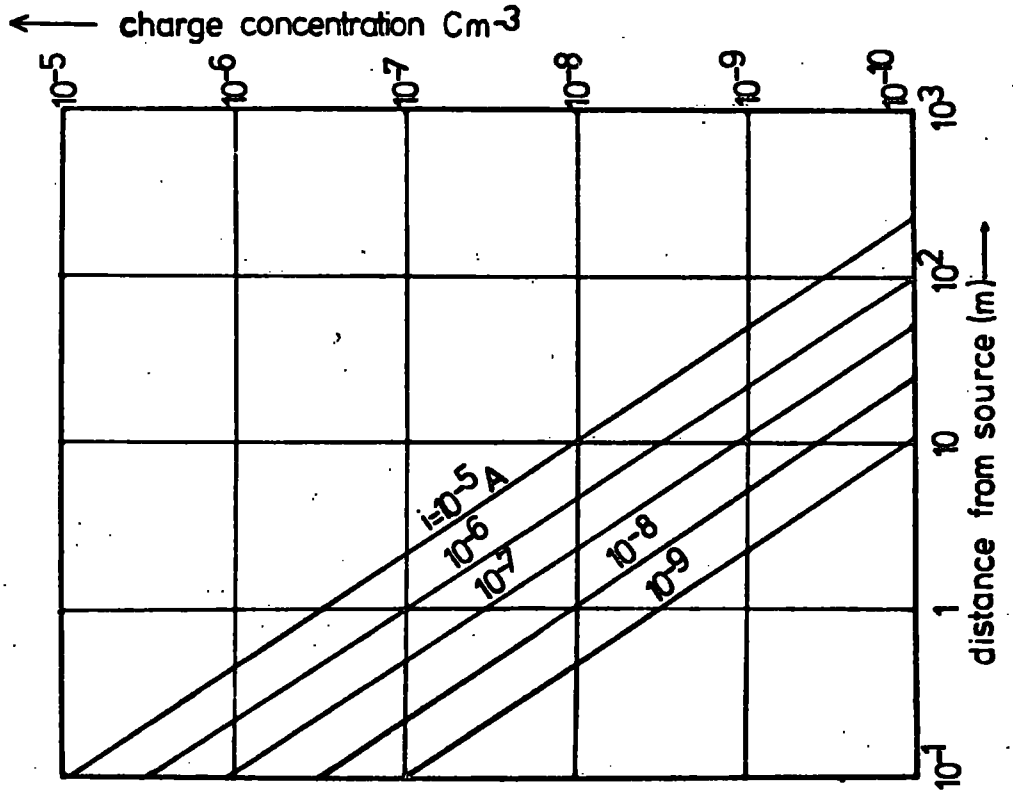

(b) behaviour of electric field

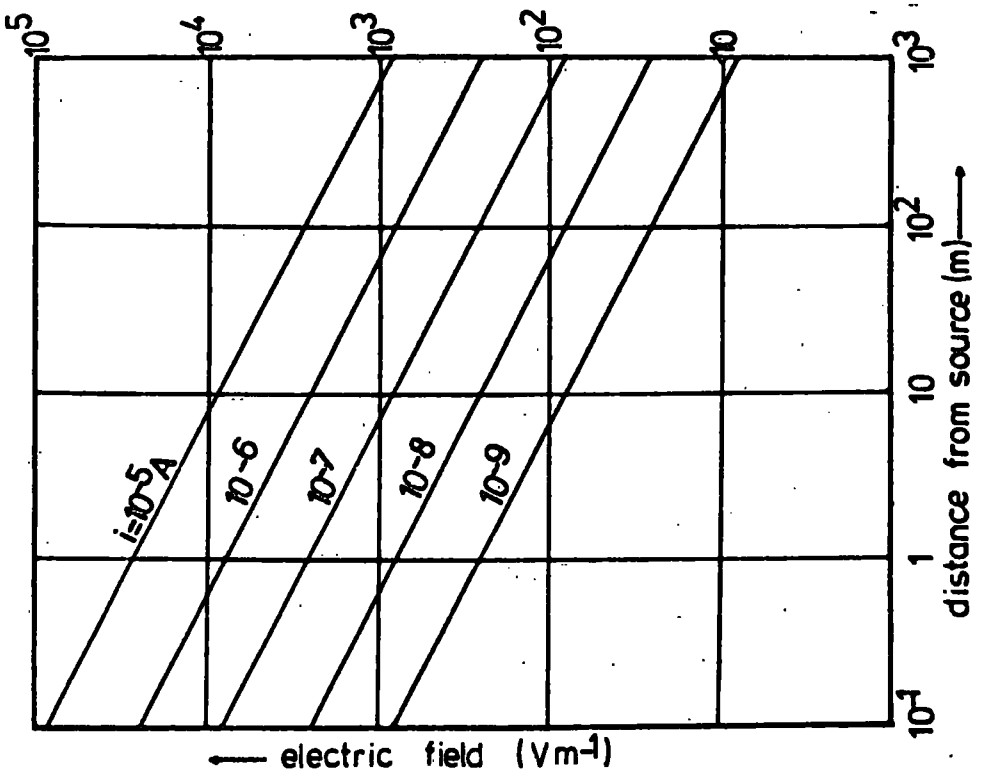

This equation is plotted, for various values of i, in Fig. 3.9(b). In this project the ion generator output was $0.3\mu A$, and for example, we note from the figure that at $10\,m$ from the source the electric field predicted is about $1\,kVm^{-1}$. A field of this magnitude would be readily detectable and accordingly there should be no experimental difficulty in establishing the validity, or otherwise, of equation (3.44).

We may also estimate, using Fig. 3.9(b), the outward radial velocity of the ions. In the situation above, for instance, where E_r was $1\,kVm^{-1}$, we find that, with a small ion mobility of $10^{-4}\,ms^{-1}$ per Vm^{-1} their radial velocity is $0{,}1\,ms^{-1}$. This illustrates in a very practical way that the analysis applies for only extremely low wind speeds.

Finally, we must consider, and this also applies to the previous cases, the effect of the ion motion on the air through which they pass. To establish whether any effect is present, we shall investigate the circumstances in which we suspect it to occur most markedly. It seems reasonable, on common sense grounds, that such effects, if any, are most likely to occur at short distances from powerful ion sources. Let us therefore consider a point $1m$ away from a $10\,\mu A$ source. We note from Fig. 3.9(a) that at this distance the ion concentration is $3 \times 10^{-7} C\,m^{-3}$, whilst from Fig. 3.9(b) we observe that the electric field is $30\,kVm^{-1}$. Hence the outward velocity of the ions is

$$v_r = \mu E_r = 3\,ms^{-1}$$

With this charge density, assuming singly charged ions, the number of ions, n , per cubic metre is given by

$$n = \frac{3\times10^{-7}}{1.6\times10^{-19}} = 2\times10^{12} \quad \text{approx.}$$

By comparison, the number of molecules, N , in a cubic metre of air at NTP is

$$N = 2.7\times10^{25}$$

and we note that the ratio n/N is approximately 10^{-13} . Therefore we conclude that if any electrically driven air motion does actually occur it will be a very small effect.

3.5.5 The Effect of Image Forces on Simple Charge Systems

3.5.5.1 Opening Note

A precise theoretical investigation of the effect of these forces, even on quite simple systems, is, because of its complexity, beyond the scope of this project. In this section we shall consider, as before, two simple cases and then apply the results obtained from them to ion plumes. It must, of course, always be borne in mind that the expansion processes discussed previously will operate in addition to the image effects now being considered.

3.5.5.2 Spherical Charge

This is shown in Fig. 3.5(b), the labels 1, 2 and 3 indicating successive positions of the spherical charge as it moves downward under the action of image forces. In reality, the upper part of this charge will, to some extent, be screened from image forces by the lower part. As a result of this, the image forces will exert a stronger effect on the lower parts of the charge and therefore will cause it to be distorted from its original spherical shape. Ultimately, as the charge descends

it will become pear-shaped, or even cigar-shaped. For the purposes of this analysis we shall not consider this aspect any further but content ourselves with a very simple analysis of the image effect.

Suppose the distributed space charge illustrated in Fig. 3.5(b) were reduced to an equivalent point charge q. This charge is placed at O, a height h_0 above the ground. The electric field E_i at the charge due to its own image is given by

$$E_i = \frac{q}{4\pi\epsilon_0 (2h)^2} \qquad (3.45)$$

Therefore, for a cloud of ions of mobility μ, the initial downward speed is given by

$$\frac{dh}{dt} = -\frac{\mu q}{16\pi\epsilon_0 h^2} \qquad (3.46)$$

Integrating (3.46), and remembering that at $t=0, h=h_0$, we find that

$$h = \left[h_0^3 - \frac{3\mu q t}{16\pi\epsilon_0} \right]^{1/3}$$

If the charge is being blown along by a wind of velocity u we can replace t by x/u in the above equation. Here x is the distance of travel from the point where the charge was at the original height h_0.

Hence

$$h = \left[h_0^3 - \frac{3\mu q x}{16\pi\epsilon_0 u} \right]^{1/3} \qquad (3.47)$$

We illustrate the magnitude of the effect predicted by (3.47) by considering two simple examples. Suppose $h = 10{,}00\,m$, $q = 0{,}1\,\mu C$, $u = 5\,ms^{-1}$ and $x = 50\,m$. In these circumstances h is found to be $9.99\,m$ and the image effect is negligible. Now suppose $h_0 = 1\,m$, with the remaining quantities as before.

Here we find that h is now $0.67m$ and in this case the image effect is substantial.

It is clear that we cannot always ignore image effects and, in fact, with low level ion sources the progressive reduction in height of the space charges must be taken into account. Ultimately some of the ions will arrive at the ground and, in so doing, will either remain there or be discharged. Moreover even if any undischarged ions reside at the ground they can no longer produce any electrical effects and thus, effectively, have also been removed from the plume.

We now move on to consider a simple plume analogy derived from a line charge concept.

3.5.5.3
Cylindrical Charge

If we consider the image force on a line, instead of a point charge, we find that the height decreases with time according to

$$h = \left[h_o^2 - \frac{\mu \lambda t}{\pi \epsilon_o} \right]^{1/2} \qquad (3.48)$$

(λ is the charge per unit length)

By employing similar arguments to those used in Sec. 3.5.3. we may apply this result, albeit rather naively, to an ion plume. It is found that

$$h = \left[h_o^2 - \frac{\mu i x}{\pi \epsilon_o u^2} \right]^{1/2} \qquad (3.49)$$

The predictions of this important equation in regard to the particular conditions of this project are shown in Figs. 3.10 (a) and (b). The implications of the results are not discussed here as they will be fully dealt with later. Nevertheless, it should be pointed out that, particularly when the

The effect of image forces on ion plumes

(a) ion source 0,3μA at 10m

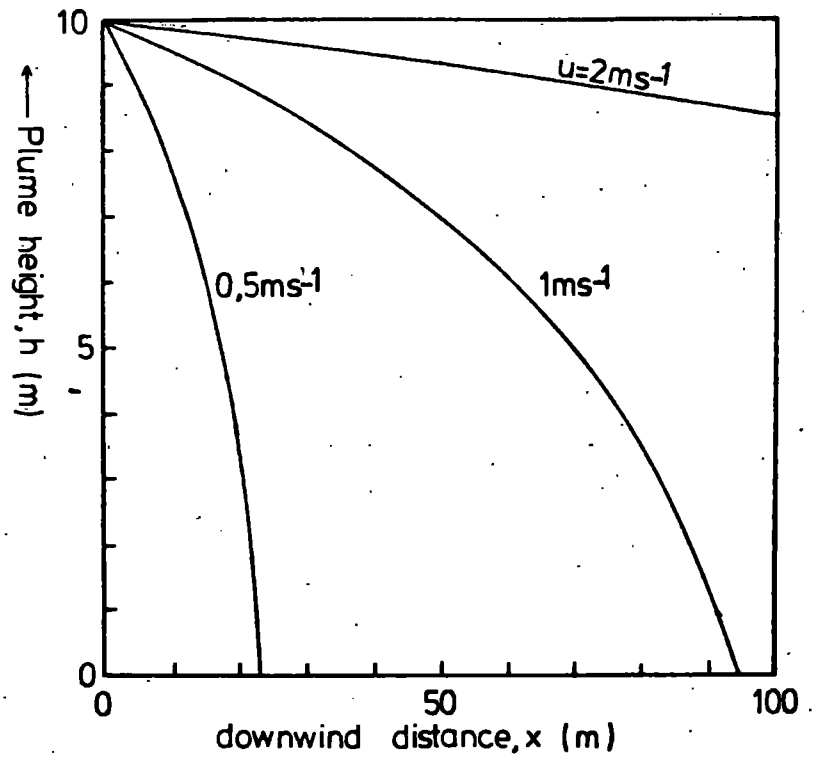

(b) ion source 0,3μA at 2m

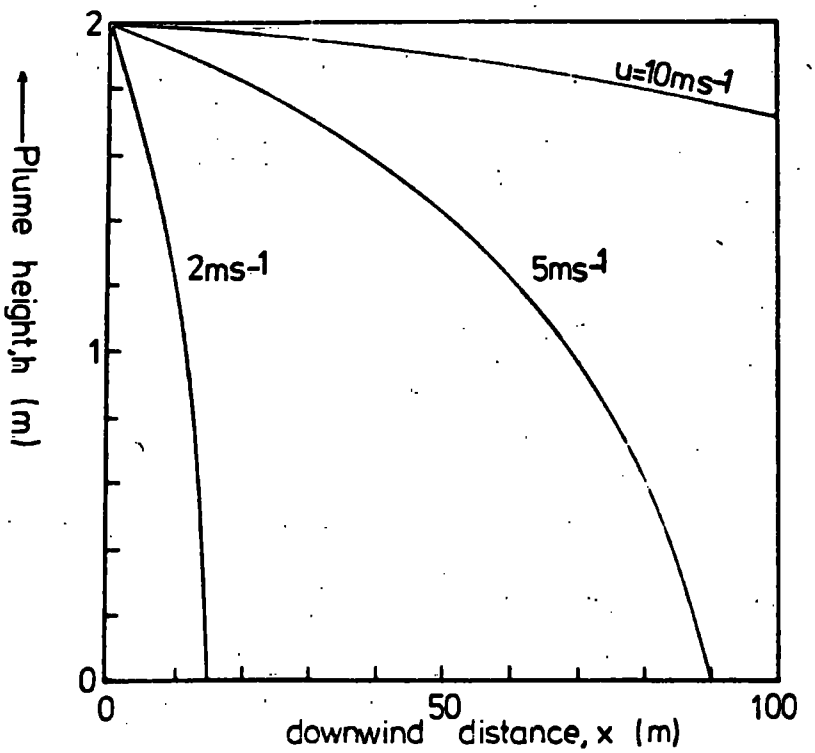

ion source was at $2m$ the image forces were evidently of considerable importance in determining the plume behaviour.

3.6 The Relation between the Electric Fields at Different Points under an Ion Plume

So far we have considered techniques for estimating the electric field at any given point under an ion plume. In this project four field mills were operated simultaneously and therefore it is of interest to be aware of any relationships that might exist between the various field records.

At any point under the plume the electric field changes constantly in response to the varying charge distribution. However, quite frequently, certain features such as kinks and loops (see Sec. 2.7) develop in plumes, and, when features of this nature pass over a given point distinctive electric field patterns are often produced. In addition, if the kink passes over (or near) two points in succession we would expect similar field patterns to be recorded but with an appropriate time displacement between them.

One type of behaviour is illustrated in Fig. 3.11(a). A vertical kink (k) develops in a plume and then travels downwind. This situation might result from a sudden short-lived burst in the downward velocity component (w). It is fairly obvious that the presence of such a kink near a measuring point would result in an enhanced electric field. In the diagram M1 and M2 represent the positions of typical recording stations and the graph indicates the type of electric field variations to be expected. The electric field records will each attain a maximum as the feature passes overhead but these maxima will

be displaced by an amount t_d depending on the separation of the points *M1 M2* and the mean wind speed (u). A cross-correlation analysis (see Sec. 6.2) of the field records would therefore reveal a maximum value at a lag number corresponding to t_d. In practice, a kink or loop will usually become less well-defined as it travels downwind and, as a result, the cross-correlation coefficient at t_d will reflect, in a sensitive manner, the relative "power" of the turbulent diffusion processes operating.

A second possibility is shown in Fig. 3.11(b). In this case a horizontal kink develops and travels downwind. Let us suppose that field mills are arranged across wind as illustrated. It is clear that, as the kink moves downwind towards *M2*, the electric field will increase there, ultimately reaching a maximum value and then declining as the feature moves away. During this time, however, the field mill at position *M1* has seen the plume first recede and then advance after the passage of the kink. Consequently the electric field here falls to a minimum as the feature passes by. A cross-correlation analysis of the *M1* and *M2* records would therefore show a negative value at zero time lag, as a result of the out-of-phase nature of the two records. It is also possible, with this arrangement of field mills, to make certain deductions about the ion plume width. For example, if there were negative correlation between records such as *M1 and M2* then the plume could not have been wider than the distance y between *M1* and *M2*. Therefore if we place field mills at various distances apart in a cross-wind line and then examine the cross-correlation coefficients between their records it should be possible to arrive at useful conclusions about the

The relation between the electric fields at different points under an ion plume

(a) the effect of vertical kinks

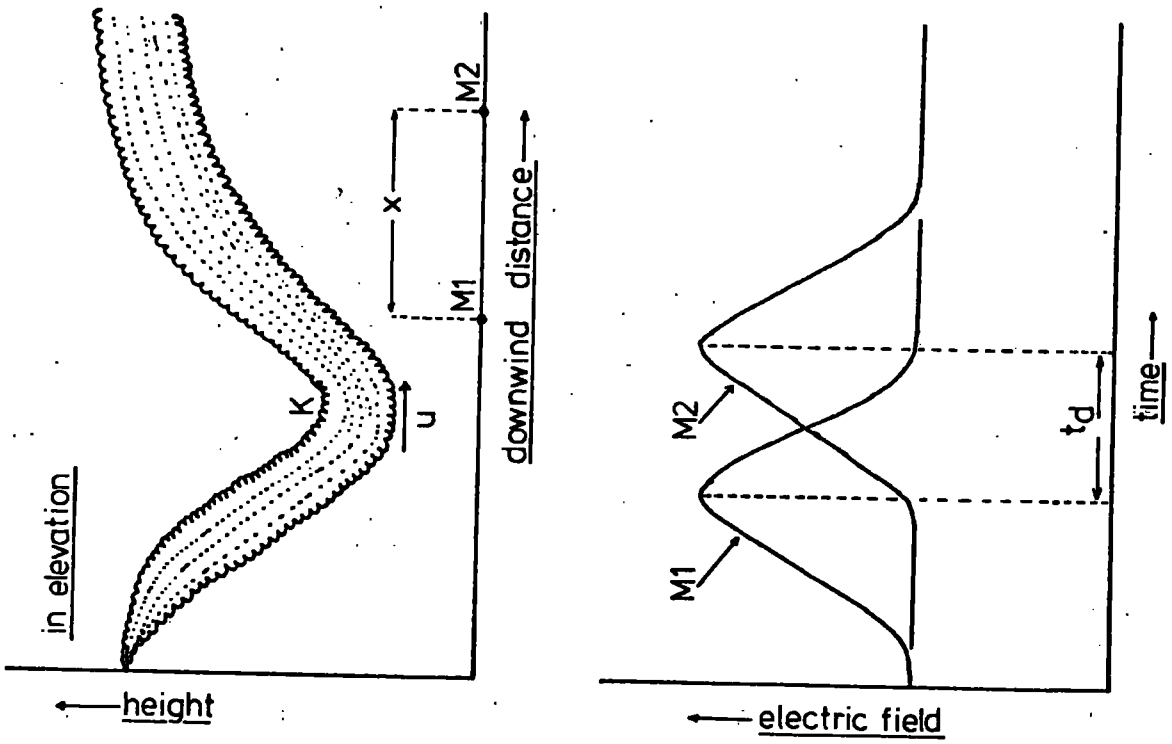

(b) the effect of horizontal kinks

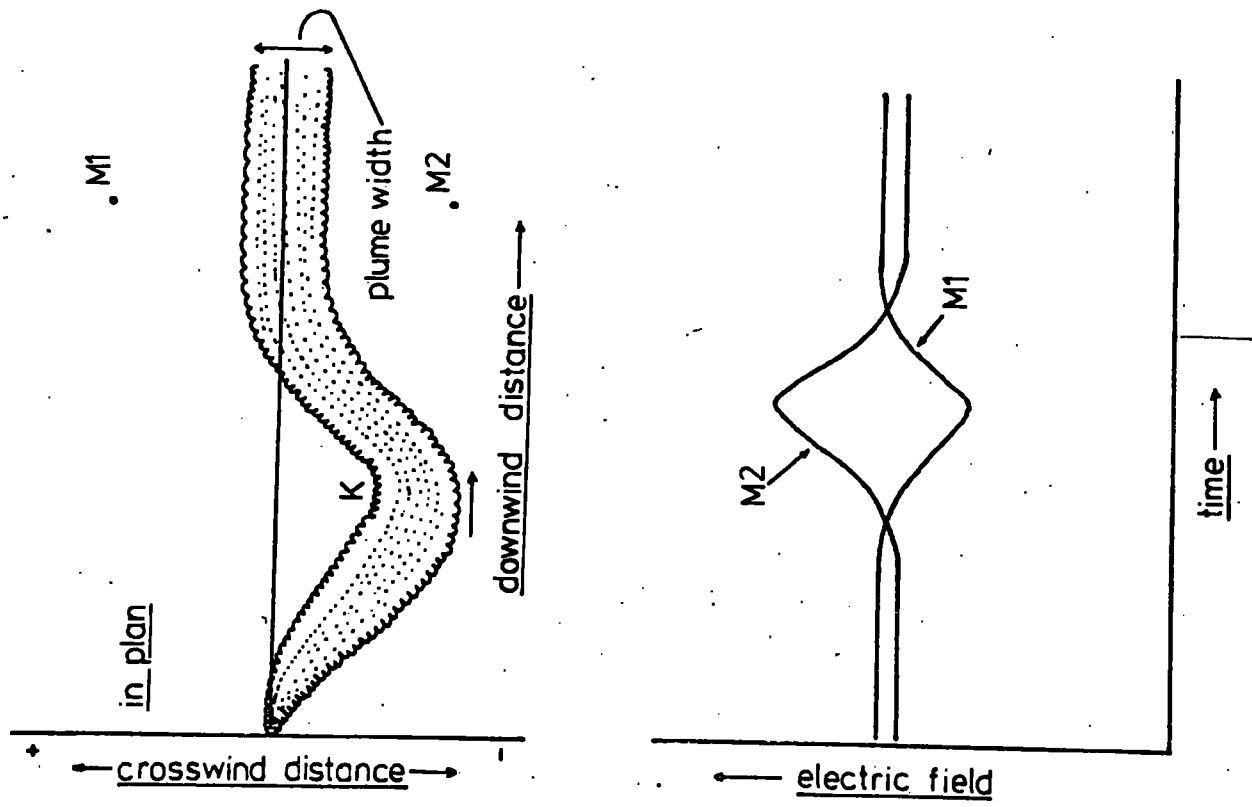

ion plume dimensions.

The above concepts have been found invaluable in the analysis of experimental results and will be referred to again in Ch.7.

3.7 The Presence of the Natural Electric Field

The existence of a natural electric field at the Earth's surface is well known, having been first detected by LEMONNIER as early as 1752. The presence of an "external" electric field in addition to that of the ion plume might possibly confuse any experimental results and therefore the likelihood of interference from this cause had to be investigated.

SHARPLESS (1968) carefully observed the behaviour of the natural field at an unpolluted site and concluded that, during fine weather, the average potential gradient was approximately $100\ Vm^{-1}$. WHITLOCK and CHALMERS (1956) made a special study of the short period variations and discovered that, in fine weather and with little low cloud present, any changes were relatively small. On the other hand, in disturbed weather conditions, mostly frontal precipitation, showers and thunderstorms, the potential gradient is large and often displays rapid fluctuations - see ASPINALL (1969). Very frequently potential gradients exceed $1\ kVm^{-1}$ and, during thundery weather, values as large as $10\ kVm^{-1}$ are not uncommon.

It was expected, largely on the basis of the plume models described herein, that the electric fields associated with ion plumes would range up to approximately $2\ kVm^{-1}$. Consequently, it seemed evident that the variations of the natural field

occurring in disturbed weather would often be large enough to mask those fields caused by the ion plume. Apart from this problem, there would also be considerable difficulties in operating the equipment during wet weather. It was therefore necessary, for both these reasons, to restrict all field work to dry conditions.

On the basis of the results of SHARPLESS and WHITLOCK little interference was expected from the natural field in fine weather conditions. As a precaution, however, the relevant characteristics of the natural field were investigated early in this project. It was found that, in practice, slight interference did occur but it detracted little from the quality of the experimental results. The characteristics of the natural field, as found in this project, are presented with the rest of the experimental data, in Chs. 7 and 8.

Chapter 4: THE MEASURING EQUIPMENT

4.1 Introduction

The following items of equipment were required:-

(a) Ion generator,

(b) Ion detectors - in the form of field mills or ion collectors,

(c) Apparatus for monitoring the micro-meteorological environment,

(d) Certain photographic equipment for the smoke plume investigations,

(e) A suitable mast to support certain of the above items.

(The mast used for this project, made by A. C. CLARKE & CO., Binstead, Isle of Wight, consisted of six telescopic sections. It could be raised to a maximum height of 12*m* by air pressure generated from an attached hand pump. The mast gave no trouble throughout the project.)

4.2 General Design Criteria

Ideally for this investigation a permanent installation would have been desirable but the only location where this might have been possible, Durham University Observatory field, was too small and insufficiently level. Therefore, there was no choice but to design and construct instruments which could be transported to a site, be set out and operate independently of a mains supply. At one stage use of the Group's Honda generator , giving 240 *V* AC, was considered, but this idea was rejected when it was discovered that its internal combustion engine was a prolific source of ions. Hence the employment of batteries as the means of power supply appeared the only solution. It was necessary that the equipment should be capable of running

for at least 5*hr* before requiring renewal or recharging of batteries. Certain items of equipment requiring only small currents were powered by conventional dry batteries, whilst apparatus needing larger currents, such as field mill motors, were supplied by rechargeable batteries. This approach enabled costs to be kept to a minimum commensurate with satisfactory equipment performance. One of the most undesirable features of all batteries is their progressive reduction in voltage which takes place as discharge proceeds. Much of the equipment was sensitive to supply voltage alterations and therefore great care had to be taken to minimise any effects due to this.

The apparatus needed to be mechanically robust as it would be transported long distances by Land Rover over rough ground. Overall system reliability needed to be good as only the most minor of breakdowns could be repaired in the field.

At this stage it was also necessary to decide on the type of output signal that the measuring instruments should produce. It was proposed that each instrument should give a small direct voltage output, the value of which was linearly proportional to the magnitude of the parameter being measured. The actual voltage range employed was 0 to 1.0 *V*, the lower figure always corresponding to the minimum value of the parameter, the upper to the maximum.

4.3 The Field Mills

4.3.1 Design and construction

The fundamental principles of field mills have been thoroughly documented elsewhere and therefore will not be discussed here. The field mills used in this project, although largely of standard design, do, however, incorporate one or two innovations which were a result of the particular requirements of this project. We now examine these features in more detail.

Early work indicated that electric fields as large as $3\,kVm^{-1}$ occurred near ion plumes. In contrast, if a field mill were placed a considerable distance from such a plume it would register an electric field close to the natural value ($100-300\ Vm^{-1}$ in fine weather). It was clear therefore that the field mills would need various ranges if accurate measurements were desired. The nominal ranges chosen, giving a 0 - 1.0 volt output were (1) $0 - 200\,Vm^{-1}$, (2) $0 - 400\,Vm^{-1}$, (3) $0 - 1\,kVm^{-1}$, (4) $0 - 1{,}6\,kVm^{-1}$ (5) $0 - 3\,kVm^{-1}$ and (6) $0 - 6\,kVm^{-1}$. The type of field mill used responded equally to potential gradients of either sign as it consisted of a simple rotor and stator system without bias plate. It was originally hoped to incorporate sign discrimination by modifying the existing stator to act as a bias plate, at the same time introducing a new stator. However, this modification was never performed. This lack of sign discrimination was of no importance when studying positive ion plumes in fair weather as the resulting potential gradients were always positive. However, on those few occasions when negative ion plumes were investigated, sign ambiguities, although present, were not too troublesome.

OGDEN (1967) has constructed portable field mills but in my opinion his design seemed unnecessarily cumbersome. Portable field mills, using DC motors, are inevitably very susceptible to electrostatic interference from the motor commutator brushes. Ogden overcame this problem by isolating the motor from the field mill proper by means of a long flexible coupling. It was hoped that, by using a high speed motor with a reduction gearbox and modifying the standard amplifier design (see SHARPLESS 1968), this long coupling could be eliminated. Such modifications were most desirable as they would considerably reduce the size of the instrument. In practice a 6 V DC motor, with a nominal speed of 7500 RPM, was used to drive the field mill rotor via a 5:1 reduction gearbox. In this way it was thought that most of the brush interference from such a system would be at frequencies considerably higher than the mill signal frequency. After construction it was found that there was still some brush noise present, even though the motor had been carefully shielded. As development continued it appeared that the only really satisfactory method by which the interference could be eliminated was by reducing the input impedance of the amplifier to about 5 $M\Omega$. This, however, immediately raised another difficulty. MAPLESON & WHITLOCK (1955) have shown that, for a field mill output to be independent of signal frequency, f , the criterion $fCR > 1$, where C is the input capacitance and R the input resistance, must be met. Reducing the input impedance to 5 $M\Omega$ drastically violated the above relation and hence a compromise solution had to be found. This was achieved by using a tuned field mill amplifier, shown in Fig. 4.1. The amplifier gain was arranged to change with frequency in such a way that as

THE FIELD MILL AMPLIFIER

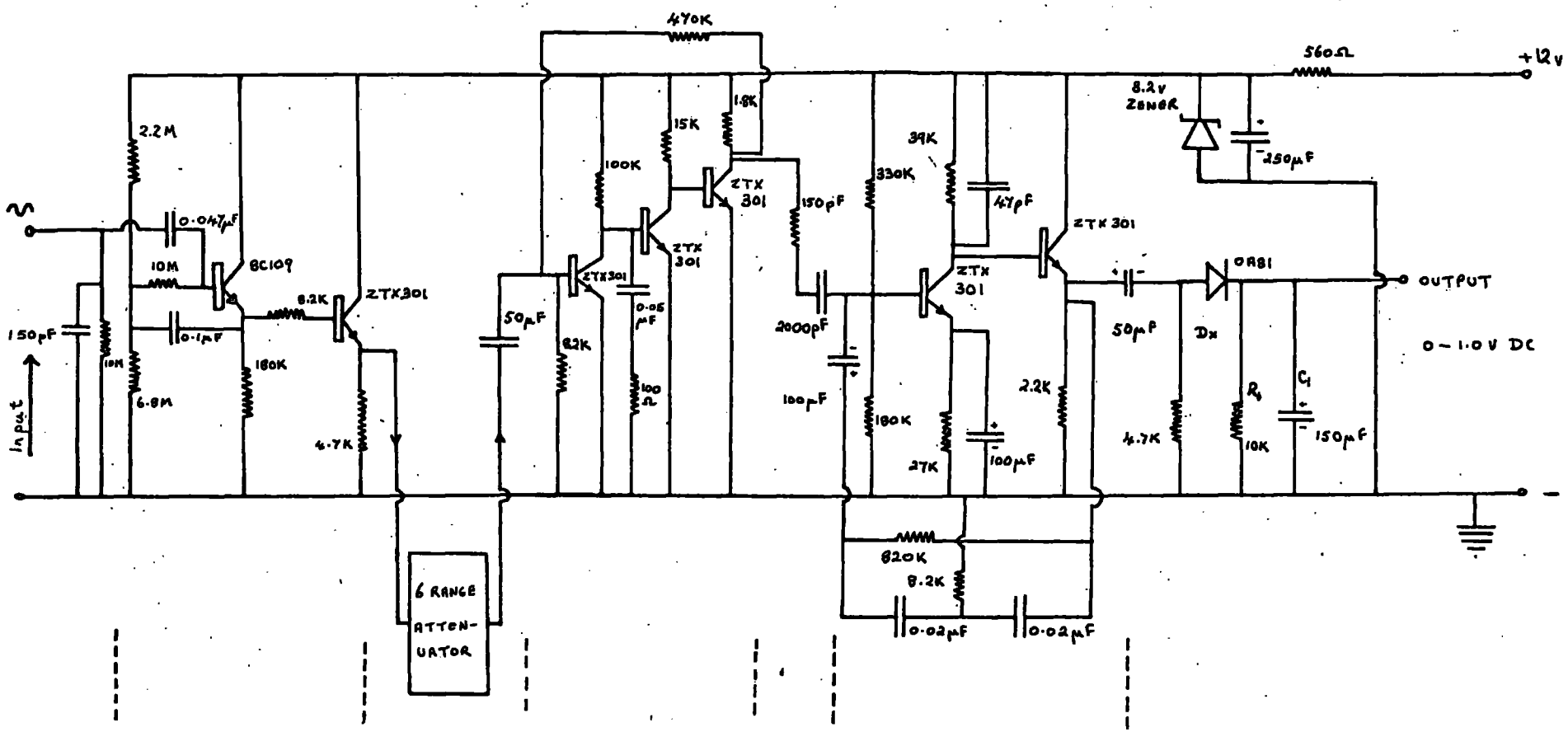

the rotor speed varied the output voltage, for a given electric field, would tend to remain constant. Independence of mill output from changes in rotor speed is, of course, very important with battery-driven mills as the rotor speed progressively decreases as the battery discharges. By carefully tuning the amplifier it was possible to maintain a mill output within 5 per cent of its calibration value.

The rotor and stator were constructed from 20 SWG aluminium sheet and were of 0.17 *m* diameter. A small phosphor-bronze brush was used to make an earthing contact to the rotor shaft. Very occasionally trouble was experienced with contact potentials between the rotor and stator. Stripping down and thoroughly cleaning the rotor and stator assemblies invariably cured this difficulty.

Four field mills were constructed for this investigation and, complete with batteries, a field mill weighed just under *3 kg*.

4.3.2 Calibration and Performance

It was anticipated that electric field in the vicinity of ion plumes would exhibit large and rapid fluctuations; further, field measured at two points separated by only a short distance might be quite different. We would expect, however, that as the distance between a field mill pair was decreased their readings would become progressively more similar. It was hoped to be able to calculate means and standard deviations of the electric field at various points and, later, possibly to investigate the correlation between the records of pairs of mills in order to test certain hypotheses about ion plume behaviour (see Sec. 3.6.).

Taken together the above experimental desiderata imply quite stringent performance criteria for the field mills. Consequently, in these mills, factors such as accuracy, short-term stability and frequency response were particularly important. It was hoped that the absolute accuracy of the mills would be better than 10 per cent whilst to make meaningful comparisons between pairs of records the short-term stability should be no worse than 2 per cent. (In this context the expression short-term refers to the duration of one run, i.e. 24 min.). Relevant features of the calibration and performance are now discussed.

The four field mills were individually calibrated on each of their six ranges for electric fields of both positive and negative polarities. A uniform electric field was set up in the laboratory by applying a stabilized voltage between two large parallel circular plates. These plates were separated by perspex insulators, 0.1 *m* long, and in the centre of the lower plate there was a circular hole of 0.18 *m* diamter. A field mill was placed under the apparatus in such a way as to render the stator flush with the lower plate. It was then possible, by varying the voltage between the plates, to impose any desired field on the mill. Early calibration work was carried out with the system housed in a Faraday cage. Later, however, it was discovered that the cage was not really necessary as the upper plate was an effective shield from external fields. During calibration the output voltage of the mill amplifier was plotted against various values of applied field, the procedure being repeated over the six ranges of each instrument. Calibration curves were then constructed. These curves

were found to be linear within a few per cent and, as the field mill readings were to be ultimately processed by computer, it was convenient to represent the mill transfer characteristic in the form of a linear equation. Thus

$$F = mV + C \qquad (4.1)$$

where F is the potential gradient,

V the mill output voltage

and m and C are constants for any particular mill and range.

The value of the offset electric field (C), most likely the result of contact potential effects, was nearly always less than $20\ Vm^{-1}$ and, except on the lowest ranges, could be ignored.

The quantity m in the relation above is a function of the sensitivity of the particular field mill. Consequently values of m had to be calculated for each mill and each sensitivity range, making 24 values in all. The calibration curves were found to be symmetrical about the origin and hence if negative potential gradients were being recorded these could be catered for simply by reversing the sign of m in the computer programmes.

Calibration checks were performed at monthly intervals during the early service of the field mills. Little change was noted in the characteristics of the mills over such periods and, as re-calibration was a lengthy procedure, later checks were undertaken every three months. On one occasion, after the equipment had suffered very severe mechanical shocks when the Land Rover was driven into a deep pot-hole, a special calibration check was thought advisable. Although slight departures from the nominal calibrations were detected from time to time none of these was large enough to warrant amending the

calibration equations.

A feature of particular interest in this investigation was the frequency response of the field mills. Portions of the ion plume passing close to a mill could readily produce field variations as fast as 0.2 Hz or possibly even faster. Hence the field mills had to respond adequately to variations of such frequencies. In practice, the effective frequency response of the mills and other measuring systems was further complicated by the characteristics of the data sampling system. It is sufficient to say here that mill time constant needed to be no longer than 2 s to ensure a satisfactory high frequency performance. An inspection of Fig. 4.1. indicates that the time constant of the mill amplifier is, to a large extent, determined by R_1 and C_1 . It was necessary to maintain R_1 at 10 $k\Omega$ to correctly match the input circuits of the sampling system (see Sec. 5.3). Thus in theory a time constant of 2 s could be achieved by setting C_1 at 140 μF . The value of this time constant also controls the degree of smoothing that is applied to the alternating signal after rectification by D_x . An insufficiently large time constant would, whilst providing a very swift mill response, unfortunately produce a signal with an intolerable ripple content. Such a signal would, of course, be quite unsuitable for recording. Calculations show that for a signal frequency of 100 Hz the ripple signal will be less than 1 per cent of the mean value when the time constant is 2 s. This was quite acceptable.

It was thought worthwhile to determine the frequency response of the field mills experimentally. Undirectional, but sinusoidally varying, voltages were applied to the parallel plate

FIELD MILLS - FREQUENCY RESPONSE

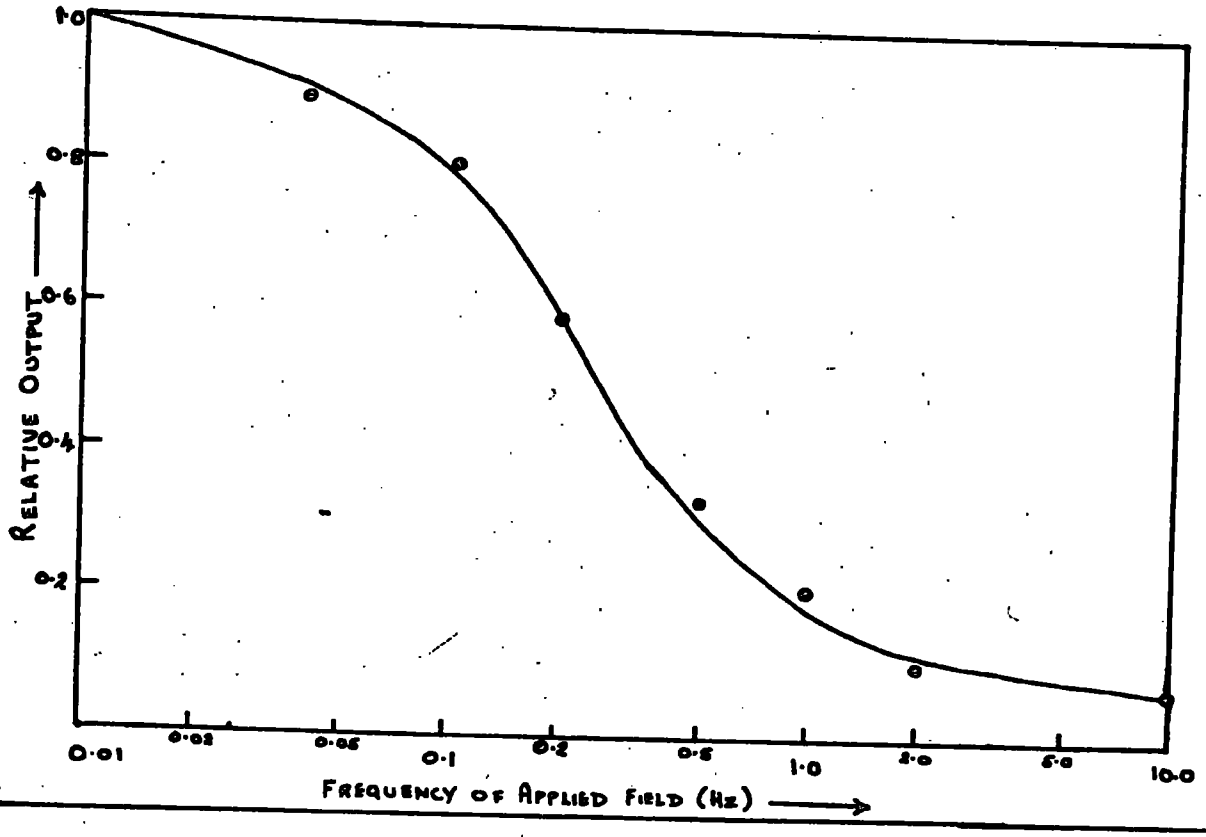

THE ION COLLECTOR - CIRCUIT PRINCIPLES

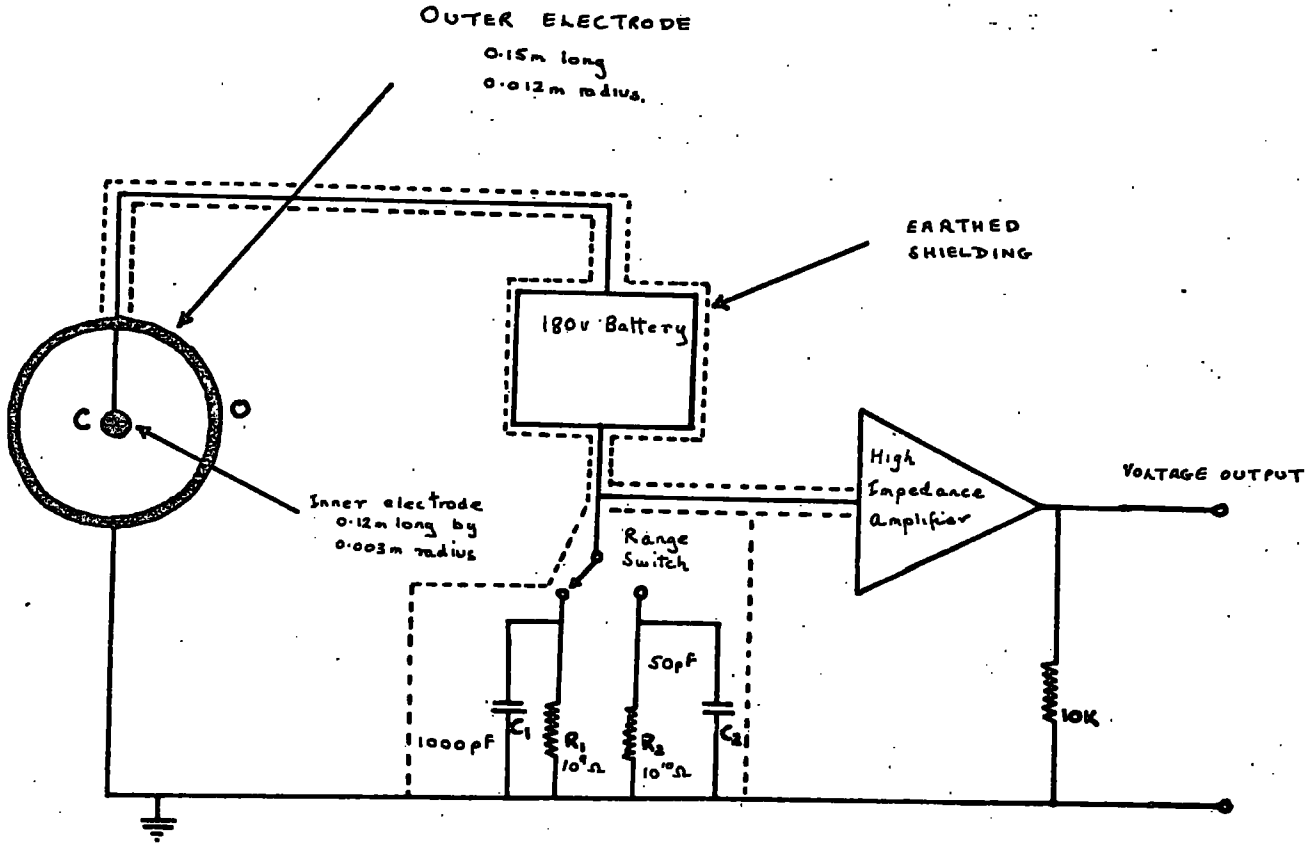

A portable field mill

calibration system by means of a special function generator. By maintaining the amplitude of the imposed field variations constant and measuring the output voltage of the mill amplifier as the field frequency was altered, it was possible to derive the frequency response of the field mills. The mills differed very little from one and another and the averaged response is shown in Fig. 4.2. These results accord well with theoretical calculations based on a 2s value for the time constant.

A characteristic of considerable relevance was the degree of similarity that could be expected between the readings of two field mills experiencing identical field variations. Alternatively, if one obtained a low cross-correlation (see Sec. 6.2.) between a pair of mills for a particular run one must know whether it was real or just a result of limitations in field mill performance. In order to investigate this, pairs of mills were subjected to identical, but varying, electric fields in the laboratory. This *test* field had a frequency of 1 cycle min^{-1} and a mean amplitude of 100 Vm^{-1}. Table I shows the results of these investigations. The coefficient of variation (see Sec. 6.2) of the applied field is listed against the correlation coefficient obtained. Average values for all four mills are presented.

TABLE I

Coefficient of Variation	Cross-correlation Coefficient
0.3	1.00
0.1	0.99
0.06	0.89
0.02	0.57

We note the excellent correlation between mill pairs when the coefficient of variation exceeds 10 per cent. On all but very few occasions the coefficient of variation of fields measured near the ion plume greatly exceeded 10 per cent. Therefore, the mill performance imposed little restriction on the validity of correlation measurements in these circumstances.

Some investigations were made of the Earth's natural electric field and the mill limitations had, of course, also to be borne in mind on these occasions. It is worth noting also that as these cross-correlation tests were performed with a low frequency field, it was anticipated that, near the high frequency limit of the mills, correlations would be lower due to signal phase shift effects in the amplifiers. The results of some mill correlations checks performed in the field are presented in Ch. 7.

As can be seen, the field mills have been subjected to stringent tests to ensure their fitness for this project. Their performance in the field has been excellent.

4.4 The Ion generator

4.4.1 Basic theory and principles of design

It is quite easy to ionize air by the application of a sufficiently large electric field. Such a field would normally be produced by the use of a high voltage supply connected to a suitable electrode system. In this project ions of only one sign were required at any particular time and these ions, once created, had then to be somehow removed from the electric field that produced them. In practice a coaxial cylinder

electrode system is very convenient for producing large electric fields without risk of breakdown. The feasibility of such a system was duly investigated and, after considerable experimentation, was finally chosen for the ion generator.

We now review the underlying principles of operation of the generator and, perhaps it should be stated at the outset, that as the physics of gas discharges is very complex, only the basic physics of the apparatus can be discussed here. A fuller description of this, and related, topics can be found in LOEB (1965).

It can be shown from elementary principles that the electric field, E , between coaxial cylinders is given by

$$\boxed{E = V/(r \ln(b/a))} \qquad (4,2)$$

where V is the applied voltage,

r the radius at which the electric field is to be calculated, and

a and b the inner and outer radii, respectively of the coaxial system.

Strictly, this relation applies only to infinitely long cylinders and to systems in which there is no space charge present. Clearly these are somewhat severe limitations, particularly in the present case, but equation (4.2) will, however, suffice for the approximate analysis given here.

In designing the ion generator the radii of the outer and inner cylinders could be varied but their dimensions could obviously not exceed certain limits. Naturally it was hoped that the ion generator could be made quite small so that it might be easily placed on a light mast. Ideally therefore the radius of the

outer cylinder should not be greater than about 0.1 *m* Also the inner cylinder, or wire, should not be too small, because if it were, it would not withstand normal mechanical shocks. In fact, it proved possible to use a tungsten wire of only 6 *μm* radius in the ion generator; the advantage of using such a thin wire being, of course, that even with a relatively modest high voltage supply, very large electric fields could be produced, thus causing intense ionization. At this stage the design of the high voltage supply had therefore to be considered. It is, in fact, possible to construct, quite easily, portable power supplies capable of giving 100 *kV DC*. However, I did not wish to use such high voltages, mainly for reasons of safety. Consequently it was decided that a 20 *kV* supply was the maximum that could be handled in the field.

Substantial ionization occurs in regions where the electric field exceeds some critical value, say E_c . The ions are, of course, produced by collision processes and, in air at normal pressures, E_c is about $10^6 Vm^{-1}$. In the present ion generator this field is exceeded within about 2*mm* of the central wire. (This figure was obtained by inverting equation (4.2), specifying appropriate values for *a*(6 *μm*) , *b*(50 *mm*) and *V*(20 *kV*), and then solving for *r* .) Consequently all ionization is confined to a cylindrical region around this central wire.

Let us now consider how those ions that are created in this region behave under the influence of the electric field that is present. For the sake of argument, imagine that the central wire is positive with respect to the outer cylinder. (The outer cylinder was, in practice, always earthed.) Ions of both polarities are created in the inner region and the prevailing electric

field will cause negative ions to be attracted toward the central wire whilst positive ions will be repelled toward the outer cylinder. The electric field is, however, very large near the inner wire but relatively small in the vicinity of the outer cylinder. Therefore the transit time of a positive ion to the outer cylinder will be very much larger than that of a negative ion to the central wire. Theoretical calculations (see CHALMERS 1967) show that a positive ion will require about $5\,ms$ to reach the outer electrode whereas a negative ion (or electron) will be discharged at the central wire only a few μs after its creation. It appears therefore that the region from the outer cylinder to within $2\,mm$ of the inner wire will be filled with relatively slow moving positive ions. In view of this it seemed there might be a possibility of expelling some of these positive ions from the system by blowing a brisk current of air along the axis of the apparatus. We can test this idea by means of a very simple calculation. Suppose the length of electrode system were L , the transit of time of the positive ions across the system t and velocity of air through the generator v . Then if

$$\boxed{v \geq L/t} \qquad (4.3)$$

all the positive ions generated should clear the outer cylinder. The above reasoning, admittedly crude, does provide us with an idea of the practicability, or otherwise, of the proposed technique for expelling the ions. Substitution of appropriate values into equation (4.3) indicates that an air velocity of $5\,ms^{-1}$ should be sufficient for the design contemplated. Fortunately, this is a realistic figure for a blower and thus the construction of an ion generator seemed a feasible proposition.

It should be added here that a similar analysis can be performed in the event of the central wire being at a negative potential and this suggests the interesting alternative possibility of generating negative ions.

In conclusion, I would like to point out that some factors have been deliberately omitted in the above theory. It is, for instance, possible to treat the system in a more sophisticated manner by considering the effect of space charge on the electric field distribution inside the generator. However, theoretical treatments rapidly become involved and, from my point of view, it was thought better, having established the basic principles of the device, to proceed with the construction of an ion generator.

4.4.2 Construction and Performance

An ion generator was constructed in accordance with the ideas discussed in the last section. The electrode assembly, expeller motor and fan were all mounted in a perspex tube 0.3 m long and 0.1 m in diameter. The arrangement is illustrated in Fig. 4.3. Three rectangular windows were cut in the perspex cylinder thereby permitting the earthed cylindrical electrode to be mounted on the outside of the tube. A small, easily removable, carrier was used to support the central wire. The framework of the carrier was made of thin perspex rod whilst copper pins mounted in PTFE bushes were provided at two suitable points at which to solder the gold-plated tungsten wire. The length of the central wire was 2.5 cm.

It was hoped to determine the ion output of the generator by monitoring the current flowing in the high voltage circuit.

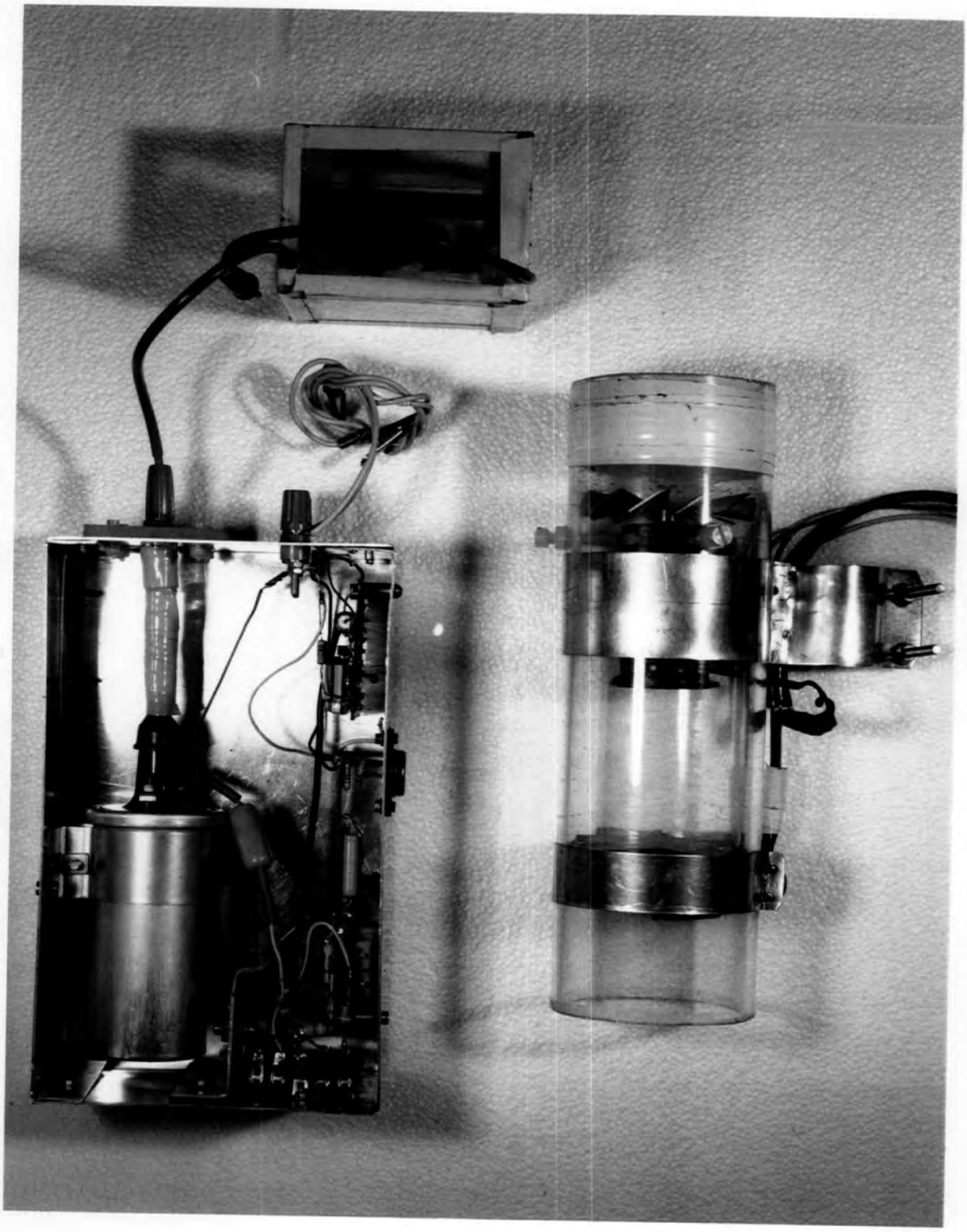

ION SOURCE - EHT SUPPLY - RECTIFIER

Early experiments soon convinced me that this idea was not feasible because the total discharge current bore little relation to the actual quantity of ions being expelled by the generator. It appeared that many of the ions produced were not blown out but instead were ultimately collected by the outer electrode. The blower unfortunately produced a very turbulent air flow through the electrode system and it is felt that the enhanced ion transport due to this turbulence may have considerably increased the collection efficiency of the outer cylinder. Some attempt was made to improve the performance by placing straightening vanes in the air flow but this did not remedy the situation.

The output of the ion generator could, however, be readily assessed by an indirect method. The generator was mounted on a suitable mast at a few metres above ground level and a field mill was placed approximately 10 m downwind of the mast. Theoretical calculations (the steady-state model) had already provided values for the magnitude of the electric field disturbance to be expected from the presence of the ion plume. Hence it was possible, in theory at least, to deduce the ion generator output from the field mill readings. In practice this method, although a little cumbersome, worked very well and was invariably used to estimate the generator performance whilst development was proceeding.

It was later discovered accidentally that the output of the ion generator could be considerably increased by coating the outer electrode with a thin layer of varnish. It is thought that this varnish layer, whilst not materially affecting the electric field distribution within the generator, may consi-

derably decrease the collection efficiency of the outer electrode, thereby resulting in an increase in the ion output. It should be emphasised that this explanation has not been verified experimentally and may, therefore, be incorrect.

The blower used in the generator consisted of a 12-bladed rotor fan powered by a 6 *V* DC 6000 RPM motor. The current consumption was 1 A and the flow velocity exceeded 7 ms^{-1}.

The ion generator has been in service for over a year and, except for one occasion, has functioned quite satisfactorily. The generator failed late one evening in very damp conditions, probably only after the perspex insulation had absorbed considerable moisture. A more serious fault, however, was only noticed after the generator had been in use several months. It had become apparent that the ion output was rather erratic in high winds. This behaviour was, after some investigation, attributed to the action of strong winds disturbing the air flow over the electrode system. The problem was solved by mounting the generator with its axis horizontal, instead of vertical as previously, and then attaching a right-angle cowl over the air intake.

The output of the ion generator, estimated from numerous observations, is 0.3 μA when producing positive ions and 0.5 μA when producing negative. (The difference between the positive and negative ion outputs is not determined by the generator itself but depends on the differing mobilities, and other properties, of ions of the two signs.)

4.4.3 The High Voltage Supply

A schematic drawing of this is shown in Fig. 4.3. The high voltage supply was powered by a 12 *V* 4.5 Ah rechargeable battery, the current consumption of the system being o.4 A. The operation of the supply is now briefly discussed.

The inverter converts the 12 *V* DC supply into a 250 *V* 15 *kHz* alternating voltage which is then rectified and smoothed by D_1 and C_1 respectively. In the absence of a positive pulse from the multivibrator, the thyristor T is effectively an open-circuit between the points X and Y. The capacitor C_2 is thus charged to approximately 350 *V* via R_2, the primary of the ignition coil being of negligible resistance. The arrival of a short positive pulse at the gate electrode, G, of the thyristor causes it to rapidly become conducting. Hence X and Y are now effectively connected together. This results in the capacitor C_2 being discharged into the primary of the ignition coil thereby producing a very high voltage at the secondary terminal. After this the thyristor again becomes non-conducting, allowing C_2 to recharge. The process is then repeated at a frequency determined by the time constant of the multivibrator. In practice, of course, the charging time constant of R_2 and C_2 must be made sufficiently small so that C_2 is fully charged each time the thyristor conducts. The repetition frequency in this apparatus was 30 Hz.

The secondary output was rectified by a special "silicon stack" enclosed in a separate perspex box. This arrangement was necessary so that the rectifier could be connected either way round into the high voltage system. This enabled negative or positive ions to be generated as required. Initially a capacitance

of 500 pF was placed across the rectifier so as to provide a smoothed supply. However, the presence of a 500 pF capacitor charged to a potential difference of 20 *kV* was most undesirable as it could give a serious, possibly even fatal, electric shock to anyone accidentally touching it. As an alternative the distributed capacitance, amounting to 150 pF, between the cable carrying the high voltages and the earth return wire was used for smoothing. Whilst considerable charge was retained in the cables, their self inductance obviated, to a large extent, the risk of a dangerous shock.

4.5 The Ion Collector

This simple device was designed to supplement the field mill observations. After theoretical investigations it had emerged that the ion plume would initially expand very rapidly, both laterally and vertically, as a result of electrostatic forces (see Sec.3.5). It was hoped that the ion collector could be used to determine the ion concentration profile in the region within about 10 m of the source. A simple calculation shows that, at this distance, ion concentrations of the order of 10^{-8} Cm^{-3} were to be expected, a figure approximately one hundred times greater than the fair weather ambient values. (See CHALMERS 1967). Consequently, it was not anticipated that the presence of relatively small numbers of natural ions would cause any difficulties.

The collector was based on the original design of EBERT (1901) and is, in principle, almost identical. Air is drawn through a coaxial cylinder electrode system, as shown in Fig. 4.2, by a suitable motor driven fan. The central electrode C is main-

HIGH VOLTAGE SUPPLY AND THE ION GENERATOR

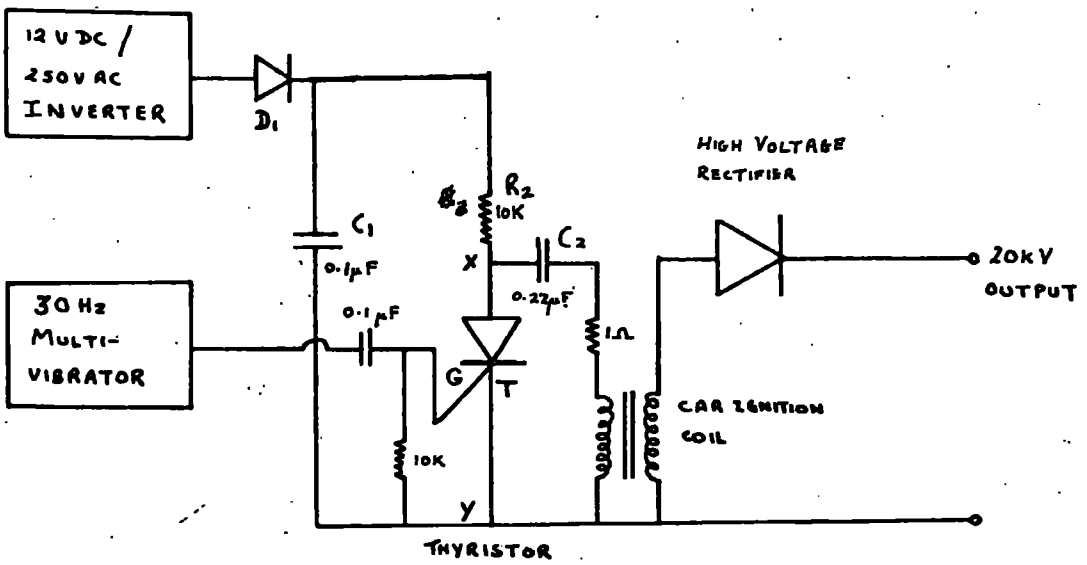

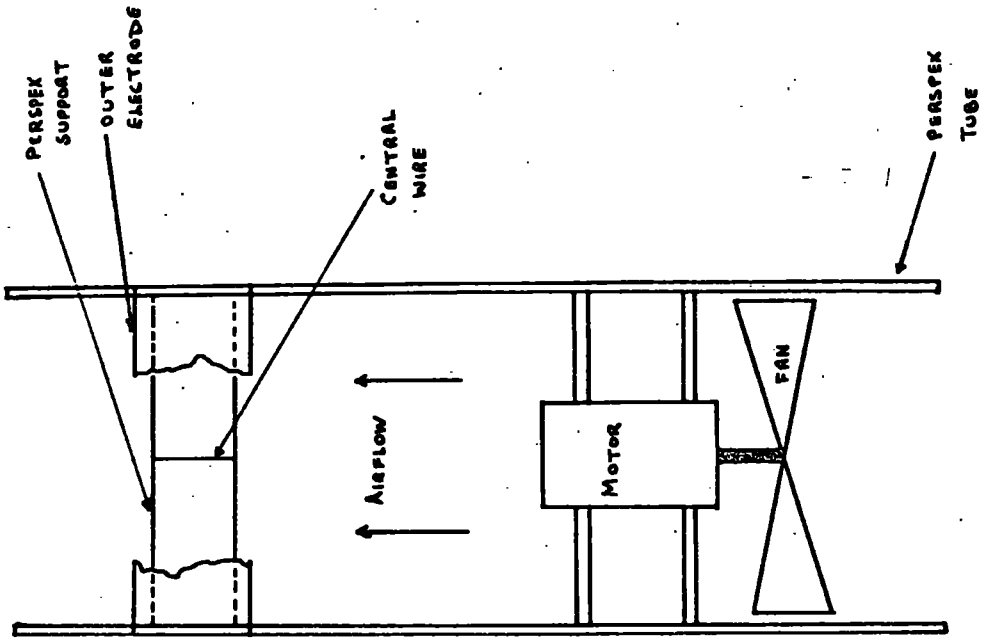

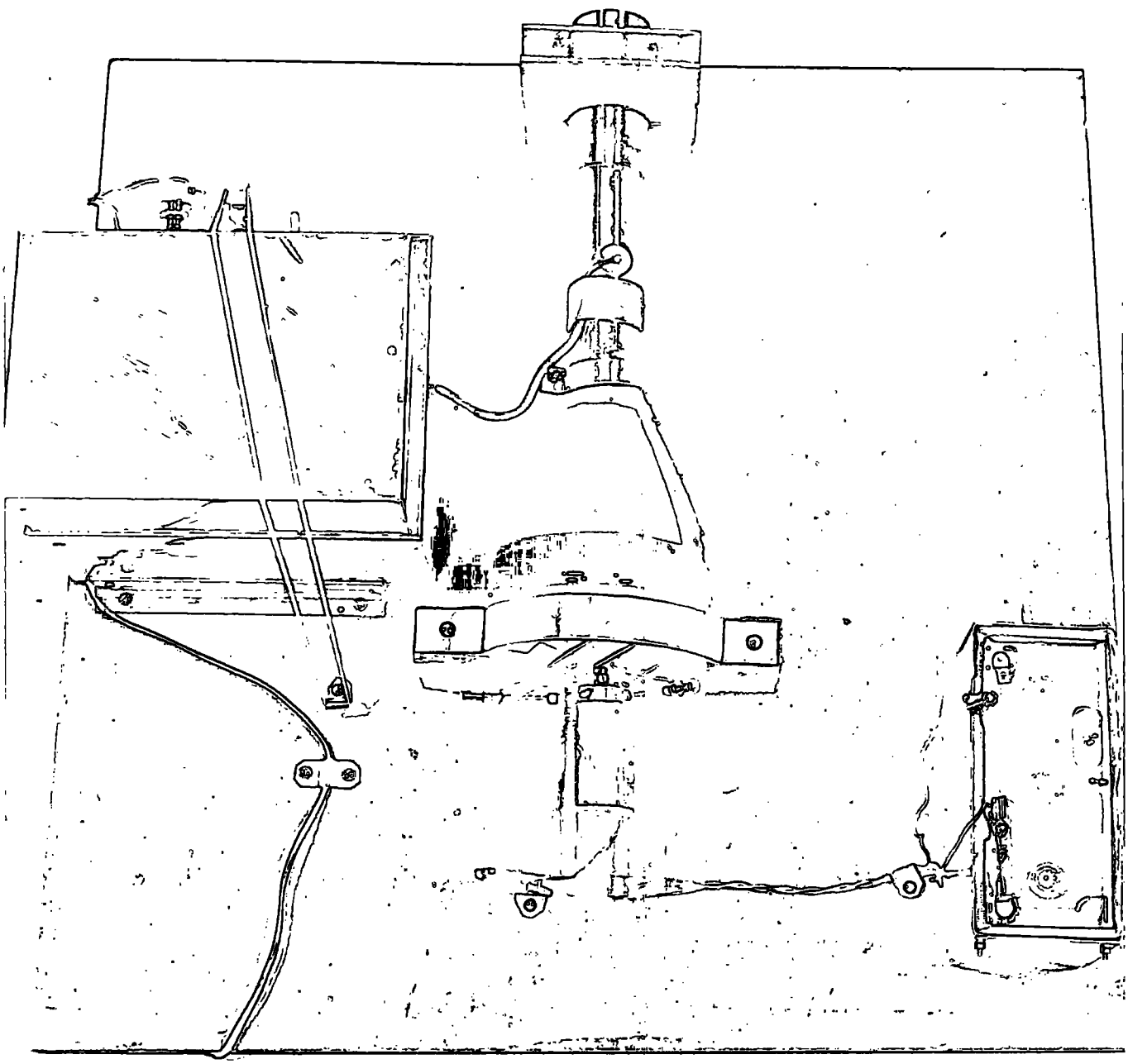

The ion collector

tained at a constant potential with respect to the outer electrode O. Ions entering the device will therefore either be attracted to or repelled from the central electrode depending on their sign. Those ions which reach this electrode before passing out of the device constitute an electric current. This current flows through the external resistor R and produces a small voltage. Ions of the opposite sign reaching the outer electrode flow to earth and play no part in the functioning of the apparatus. It is, of course, essential for quantitative work that the central electrode collects all the ions which are drawn into the apparatus. Suppose the velocity of air flow through the system were v and the length of the electrode system were L; then the incoming ions must reach the central rod in a time less than or equal to

$$L/v$$

Now by employing similar reasoning to that used in designing the ion generator, we can show that the transit time, t, of an ion from the outer cylinder to the central rod is given by

$$\boxed{t = (\ln(b/a)(b^2 - a^2))/2\mu V} \qquad (4,4)$$

where μ is the mobility of the ions,

V the central electrode potential and

a and b the inner and outer radii respectively.

Using the two relations above, we are now in a position to design an ion collector. The mobility μ of the small ions is, of course, fixed, but the quantities L, v, V, a and b are all, within reason, left to our choice. As is usual, in practice these quantities are not independent and therefore a compromise must be reached. A suggested upper limit for V was about 200 volts, as a battery of higher voltage would have

been cumbersome. It was thought that the inlet velocity, v, should be not less than 15 ms^{-1} otherwise gusty winds might adversely affect the performance of the apparatus. The length, L, was set to 0.15 m and, from equation *(4,4)*, it was found that the dimensions of a and b were perfectly reasonable. (The exact dimensions are shown on the figure.)

Capacitors C_1 and C_2 were placed across the input resistors R_1 and R_2 to establish a definite time constant for the collector. A value of 1*s* was, in fact, chosen. (It should be remarked that as the self capacitance of the electrode system and wiring was approximately 50*pF* C_2 only needed to be 50*pF* to obtain the desired time constant). The voltage across R_1C_1 (or R_2C_2) was then amplified by a special FET integrated circuit DC amplifier having an input impedance of not less than $10^{11}\Omega$. The output current from this device was fed to earth via a 10*k*Ω resistor, thus producing a voltage output suitable for recording. In the final design a commutating switch was provided so that the polarity of the voltage on the central electrode could be reversed. This enabled the concentrations of both positive and negative ions to be determined, though not, of course, simultaneously.

After construction, the collector was checked to make certain that it was responding to all the small ions which passed through it. A small radioactive source, of Americium 241, was placed near the inlet tube of the device and the 200*V* battery was replaced by an isolated variable voltage supply. The voltage applied to the central electrode was then altered and the effect on the output voltage noted. The results of this test

indicated that at the normal working voltage 99 per cent of incoming negative and 95 per cent of incoming positive ions were collected.

This ion collector responds to the rate of arrival of ions of one sign at the central rod. From a knowledge of the air flow rate through the apparatus, it is therefore possible to calculate the charge concentration. Previous workers, e.g. OGDEN (1967), have measured the flow rate through their much larger space-charge collectors by means of gas meters. The use of such a technique was thought most unlikely to succeed in this case because gas meters require a comparatively large pressure drop to operate them satisfactorily. A crude estimate of the flow rate was, however, obtained by using a sensitive small probe hot wire anemometer to establish the mean velocity profile across the collector inlet. This was not an accurate measurement and the volume flow rate derived from it could be as much as 20 per cent in error. The mean intake velocity was found to be 14 ms^{-1} , which is close to the design figure.

The ion collector functioned quite well in the field, although the output signal was rather noisy on the more sensitive range.

4.6 The Micrometeorological System

4.6.1 Purpose of the System

Clearly the behaviour of the ion plume depended to a great extent on its local meteorological environment. It was the purpose of the instruments described herein to monitor that environment by the measurement of appropriate physical quantities. In Sec. 2.7 it was shown how the atmospheric stability had a marked effect on the behaviour of a plume. For

this reason it was decided to measure the wind speed and temperature gradients near the ground so that the Richardson number could be determined. Obviously the wind speed itself is also of considerable importance and therefore this too was measured.

Later experiments featured the use of a bivane as it was found that stability measurements, although useful, were not providing as much information as was originally hoped.

The individual instruments are now discussed.

4.6.2 The Anemometer System

4.6.2.1 General Features

Two Casella type T 16108/2 sensitive cup anemometers were obtained for this project. These anemometers were compact, simple to use and proved very reliable. The manufacturer specified a starting speed of not more than 10 cms^{-1} and an accuracy of better than 0.3 ms^{-1} . Hence their performance was adequate for the application envisaged. These anemometers provided a single 12 V pulse per cup shaft revolution. This pulse was derived from the rotation of a sectored disc, attached to the cup shaft, which interrupted the light beam between a photo cell and lamp. The photo cell output was fed into a Schmitt trigger circuit which produced the 12 V pulses.

The anemometers were attached to the Clarke mast by suitable clamps and booms. Care was always taken to site the anemometers upwind of the mast in order to minimize the effects of wind flow disturbance on the observations. The anemometers were placed at

MICROMETEOROLOGICAL INSTRUMENTS - Electronics system

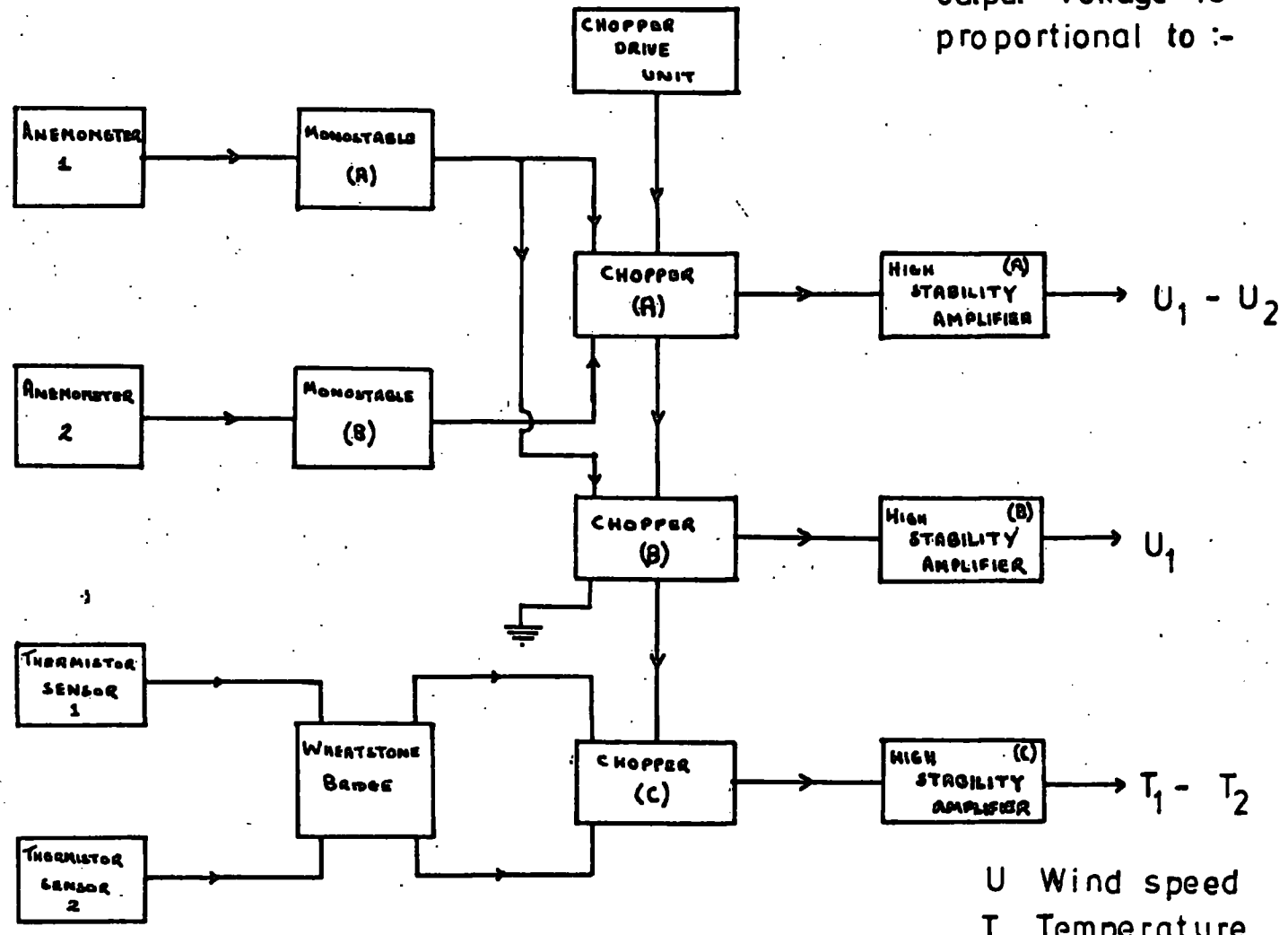

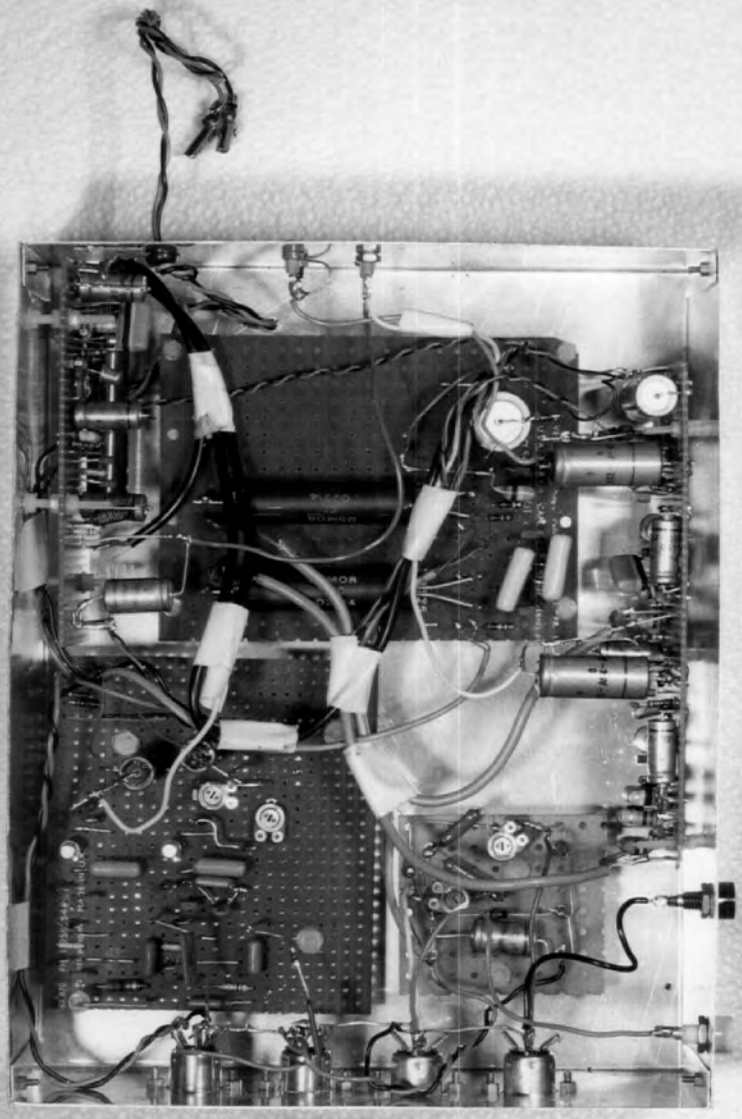

THE MICRO METEOROLOGICAL
SYSTEM ELECTRONICS

standard heights, 2 m and 9 m, and were connected to their electronics system, which was at ground level, by lengths of twin core shielded microphone cable. No trouble was experienced with *interference* from the 20 *kV* ion generator power supply although it had been expected.

4.6.2.2
The Electronics System

A schematic diagram of the anemometer signal processing arrangements is shown in Fig. 4.4, whilst details of the individual circuits can be seen in Fig. 4.5. The anemometer electronics system was designed to produce two outputs. Firstly a 0 to 1.0 *V* analogue output proportional to the wind speed at 9 m and secondly, a similar output proportional to the difference between wind speeds at 9 m and 2 m. It would, of course, have been possible to measure and record the wind speeds at these heights entirely independently and then later compute the wind speed difference by substraction. In retrospect I would now consider the latter alternative as the more satisfactory. However, mainly due to lack of experience, it was not unfortunately adopted. Nevertheless the system based on the original proposal, despite its unnecessary complexity, did work well.

The 12 *V* pulses appearing at the anemometer outputs were not of standard width, the actual pulse width being a function of wind speed. In the pulse counting system contemplated it was, however, necessary that the incoming pulses were of constant width. To achieve this the pulses from the two anemometers were shaped by the monostable multivibrators A and B. After conversion to standard width the pulses were integrated and DC

outputs proportional to their repetition rates were produced at point B. The time constant of the integrating circuits was 3.5 s, this being determined by the value of R_1 and C_1 in Fig. 4.5.1.

The DC voltage appearing at B was not suitable for recording because the input impedance of the recording system would have seriously disturbed the action of the integrating circuit. Thus some type of buffer amplifier was needed to give a suitable output. A simple DC amplifier was constructed but, unfortunately, output voltage drift, due largely to temperature changes, precluded its use. This, of course, was especially so in field work where hot sunshine anc cool breezes might alternate thus producing large temperature variations. After some experimentation a chopped DC amplifier was found to offer the most promise. The input of such an amplifier is alternately switched from the DC voltage to be amplified to a fixed reference voltage and vice-versa. Thus a square wave is produced at the input and this can, of course, be handled by a conventional AC amplifier. The advantages of such a system are, firstly drift is eliminated and, secondly, it is possible to design sensitive and stable circuits quite simply. A major disadvantage is that there is a difficulty in establishing the sense of the input signal as the amplifier responds only to the magnitude of the difference between the input and reference signals. In practice, this was not serious because it was found that the wind speed at 9 m was invariably greater than that at 2 m. Hence, by employing two chopper DC amplifiers it was quite simple to produce the desired output signals. Inter-connexion details of the various amplifiers are shown in Figs. 4.4 and 4.5.

MICROMETEOROLOGICAL SYSTEM ELECTRONICS I

1. Anemometer pulse convertor

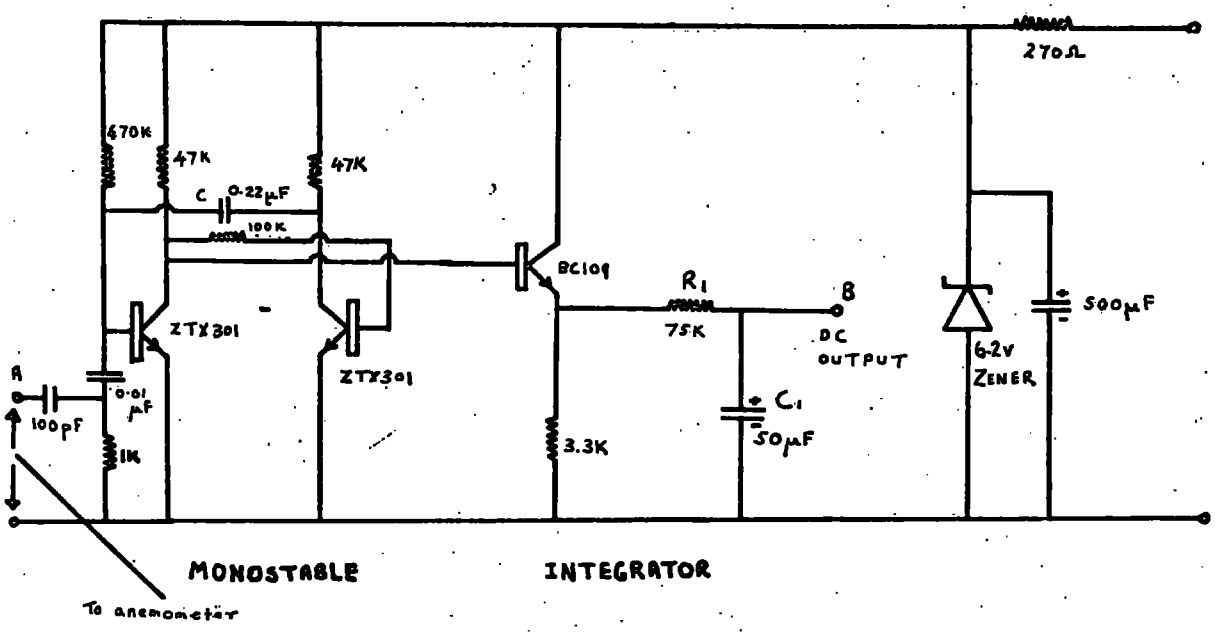

2. High stability amplifier

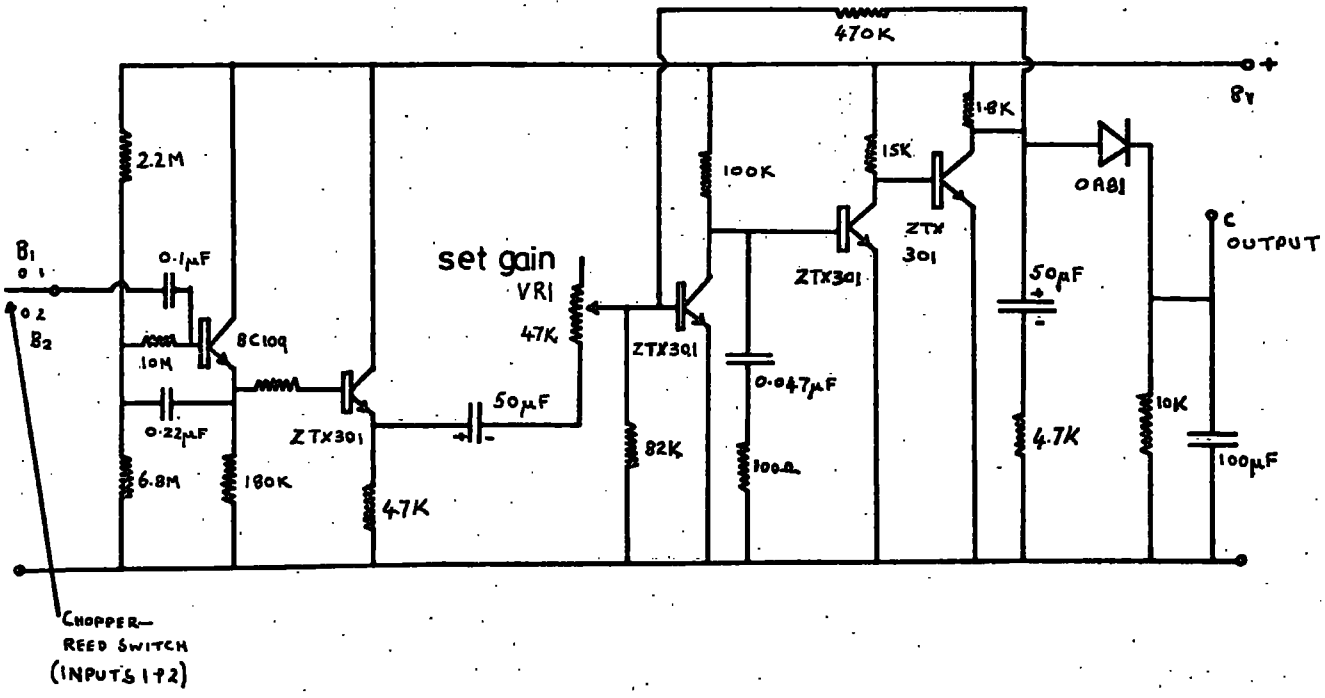

MICROMETEOROLOGICAL SYSTEM
ELECTRONICS II

3. Chopper drive unit

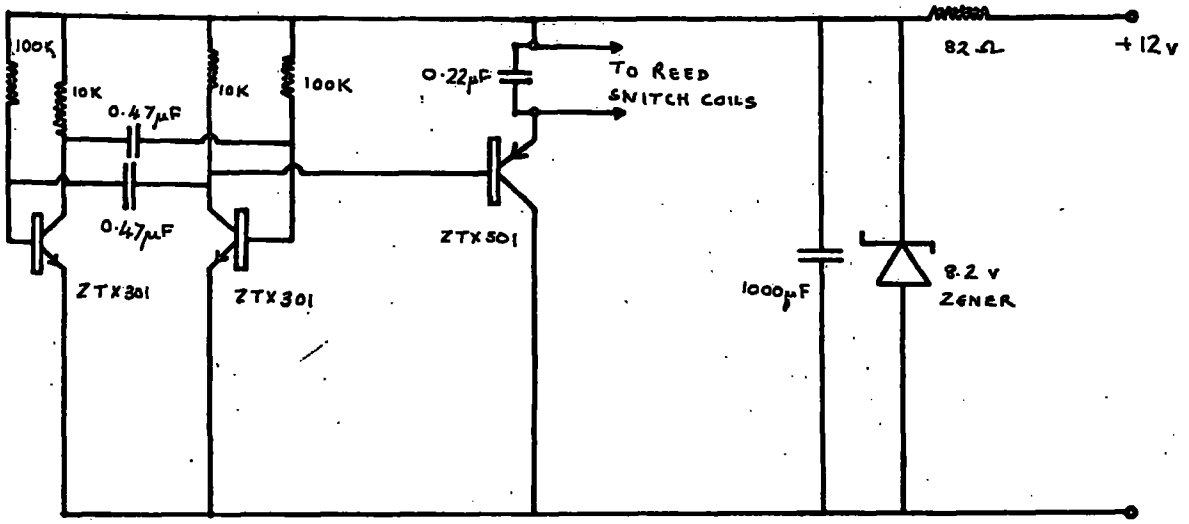

4. Thermistor bridge circuit

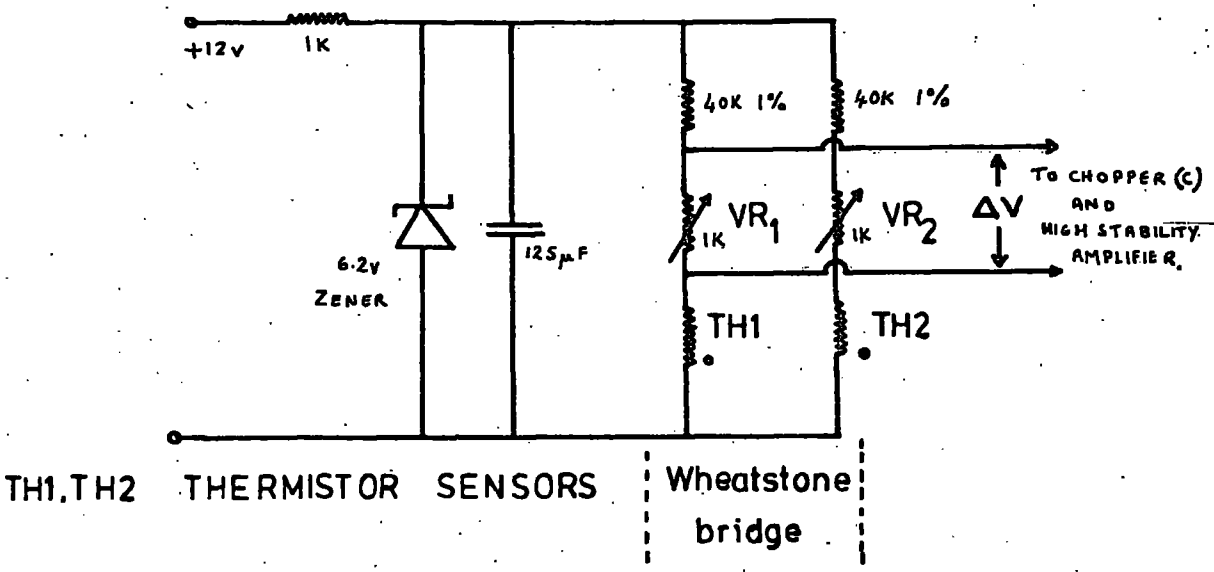

In the anemometer system two changeoever reed switch choppers were used. The driver circuit for the chopper system is shown in Fig. 4.5.3., and is conventional in all respects. The chopping frequency was approximately 30 Hz. A small 0.22 μF capacitor was placed across the reed switch to ensure that inductive effects did not damage the driver transistor.

4.6.2.3
Calibration and Performance

The manufacturer supplied standard calibration curves with these anemometers. These curves consisted of output pulse rate plotted against the actual wind and were substantially linear within the range 1-10 ms^{-1} . The two anemometers used in this investigation were never checked in a wind tunnel but, later, a third, individually calibrated, anemometer was acquired and the readings of all three anemometers were very carefully compared. It was concluded that the original two anemometers were well within their nominal calibration even after two years of service.

The output pulse rate of the anemometers was 40 pulses per minute per ms^{-1} , and thus at a wind speed of 1 ms^{-1} , a pulse occurred every 1.5 s. As the time constant of the integrating circuit was 3.5 s, considerable ripple was apparent on the output signal at very low wind speeds. This was of little importance however, as few observations were made in wind speeds of less than 2 ms^{-1} .

The anemometer electronics system was calibrated by means of a specially designed pulse generator having two individually variable pulse rate outputs. Such a pulse generator enabled both different wind speeds and wind speed gradients to be

precisely simulated. The gain of the high stability amplifiers was controlled by VR 1 (see Fig. 4.5.2.) and setting this controlled the calibration span of both systems. The calibration curves for the anemometer systems are shown in Fig. 4.6. Some slight non-linearity is evident in the curves, but it was not large enough to be of great importance. These curves were, in fact, expressed in the form of a linear equation, this being convenient for computer processing of the data.

The electronics system, although complex, worked quite successfully in the field and suffered no major faults throughout the duration of the project. Calibration checks were performed at three-monthly intervals, very little alteration in the system being evident.

A further check of the wind speed gradient system could be made in the field. If the anemometers were placed as close as possible together, then, theoretically, they should indicate a zero wind speed difference. In practice a figure of 0.2 ms^{-1} or less was usually achieved. This was regarded as quite satisfactory.

4.6.3 The Differential Thermistor System

4.6.3.1 General Features

Two aspirated temperature sensors were constructed to enable the mean temperature gradient between 9 m and 2 m to be determined. The aspirated thermistor systems were similar in design to those of OGDEN (1967) although in this case a cylindrical rather than rectangular, arrangement was employed to facilitate

ANEMOMETER SYSTEM - Performance curves

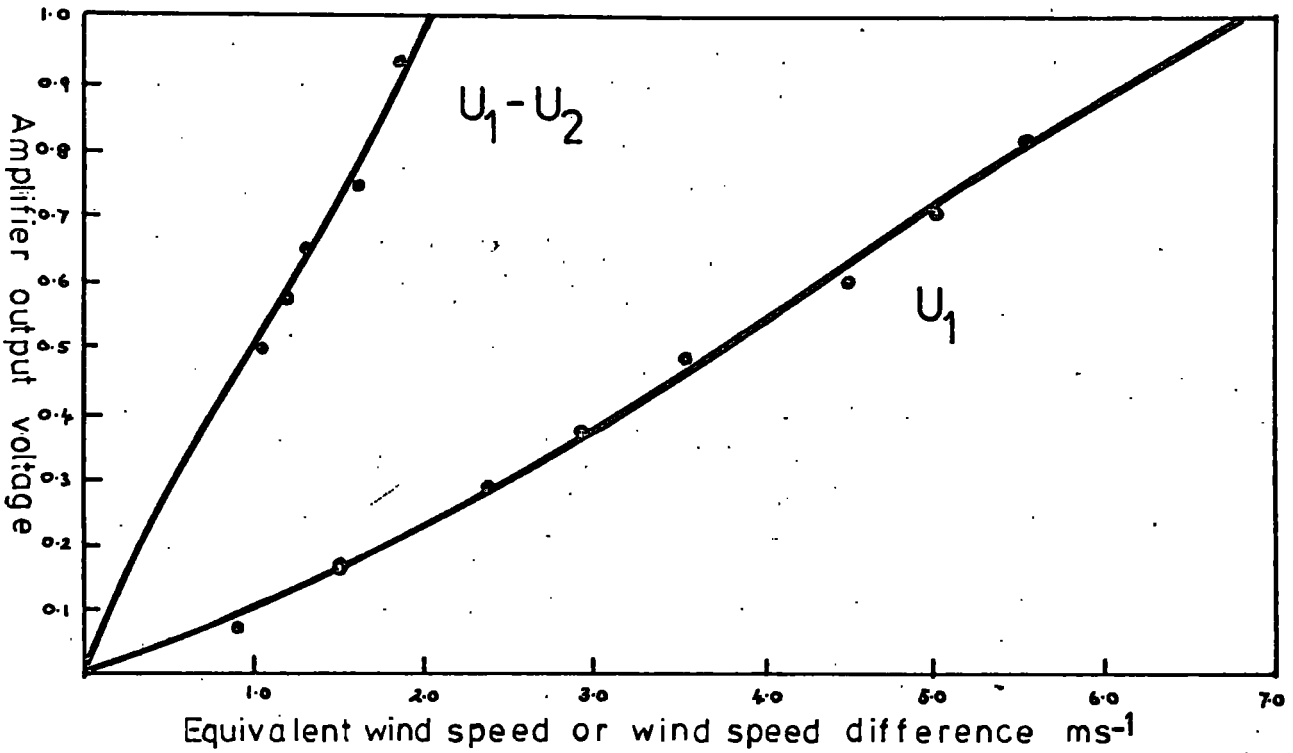

DIFFERENTIAL THERMISTOR SYSTEM
Performance curve

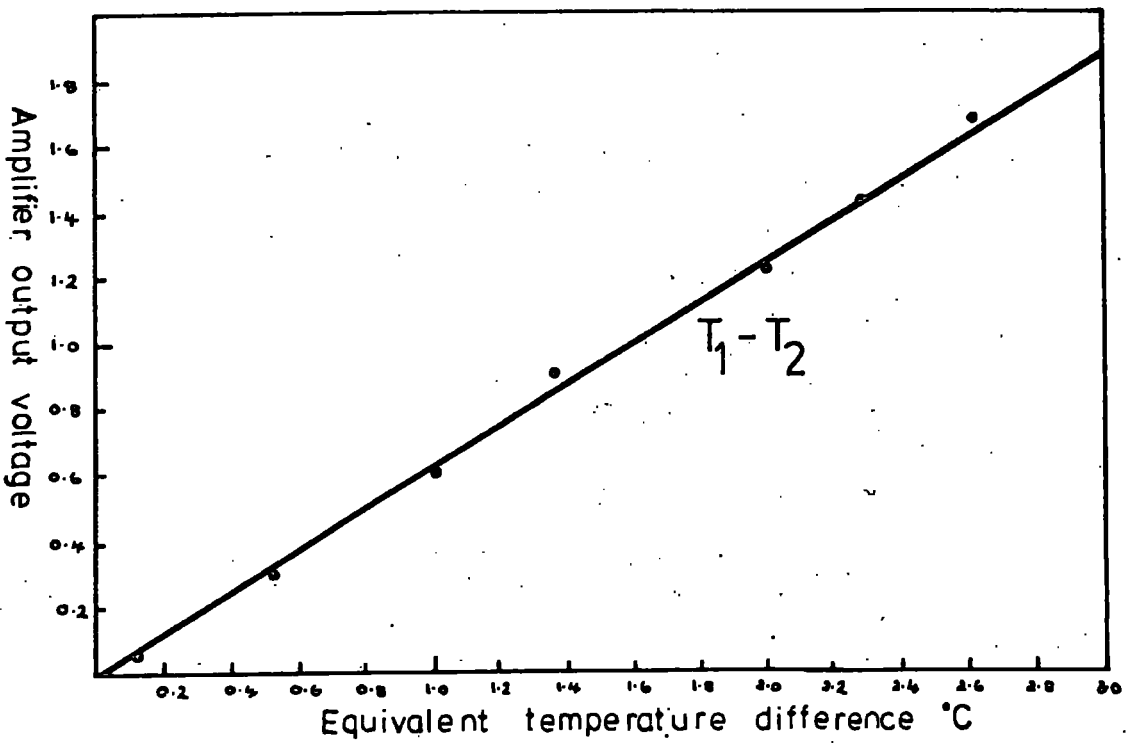

construction. A sectioned drawing of an instrument is shown in Fig. 4.7, the external surface being, as usual, painted white to minimize radiation effects.

The thermistors used, manufactured by the Yellow Springs Instrument Co., have the following specification:-

TYPE YSI 44032

INTERCHANGEABILITY 0.1°C in the range -20°C to + 70°C

RESISTANCE 30.00 $k\Omega$ at 25°C

RESPONSE TIME IN STILL AIR 10 s

DISSIPATION CONSTANT 1 $mW\ ^{\circ}C^{-1}$

The thermistors were aspirated throughout a field run by means of a small motor and fan. The air velocity in the large tube was 0.6 ms^{-1} and, a simple calculation shows, in the region of the thermistors the flow velocity was about 3 ms^{-1}. Experiments indicated that, at this aspiration rate, the time constant of a thermistor was less than 2 s. This was satisfactory.

The two thermistor sensors were connected, by means of ordinary twin wire, into the bridge circuit shown in Fig. 4.5.4. As the thermistors were matched to within 0.1°C they could be used directly to indicate temperature difference. Nevertheless small trimming resistors, VR1, 2, were included in the bridge to balance out any slight differences between the thermistors. In fact no differences were ever found and consequently the trimmers were never used. Precision resistors were, of course, employed in the two remaining arms of the bridge. The voltage supply to the bridge was fully stabilized by means of the 6.2 V zener diode arrangement shown.

The voltage difference, ΔV, produced at the bridge output was 73.0 mV per deg. C difference between the thermistors. It was, in fact, possible to calculate accurately the voltage output for given termperature differences at various temperatures as the manufacturer supplied very precise resistance tables with the thermistors. When such calculations were performed it was discovered that the value of the output voltage, per unit temperature difference, depended little on the actual temperature. Within the range 5-20°C the change in ΔV for a given temperature difference was less than 3 per cent and could therefore be ignored. A further, and very useful, feature of this bridge circuit was that for relatively small temperature differences, say less than 3°C, the output voltage versus temperature difference characteristic was linear.

4.6.3.2
The Electronics System

The chopper amplifier used to process the temperature difference signal produced by the thermistor bridge was virtually identical with that in the anemometer electronics system. Consequently the remarks made in Sec. 4.6.2.2. also apply, mutatis mutandis, here.

4.6.3.3
Calibration and Performance

The temperature difference sensing system was calibrated by substituting the thermistors with precision resistance boxes and, by varying the resistance, various temperature difference could be readily simulated. The results of such a calibration are shown in Fig. 4.6, the high degree of linearity being clearly evident. Calibration checks were undertaken at three-monthly intervals, no indication of any charge in the performance was ever apparent.

THERMISTOR TEMPERATURE SENSORS

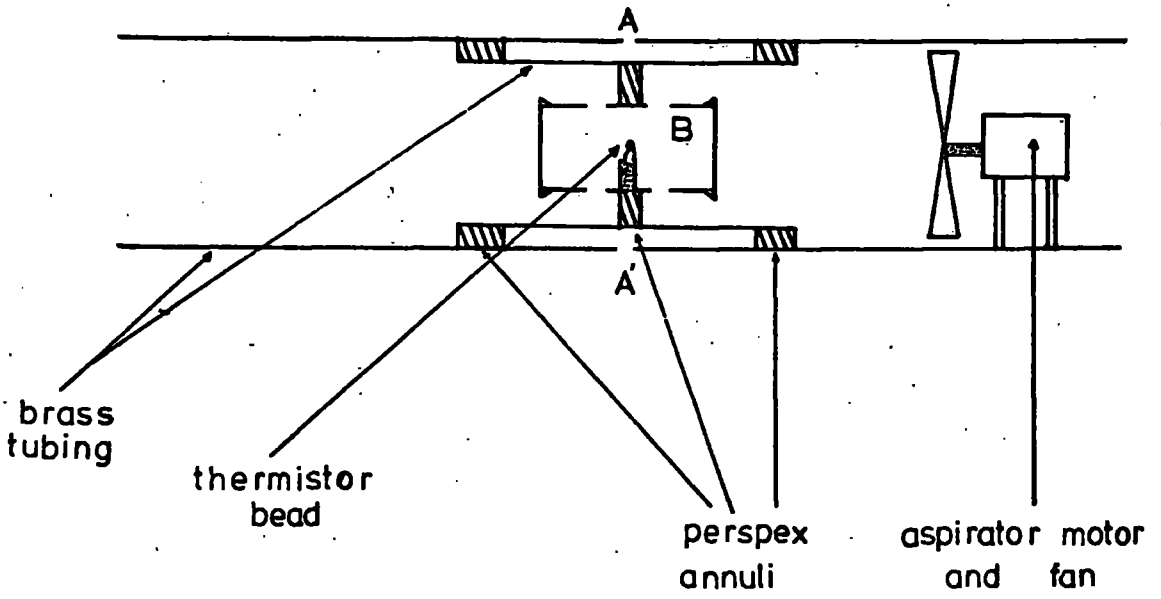

Dwg to 1/2 scale

BIDIRECTIONAL VANE - Sensing circuits

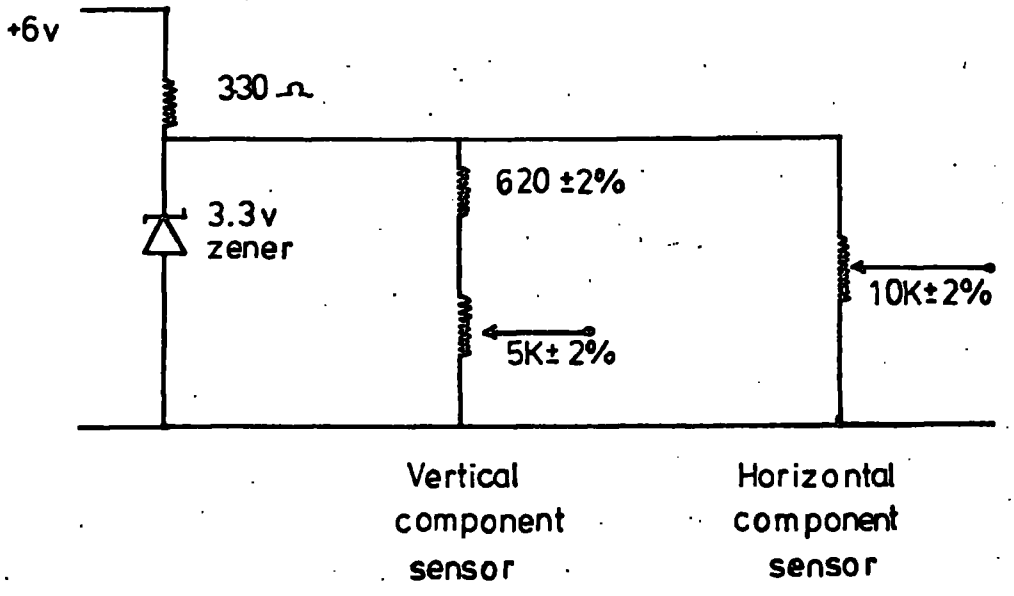

Occasionally a test was conducted in the field to check the coincidence of the thermistor characteristics. The sensors were placed at the same height on the mast and the indicated temperature difference noted. Ideally, of course, the value should be close to zero and, in fact, those observed were invariably less than 0.1°C. This was regarded as quite satisfactory.

It became obvious as experimental work progressed, that when designing the sensor amplifier, an importance factor had been overlooked. At that time it was not appreciated that when the conditions were near neutral (see Sec. 2.6.2.) the temperature gradient near the ground would quite frequently change from a small positive to a small negative value and vice versa. In Sec. 4.6.2.2. it was mentioned that the chopper amplifier employed only responded to the difference in voltage of the input signals, or, in other words, the amplifier indicated the magnitude of the temperature gradient but not the sign. The problem was alleviated in later work by placing a very high input impedence digital voltmeter across the bridge output whilst field work was in progress. This instrument indicated the polarity, as well as the magnitude, of the voltage across the bridge. A written note of the sign of the temperature gradient could then be taken in near neutral conditions.

Apart from this sign ambiguity, the temperature gradient system functioned very well. On one occasion, however, the system failed completely. This was later attributed to a faulty plug connector on one of the thermistor housings.

4.6.4 The Bidirectional Vane

4.6.4.1 General

Neither the author *nor* the Atmospheric Physics Group at Durham had had any previous experience with bi-directional vanes (bivanes). Although many published designs exist in the literature, e.g. CRAMER, GILL AND RECORD (1957), it was felt that these were unnecessarily complex for the project in view. Such instruments had been designed for applications involving surface stress measurements and, in consequence, were required to respond to the entire spectrum of turbulent energy. However, as far as this project was concerned, interest was centred mainly on those larger eddies which might cause the ion plume to be displaced bodily. In order to restrict the response of the bivane to these lower frequencies, its dimensions were made rather larger than usual. In fact, the total length of the bivane was over 1 m.

4.6.4.2 Construction of the Bivane

Fig. P 7 shows clearly the construction of the device. The horizontal and vertical sensing vanes, which were very carefully balanced, were attached to suitable axles and their angular position transduced by means of specially adapted potentiometers . (Limit stops were provided on the horizontal component sensor to prevent damage if violent gusts occurred - these were placed at 50° from the centre position). The circuit of the system is shown in Fig. 4.7.

Potentiometers were specially adapted for this application by bending away the wiper contact slightly, thereby relieving some of the frictional resistance between wiper and track.

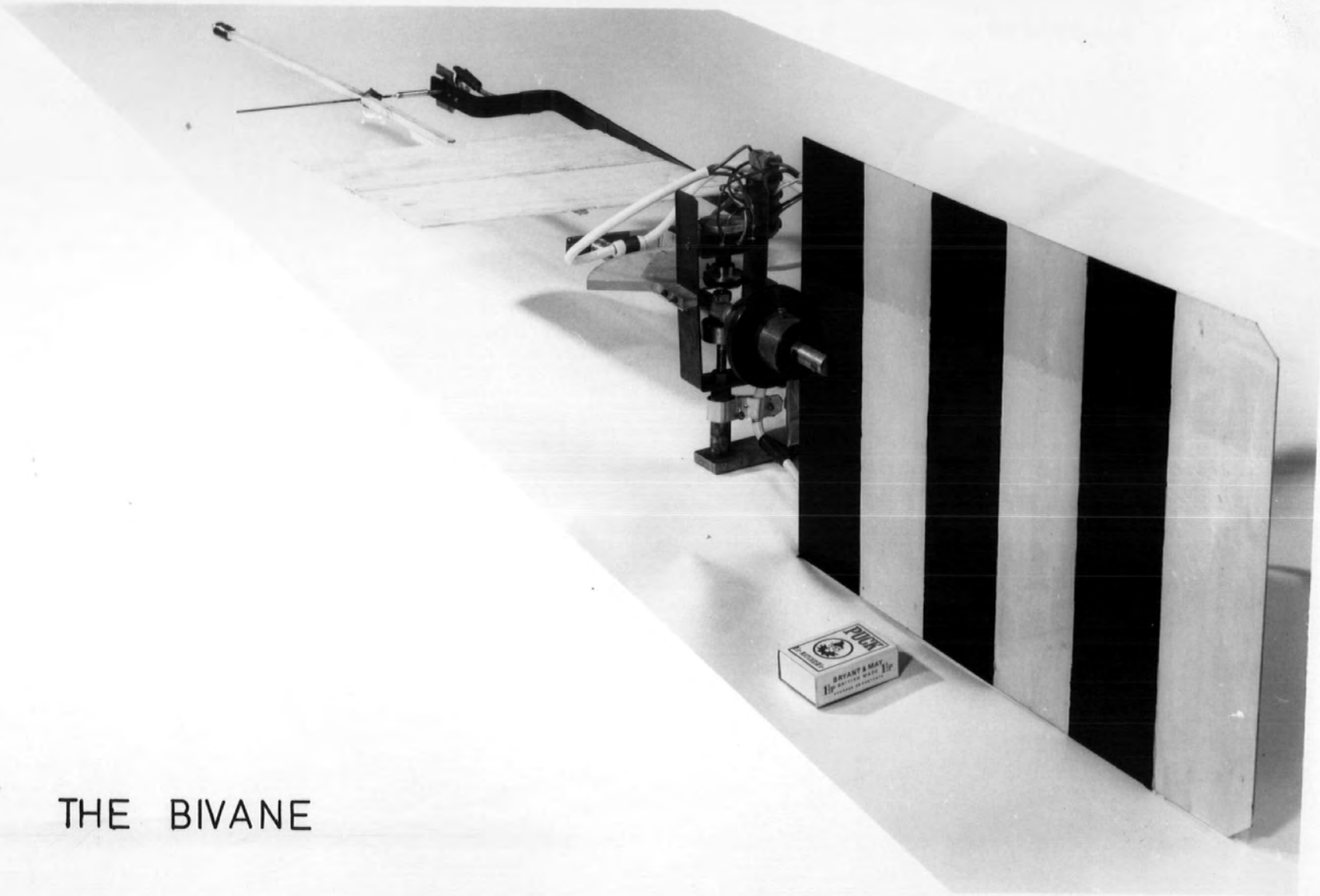

THE BIVANE

This technique was perfectly adequate for the horizontal component sensor but it was noticed, particularly in very light winds, that the vertical component sensor appeared to be sticking. Clearly this was most undesirable as it could easily lead to erroneous values for the vertical component readings. The offending potentiometer was therefore replaced by a proprietary low torque device with noble metal contacts. This potentiometer, a COLVERN type CS 08, had a starting torque of only 0.05 $gm\ wt\ m^{-1}$ and, after this had been installed, no further trouble was experienced.

The vertical sensing vane was constructed from 2 mm balsa wood sheet to achieve maximum sensitivity.

4.6.4.3
Calibration and Peformance

A ruled graticule was attached permanently to the bivane in order to enable the horizontal component sensor to be calibrated in situ. The vertical sensor was checked by fixing a protector to its axis and measuring the variation in output voltage as the sensor was manually rotated. Results of such calibrations are not shown graphically because, as was expected, they are perfectly linear. The results of the sensor calibrations were also expressed in the form of a simple equation, such a technique facilitating later data processing. The equations are given below

$$\alpha = 141 V_\alpha - 114 \qquad (4.5)$$

$$\beta = 86 V_\beta - 67 \qquad (4.6)$$

where α is the vertical component sensor angle, being positive for upward air movement and negative for downward,

β is the horizontal component sensor angle, increasing in the clockwise direction, and

V_α, V_β are the voltage outputs of the vertical and horizontal sensors respectively.

(The angles α and β were measured in degrees.)

It should be appreciated that the angles α and β are specified with reference to the appropriate axes of the bivane itself. In the construction of the bivane great care was taken to ensure that the axes of the two sensors were accurately perpendicular. Additionally, when setting up the bivane on the mast, considerable dexterity was needed to ensure that it was correctly aligned. For this to be achieved the mast needed to be accurately vertical and, further, once the horizontal component sensor had been set, the mast had to be prevented from any further rotation. A second system of guy ropes, attached to the top of the mast, was used to ensure that this could not occur. After initial difficulties, a standard procedure for accurately siting the bivane was eventually devised. The technique involved the use of a prismatic compass and binoculars and, although a little tedious, was reasonably successful.

Apart from the relatively minor difficulties of setting up the bivane in the field, the device worked very satisfactorily. The results obtained from the series of experiments using the bivane are presented in Ch. 8.

4.7 The Photographic Equipment and Smoke Generator

Cine photography of smoke plumes was employed to supplement the bivane observations in the final stages of the project.

Smoke candles, supplied by STANDARD FIREWORKS of Huddesfield, were placed as close to the ion generator as possible, and then ignited by means of long fuses. When a smoke generator

was ignited, two remotely controlled automatic 8 mm cameras, the ion generator and recording system were switched on. These cameras were placed at suitable upwind and crosswind locations, and from the ensuing photographic records, it was possible to trace, accurately, the varying configuration of the smoke plume. Small tungsten bulbs, placed in the field of view of the cameras, were arranged to light once every recording cycle. In this way accurate synchronization between the photographic and data recording systems could be maintained.

In the laboratory the smoke plume configurations were compared with those computed from the bivane data. Results obtained with this technique can be found in Sec. 8.2.4.

Chapter 5: THE DATA HANDLING SYSTEM

5.1 Basic Principles of Design and Operation

The various instruments described in the previous chapter produced analogue voltage outputs proportional to the value of the particular parameters they were measuring. The range of these output voltages lay between 0 and 1.5 *V* and any proposed data handling system had therefore to accept this input.

It might have been possible to use a multichannel pen recorder to monitor the instrument readings directly. However, it was hoped that an alternative system could be devised which would provide a digital output ultimately for computer processing. The use of a pen recorder would not have facilitated this objective and therefore, as well as for other reasons, its employment was not considered any further.

It is well known that data can be stored compactly and conveniently on magnetic tapes and, moreover, a tape recorder would be reasonably easy to handle in the field. Further, it was also possible to obtain a digital output signal from a tape recorder system. These advantages led me to the conclusion that the most satisfactory recording medium, for this project, would be magnetic tapes. Many previous workers, including some at Durham, have, in fact, used this method for recording and storing geophysical data.

An FM instrumentation recorder would, of course, have been ideal for this project, enabling the instrumental outputs to be recorded without further processing. Unfortunately, the purchase of such equipment was beyond the resources of the

Atmospherics Physics Group and consequently an alternative means had to be sought. ASPINALL (1969) was, in fact, confronted with this problem and he overcame it by the employment of a system known as time division multiplexing. In such a system the output from each measuring instrument is sampled in turn and the resulting sequence of values recorded on a single channel recorder. For example, if five parameters were being measured, then the first parameter could be recorded for the first second, the sampler then advancing and the second parameter being recorded for the next second. The system is arranged to operate cyclically and, in the above example, the first parameter would again be recorded for the sixth second.

Clearly the main advantage of this technique lay in the elimination of the need for a multichannel recorder. However, as a particular quantity was only sampled for a fraction of the total time, it was inevitable that certain features present in the variations of the parameter would be lost. The effect which this loss of information has upon the overall performance of the system is discussed in Sec. 6.2.2.4.

Consideration had also to be given, at this stage, to the accuracy of the data handling system. It was decided that, in common with the requirements of previous workers, the system must not, if possible, degrade the accuracy of the individual measuring instruments in any way. In practice, the performance of the proposed system was determined by two factors, firstly the constancy of the tape speed past the heads during the recording and playback operations and secondly, the stability and linearity of the voltage to frequency and frequency to voltage

convertors. Further discussion regarding the accuracy of the system will consequently be postponed until these circuit elements have been described.

The high quality portable audio tape recorder (EMI type L4B), used by ASPINALL in his project, was still serviceable and therefore the present system was designed to operate with this recorder. Whereas an instrumentation recorder could accept DC input voltages without modification this was not the case with an ordinary audio tape recorder, which could only deal with AC signals in a range from approximately 30 Hz to 10 KHz. Consequently, it was necessary to convert the DC signals from the measuring instruments into some type of equivalent AC signal. A technique in which the frequency of an AC signal was modulated by the DC input voltage has been used by ASPINALL. Such a system, the accuracy of which depended solely on the measured frequency of a signal and not on its amplitude, would also be insensitive to changes in recording level and the effects of minor tape defects. The alternative, using amplitude modulation, suffered from both these drawbacks and was not therefore considered suitable.

Previous workers at Durham had processed their recorded tapes to produce a punched paper tape input for the computer. However, I was advised by the Computer Unit that this technique was no longer practical and it was suggested that a more up to date approach be adopted. Fortunately, at about that time, digital voltmeters with automatic printers were just appearing on the market. Further, a colleague, Mr. K. M. DAILY, was about to construct a similar data handling system and so he too might require the use of such a device for his project. The

various possibilities were explored jointly and a WEYFRINGE type 901 "Data Capture Unit" with integral printer was finally selected as the most suitable. The range of this voltmeter was from zero to 199.9 mV, the accuracy being within 0.1 mV of the indicated value. The registered value could also be printed out (on a paper roll) by depressing the printer actuator switch. The printer, which worked at the maximum rate of one value every 3 s, could also be operated remotely and this facility offered the possibility of completely automatic playback of data tapes.

5.2 The Choice of Channel Allocation and Sampling Rate

As mentioned previously, it was proposed to record the outputs of the four field mills, the wind speed, wind speed gradient and temperature gradient systems. Therefore, seven inputs would be required if each instrument were to be allocated a single channel. It occurred to the author that, of the four different parameters chosen for recording, certain of them might be more relevant to this investigation than others. Consequently, effort was directed into assessing the most satisfactory way of allocating channels to optimize data acquisition. It was also felt desirable that a further channel be provided in order that a marker signal could be recorded once per sampling cycle. The function of this marker was to be twofold. Firstly, appearing as it did within an ordered sequence of sampled parameters, any omissions or duplications in the sampling cycling would, on playback, be immediately obvious. Secondly, if a standard voltage were to be applied during the interval in which the marker was being sampled, it would enable a useful check of the consistency of performance of the voltage

to frequency convertor to be made.

After consideration, it was decided that the field mills should be sampled twice as frequently as the micrometeorological instruments and that the inclusion of a marker was definitely worthwhile. Implementing these ideas would raise the total number of channels to twelve although, of course, four pairs of channels would be common.

Early experiments had clearly indicated the need for faster sampling than that employed in the systems used by previous workers. Even with the provision of two channels for each field mill, it was estimated, on the basis of certain theoretical relations, that the system proposed would need to cycle through all twelve channels in not more than 3 s. This relatively high sampling rate was necessary to resolve the high frequencies that were known to be present, particularly in the electric field variations.

5.3 The Sampling and Recording System

5.3.1 Purpose of the System

This system was designed to sample each of the measuring instruments in cyclic sequence and convert their output voltages into a series of AC signals suitable for tape recording. The operation of the system is represented schematically in Fig. 5.1.

THE SAMPLING AND RECORDING SYSTEMS

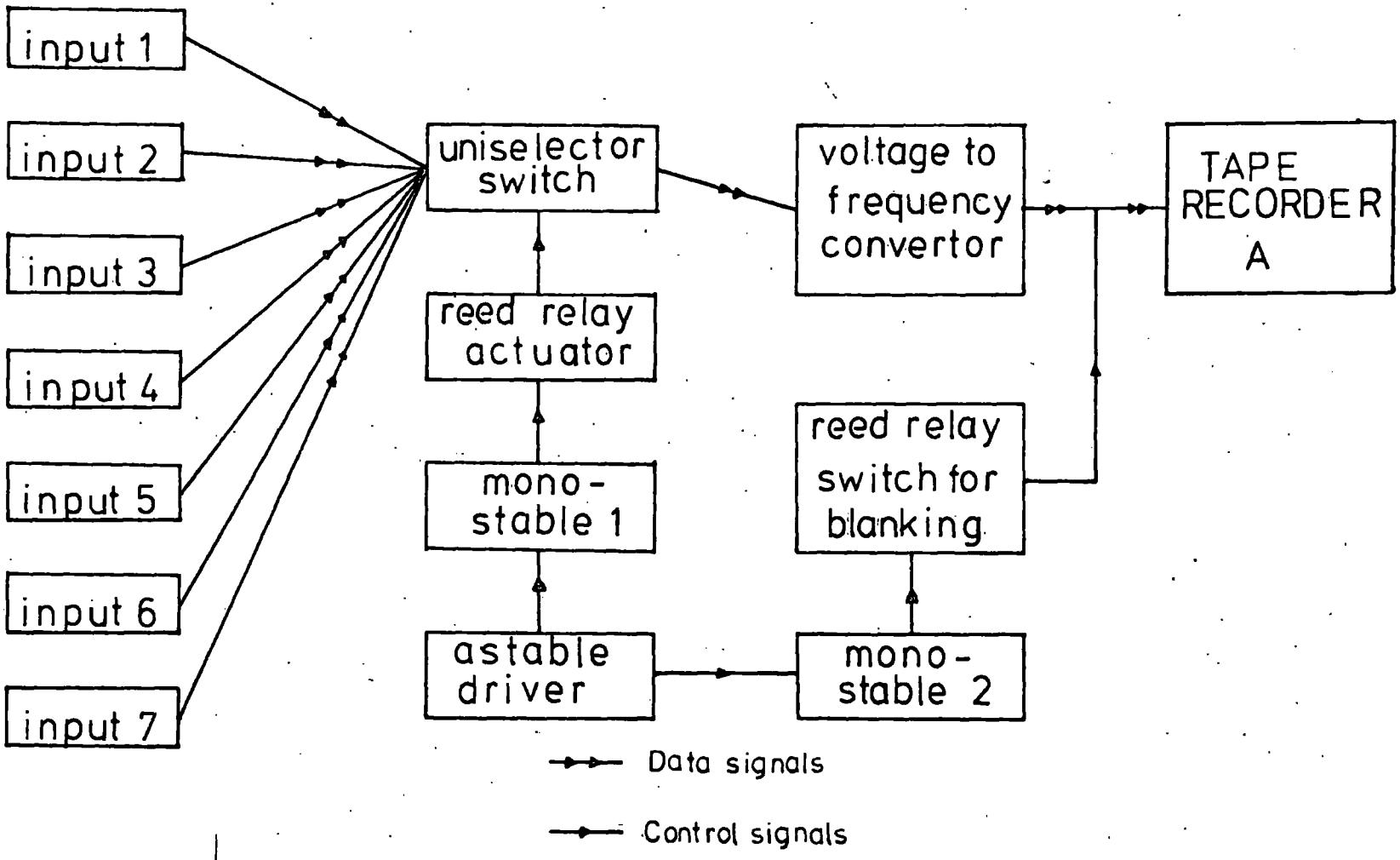

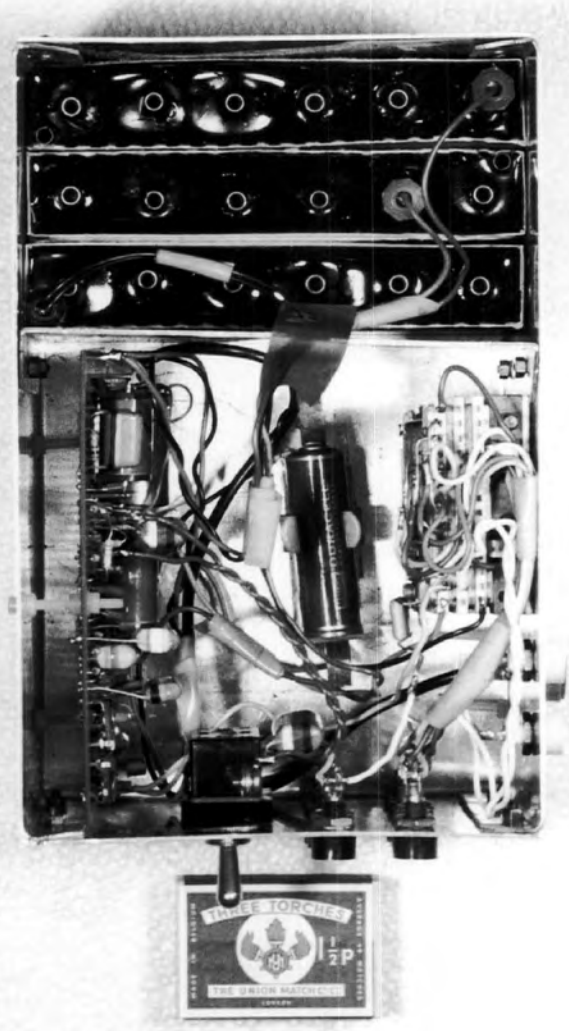

THE SAMPLING UNIT

5.3.2
The Sampling System

ASPINALL (1969) suggested that future sampling systems might be designed employing integrated circuitry. Following discussions with the electronics group at Durham, I realized that such techniques, whilst being eminently suitable for sampling AC signals, were not easily adaptable to sampling DC signals. It was recommended that the use of some type of electromechanical device would, most likely, be far simpler. ASPINALL had himself used reed relays and a quite complex logic system in his experiments. Frankly, the author found the prospect of designing and constructing a system involving twelve reed relays and associated logic a little daunting and was therefore led to consider simpler alternative systems.

The feasibility of employing a uniselector as the sampling device was consequently investigated. (A uniselector is a solenoid actuated multiway switch, a suitable current pulse causing it to advance to the next contact position). Fortunately, the Group already possessed a number of 12 way uniselectors and tests confirmed that such devices could be made to switch at the required speeds.

Fig. 5.2. shows the system that was constructed employing the uniselector. The sampling rate of the system is determined by the pulse repetition frequency of the astable driver. The output square wave from the driver was used to trigger monostable 1 and this, in conjunction with a reed relay, supplied pulses to advance the uniselector.

During the marking interval standard conditions were established in the voltage to frequency convertor by switching a

10 K resistance in parallel with its input.

5.3.3 The Voltage to Frequency Convertor

The ouput from the uniselector consisted of an ordered sequence of DC voltages and could therefore be connected directly to a suitable voltage to frequency convertor.

Previous workers at Durham have employed the circuit of DE'SA and MOLYNEUX (1962) for voltage to frequency conversion. However, the rather small range of output voltage of the measuring instruments used here required that either a different type of convertor be employed or that the signals were suitably amplified. The latter alternative was rejected as trouble had already been experienced with DC amplifiers. None of the published circuits appeared suitable and consequently it was necessary to develop a convertor specifically for this project.

It was known that the pulse repetition frequency of an astable multivibrator is very dependent on the voltage applied to the base timing resistors. The possibility of this voltage to frequency dependence being applied to the solution of the present problem was therefore explored. Suppose V_s was the supply voltage applied to the collector, whilst an excess voltage V were applied to the base timing resistors. This is shown in Fig. 5.2. (In this case the base resistors are R_5 and R_6, the collector resistors being R_7 and R_8). Simple theory indicates that the pulse repetition frequency, f, of such an arrangement is given by the expression

$$f = \frac{1}{2RC \ln\left(\frac{2V_s + V}{V_s + V}\right)} \qquad (5.1)$$

THE SAMPLING AND RECORDING SYSTEMS - Circuit Diagram

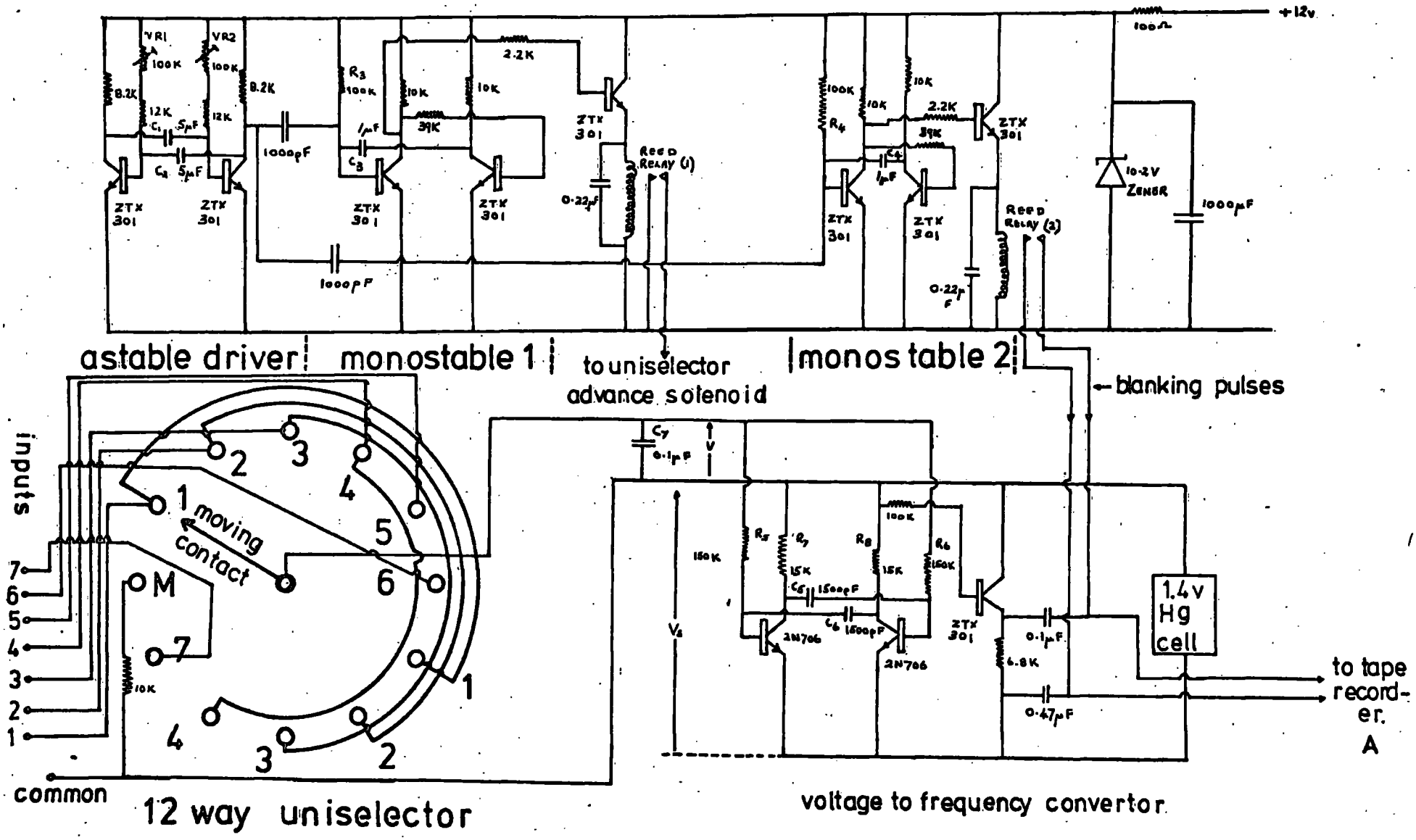

where R is the base timing resistance

and C the timing capacitor value.

(It is worth noting that equation (5.1) reduces to

$$f = \frac{1}{2RC \ln 2} \qquad (5,2)$$

when V = 0. This latter expression, of course, represents the relation between frequency and circuit values for a conventional astable multivibrator).

At this stage a trial circuit was constructed to establish the validity, or otherwise, of expression (5.1). Tests revealed that, not only was the theoretical relation closely adhered to, but also, by a suitable choice of V_s, the collector supply voltage, the voltage-frequency characteristic could be made virtually linear. It was found that, for this project, the optimum value of V_s was about 1.4V It should be noted, however, that as the frequency is also dependent upon the value of V_s, as well as of V, the V_s supply would need to be very stable. High stability was achieved in practice by specifying a mercury cell for this supply. (A mercury cell has a very flat voltage-time discharge curve, thus rendering it eminently suitable for the application in view). A further, and very useful, feature of this design of convertor was its minute current consumption, this being typically about 150μA.

A computed voltage to frequency characteristic for the particular circuit values employed here is shown in Fig. 5.3.

5.3.4
The Blanking Circuits

Early trials with the sampling system revealed that considerable contact noise and other interference was present on the output signal of the voltage to frequency convertor during interchange between input channels. Various attempts to eliminate this interference were unsuccessful, and therefore it was necessary to blank off the output signal during these changeover periods. Later, it was realized that the blanked interval in the signal could be used to trigger the printer on the digital voltmeter and thus make a separate synchronized trigger pulse unnecessary. The blanking signal was generated by monostable (2) (see Fig. 5.2.) The signal, after being passed through a driving transistor, was used to close a reed relay for a suitable length of time during the interchange. After trials the blanking pulse length was set to 70 ms.

Fig. 5.4 shows the types of wave form present in the voltage to frequency convertor and sampling system.

5.4
The Design and Operation of the Playback System

5.4.1
Preliminary remarks

During recordings each parameter was sampled for approximately 0.28 s, the exact duration depending on the setting of the astable driver circuit in the sampling unit. Consequently, if a tape were played back at the same speed as it had been recorded at, then the resultant output signal would consist of a series of tones each about 1/4 s in length. However, the fastest speed at which the digital voltmeter could reliably operate was one value per 3 s. It was decided, therefore, that a second tape recorder would be needed in order to playback

Computed voltage to frequency convertor characteristic

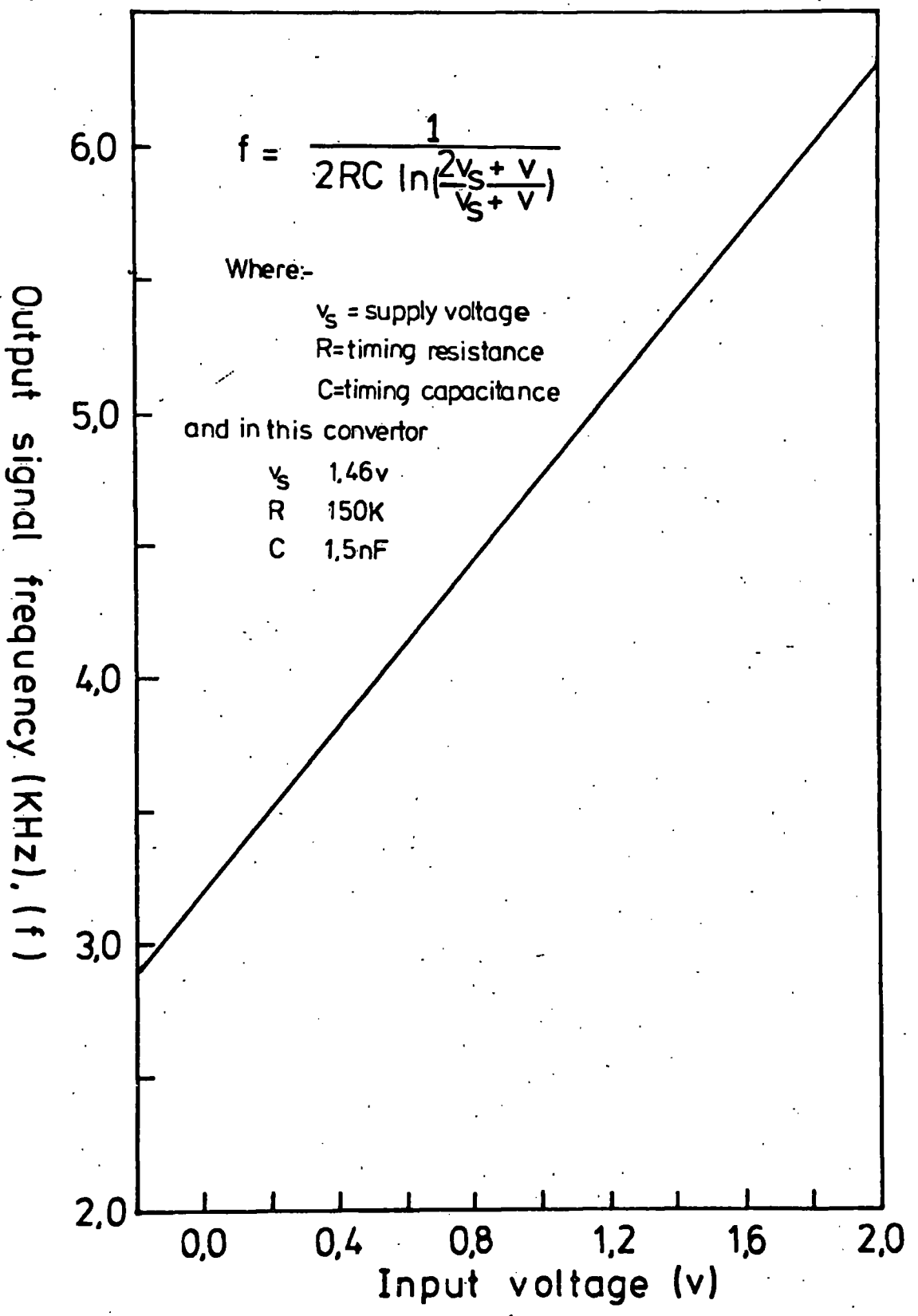

THE WAVEFORMS IN THE SAMPLING AND RECORDING SYSTEMS (not to scale)

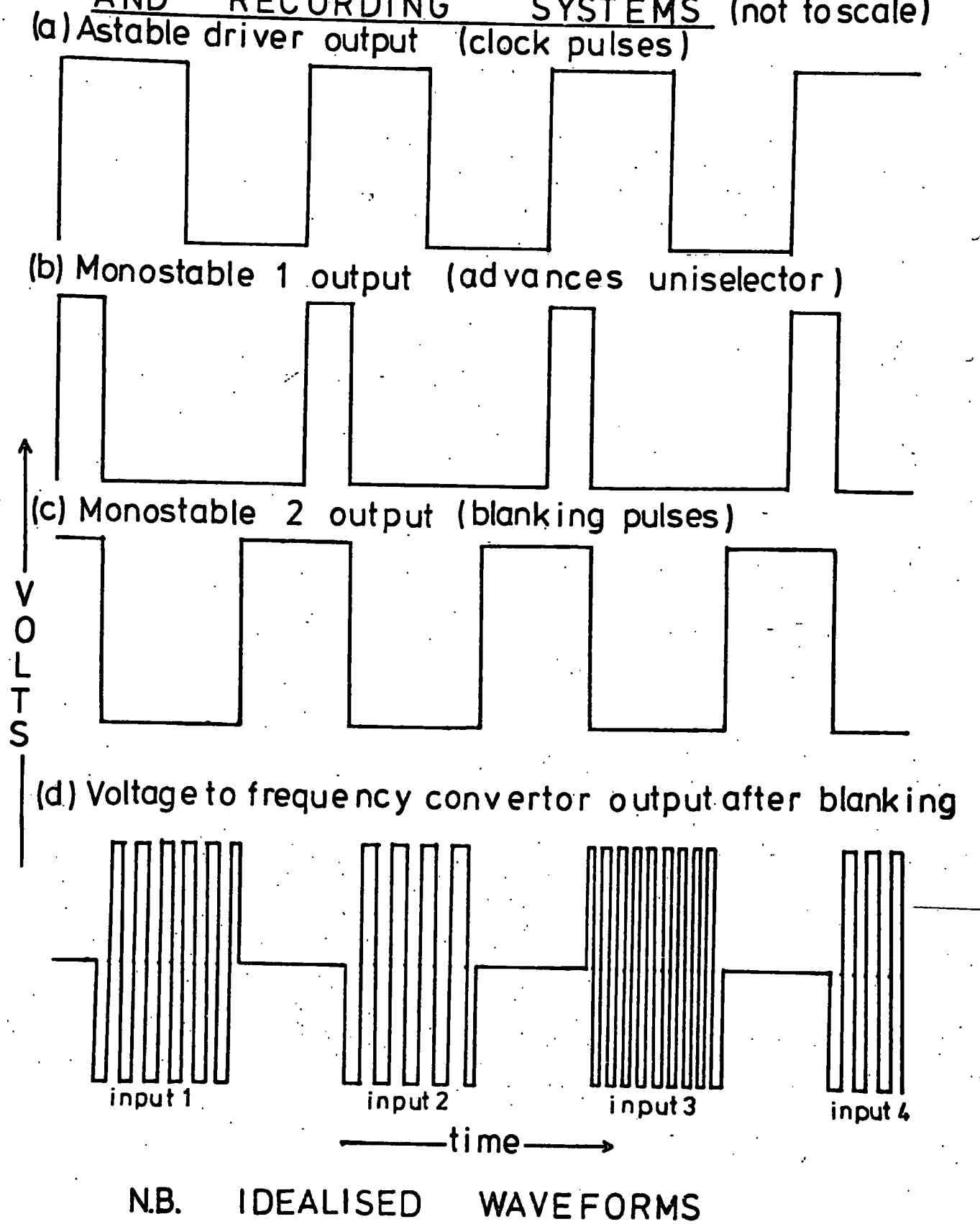

N.B. IDEALISED WAVEFORMS

tapes at a speed sufficiently low for the digital voltmeter to work satisfactorily. The portable tape recorder used for recording in the field operated at 7 1/2 IPS (inches per second) and consequently, in order to dilate the recorded signals sufficiently, it was necessary for the second tape recorder to operate at 0.6 IPS or less. A possible alternative might have been to record data tapes at speeds much higher than 7 1/2 IPS but this was regarded as unsatisfactory because, amongst other problems, vast amounts of tape would be required for any reasonable duration of recording.

A conventional mains-powered domestic tape recorder was obtained, and, by carefully modifying the drive system, it was possible to achieve a tape speed of just under 0.5 IPS. This was done by attaching additional reduction pulleys between the motor and existing systems and by carefully grinding down the capstan shaft to half its original diameter. A very high degree of concentricity needed to be maintained in the ground down capstan because any error would have caused tape speed variations. Wow and flutter would hence be created on the playback signal and this would result in a serious loss in the accuracy of the system.

This specially modified tape recorder will henceforth be referred to as tape recorder B. To emphasise this distinction, the portable tape recorder employed in the field will be termed tape recorder A.

5.4.2

The Frequency to Voltage Convertor

The function of this system was to convert the series of tones appearing at the output of tape recorder B into a sequence of DC voltages suitable for logging by the digital voltmeter. The rôle of the convertor is represented schematically in Fig. 5.5.

The voltage to frequency convertor in the recording system operated in the range 2 - 6 KHz. The tape speed during playback was about 1/15th of that during recording and hence the frequency of the playback signals was in the range 130 - 400 Hz. This wide difference between the recording and the playback signal frequencies had, of course, to be borne constantly in mind when designing both systems. Setting the voltage to frequency convertor range too low would not have allowed the frequency to voltage convertor to operate correctly. Alternatively, if the voltage-frequency convertor range had been set too high the limited response of the portable tape recorder would have inhibited the performance of the system. In practice, the choice of frequency ranges proved quite satisfactory for both convertors.

The operation of the frequency to voltage convertor is briefly as follows. Incoming trains of pulses from tape recorder B are fed into the Schmitt trigger circuit (see Fig. 5.6.). This serves to increase the squareness of the pulses and to remove unwanted noise. The shaped pulses are then allowed to trigger monostable A. The output of this circuit consisted of a series of pulses of constant width, their frequency, of course, being equal to that of the incoming signal. These pulses are then clipped in the emitter follower circuit by a zener diode. After clipping, the pulses are integrated by an RC network, and

THE PLAYBACK SYSTEM

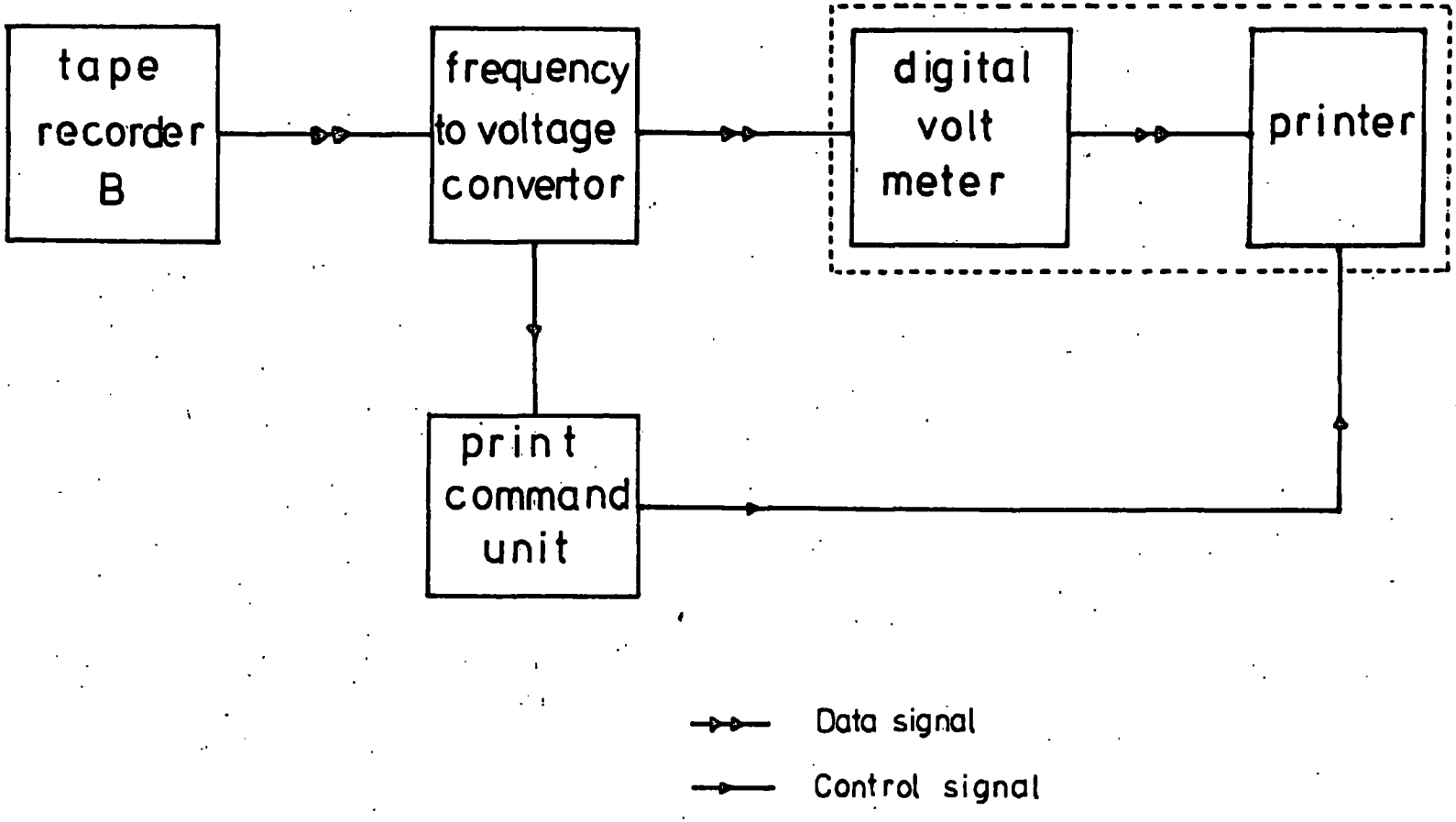

THE PLAYBACK SYSTEM - Circuit Diagram

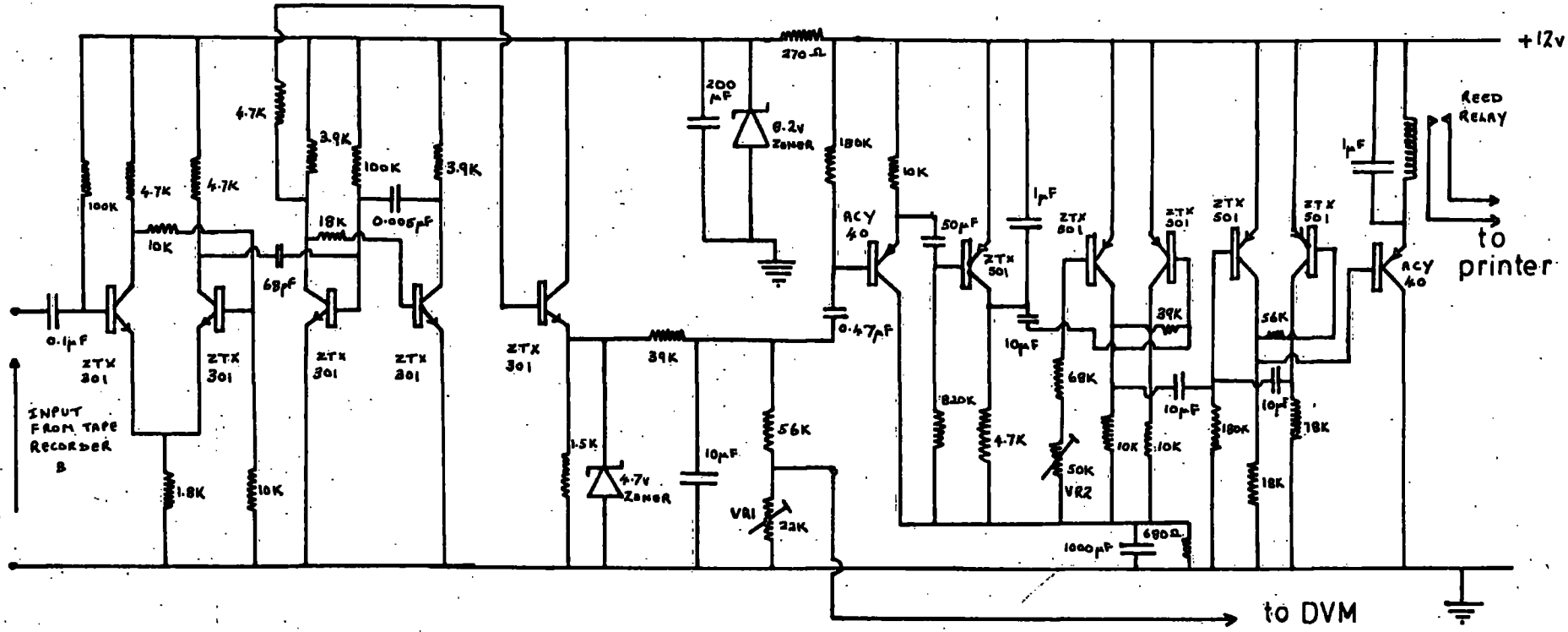

Schmitt Trigger	Monostable A	Emitter follower & pulse-rate integrator	Differentiator	Monostable B (Delay)	Monostable C	Output Driver

FREQUENCY TO VOLTAGE CONVERTOR | PRINT COMMAND UNIT

because of the constant height and width of the pulses, the output of this circuit depended only on the pulse frequency.

The time constant of this integrating circuit is of crucial importance to the correct functioning of the convertor. Too long a value would not have allowed the output voltage to have reached its final value within the span of the pulse train, whilst too short a time constant would have resulted in there being unnecessary ripple on the output voltage. In the present system the value of this time constant was set to 0.3 s. This ensured that the output voltage was within 1 per cent of its ultimate value before it was printed by the digital voltmeter. The form of the integrator output voltage, together with other waveforms, is shown in Fig. 5.7.

5.4.3 The Print Command Unit

It proved possible to derive a print trigger signal from the output of the integrator in the voltage to frequency convertor. This output, after being taken through a buffer amplifier, was differentiated by a long time constant CR network. The type of output produced by this circuit is shown in Fig. 5.7(c). It will be noted that a positive pulse is produced on the arrival of each train of pulses from tape recorder B. Consequently, if a suitable delay circuit were triggered by the arrival of these positive pulses then it should be straightforward to provide a trigger signal at an appropriate time. The optimum moment for such trigger pulses to occur is indicated by the X's in Fig. 5.7(b). A satisfactory delay circuit was developed employing, as is conventional, a monostable multivibrator, the trimming resistor VR2 being used to adjust the delay to the desired

value (monostable B). A further monostable (C) was then employed to supply the reed relay coil with a suitable current pulse, the digital voltmeter printer operating on closure of the relay contacts.

It should be mentioned here that the use of p-n-p transistors in this unit, instead of the n-p-n types as elsewhere, was a result purely of availability, the unit having been originally designed to use the n-p-n variety.

5.5 The Calibration of the Data Handling System and its Subsequent Performance in the Field

5.5.1 Considerations affecting the Accuracy of the System

System accuracy would depend largely on the following factors:

(i) The performance of the voltage to frequency and frequency to voltage convertors.

and (ii) the constancy of tape speed in both tape recorders.

It was decided, before any attempt be made to calibrate the system as a whole, that those units on which the accuracy depended most heavily should be individually assessed.

The voltage to frequency convertor was already known to be satisfactory in terms of linearity and stability of output, these features having been closely investigated during the development of a suitable circuit. It was, however, discovered that, with the design of convertor being used, a small reverse voltage was generated across its input terminals. The origin of this voltage was traced to the effect of the base current flowing to the transistors in the convertor. This current, when flowing through the output resistance of voltage source connected to the convertor, produced the small reverse

WAVEFORMS IN THE PLAYBACK SYSTEM (not to scale)

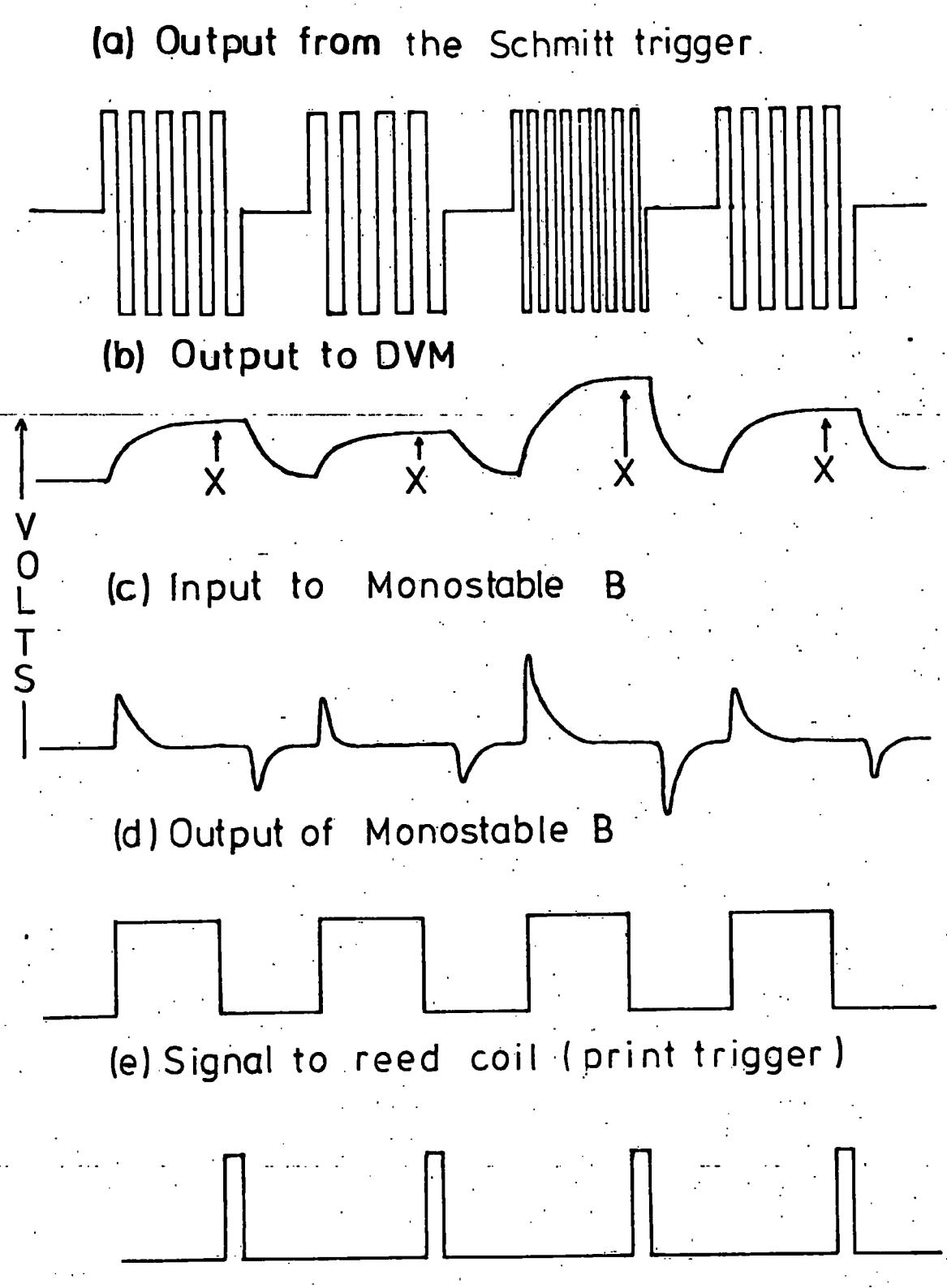

N.B. IDEALISED WAVEFORMS

Playing-back a data tape

voltage. Typically this voltage was no greater than 0.1V and, once its existence was appreciated and understood, no further difficulty was experienced.

The frequency to voltage convertor was tested directly by applying a square wave signal, whose frequency could be varied, and monitoring the output voltage. The results of such a test are shown in Fig. 5.8(a) and indicate a very satisfactory performance.

The tape recorders were checked by the following method. A constant frequency signal of suitable amplitude, provided by a high quality signal generator, was recorded onto magnetic tape by one of the tape recorders. The tape recorder under test was then made to playback the recorded tape into the frequency to voltage convertor, the output being connnected to a pen recorder. During playback some small random variations were apparent in the outputs of both recorders, the large fluctuations being, as expected, in tape recorder B. The magnitude of these speed variations was never greater than 2 per cent of the average value and thus caused only a minor loss of accuracy.

It was possible, with all but the earliest observations, to provide some compensation for these minor tape speed variations. This was achieved during computer processing of the data, the ratio of the actual value of the marker signal (see Sec. 5.2.) to its value during calibration being used as a correction factor. The use of this technique, whilst not completely eliminating errors from speed variations, provided a convenient and effective means of substantially reducing them.

5.5.2
Calibration of the Data Handling System

Attention was now directed to establishing the characteristics of the data handling system as a single entity. The relationship of principal interest was, naturally, that between the input voltages presented to the sampler unit (and recorded as tones on magnetic tapes) and those voltages ultimately printed out by the digital voltmeter during playback. It was evident from previous work that the relationship would be closely linear, but a feature of equal, if not more, importance, was the long-term stability of the entire system.

The most obvious method of calibrating the data handling system appeared that of maintaining a number of stable and accurately known voltage inputs to the sampling unit, recording a tape, and then playing that tape back over the playback system. Standard voltages were obtained from three potentiometer networks supplied by a stable voltage source. The voltages chosen for the tests were 0, 0.5, 1.0 and 1.5, these values representing the full working range of the system. The stability was better than 1 mV for the duration of a recording. The recorded tape was played back in the normal manner.

After this test it was possible to accurately determine the voltage transfer characteristic of the system. The values printed out by the digital voltmeter were punched onto computer cards, and with the aid of a suitable computer program, their means and standard deviations found. The mean output voltages versus the input voltages are shown in Fig. 5.8(b). The standard deviations, which are too small to be illustrated

RECORDING AND PLAYBACK SYSTEM

(a) Frequency to voltage convertor performance

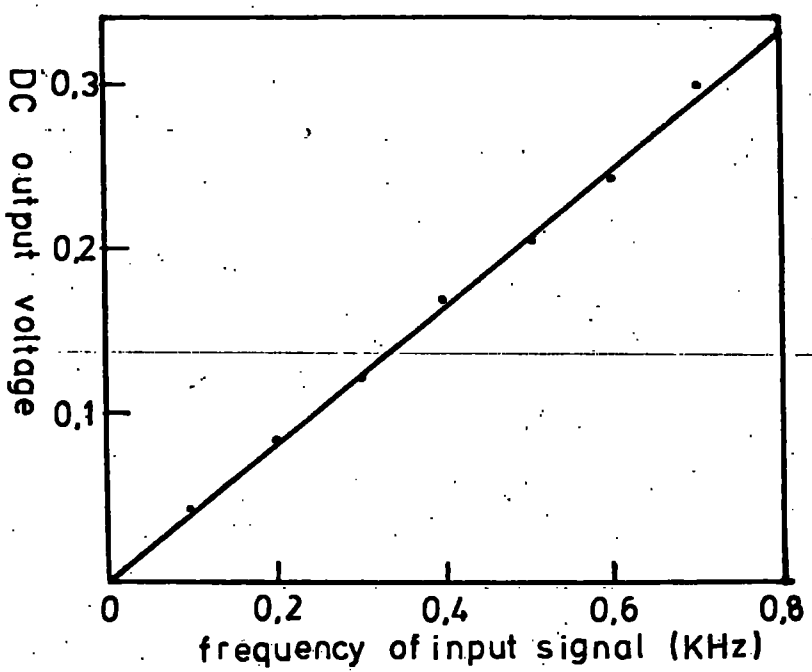

(b) Over-all performance

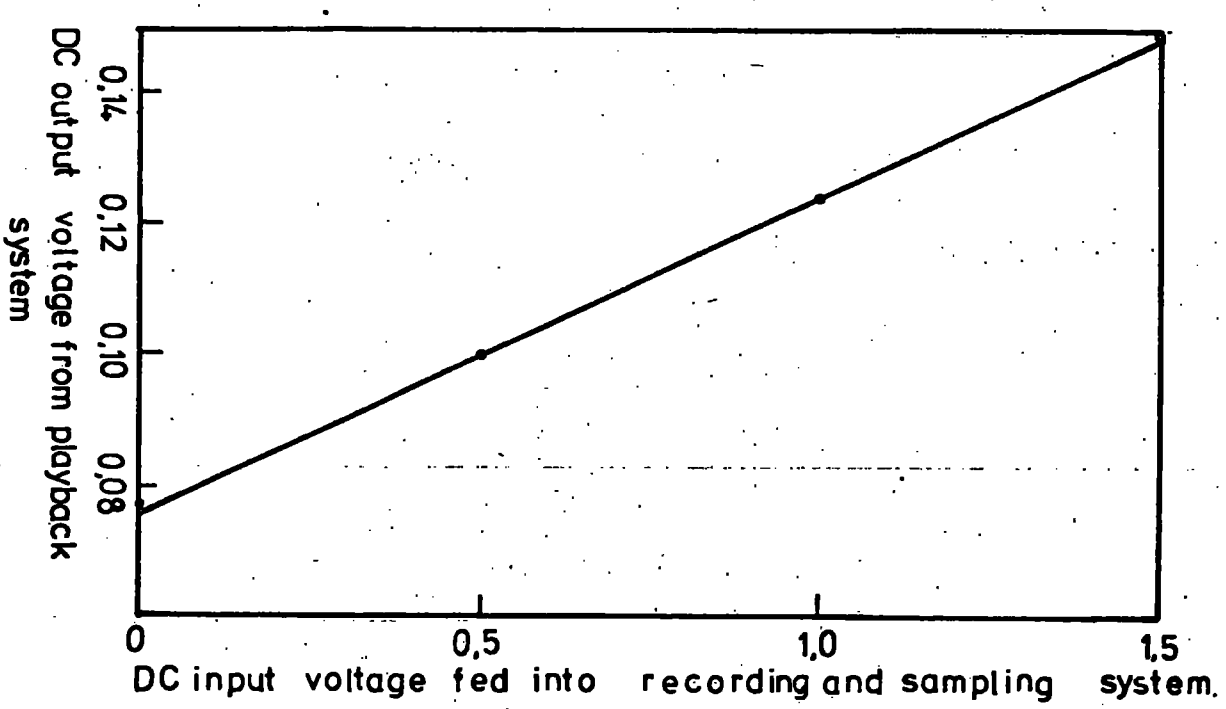

in the figure, were less than 1 per cent of the mean values at all four calibration points. This was most satisfactory and, at this point the data handling system was considered ready for service in the field.

As a precaution the entire calibration procedure was repeated at monthly intervals. After a few months it was found that departures from the original calibration were quite negligible, and because of this, subsequent calibration checks were only considered necessary at three monthly intervals. It emerged, as a result of these periodic tests, that the long-term stability was only marginally less good than the short-term performance.

5.5.3 The Performance of the System in the Field

Despite the careful design and rigorous testing of the system in the laboratory prior to field work, some irritating, though relatively minor, faults did appear.

Upon analysis of the recorded data it became clear that the voltage to frequency convertor was more sensitive to temperature variations than had been expected. This posed problems, particularly during intermittent sunshine, as the temperature of the convertor could change by as much as 20°C. In total these shifts in characteristic never exceeded 3 per cent and were therefore not too serious. Once the effect had been noticed the sampling and recording unit was always placed in a shady position. The problem did not recur once this action was taken.

After some use the uniselector switch contacts became dirty and this resulted in erratic voltages being transmitted to the voltage to frequency convertor. The application of a proprietary contact cleaning fluid at regular intervals cured this problem.

Apart from the occasional difficulties mentioned above, the system functioned extremely well, and, once recording had been started, could be relied upon to function without further attention. This was ideal as it enabled the author to undertake any supplementary observations needed or to check that other equipment was working efficiently.

Chapter 6: TECHNIQUES USED TO ANALYSE THE OBSERVED DATA

6.1 Introductory Topics

6.1.1 The Series I and II experiments

The relationship between the behaviour of a plume and the prevailing atmospheric stability was discussed in Sec. 2.7., whilst particular electric field patterns that might be associated with various plume configurations were mentioned in Sec. 3.6. Field work was therefore directed, at least initially, to the recording of electric fields under ion plumes in various conditions of stability. The electric fields were measured by four field mills whilst the atmospheric stability was monitored by the two anemometers and thermistor system. The wind speed and temperature gradient measurements would ultimately be used to compute the Richardson number, thus allowing comparisons between different field runs to be made.

After considerable experimental work of the type described above had been undertaken it emerged that the results, though excellent in themselves, were not really providing as much information as was hoped. However, it had been realized by then that the introduction of a recording bivane could be of considerable assistance in understanding ion plume behaviour (see Sec. 2.8.). Consequently such a device was constructed and employed in all later field work. In practice, it proved necessary to sample the bivane readings as frequently as possible and, in order to provide sufficient input channels, the existing instrumentation arrangements were modified. In fact, the number of field mills had to be reduced to three, only one anemometer could be used and the differential temperature system was dispensed with.

These two instrumental arrangements described above will be referred to subsequently as the Series I and Series II systems respectively.

6.1.2 The form of the data and the need for statistical analysis

In both the Series I and II field work all data was recorded on magnetic tapes by the methods described in Ch.5. These data tapes, once recorded, were returned to the laboratory for processing by means of the playback system. During recording, parameters were sampled in cyclic order, and therefore the series of values printed out by the digital voltmeter on playback would be in a corresponding sequence. The actual sequence depended, in practice, on the nature of the particular run and, of course, on whether a Series I or II type of experiment was being conducted.

During any particular field run, most of which lasted 24 min., a different parameter was sampled every 0.28 s and, as a result, in the region of 6000 'values' would be recorded on a single tape. On playback the same number of values was printed on the paper roll, there being approximately 1000 values per double channel and 500 each for the remaining single channels (see Sec. 5.2.).

The direct analysis of such a large amount of data, particularly in the form of a long roll, was almost impossible. Therefore techniques had to be devised to cope ultimately with many similar volumes of data. The need for a statistical treatment of some type was quite evident from the sheer quantity of data. However, it was hoped that the recorded data could also be processed to render graphical records so that the behaviour of the various

quantities could be examined visually. A further possibility was that of comparing the observed data with results obtained from the plume models. This is discussed in Sec. 6.4.

6.2 The Application of Statistical Techniques to the Analysis of Observed Data

6.2.1 The choice of suitable methods

There was little doubt that the electric field under an ion plume would vary in complex manner with time and space, the variations being, of course, the result of both the localized nature of the ion plume and the fluctuations of concentration within it due to turbulence. It was expected that, whilst the nature of the field variations themselves would be complicated, certain of their overall characteristics might depend in a fundamental way on the atmospheric stability and other experimental circumstances. (Here, the term 'overall characteristics' is used to refer to the general impression one might gain by a casual glance at a potential gradient record. Thus, for example, one would be immediately aware of the presence of large oscillations in the potential gradient values).

In order to compare the results of experimental runs made in different conditions, it was obviously necessary to devise methods of assessing this overall character of the recorded variations. Graphical presentations of the data might have been useful in this respect but it was felt that comparisons between records would be very tedious and, as a result, time consuming. Consequently, statistical methods were regarded

as being more suitable. Incidentally, it was hoped that inspection of graphical records would serve better as a means of analysing particular events rather than entire runs. In view of this we shall now consider how we can expect the electric field to depend on various parameters, and after arriving at some simple conclusions, propose a scheme of statistical analysis.

It seems obvious that, close to an ion plume, the mean electric field would be considerably larger than at a distance. Further, because of the erratic behaviour of all plumes, the variations of electric field would most likely also be greater near the plume. Thus, in statistical terms, the values of the mean and standard deviations of the electric field should depend, to a considerable extent, on the closeness of the measuring point to the ion plume. Of course, at large distances downwind, where the artificial ion concentration would be very low, both the mean and standard deviation of the electric field will approach their natural values.

The mean and standard deviation, although clearly of great importance in characterizing the electric field, tell us nothing about the speed with which the variations occur. The rapidity of the field changes depends on many factors, but principally on the height of the moving charges and their velocity. In practical terms this implies that the frequency of the electric field variations should be largely determined by the ion source height and the wind speed.

As well as the importance of the time scale of the variations, it would often be useful to be able to estimate the connexion between sets of observations taken at different locations. This is important because the relationships between such measurements

were expected to reveal considerable information about the nature of the ion plume (this aspect is discussed further in Sec. 3.6.).

Initially therefore, the means, standard deviations and correlations would be computed for each set of data. Later it was expected that, in the light of experience, certain additions and refinements to the techniques would be required. A discussion of the statistical methods, including the later modifications, now follows.

6.2.2 A synopsis of the statistical methods

6.2.2.1 Introduction

The application of statistical techniques to the analysis of geophysical data is by no means novel. In studies of atmospheric turbulence particularly, statistical approaches have been regarded as virtually standard since the classical work of TAYLOR (1935). In atmospheric electricity statistical methods have also been applied but their use has not been so widespread as in the previous case. Several workers at Durham, e.g. SHARPLESS (1968), have used simple statistical concepts in their data analysis. However, ASPINALL (1969) extended these methods in analytical work on frontal precipitation. In fact, his techniques have much in common with mine, even though, of course, they were devised for a very different purpose. ASPINALL includes a comprehensive discussion of the statistical methods he employed and therefore only a summary is presented here.

6.2.2.2
Means and standard deviations

Mean values were computed in the usual manner, that is by a calculation of the type

$$\bar{X} = \frac{1}{n}\sum_{i=1}^{n} X_i \qquad (6,1)$$

Here, as before, the overbar denotes the mean value, while X_i , $i = 1, 2, 3, 4 \ldots\ldots n$, represents the series of values whose average is required.

The standard deviation, σ_x , of the values of X was computed as is usual, by the following relation

$$\sigma_x^2 = \frac{1}{n}\sum_{1}^{n} (X_i - \bar{X})^2 \qquad (6,2)$$

The quantity σ_x^2 is known as the variance, and both this and the standard deviation indicate the amount of variation present in the values of X.

Sometimes it is of interest to consider the relative, rather than the absolute, variation in a quantity. A useful measure of this, known as the coefficient of variation, CV , is defined by the ratio

$$CV = \frac{\sigma_x}{\bar{X}} \qquad (6,3)$$

6.2.2.3
Cross-correlation techniques

The application of cross-correlation techniques to establish the relationship between pairs of variables is well known, see for example RACTLIFFE (1962). As a first step the cross-

covariance C_{xy} of the variables X and Y is formed by using the relation

$$C_{xy} = \frac{1}{n} \sum_{1}^{n} (X_i - \bar{X})(Y_i - \bar{Y}) \qquad (6,4)$$

A cross-correlation coefficient, R_{xy}, can then be obtained by normalising C_{xy} by the product of the standard deviations of each variable. The modulus of R_{xy} varies between zero, in which case the variables are essentially uncorrelated, and unity which implies perfect correlation - either in phase or in anti-phase depending on the sign. Expressing this mathematically we have

$$R_{xy} = \frac{C_{xy}}{\sigma_x \sigma_y} \qquad (6,5)$$

It will be observed in equations (6.4) and (6.5) that corresponding elements of each series have been correlated. That is the i^{th} element of the X series has been correlated with the i^{th} element of the Y series. Suppose the electric field were being recorded at two points downwind of the ion plume. This is shown diagrammatically in Fig. 3.11(a). It is clear from the electric field records depicted in the figure that a maximum cross-correlation will occur when either of the records is displaced in time by an amount equal to the transit time of the feature causing the field variations. Thus we could profitably extend the calculation of the 'simple' cross-covariance in equation (6.4) to include cases where the two sets of variables have been displaced with respect to each other. We now express this idea mathematically, denoting the cross-covariance at a displacement of l intervals by the quantity $C_{xy}(l)$. Hence

$$C_{xy}(l) = \frac{1}{n-l} \sum_{i=1}^{n-l} (X_{i+l} - \bar{X})(Y_i - \bar{Y}) \qquad (6,6)$$

The quantity l is usually known as the lag number and for meaningful results to be obtained it should not exceed $i/10$.

In a similar way we can normalise equation (6.6) to obtain the cross-correlation coefficient $R_{xy}(l)$ at lag number l. Thus

$$R_{xy}(l) = \frac{C_{xy}(l)}{\sigma_x \sigma_y} \qquad (6,7)$$

As a particular, but very important, case of cross-correlation analysis we can compute the correlation of a particular variable with itself at various time lags. Denoting this autocovariance, as it is known, by $C_x(l)$ we can write

$$C_x(l) = \frac{1}{n-l} \sum_{i=1}^{n-l} (X_{i+l} - \bar{X})(X_i - \bar{X}) \qquad (6,8)$$

Similarly we may normalize $C_x(l)$ by the variance of X to produce the autocorrelation coefficient at lag number l, $R_x(l)$; hence

$$R_x(l) = \frac{C_x(l)}{\sigma_x^2} \qquad (6,9)$$

The importance of $R_x(l)$ is that as it expresses the correlation of a variable with itself at various time lags it is consequently a sensitive measure of the time scale of the variations present in X .

In order to assist the reader various types of auto- and cross-correlation behaviour are shown in Fig. 6.1, together with notes concerning the nature of the variations giving rise to them.

It should be noted here that the lag number l is related to the displacement time τ, by the expression

$$\tau = sl$$

where s is the sampling interval.

6.2.2.4 Spectral analysis

It is intuitively reasonable to expect that a connexion might exist between the shape of an auto-correlation function and the variations when expressed in the form of a spectrum. Thus for example, in Fig. 6.1(a), the auto-correlogram which falls off the more rapidly (A) would obviously contribute a greater proportion to the variance at higher frequencies than the less rapidly varying autocorrelation function (B). It can be shown, subject to certain limitations which need not trouble us here, that the autocorrelation function and spectral density can be expressed as Fourier transforms of each other. In mathematical terms we have

$$G_x(f) = 4 \int_0^\infty C_x(\tau) \cos 2\pi f \tau \, d\tau \qquad (6, 10)$$

where $G_x(f)$ is known as the power or variance spectral density of the variate X. In fact, $G_x(f)\,\delta f$ represents the contribution to the variance of X arising from variations

within the frequency range f to $f+\delta f$. It should be noted that in the evaluation of $G_x(f)$, the quantity $C_x(\tau)$ is, by implication, a continuous function of τ . This may be so in some cases but in this project, owing to the discrete nature of the recorded data, the autocorrelation can only be calculated at those time intervals which are multiples of s , the sampling interval. Further, as the upper limit of integration is infinity, we apparently need to know the variation of $C_x(\tau)$ for all time. Clearly this is a practical impossibility, for we can only obtain realistic values of $C_x(\tau)$ up to a time equal to $ns/10$. The practical effects of these limitations are twofold, firstly the spectrum can only be evaluated within a particular range of frequencies and secondly, the contributions to the variance must be estimated in discrete bands. Actually by a suitable choice of sampling interval and running time, which controls n , these limitations need in no way be detrimental to the results.

A further source of trouble resulting from discrete data is that it can give rise to an effect known as aliassing. Variations which occur at frequencies higher than $1/2s$ cannot be resolved from those which occupy slightly lower frequencies. Consequently when a variance spectrum is computed from such data, contributions arising from frequencies higher than $1/2s$ are 'folded' into the spectrum near this high frequency limit. In view of this, caution must be exercised when considering the magnitude of the spectral density function near the high frequency limit. For a fuller discussion on this and related topics the reader is referred to BENDAT & PIERSOL (1966).

Typical auto- and cross-correlation patterns

(a) autocorrelation behaviour

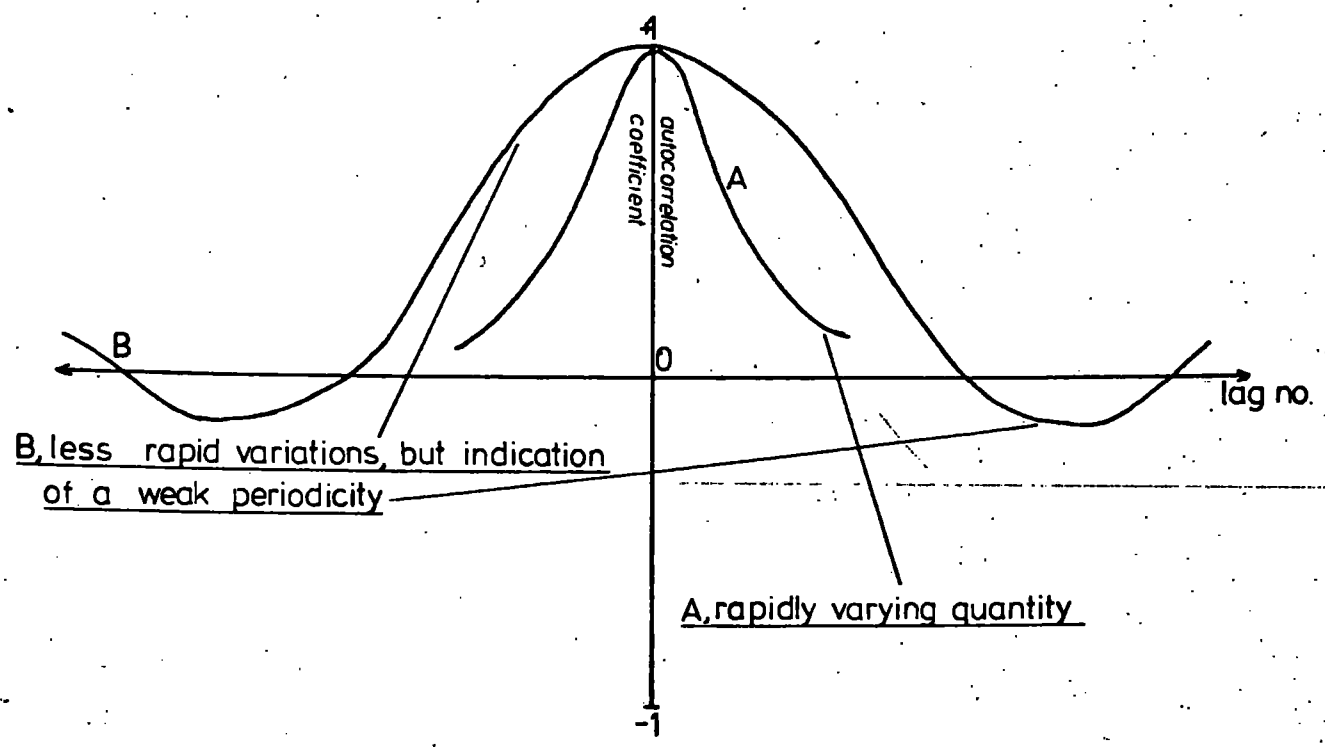

(b) crosscorrelation behaviour

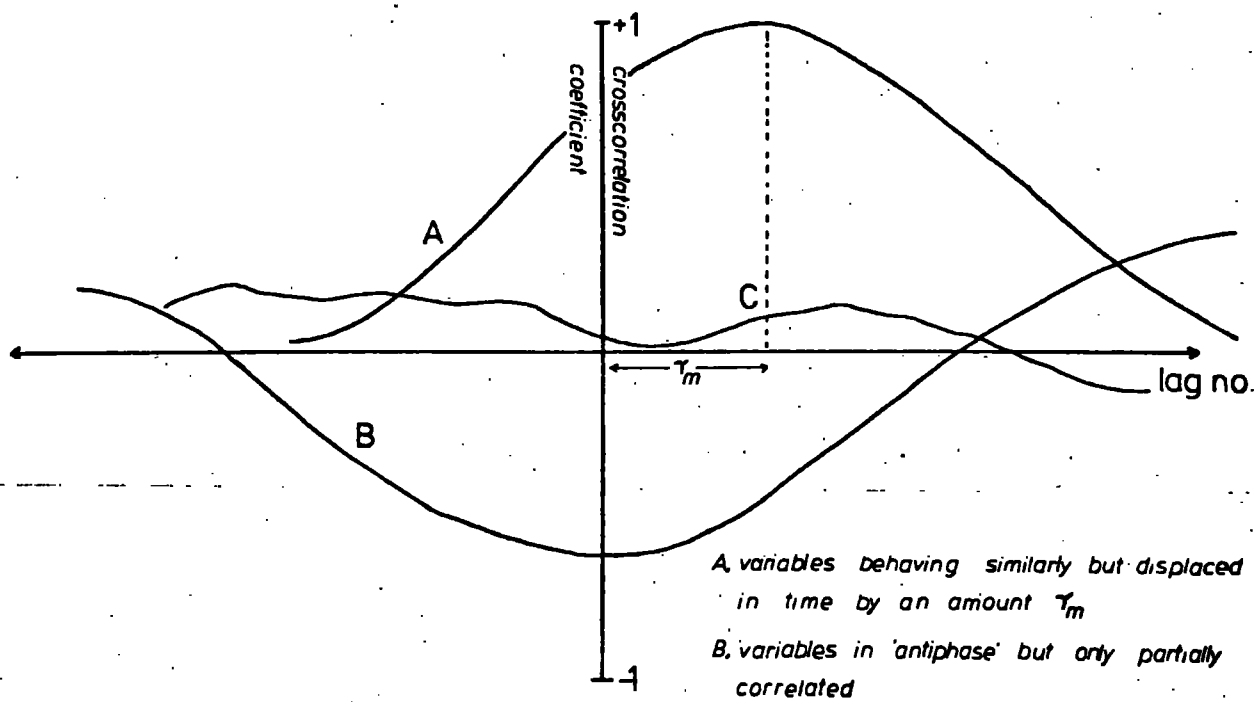

A, variables behaving similarly but displaced in time by an amount τ_m

B, variables in 'antiphase' but only partially correlated

C, variables virtually uncorrelated

It is also possible to form spectra by applying Fourier transform techniques to the *cross-covariance* functions. In this case, however, the situation is more complicated because of the mathematical nature of the cross-covariance. It is found, on taking the Fourier transform, that the resulting spectrum is a complex quantity and has the general form

$$G_{xy}(f) = Co_{xy}(f) - j\,Q_{xy}(f)$$

The real part is known as the cospectral density function whilst the imaginary part is referred to as the quadrature spectral density function. A discussion on the significance of $Co_{xy}(f)$ and $Q_{xy}(f)$ is beyond the scope of this thesis and in any case is well documented in the literature.

The quantity

$$Coh_{xy}(f) = \frac{\left[G_{xy}(f)\right]^2}{G_x(f)\,G_y(f)} \qquad (6,11),$$

which is known as the coherence of the variables X and Y at the frequency f, does however, have a simple physical interpretation. It represents, in fact, the relative contribution made to the total cross-correlation by variations occuring at the frequency f. As the value of such a concept may not be immediately obvious we shall illustrate its use by means of an example.

At a given wind speed and ion source height the rapidity of an electric field variation will depend on the dimensions of the charge system being blown past the measuring point. Obviously

a larger system will cause lower frequency variations than a smaller one. Suppose now we consider the connexion between the electric fields measured at two points separated in space. It should be clear that similar low frequency variations are likely to appear on both records because of the large scale charge systems producing them. (This argument, of course, only applies when the separation between the two points is not too great.) However, the high frequency variations, which arise from the movement of more local and smaller-scale charges are unlikely to be similar at both measuring stations. Expressing this idea in statistical terminology we would say that, in the above situation, the coherence between the records is larger at the low frequency end of the spectral range. The use of coherency analysis, which enables us to quantify the variation of cross-correlation with frequency, might therefore be of assistance in establishing the dimensions of the charge systems causing the field changes.

In a similar manner we may also consider the relative phase between the two electric field variations as a function of frequency. This is expressed mathematically by the relation

$$\phi_{xy}(f) = \tan^{-1} \frac{Q_{xy}(f)}{Co_{xy}(f)} \qquad (6,12)$$

the quantity $\phi_{xy}(f)$ being known as the phase spectrum of the variables X and Y .

6.2.2.5
Shape Analysis

After a number of graphical records of electric field had been examined it was evident that the variations were often of a characteristic shape. The larger electric field peaks were relatively narrow with sharp maxima, whilst the smaller peaks were broader and rounder. We may readily explain this by considering the behaviour of the electric field variations caused by two similar moving charges, one of which passes close to the measuring point, the other remaining more distant. The vertical electric field, due to a given charge, is proportional to $(\sin\phi)/R^2$ (see Sec. 3.3.). In the case of the more distant charge both the $\sin\phi$ and $1/R^2$ terms change only slowly, the $1/R^2$ term never becoming large. On the other hand, these terms change rapidly during the passage of a charge near the measuring point, and at the minimum distance of separation, the $1/R^2$ term can attain large values.

The effects described above result in the electric field variations being asymmetrically distributed about their mean value, rather in the manner shown in Fig. 6.2(a). It is, in fact, possible to quantify this 'skewness' of a variation by computing its third moment about the mean, and then normalizing by division with the cube of the standard deviation. (Further details can be found in LUMLEY & TENNEKES (1972)). Expressed mathematically the skewness, S_x, is given by

$$S_x = \frac{\sum (X_i - \overline{X})^3}{n\,\sigma_x^3} \qquad (6,13)$$

A further quantity of interest is the kurtosis or flatness factor. This function 'weighs the tails' of the distribution and responds strongly to the different types of variation

shown in Fig. 6.2(b). The kurtosis is expressed by the formula

$$K_x = \frac{\sum (x_i - \bar{x})^4}{n\ \sigma_x^4} \qquad (6,14)$$

(Again further details may be found in LUMLEY & TENNEKES).

This completes the discussion on the statistical methods.

6.3 The computer programmes used to process the data

6.3.1 *Introduction*

It is not the intention of this section to consider the 'text' of the computer programmes as such a discussion would be inappropriate in this thesis. Copies of the programmes, which were written in FORTRAN IV, are, however, included for reference (see appendix).

A computer programme, once written, was transferred onto punched cards and then, together with the appropriate data and control cards, was submitted to the computer. After the programmes were known to be functioning satisfactorily they were 'stored' under their 'name' on magnetic discs. During subsequent computing, access to any particular programme could be obtained by referring to that name. It was also found worthwhile to store programmes in compiled form as this saved considerable computer time when processing data.

A valuable additional feature available at Durham was that of computer plotting facilities. The 'plotter' which worked in a similar manner to a conventional chart recorder, enabled both observed data and theoretically derived results to be presented graphically. Extensive use has been made of this facility

The skewness and kurtosis of a varying quantity

(a) skewness

a function with positive skewness

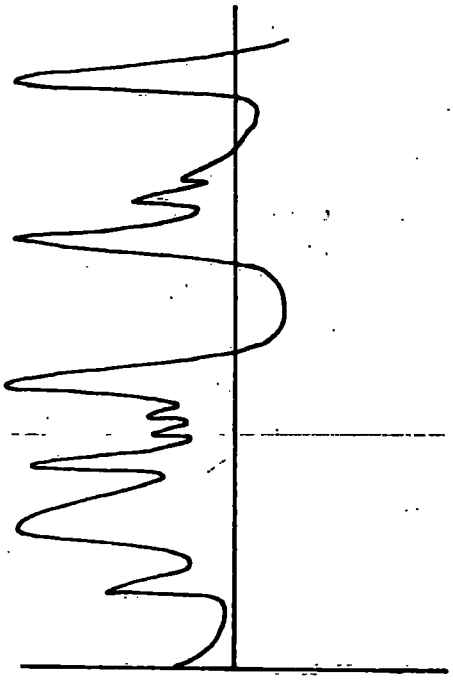

a function with negative skewness

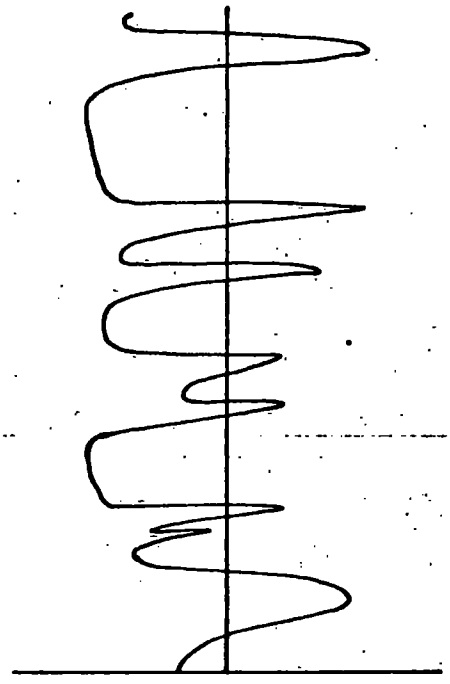

(b) kurtosis

a function with small kurtosis

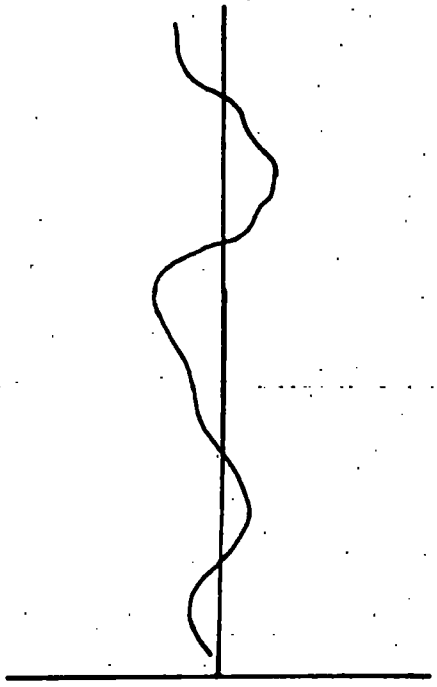

a function with large kurtosis

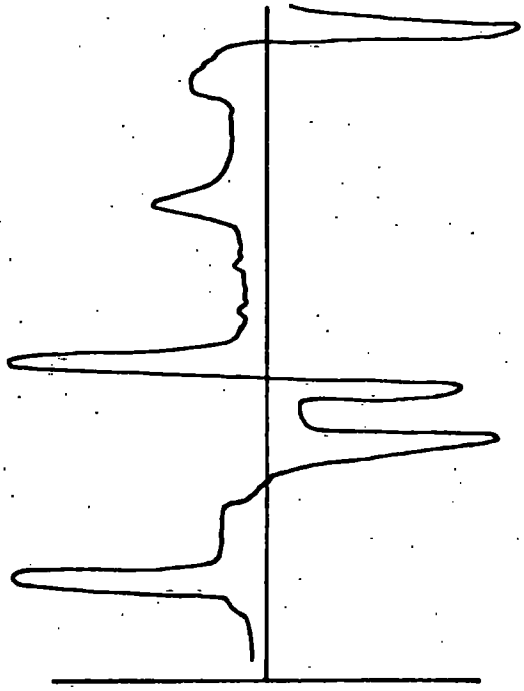

in preparing the observed data for analysis.

6.3.3.2 The Series I Programmes

The elements of these programmes are shown in Fig. 6.3., little additional comment being required here. Originally all analysis was undertaken using DATAPROG. Later, when interest was centred on the spectral and shape aspects of the data further analysis was performed with SUPPROG (supplementary programme).

The rôle of the digital filter will be discussed in Sec. 6.3.4.

6.3.3.3 The Series II Programmes

The basis of the two programmes used to process this data is shown in Fig. 6.4., the bulk of the computing being undertaken with BIVANEPROG.

Final experiments in this series involved the visual comparison of computed plume configurations, derived from bivane data, with those obtained directly from the cine photography of a smoke plume. In order to facilitate these comparisons the derived plume configurations were plotted with the aid of PLMPOSNPROG (plume position programme). Details of this experimental technique are given in Sec. 4.7., whilst results obtained with it are discussed in Sec. 8.2.4.

It was felt worthwhile, having already determined values for the three wind velocity components u, v and w, to compute the magnitude of the surface stress. This quantity was calculated using equation 2.7., and the reader is asked to consult Sec. 2.3. for the details. The numerical value of this stress,

while having little direct bearing on this work, is nevertheless of considerable interest. A great deal of published data exists on the surface stress and comparisons between these values and those observed might indicate, if nothing else, whether the bivane system was working satisfactorily. As observed values of the surface stress are presented in Ch. 8., comments on the bivane performance are reserved until then.

6.3.4
The use of digital filters

It should be understood that the rôle of a digital filter is essentially no different from any other type of filter, the idea being, in all cases, to suppress unwanted features of incoming data or signals.

It was found that spectral analysis of the electric field data often revealed the existence of very large variance contributions from the lowest frequencies. These contributions were, in fact, the result of large scale charge systems, e.g. clouds, passing over the field work area. Such very low frequency variations were of little relevance to this project but unfortunately their presence detracted from the overall quality of the computed spectra. This problem also confronted ASPINALL (1969) and his remedy was to filter the data prior to spectral analysis. A similar approach was discovered to be equally satisfactory in this case and ultimately a high pass filter of the type

$$X(K) = X(K) - P.X(K+1)$$ (as in FORTRAN usage)

Computer processing of Series I data

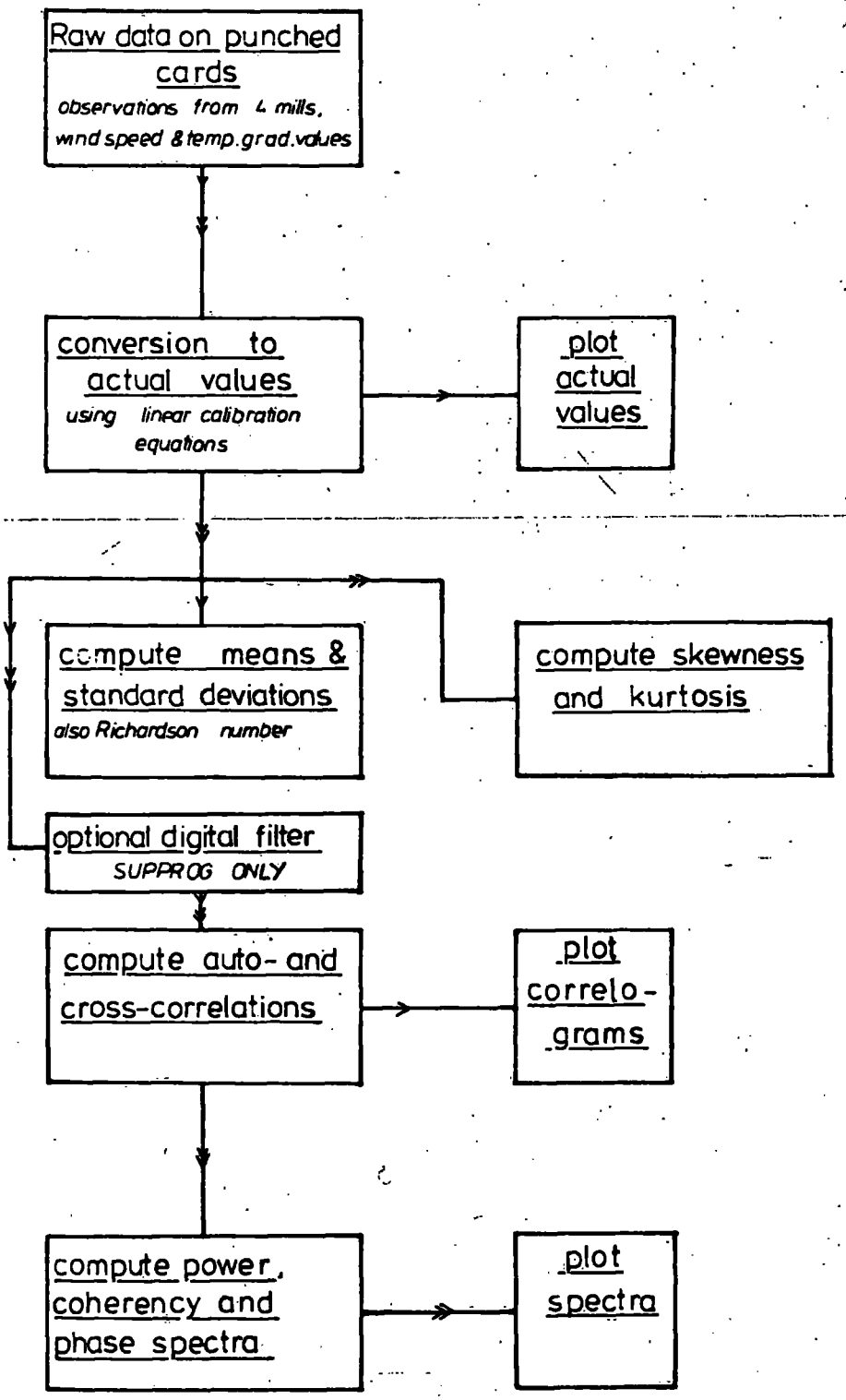

PROGRAMMES → DATAPROG →→ SUPPROG

Computer processing of Series II data

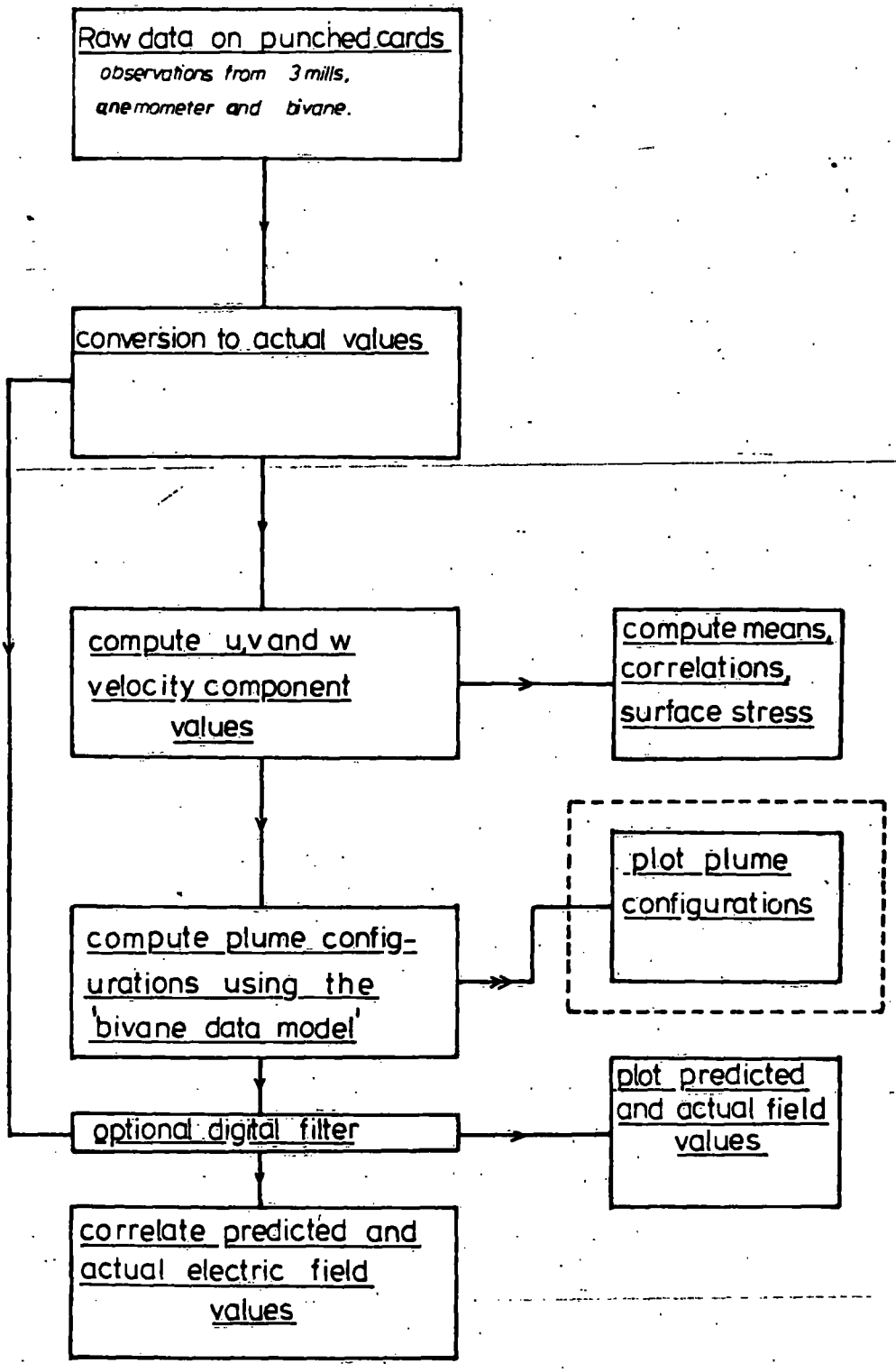

PROGRAMMES → BIVANEPROG →→ PLMPOSNPROG

was chosen. (See ACKERMANN (1964)). (Here $X(K)$ represents the K^{th} value in a sequence of values of X). Filtering action was obtained here by subtracting out any trends which were present in the data. The coefficient P , which must be ascribed a value between zero and unity, is used to control the degree of filtering. In practice, its value was adjusted empirically to obtain balanced spectra.

In the case of the Series II data analysis, inspection of the predicted and actual electric field records revealed that most of the disagreement between them was in the 'fine structure' of the variations. This was, of course, only to be expected, because the bivane data model, with its relatively coarse integration steps, could not possibly predict the details of the field variations. Thus, to suppress the higher frequencies, where it was unrealistic to demand good agreement, the two sets of values were put through a suitable low pass digital filter. The type of filter employed, which was originally intended for smoothing spectral estimates, is of the form

$$X(K) = 0,25.X(K-1) + 0,5.X(K) + 0,25.X(K+1)$$

and, in effect, takes a running mean of the quantity to be filtered. Further details of the method, which was originally due to HANN, can be found in BLACKMAN & TUKEY (1958).

6.4 Typical results obtained with the steady-state and oscillating plume models

6.4.1 Introduction

In practical terms, the steady-state and oscillating plume models proved rather disappointing. Neither model was capable of imitating the most important feature of all turbulent motion - its irregularity. Although the existence of this randomness was appreciated from the outset its importance was underestimated and this resulted in the models being, frankly, rather unrealistic. More successful models of turbulent diffusion have been based on numerical techniques used in conjunction with a random number generator, e.g. THOMPSON (1971). Originally it was hoped to compare observed electric field data with that obtained from the models but in many cases this was a rather futile exercise. However, despite their inherent limitations, the results obtained from the models are of some interest and demonstrate, at least in a general way, certain features which do occur in reality.

6.4.2 The steady-state model

The electric field under the 'steady-state' plume was calculated in the manner detailed in Sec. 3.4.2. Fig. 6.5. shows results, in typical conditions, of such calculations made at various points under an ion plume. (The validity of assuming a plume configuration of this type has already been considered elsewhere and no additional comments are needed here - see Sec. 2.8.)

If the plume were treated as a line charge then the electric field would continue to increase as one moved downwind

Computed electric field values obtained with the 'steady-state' plume model

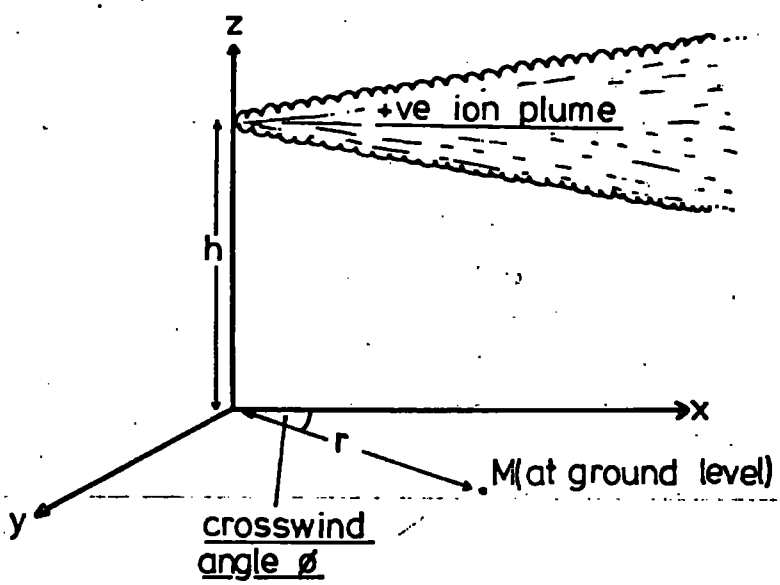

Conditions for this run:-
ion source +0,3uA 10m
wind speed 1ms^{-1}
plume dimensions were appropriate to neutral conditions

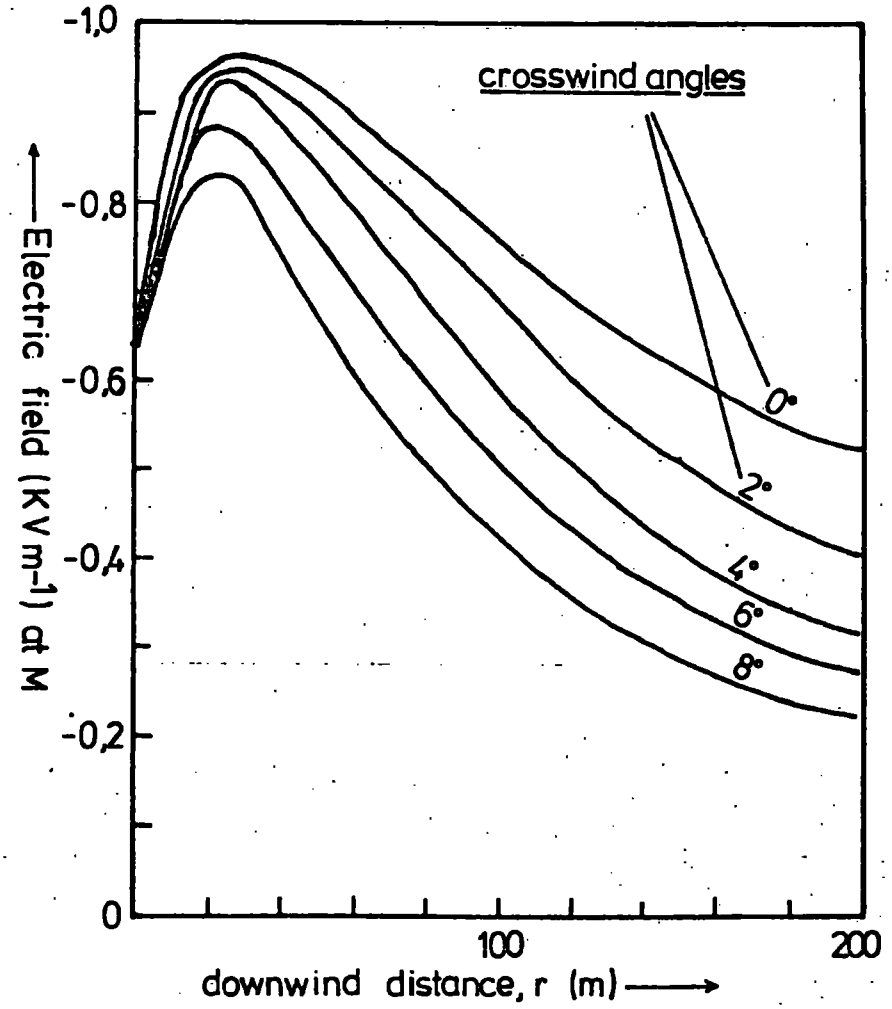

directly beneath it; however, in reality this effect must be offset against those of turbulent diffusion and electrostatic forces which tend to broaden the plume. In practice, and in the model, the combination of these various factors results in the electric field attaining a maximum value at a definite distance downwind.

It was found, after a number of computer runs with the steady-state model had been completed, that certain useful conclusions could be drawn. At any particular point, M say, the electric field E_m , for a given eddy diffusivity, depended on the source height h , the source current i and the wind speed u , in the following way

$$E_m \propto i$$
$$E_m \propto 1/u \qquad \text{VERY APPROXIMATE}$$
$$E_m \propto 1/h$$

(These relations could, in fact have been deduced on the basis of the relevant equations in Chs. 2 and 3). The main use of such relations was that they permitted electric field values to be determined, at least approximately, in other conditions without recourse to the computer.

Also of interest, though only indirectly in this work, are the values of electric field away from the surface. In these circumstances, of course, the horizontal components are no longer zero, the total electric field at any point being the vector sum of its three components. A calculation, using a steady-state model, was undertaken for a plume of the type found in stable conditions, some results being shown in Fig. 6.6. It should perhaps be emphasised again that the magnitudes of the electric field values obtained with this model

are not realistic because electrostatic expansion effects have been ignored. However, the various trends shown in the behaviour of the field components should persist regardless of the plume width. No further comments are included here as unfortunately it was not possible to actually measure the horizontal components and therefore comparisons with observed data cannot be made.

6.4.3 The oscillating plume model

This model, which has been described in detail in Secs. 2.8.3. and 3.4.4., was an attempt to simulate the looping plume characteristic of unstable conditions. Thus, in the sense that the computed electric field was not constant but varies with time, this model was more realistic than the steady-state model. The main weakness of the model was, as expected, the omission of crosswind and vertical diffusion in the modelled plume. The importance of this factor was appreciated at the outset, but it was estimated that a single computer run, incorporating these diffusive effects, might take longer than one hour. Unfortunately, such amounts of computing time were not easily available and therefore the limitations of the model had to be accepted. (Perhaps this is an appropriate point to emphasise that the concept of a looping plume with crosswind and vertical diffusion is thought to approximate quite closely to reality).

A set of results which typify those obtained using this model are now discussed. The values of electric field underneath a plume executing vertical loops are shown in Fig. 6.7. The electric field is, of course, a varying quantity and, in con-

Some results obtained using the 'steady-state' plume model

Computed electric field components near an ion plume

ELECTRIC FIELD VALUES ARE AT 100m DOWNWIND. CROSSWIND ANGLES AS SHOWN.

ION SOURCE 1μA at 10m WIND SPEED 1ms^{-1}

PLUME DIMENSIONS APPROPRIATE TO STABLE CONDITIONS

Some typical results obtained using the 'oscillating plume model' (see also fig 2.5)

This run simulated a plume with vertical loops. Values ascribed to the various parameters were:-
$A_y=0$, $A_z=0{,}17$, $F_y=0$, $F_z=0{,}03$, $U=1 ms^{-1}$, $H=10m$, $1\mu A$ ion source

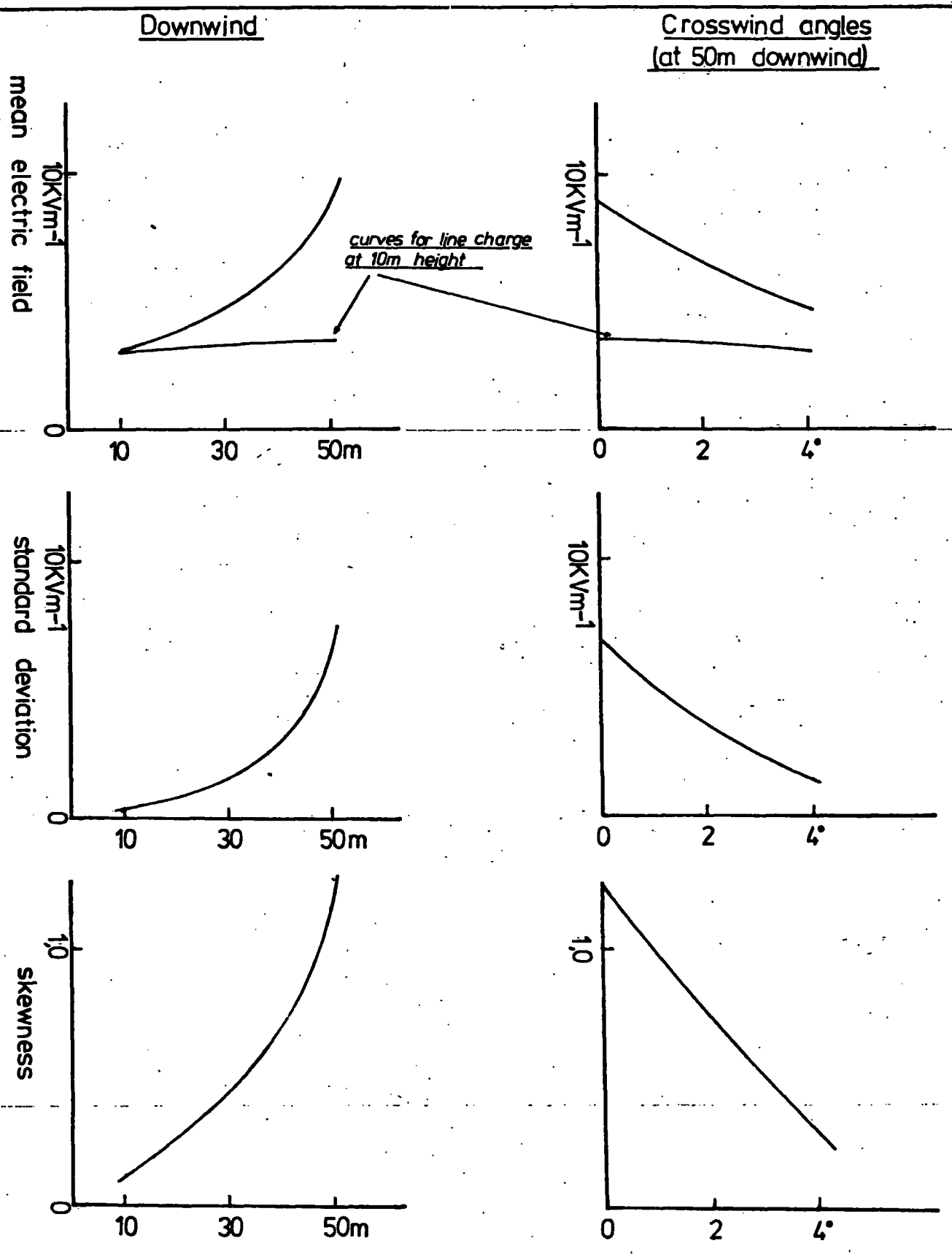

sequence, we may calculate its mean, standard deviation and other statistical quantities. In this example the field has been computed at 10, 30 and 50 m downwind of the ion source and also for crosswind angles of 2^{o} and 4^{o} at the 50 m position. The value of the constant A_z was chosen so as to make the plume descend, in its looping action, to within 1.5 m of the 50 m downwind point. In the model the amplitude of the oscillations was arranged to increase linearly with downwind distance and therefore at 10 m and 30 m the amplitude is correspondingly smaller. The efect of this increasing amplitude of the loops is shown by the dramatic increase in the mean, standard deviation and skewness (see Sec. 6.2.2.5.) of the electric field as one progresses downwind. It is, of course, not very meaningful to enquire how the electric field behaves at greater distances downwind, where the plume may reach the ground, because at that stage the concept of a line charge becomes totally unrealistic.

Many of the features described above actually occur in practice and further reference to them will be made in the next chapter. The magnitudes of the electric fields predicted, even taking into consideration the $1\mu A$ source used in the model, are larger than was measured. There can be little doubt that the reason for this was that the charge was too localized in the model. This again emphasises the need for the inclusion of crosswind and vertical diffusion in the model.

Chapter 7: THE SERIES I EXPERIMENTS

7.1 Introduction

The field work had to be conducted with portable equipment because there was no suitable site at which to install a permanent system. The lack of a permanent installation required that all equipment had to be erected before and dismantled after each series of experimental runs, a complex and lengthy procedure. Normally it took about an hour to erect the mast, attach the meteorological instruments and ion generator, and place the field mills at their allotted positions. Early field work was undertaken at the Oxen Law site (see Ch. 1.), approximately 20 miles from the University, and thus a further half hour was necessary to transport the equipment to this destination.

Once operational conditions were established, five or six field runs would be attempted. Each recording only lasted 24 min., but in between runs, field mills might have to be re-sited, or the height of the ion generator altered. As a result of these, and other, adjustments the total time required to perform the field runs was sometimes as much as five hours.

The complexity of the experimental system at times required the expenditure of considerable effort, both mental and physical, to assure its correct functioning. It was found that these human factors were restricting the amount of field work that could be done and to ameliorate this an experimental site nearer the University was sought. Later field work was,

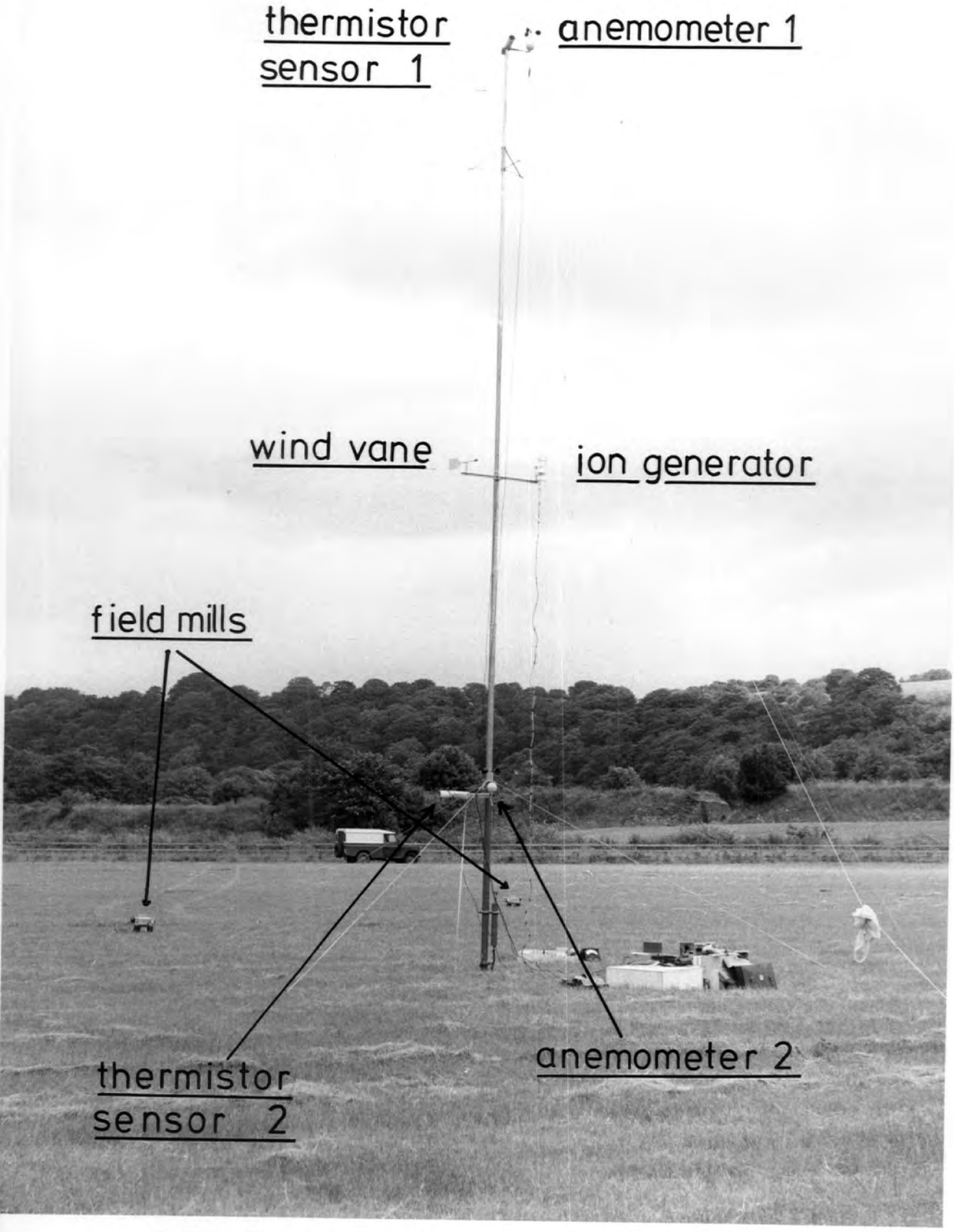

FIELD WORK IN PROGRESS 1

in fact, carried on in one of the playing fields at the University Sports Centre, Maiden Castle, (see Ch. 1.). In many ways this was an ideal site being only half a mile from the laboratory. However, one or two minor disadvantages did become apparent and these are mentioned in the next section.

7.2 The nature of the experiments and choice of weather conditions

The aims of the experiment were quite simple, being first to explore the electric field in the vicinity of ion plumes and then secondly to relate these results to the prevailing micro-meteorological conditions.

The ion source, anemometers and differential thermistor sensor were placed at standard heights on the Clarke mast. In practice the standard heights were 9 m and 2 m, whilst the ion generator could be attached at any of three heights, namely 9 m, 5 m and 2 m. The retracted mast, 2 m high, was held vertically by guy ropes and the various items of equipment bolted to it. The mast was then extended to its full height by means of the hand pump provided and the top guy ropes secured. After this the anemometers, thermometers and ion source were connected into their appropriate electronic systems and functional checks performed.

It was found very helpful to attach a small wind vane to the mast at the same height as the ion generator. Observation of this vane enabled the local wind direction to be accurately determined thus facilitating the correct placing of the field mills. Generally the mills were set in arcs or lines downwind of the ion source, the exact arrangement depending both on the

meteorological conditions and the particular objectives of the experiment. As a rule, field mills were not placed more than 100 m from the source, because, although ions could certainly be detected at much greater distances, the time involved in setting out cables of such lengths would have proved detrimental to the experiments as a whole.

A typical experiment is shown in progress Fig. *P10* , whilst additional details are presented in Sec. 6.1.1.

During the period 21st April 1972 to 10th August 1972, forty-seven 24 min. data recordings were made - mostly at Maiden Castle. Nine of these recordings were of the natural potential gradient whilst the remainder was concerned with the ion plume.

Ideally it was hoped to obtain results in as wide a variety of meteorological conditions as possible. There were however certain limitations to be considered, both in the performance of the equipment and in the technique itself. In particular, field work was impossible in rain or snow for reasons explained in Ch. 4. The equipment, notably the ion source, could be damaged by anything more than a light shower and therefore this eventuality had to be avoided. Consequently all field work was restricted to lightly clouded conditions so that there was little likelihood of any precipitation. Choosing such conditions also meant, conveniently, that the natural potential gradient variations would be small and therefore not interfere with the experiments. Occasionally, at the Maiden Castle site, diesel fumes from local land reclamation operations resulted in large fluctuating potential gradients being

measured (see also OGDEN (1967)). There was no choice but to abandon field work in these circumstances.

Positive ions were used throughout this series of experiments to avoid any ambiguities in the sign of the potential gradient downwind of the ion source. (The results of the Series II experiments indicate that the behaviour of ions of both signs is substantially the same). In many later experiments the natural potential gradient was not actually recorded because, if a field mill were reserved for this task, only three would remain for recording under the ion plume. Thus, in order to make maximum use of the equipment, all four field mills were sited for recording under the plume, the natural potential gradient being monitored at the beginning and end of each run to ensure that it was close to its normal value.

The complicating effects of topography and changing synoptic conditions were mentioned in Ch. 2. In practice by far the largest problem was that caused by the arrival of a sea breeze, the onset of which, usually about noon, could ultimately change the wind direction by as much as 90^{o}. Further, the character of the sea breeze was such that after its arrival the atmosphere tended to be less unstable than previously. This disturbed the continuity of any experiments because, under these circumstances, the field mills had to be completely re-sited. Later, as experience was gained, the likelihood of a sea breeze could be anticipated and, by deploying the equipment appropriately, any irritating effects minimised.

The Summer of 1972, during which this field work was conducted, was rather cloudy and consequently stable and unstable condi-

tions occurred only infrequently. Nevertheless, some quite successful field runs were performed during unstable conditions, but obtaining results in stable conditions presented something of a problem. It will be recalled (see Sec. 2.6.) that stable conditions usually occur at night. The operation of the equipment in darkness would have been extremely difficult and was not seriously contemplated. Despite these obstacles, some useful data was obtained late one evening in thoroughly stable conditions.

7.3 Presentation and Discussion of the Experimental Results

7.3.1 Initial Considerations

The field data was processed in accordance with the analytical procedures described in the previous chapter, two computer programmes (DATAPROG and SUPPROG) being written for this purpose. Statistical techniques were of undeniable value as their use enabled a particular run to be precisely characterized and thus compared with other field runs. However, such methods did not necessarily convey to best advantage certain features present in the records themselves. It was thought preferable therefore, by way of introduction, to briefly describe those important and recurrent characteristics which were immediately apparent even from a visual examination of the records. It is hoped that the results of the more complex analyses will then be more easily understood once the reader has a clear idea of the nature of the variations themselves. Unfortunately, space does not permit the inclusion of entire records here but selected portions are presented in Figs. 7.1. and 7.2.

SIMULTANEOUS POTENTIAL GRADIENT RECORDS AT FOUR POINTS IN A LINE DOWNWIND OF THE ION SOURCE

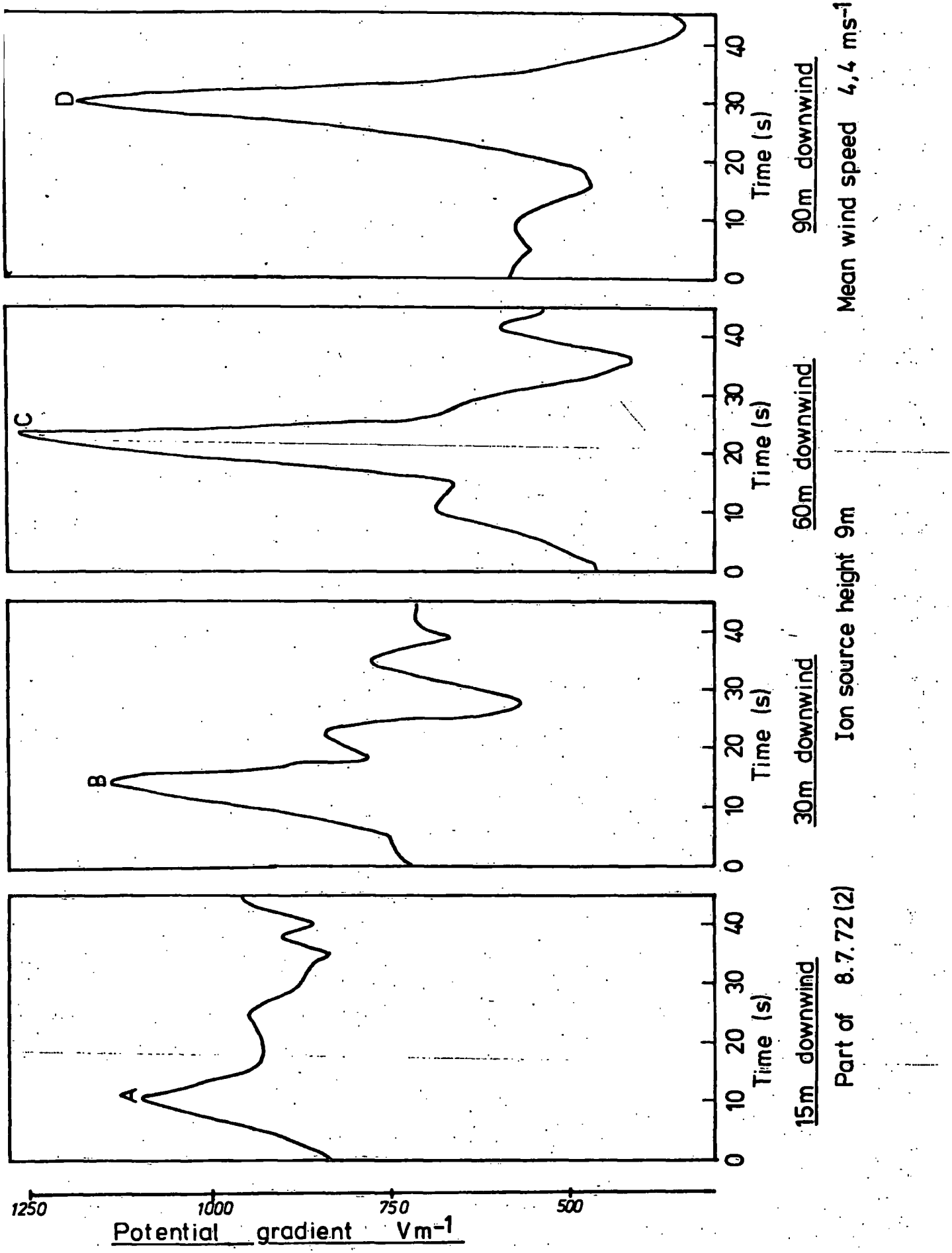

Fig. 7.1. shows a series of simultaneous potential gradient records taken at various distances downwind of the ion source. In this run (No. 4, 8.7.72) the ion source was at a height of 9 m, whilst field mills were placed at distances of 15, 30, 60 and 90 m downwind. We note that, in the record taken at 15 m from the source, a small peak (A) of potential gradient occurs 11 s after recording commenced. It should be remarked that the maximum value of potential gradient attained here, 1100 Vm^{-1} , was far in excess of the natural value.

We now make the reasonable assumption that, whatever the charge distribution was that caused the peak A to occur, that charge would inevitably be blown along by the wind. This idea was, in fact, introduced in Ch. 3 and the reader is referred there for further details. In accordance with this assumption we might reasonably expect similar peaks (B, C and D) to occur in records taken at greater distances downwind, but of course, at correspondingly later times. We can estimate the velocity of travel of the charge parcel on this basis, and in this case, it was found to be 4.4 ms^{-1} . The fact that this figure is exactly the same as the mean wind speed for the run is fortuitous but the agreement does indicate the plausibility of the above hypothesis. Also of interest is the fact that the peak attains a maximum size in the record taken 60 m downwind of the source. It seems from this that the charge parcel, as well as travelling along with the wind, appears to change as it does so. In practice, it was thought that the parcel moved gradually nearer the ground, possibly under the action of image forces (see Sec. 3.5.5.), as it was blown along. Naturally the parcel was also dispersed, both by turbulent and electro-

static agencies, as it moved downwind and therefore at greater distances the electrical effects begin to diminish.

An additional feature of relevance was the behaviour of the background, as distinct from the natural, potential gradient in these records. In fact, we can observe a systematic decrease in this as the downwind distance increases. This is substantially in accordance with the steady state model discussed in Ch. 6 and is, of course, a result of the general increase in ion plume dimensions as it travels downwind.

Typical results obtained with the alternative arrangement of field mills, i.e. across the width of the plume, are shown in Fig. 7.2. In this record, part of No. 3, 13.7.72, the ion source was at a height of 4.85 m, the mean wind speed being 2.3 ms^{-1} . As anticipated in Sec. 3.6. the relationship between the potential gradient records is now quite different, although their individual character is much the same. We note that in the record of mill 3 a peak (A) occurs at the same time as a trough (A') in the mill 2 record. A similar, but more pronounced, example of this is demonstrated by the features B and B'. It is clear, that in order to produce these out-of-phase variations, the ion plume (or part of it) must have moved toward mill 3 and away from mill 2. This movement could occur in two ways. Firstly, as shown in Fig. 3.11, a horizontal loop could have passed over mill 3, or secondly, if the plume were already nearer mill 3, then the passage of a vertical loop would have produced the same effect.

SIMULTANEOUS POTENTIAL GRADIENT RECORDS AT THREE POINTS IN A CROSSWIND LINE DOWNWIND OF THE ION SOURCE

Part of 13.7.72(3) Ion source height 4,85m

Mean wind speed 2,3 ms^{-1}

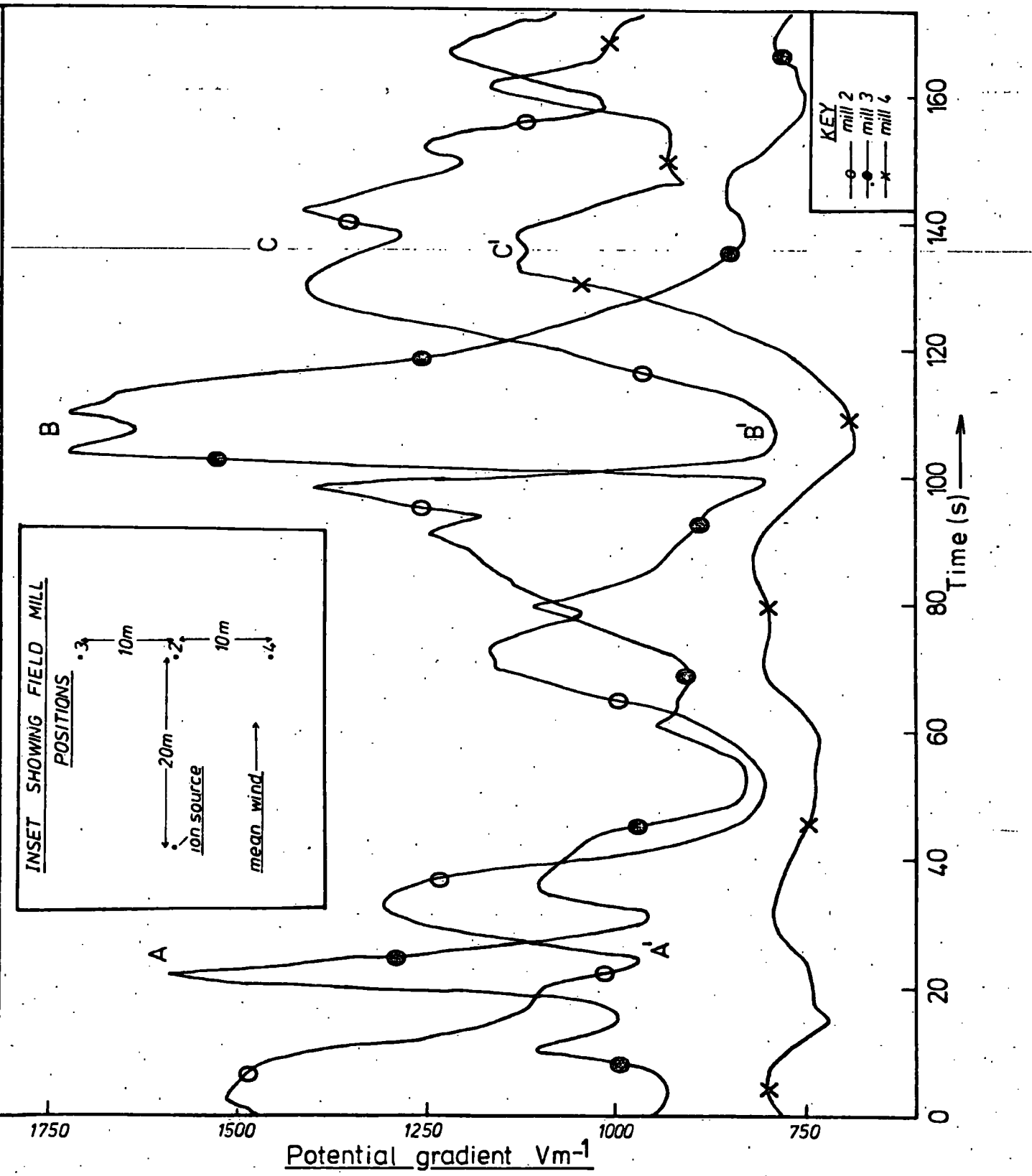

A different type of behaviour is indicated by the in-phase peaks C and C'. Here the charge parcel must have been moving nearer both field mills simultaneously and again there are a number of ways in which this could have occurred. Calculations show, however, that in order to produce these two peaks of roughly the same size, it is most likely that a charge parcel passed between field mills 2 and 4 rather than to one side of them.

Unfortunately, as can be seen, it is not possible to specify precisely the type of movement that produces these potential gradient variations, but the indications are that, because of the out-of-phase nature of some of the variations, the size of the features causing them is relatively small. The statistical analyses, to be discussed next, do, however, give a clearer idea of the size of these charge features.

7.3.2 The Statistical Analyses

7.3.2.1 Purpose of the Analysis

The main purpose of this investigation was to establish the basic features of ion plume behaviour. Consequently it was thought more appropriate to take a collective view of the statistical results rather than attempting to ascribe too much significance to any particular run. It seemed obvious that the meteorological conditions and ion source height would profoundly affect the potential gradient variations and therefore the statistical results were considered in relation to these, and other, factors. Further, the existence of the

electrostatic effects, described in Ch. 3, could also be clearly demonstrated by such an approach. The results of the statistical analyses are presented graphically in Figs. 7.3. - 7.11., verbal comments being included below.

7.3.2.2
Mean potential gradient v. distance downwind

This is shown in Fig. 7.3., distinction between runs with different source heights being made by the use of the symbols indicated. The mean values are widely scattered but, nevertheless, certain general trends are apparent. The lines, drawn by eye, indicate the overall tendency of the mean potential gradient as a function of distance downwind. Reference to Fig. 3.10. shows, that for the 9 m plume, we would not expect either image or repulsion effects to be large, except in the lightest winds, and thus the behaviour of the plume is largely determined by the meteorological conditions. The values of the mean potential gradient are, in this case, in reasonable agreement with those predicted by the steady-state model (see Fig. 6.5.)-but it should be emphasised that this does not necessarily imply that the actual ion plume was in a steady state. However, when the ion source was at 2.3 m, Fig. 7.3. shows that, in winds of a few metres per second, image effects appear capable of bringing the plume down to ground level within about 50 m of the source. It is not possible to be categorical here because of the paucity of data but the results *do* seem to indicate an abrupt disappearance of the plume at about 50 m downwind.

MEAN POTENTIAL GRADIENT versus DISTANCE DOWNWIND FROM ION SOURCE (all runs)

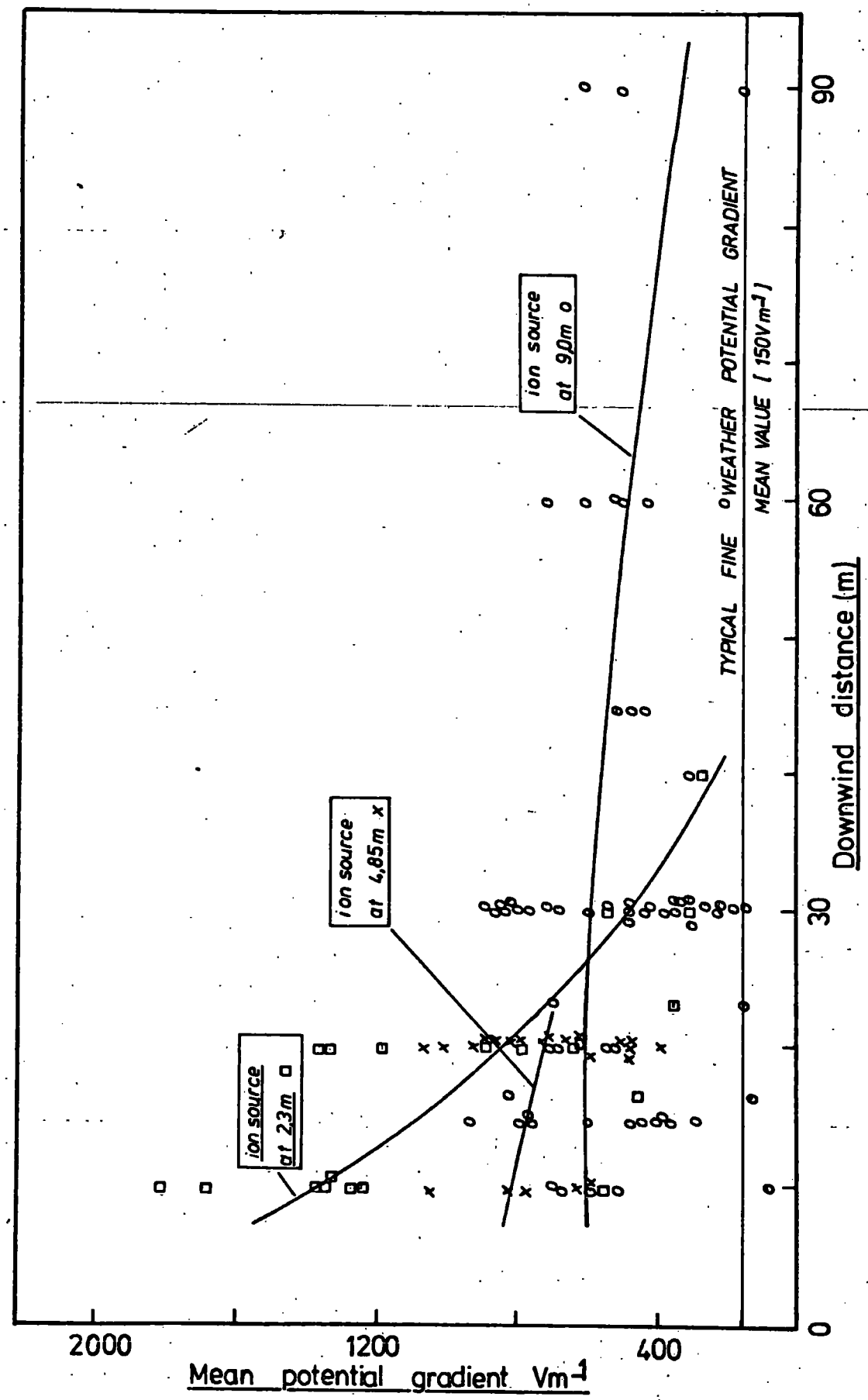

STANDARD DEVIATION OF POTENTIAL GRADIENT versus DISTANCE DOWNWIND FROM ION SOURCE (all runs)

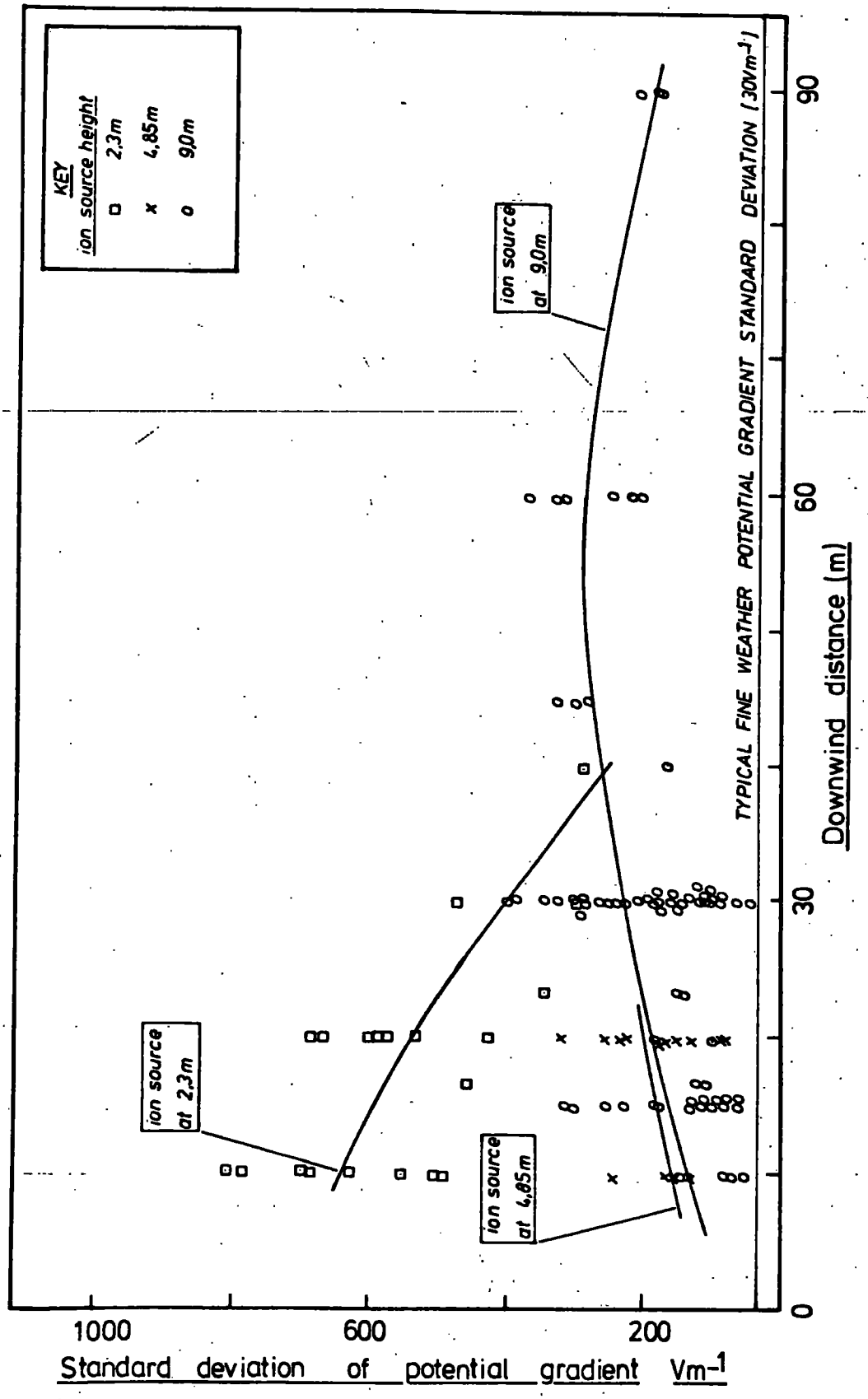

7.3.2.3

Standard deviation of potential gradient v. distance downwind

This is shown in Fig. 7.4., and again there is considerable scatter in the results, but as before, trends are apparent. It can be seen that, in those cases when the ion source was at 9 m, the standard deviations show a broad peak at about 50 m downwind. The existence of this peak is thought to be a result of two opposing effects. Firstly, the gradual motion of some plume elements toward the ground, caused both by image forces and certain larger scale turbulent motions (e.g. looping - see Sec. 2.7.), results in the potential gradient variations increasing in magnitude with downwind distance. Secondly, and in opposition, are the diffusive effects of turbulence and electrostatic repulsion. Thus, at a certain distance downwind, the field variations attain a maximum of intensity.

The rapid decrease of variance of potential gradient downwind of the ion source at 2.3 m is in accordance with the image effects discussed previously.

7.3.2.4

Standard deviation of potential gradient v. mean wind speed

This analysis, shown in Fig. 7.5., indicates a weak trend in the data obtained with the ion source at 2.3. m. It appears in this case that potential gradient variations tend to be largest when the wind speed is about 4 ms^{-1} . This can also be explained in terms of opposing effects, namely those of image forces and dilation of plume material by the wind. It was shown in Sec. 3.5.3. that the charge per unit length of the plume was inversely proportional to the wind speed. Consequently, at the higher wind speeds, the plume segments are likely to be more sinuous and dilute, and as a result, the

potential gradient variations smaller.

7.3.2.5 Standard deviation of potential gradient v. Richardson number

In contrast with previous results, this analysis, which is shown in Fig. 7.6., displays a very marked trend. We note that much lower standard deviations occur during unstable and stable, *rather than* neutral, conditions. This is, in fact, a direct result of the lessening of turbulent diffusion activity in the stable conditions; whilst on those occasions when it was unstable there was so little wind that any turbulence was almost entirely thermal. Consequently, in both circumstances the weather was very quiet and this allowed the electrostatic effects to dominate the ion plume behaviour. It was shown in Ch. 3 that, in very low wind speeds, these effects result in a very broad plume being formed with very little variation of concentration within its boundaries. We may, therefore, conjecture that an ion plume of this nature would not be capable of producing large potential gradient variations.

7.3.2.6 Cross-correlation between potential gradient records at different downwind distances

Previous reference to the evolution of plume elements has been made when discussing the correspondence between potential gradient peaks obtained when the field mills were arranged in a line downwind. It is possible *to* estimate relative changes in the charge distribution by the use of cross-correlation analysis, the results of such techniques being shown in Fig. 7.7. Further details of the method can be found in Secs. 3.6. and 6.2. In the results here, the cross-correlations are expressed

STANDARD DEVIATION OF POTENTIAL GRADIENT AT VARIOUS DISTANCES DOWNWIND OF THE ION SOURCE versus MEAN WIND SPEED

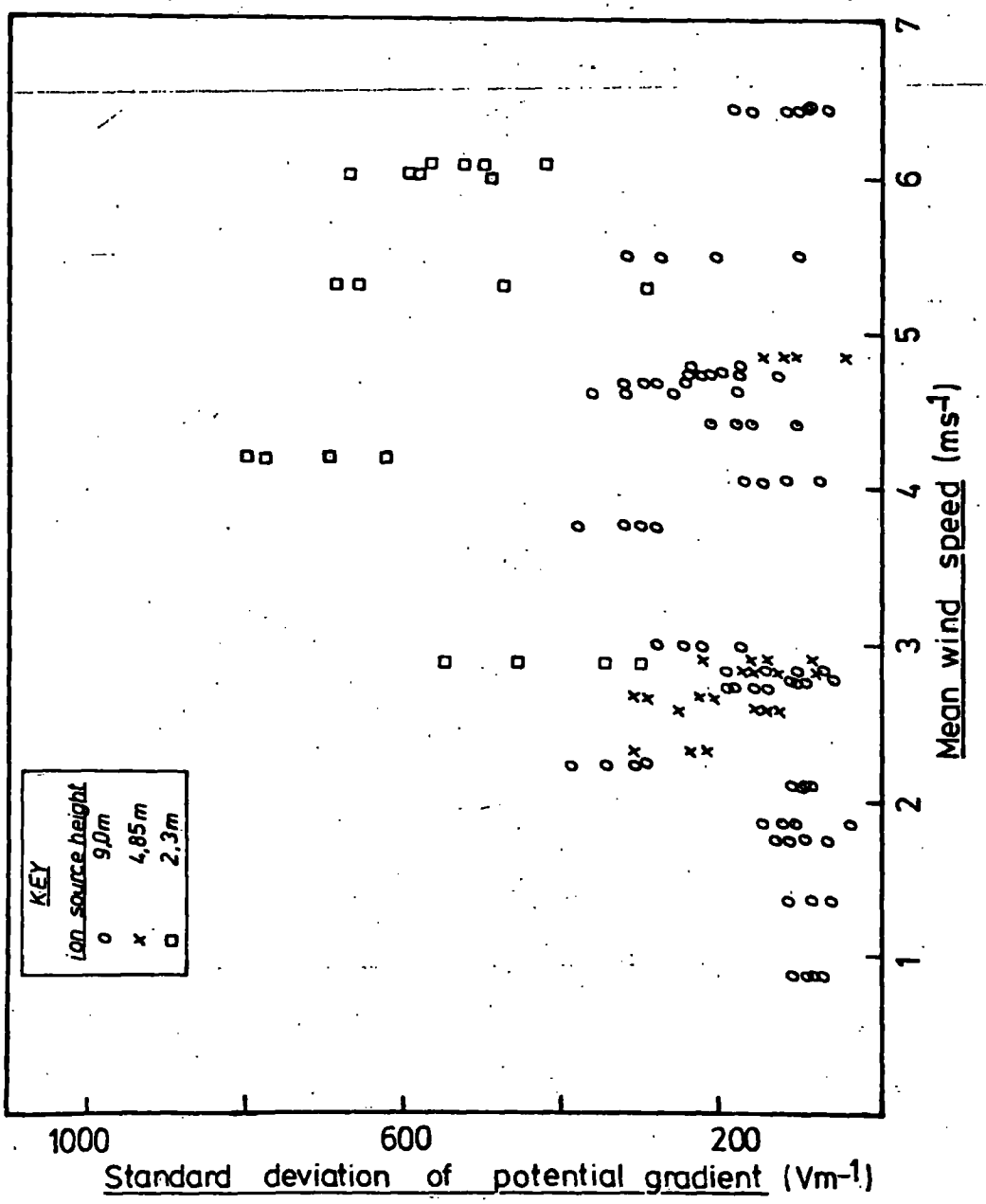

STANDARD DEVIATION OF POTENTIAL GRADIENT AT VARIOUS DISTANCES DOWNWIND OF THE ION SOURCE versus RICHARDSON NUMBER

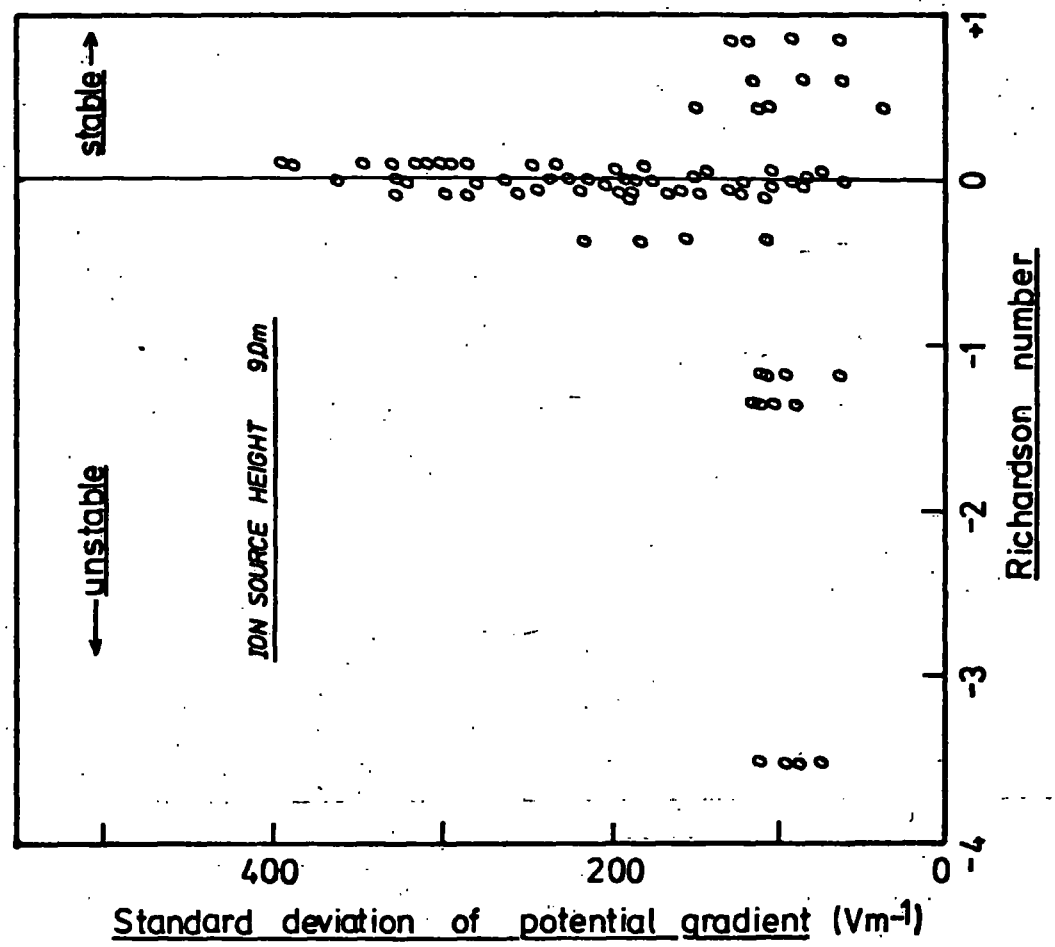

with reference to the field mill nearest the ion source, which in all cases was either 10 or 15 m downwind. The effects of time displacements between the records have been eliminated by considering the maximum cross-correlation coefficient provided that it occurred at an appropriate lag number. As we would expect the potential gradient records were almost fully correlated, about 0.99 in practice, when the field mills were together. With increasing downwind separation the cross-correlation gradually decreases, the height of the ion source having, rather surprisingly, little effect on the correlation decline. A very approximate estimate suggests that, at mill separations of greater than 200 m, the potential gradient records would be virtually uncorrelated. This does not necessarily imply that all the ions have recombined, or otherwise disappeared in this distance, but that the mixing effects of turbulence have resulted in a thorough re-distribution of the charge.

The results of the investigation of the fine weather natural potential gradient are included for reference and indicate, as anticipated, a much slower decline in cross-correlation with field mill separation. This is interpreted as being a direct result of the considerably larger scale of the natural charge elements.

7.3.2.7 Cross-correlation between potential gradient records taken at various cross-wind angles

It was only possible to draw tentative conclusions when discussing the downwind cross-correlation behaviour in the previous section. However, in this case, shown in Fig. 7.8.,

the indications are more definite. The basis of the approach has already been described in Secs. 3.6. and 6.2. and therefore only the implications of the results are dealt with here. The analyses, rather as expected, showed that, in normal conditions the ion plume width was about 20°. This is, in fact, somewhat larger than an uncharged plume and is, most likely, a result of the electrostatic expansion effects referred to in Ch. 3. Of particular interest is the ion plume behaviour in unstable and stable conditions, where the much slower decline of cross-correlation with angular separation strongly reinforces the opinions expressed in Sec. 3.3.

7.3.2.8
Relation between time-lag at maximum cross-correlation, wind speed and separation distance of field mill pair

It was pointed out in Sec. 3.3. that certain features of the potential gradient records were the result of charge parcels being blown along by the wind. One may investigate this in a more rigorous way by considering the relationship between the time lag at maximum cross-correlation, wind speed and mill separation. Such an analysis, depicted in Fig. 7.9., indicates conclusively that the potential gradient variations were caused either by features of the entire ion plume or plume segments travelling along with the wind.

7.3.2.9
Potential gradient variance spectra

Although a considerable number of variance spectra were computed, the results, though interesting, did not reveal as much as was hoped. The data was passed through a digital high pass filter, described in Sec. 6.3.4., prior to spectral analysis in order to remove any low frequency trends that might have been present.

THE CROSS-CORRELATION BETWEEN POTENTIAL GRADIENT RECORDS TAKEN AT VARIOUS DISTANCES DIRECTLY DOWNWIND OF THE ION SOURCE *(VARIOUS RUNS)*

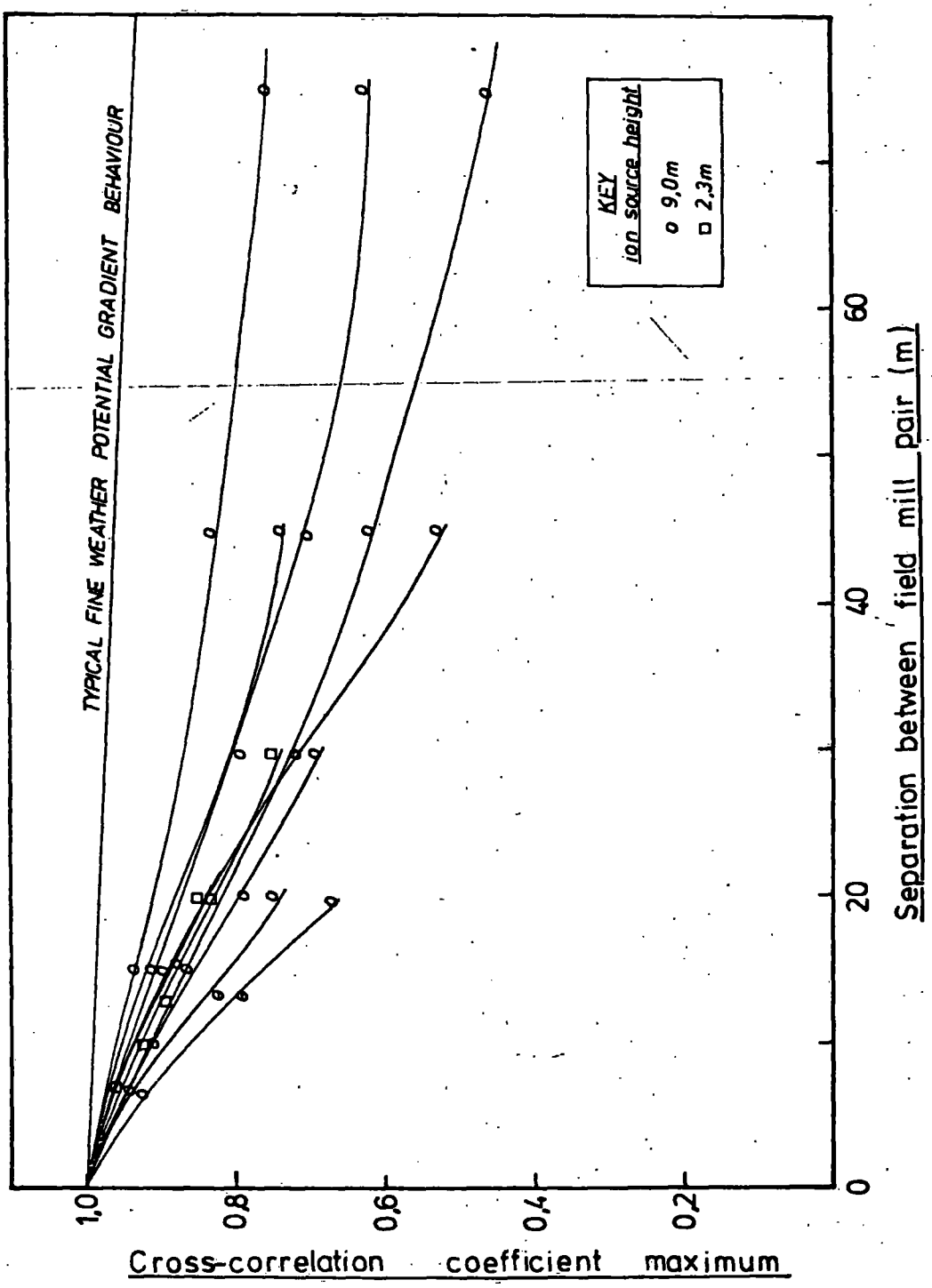

THE CROSS-CORRELATION BETWEEN POTENTIAL GRADIENT RECORDS TAKEN AT POINTS WITH VARIOUS CROSSWIND ANGULAR SEPARATIONS

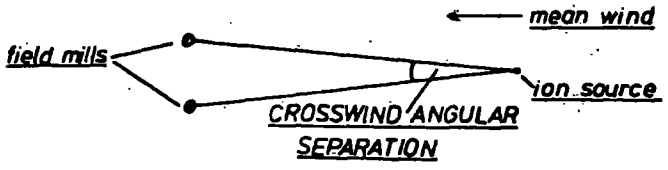

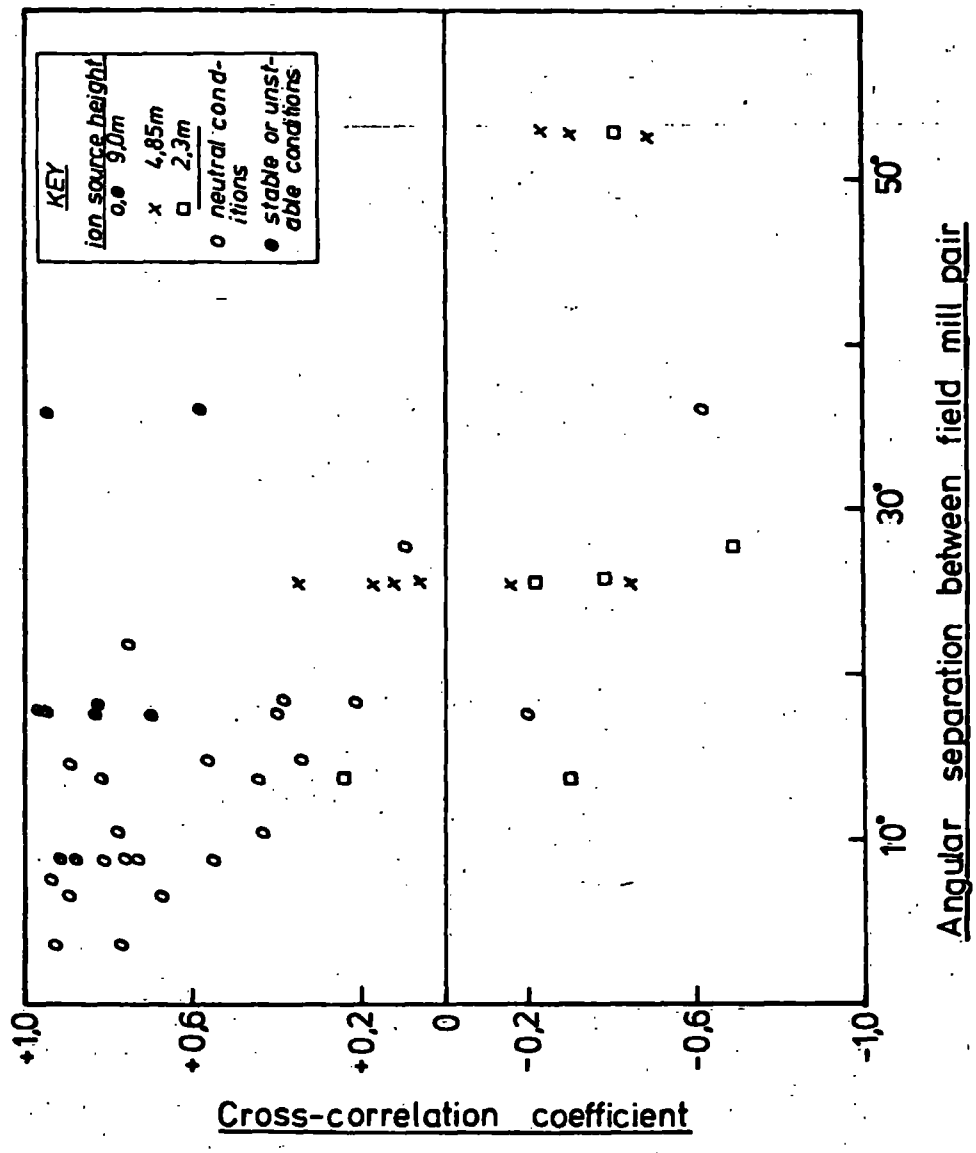

THE RELATION BETWEEN TIME-LAG AT MAXIMUM CROSS-CORRELATION, WIND SPEED AND SEPARATION DISTANCE OF FIELD MILL PAIR (Field mills directly downwind of the ion source)

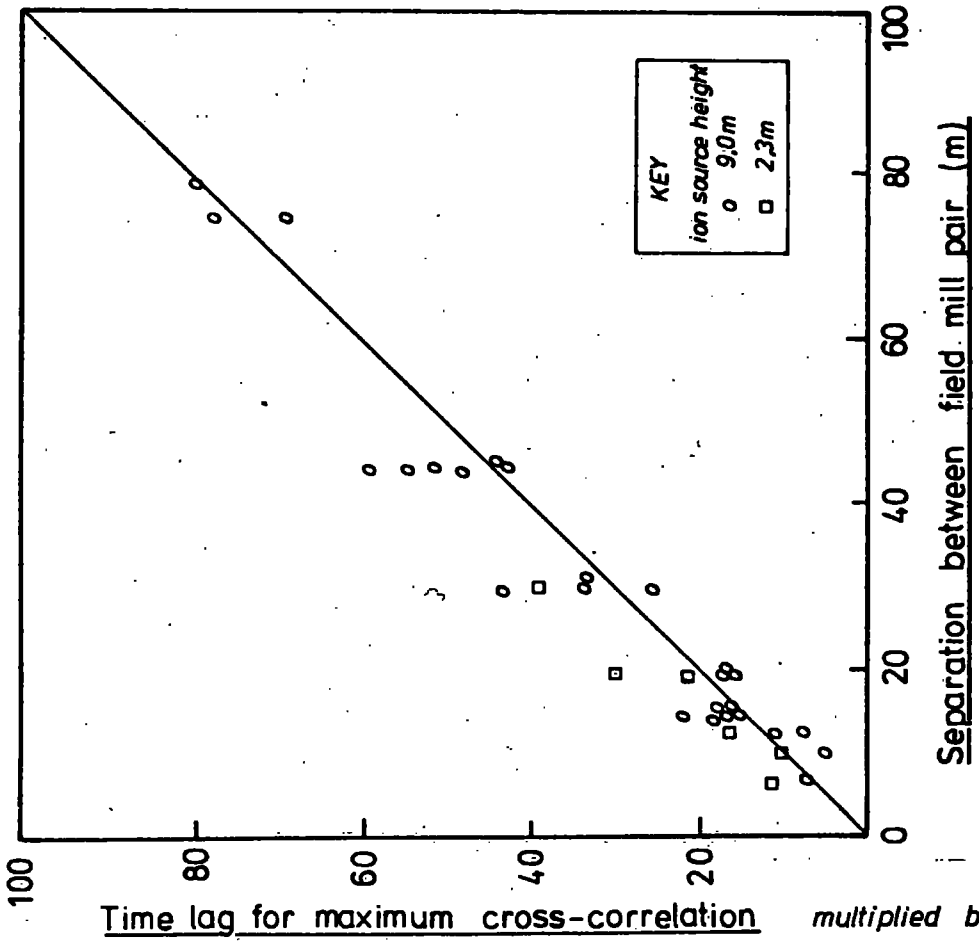

Typical results are shown in Fig. 7.10. and these bring out clearly the considerable effects that the plume has at all frequencies. The effect of the ion source height on the variance spectrum is also shown, indicating that the potential gradient variations are larger throughout the frequency range with a lower source.

A feature not revealed by the spectra was a tendency, in similar conditions, for the autocorrelation of the potential gradient to fall off faster when the ion source was lower. This implied the presence of relatively more high frequency energy in that case and follows directly from the elementary reasoning regarding moving charges presented in Sec. 3.3. It remains obscure why this point is not evinced by the variance spectra.

Finally, it should be mentioned that there is still a considerable variance contribution at the high frequency limit of the spectra and therefore it would be advantageous if the frequency response of the field mills and recording system could be extended in future investigations.

7.3.2.10
Potential gradient coherence and phase spectra

Typical spectra are shown in Fig. 7.11. not because they convey any new information but rather the spectra indicate the complexity of the processes operating. Despite the intricacy of the spectra, certain general features can be distinguished. Firstly, the coherence was greater at all frequences when the field mills were closer together and also, in that case, it fell-off more slowly with frequency.. Secondly, the phase

difference increased much more rapidly in the case of the widely separated mills. These general trends can, in fact, be deduced from simple geometrical arguments but the complex nature of the actual spectra was thought to be a result of two additional factors. On *the occasion shown* a very wide variety of eddy sizes was present in the wind and this would naturally result in there being a similarly sized assortment of ion plume segments moving downwind. Further, whilst the plume segments were travelling between the field mills, the action of turbulence was constantly re-arranging the ion distribution within them.

7.3.2.11 Skewness and Kurtosis analysis

The potential gradient records were subjected to the skewness and kurtosis analysis proposed in Sec. 6.2.2.5. The skewness of the potential gradient under the ion plume was invariably a small positive value which did not vary systematically with the meteorological conditions, ion source height or any other parameter. The sign of the skewness was a direct result of the fact that a positive ion plume had been used in this investigation. Inspection of the potential gradient records indicates that, although occasionally highly skew peaks do occur, it seems most likely that, statistically speaking, these peaks would be masked by the large number of small and much less skew peaks present in most of the data.

The result of the kurtosis analysis was similarly inconclusive.

Typical potential gradient variance spectra

THESE SPECTRA WERE OBTAINED IN SIMILAR METEOROLOGICAL CONDITIONS AND ARE THEREFORE COMPARABLE

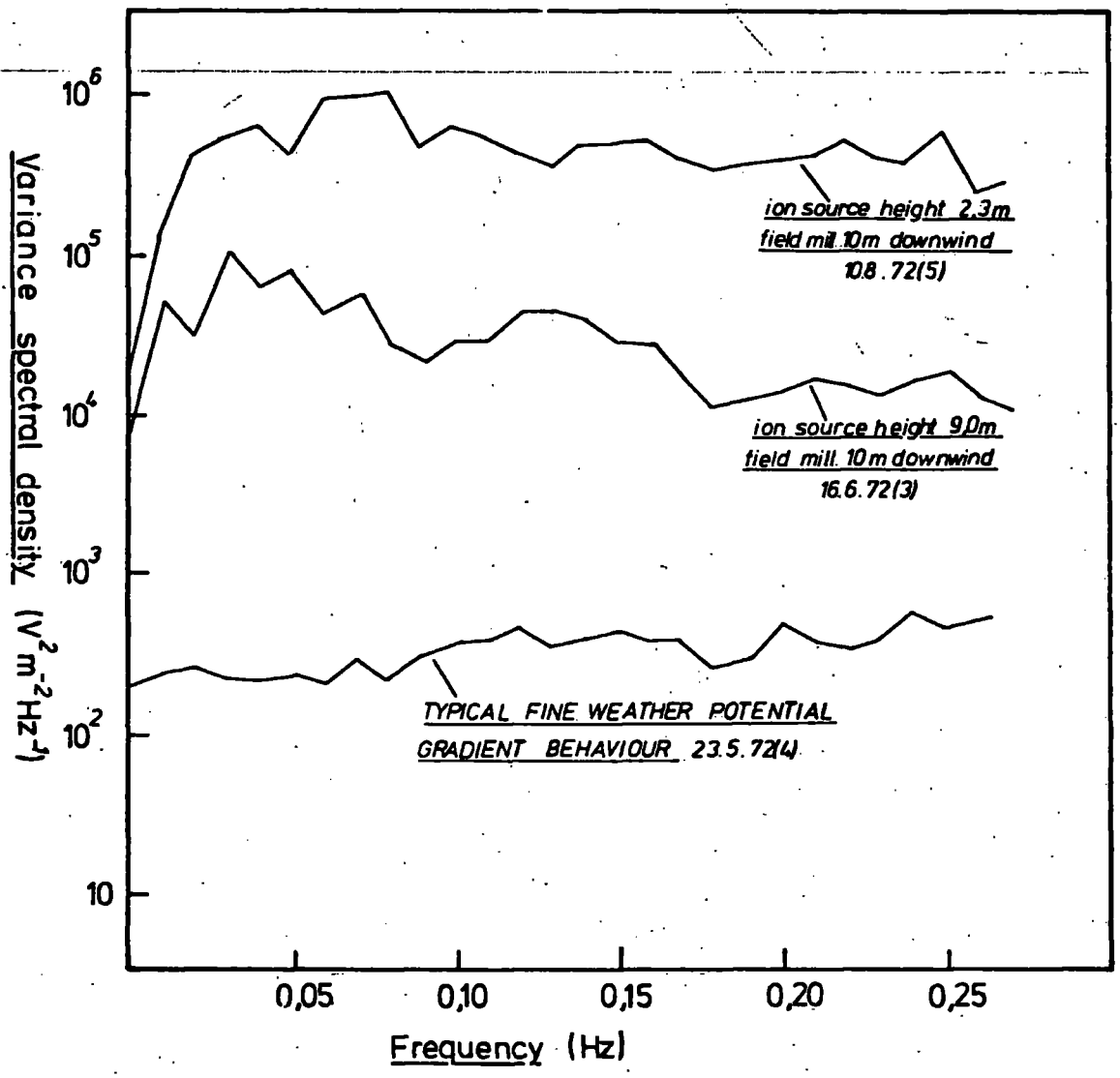

Coherence and phase spectral analysis of potential gradient records obtained from field mills at various distances downwind of the ion source

ION SOURCE HEIGHT 9,0m
5.6.72 (4)

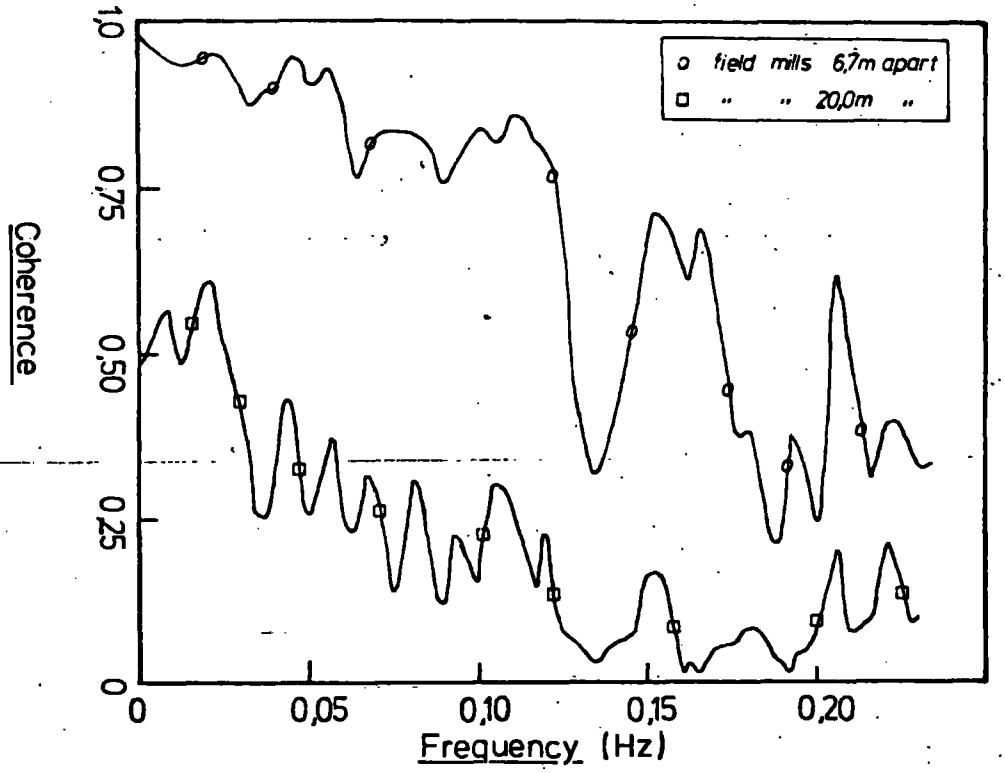

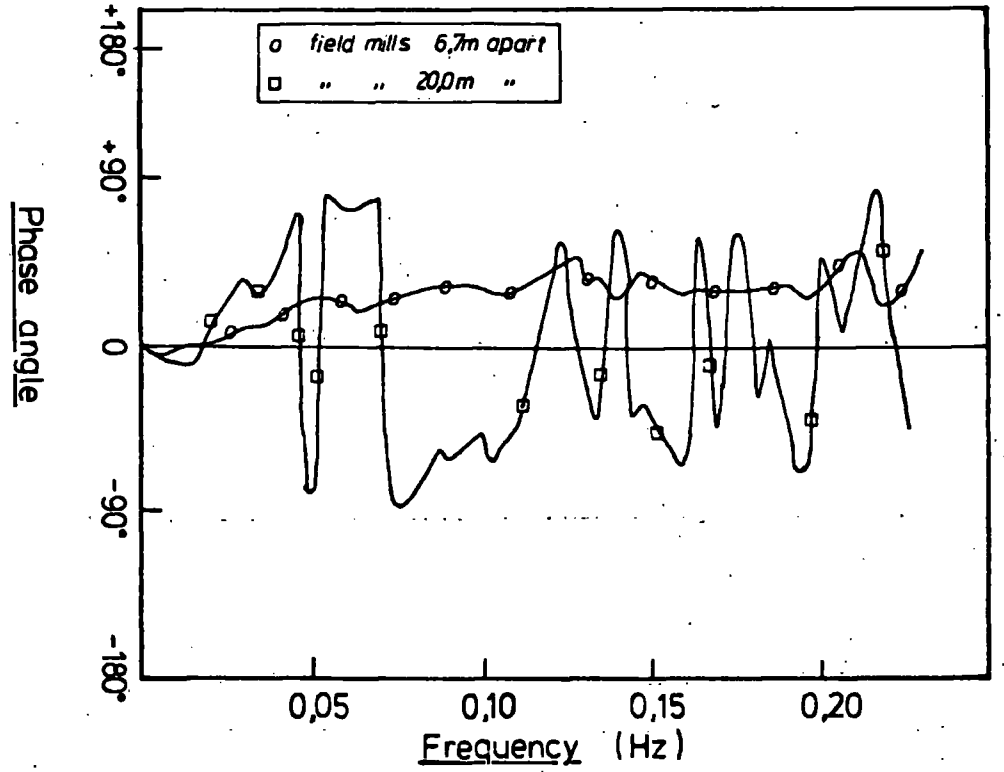

7.4
Criticisms and Conclusions

The results indicate that the potential gradient variations are caused by a haphazard sequence of charge distributions passing over the measuring point. In certain conditions it would appear that portions of the ion plume become virtually detached from the main system. These charge parcels are capable of maintaining their identity over considerable distances and result in characteristic electric field patterns as they pass over an array of field mills. Cross-correlation analysis has indicated that these detached portions are of quite small size - typically a few metres across. The configuration of the ion plume and the behaviour of the detached portions is largely controlled by the meteorological conditions, as are the characteristics of a smoke plume. Two important exceptions to this must be noted however. Firstly, ions released at a low level (less than 2 m) are rapidly attracted to the ground by images forces and presumably absorbed therein. Secondly, in very light winds, less than 3 ms^{-1} or so, ion plume behaviour is dominated by the electrostatic effects discussed in Ch. 3.

It was clear at the outset that the Series I experiments would only provide general data on the ion plume. In particular, the instantaneous ion plume configuration could not be ascertained and thus the details of the charge distribution were not known, The Series II experiments, using the bivane, largely resolved this difficulty.

Chapter 8: THE ION COLLECTOR, SERIES II AND OTHER RESULTS

8.1 Introduction

The experimental results presented in the previous chapter enabled one to make various, rather general, deductions about ion plume behaviour. It would obviously be useful if a more penetrating technique were available to investigate these plumes. Reference has already been made to bivane techniques and thus the justification for the choice of this method is not discussed here. Bivane readings taken near the ion source were used to predict the changing ion plume configuration, from which values of the potential gradient were evaluated at various points and compared with those actually measured. Certain shortcomings, both in the equipment and the bivane data model, became apparent, and, in a further series of experiments, the predicted plume configurations were checked against results obtained directly from cine photography of a smoke plume.

Two related investigations were also conducted. The region near the source, that is within 10 m, was explored with the ion collector, whilst field mills set at distances of up to 1/2 km downwind were used to determine the "long-range behaviour" of the plume.

8.2
The Series II (Bivane) Results

8.2.1
General Remarks

The arrangement of apparatus in the field was broadly similar to that of the previous series of experiments. The main difference, of course, was the inclusion of the recording bivane near the ion source (see Sec. 6.1.1.). Certain difficulties had been experienced from sea breezes at Maiden Castle and consequently the Series II experiments were conducted at Oxen Law. (As these experiments were performed in the Autumn the much weaker insolation would probably have caused little difficulty with sea breezes anyway.)

Thirteen 24 min. data tapes were recorded on two slightly unstable clear days in October 1972. The predicted and measured values of potential gradient downwind of the ion source were then compared statistically. However, inspection of the graphical records also produced by the computer indicated that much of the disagreement between the values was attributable to the short-period variations. In this context the term short-period refers to variations lasting no longer than two or three seconds. The sampled nature of the bivane data implied it was clearly impossible for the computer model to predict these short-term variations accurately. In order to obtain a more realistic assessment of the value of the model, the predicted and actual potential gradient data was therefore passed through a low pass digital filter prior to statistical analysis. Before discussing these results, however, we shall consider by way of introduction, a typical section of potential gradient data obtained during this series of experiments.

8.2.2
Discussion of a Section of Typical Potential Gradient Record

Fig. 8.1. shows part of a record obtained 10 m downwind of the ion source which, on this occasion, was at a height of 5 m. The predicted and actual potential gradient variations are shown, the nature of the records being much the same as those presented in the previous chapter. The overall agreement between the predicted and actual values is self-evident and, with some relatively minor exceptions, this was so in most of the other records. Certain features are worth noting, however. Firstly, nearly everywhere on this record, the predicted values are somewhat less than the actual readings, although the magnitude of the variations is much the same. The virtually constant difference is attributed to the presence of the natural potential gradient which is, of course, superimposed on any values measured near an ion plume. The natural potential gradient, as monitored by a field mill placed well upwind of the ion source, was found to be about 250 Vm^{-1} , this figure according well with the difference between the predicted and actual data. Secondly, this record, which has not been filtered, exhibits the discrepancies in the short-term variations referred to previously.

To illustrate the nature of the ion plume motion causing the potential gradient variations two computed configurations are shown in Figs. 8.2. and 8.3. In these figures small black dots have been used to indicate the positions of successive plume elements, whilst the lines joining the dots depict the geometry of the plume as a whole. The position coordinates were obtained with the bivane data model. It should be remembered that in the calculation of potential gradient with this

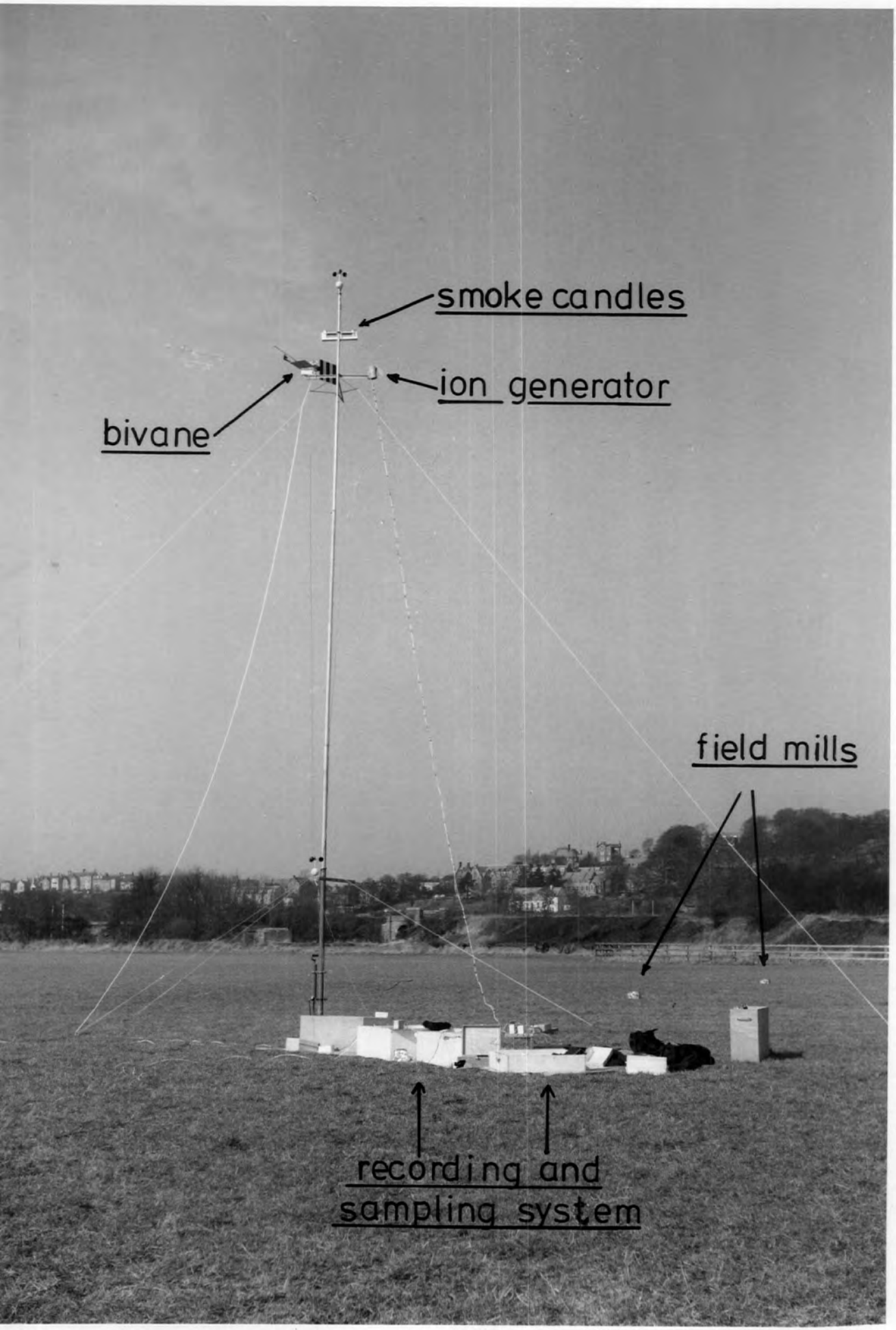

FIELD WORK IN PROGRESS 2

TYPICAL MEASURED VALUES OF POTENTIAL GRADIENT COMPARED WITH THOSE COMPUTED FROM BIVANE DATA

PART OF 4.10.72(6) *ION SOURCE HEIGHT 5m* *MEAN WIND SPEED 3.4 ms^{-1}*

CONDITIONS: slightly unstable, sky clear

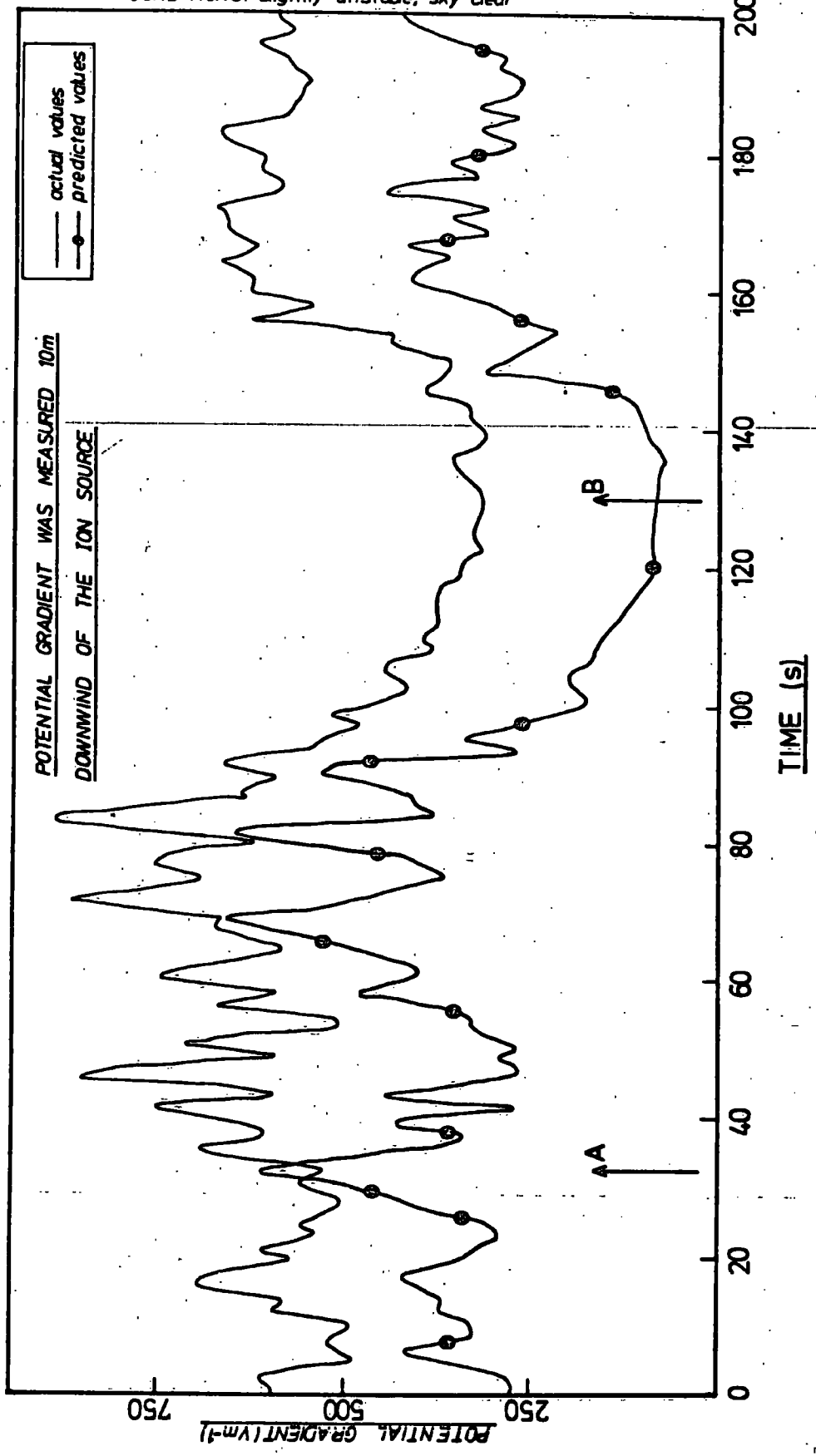

Example of computed ion plume configuration

(1) AT TIME 'A' (see fig. 8,1)

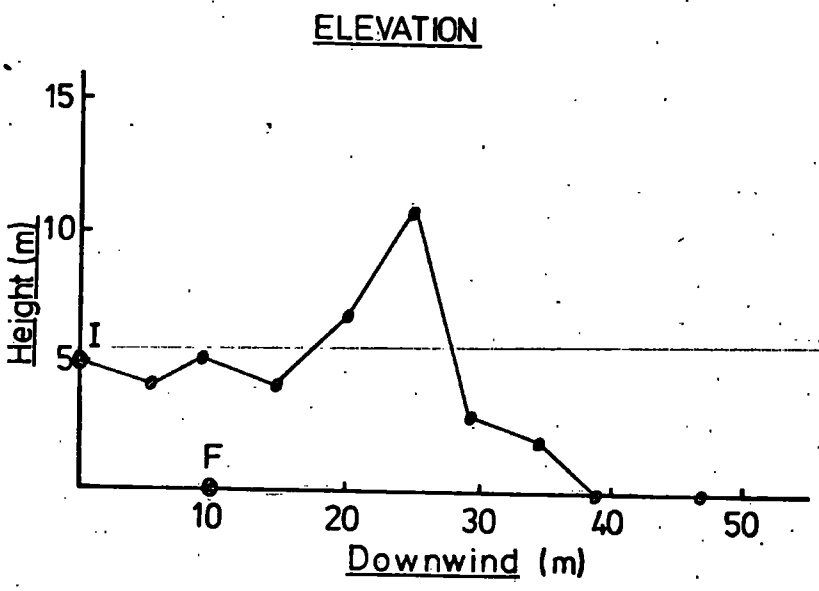

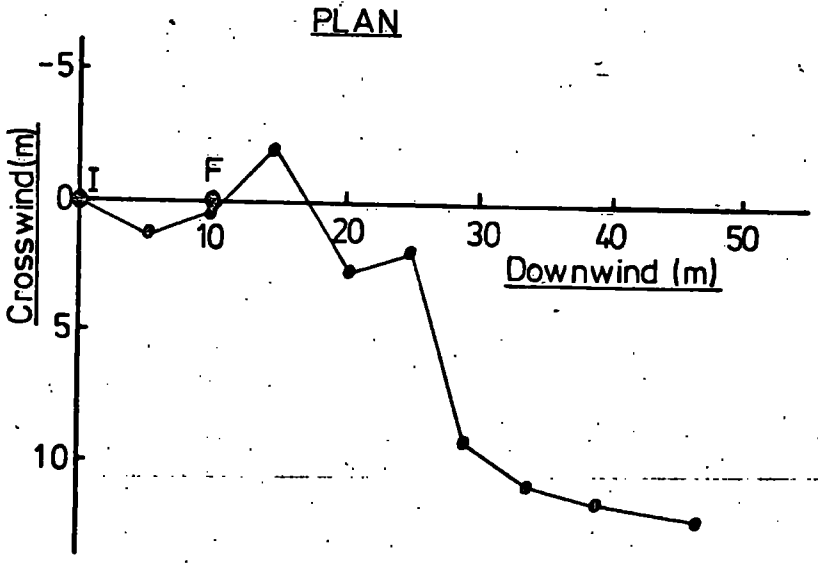

I ION SOURCE F FIELD MILL

Example of computed ion plume configuration

(2) AT TIME 'B' (see fig. 8,1)

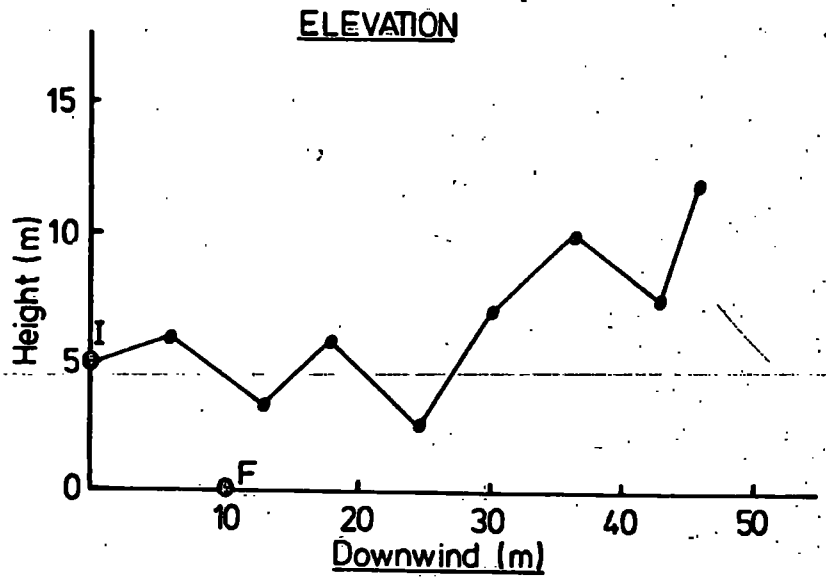

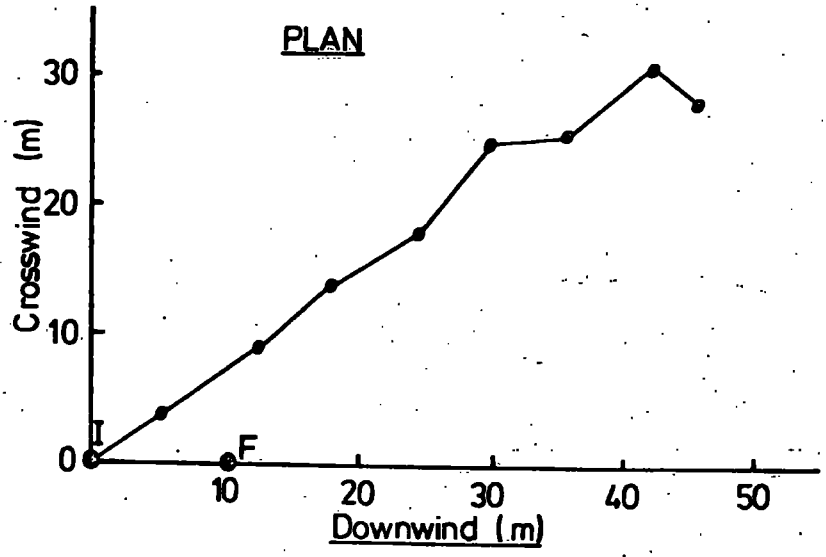

I ION SOURCE F FIELD MILL

model appropriately sized space charge parcels were supposed to reside at the plume element positions. The validity of this assumption is discussed later.

At time A (see Figs. 8.1. and 8.2.) we observe that three charge elements of the plume are almost directly above the field mill (F) and, *because* of the inverse square law, it is these three local charges which make by far the largest contribution to the predicted potential gradient. During this time the actual potential gradient behaved similarly and we thus conclude that, in all probability, the actual plume configuration was not too different from that predicted. In marked contrast with this is the situation of the ion plume at time B (see plan in Fig. 8.3.). Here the projection of the entire plume is at an angle to the mill-source line, possibly due to the passage of a large horizontal eddy or similar feature. The predicted potential gradient is, as we would expect, much lower because nowhere is the ion plume near the field mill.

8.2.3 Discussion of the Statistical Results

8.2.3.1 Opening remarks

The data obtained from the bivane, anemometer and field mills was processed by the computer in the manner described in Sec. 6.3. The cross-correlation coefficient between the predicted and actual potential gradient values was of most interest because its magnitude indicated the validity or otherwise of the bivane data model and the extent, if any, of the electrostatic effects. The standard deviations of the predicted

and actual potential gradient were also computed and in many cases the agreement was quite good. In fact, the best agreement was obtained when the source current in the model was set to $+0.3\,\mu A$ and, taking into account the Series I results, this figure was accepted as being the best available. Observations with the ion collector indicated that the ion source produced negative ions rather more copiously, see Sec. 8.3. Values of the turbulent surface stress obtained with this relatively simple equipment, although of little direct relevance to this project, were nevertheless of interest in that they provided a check on the bivane and recording system. Actually, the results obtained for the stress were close to the accepted figures and this was quite encouraging.

It will be noted from Fig. 8.4., which gives a summary of the Series II results, that negative ions were used in some of the runs. The implication of this is that near or under the ion plume the sign of the potential gradient would, at times, most likely be reversed. Unfortunately, sign discrimination was *never* incorporated on the field mills as had been originally intended and consequently there were inevitably occasions when the polarity of the recorded potential gradient was uncertain. This effect, which is discussed in more detail later, caused certain difficulties both when interpreting the graphical records and in understanding the value of cross-correlation obtained.

SUMMARY OF SERIES II DATA

DATE	RUN No.	SOURCE HEIGHT m	ION TYPE	MEAN WIND SPEED ms^{-1}	Surface stress $N m^{-2}$	STANDARD DEVIATION OF POTENTIAL GRADIENT Vm^{-1}				Correlation coefficient of actual and predicted	
						actual values		predicted values			
						mill 1	mill 2	mill 1	mill 2	mill 1	mill 2
4.10.72	3	9,0	+ve	2,8	0,16	160	160	82	180	0,04[a]	0,52
	4	"	"	2,5	0,11	140	150	84	240	0,09[a]	0,42
	5	5,0	"	3,4	0,14	91	140	180	240	0,40	0,34
	6	"	"	3,3	0,08	110	160	200	240	0,49	0,40
	7	2,3	"	3,7	0,04	410	260	460	230	0,63	0,62
	8	"	"	4,0	0,09	320	71	520	310	0,19[a]	0,34
	9	"	"	2,9	0,07	430	220	530	370	0,43	0,49
13.10.72	3	9,0	-ve	1,4	0,02	54	200	130	270	0,57[b]	-0,04[b]
	4	"	+ve	1,7	0,13	110	350	60	62	0,60	-0,43[a]
	5	5,0	+ve	1,5	0,08	150	160	600	87	0,40	0,35
	6	"	-ve	2,7	0,10	190	44	330	10	0,10[a]	-0,41[c]
	7	2,3	-ve	2,5	0,16	220	68	630	8,4	0,20[b]	0,18[b]
	8	"	+ve	2,8	0,12	180	100	390	17	0,21[a]	0,49

Notes

1. METEOROLOGICAL CONDITIONS - clear skies, slightly unstable on both occasions

2. FIELD MILL POSITIONS

4.10.72	mill 1 10m Downwind " 2 30 "
13.10.72	both mills 30m Downwind but 50 apart.

3. Predicted values of potential gradient obtained from bivane data model. Actual and predicted values were passed through a digital low-pass filter prior to statistical analysis. Ion source in model was 0,3μA.

4. Low cross correlations are superscripted by a,b or c, the letters being used to refer to the various effects causing the poor results. SEE TEXT.

8.2.3.2
The nature of the cross-correlation between predicted and actual potential gradient data

We shall now consider firstly how this cross-correlation might be expected to depend on various factors and secondly any likely sources of discrepancy between measured and predicted values of potential gradient.

The cross-correlation should be better when

(a) the wind speed is higher,

(b) the ion source height is greater, and

(c) the field mill is placed near the source.

Under circumstances (a) and (b) we would anticipate that the ion plume configuration would adhere more rigorously to the bivane data model because any electrostatic effects would be minimal. However, in conditions of high wind speed, because the sampling interval is constant, the plume elements used to evaluate the potential gradient in the model are relatively widely spaced. Inevitably, this large spacing will, at least to some extent, detract from the accuracy of any predicted electric field values. In the case of (c) above it would seem reasonable that, whatever the exact nature of the turbulence causing the potential gradient variations, the model would be more applicable nearer the source. This is because the departure from the straight line effect (on which the bivane data is based) would be less near the source than at greater distances downwind (see Sec. 2.8.).

Sources of discrepancy between the predicted and actual values of potential gradient were thought to be:

(a) Departure from the straight line effect - see Sec. 2.8.2.,

(b) Discrete, i.e. sampled, nature of the data,

(c) Omission of crosswind and vertical diffusion in the model,

(d) Disregard of electrostatic effects,

(e) Instrumental errors, principally those of bivane alignment and anemometer accuracy, and

(f) Lack of field mill sign discrimination.

The existence of the straight-line effect is, of course, fundamental to the success of the bivane data model and any departure from it would inevitably affect the results adversely. Of equal importance was the sampled nature of the data, it being suspected that many small scale features of the plume were being missed. This suspicion was confirmed in some later experiments with smoke plumes (discussed later in this chapter) during which the validity of the straight-line hypothesis was also thoroughly explored. Initially it was hoped to include the effects of crosswind and vertical diffusion in the bivane data model but this was not possible for reasons detailed in Sec. 8.3.3.2. For similar reasons, the effects of electrostatic forces had also to be omitted from the model.

Considerable effort was taken to carefully align the bivane by a procedure involving the use of compass and binoculars, more details of the technique being given in Sec. 4.6.4. Despite these precautions it is felt that, together with inaccuracies in the data transfer system, the bivane observations could have been as much as 5^{o} in error. Naturally, if the anemometer system also gave inaccurate readings, this would detract further from the reliability of the computed wind component values.

We now consider the analytical results, shown in Fig. 8.4., in the light of the previous comments. An examination of the cross-correlation coefficients indicates that if any tendencies are apparent, they would seem to be in contradiction to the proposals made above. That is, the correlation appears rather better when the ion source height was low and in light winds. However, a visual inspection of the graphical records suggested that the predicted and actual potential gradient values agreed rather better than their correlation coefficients would indicate and, in fact, on most occasions the agreement was quite good. Further, visual analysis also substantiated that any discernible trends in this agreement did apparently conform to the criteria originally suggested.

The reason for the disparity between the two methods of analysis is quite simple and is as follows. It must be remembered that the value of the correlation coefficient is very sensitive to the position of the largest peaks and, because of the nature of the system being investigated, it was in the prediction of these large potential gradient variations that the maximum error was likely to arise. The largest variations are, of course, caused by space charges passing close to the field mill and when such a variation has to be predicted the accuracy of the bivane and anemometer as well as the validity of the computer model are both severely challenged. Consequently, it was hardly surprising that whilst the agreement between the small peaks, associated with the movement of more distant charges, was frequently excellent, that between the large peaks was often disappointing. In view of this it appears that correlation analysis, in the mathematical sense, produces unnecessarily pessi-

mistic results and thus more importance was attached to the visual analysis of the potential gradient records.

Certain additional effects contributed to the poor cross-correlation obtained in some cases. The particular instances where this is applicable have been superscripted with the letters a, b or c so that the various factors causing these low figures can be discussed separately.

In the case of those values labelled with an 'a' the poor correlations were substantially a result of the effects described immediately above combining in an unfavorable manner.

The poor results carrying 'b' or 'c' labels were all obtained when negative ions were being used and we therefore suspect immediately that this may be a result of the lack of sign discrimination on the field mills. In fact, this turns out to be so but the lack of sign discrimination causes, not one, but two related effects. Let us suppose, as was the case in fact, that the natural potential gradient was small and positive throughout these field runs. Firstly, if the negative ion plume is relatively distant from the field mill, then any motion toward the mill, provided that the motion is not too large, will result in the measured potential gradient being decreased slightly. However, the possibility of computations involving negative ions (and hence negative potential gradients) was, rather stupidly, not allowed for in the bivane data model computer programme and as a result the sense of the predicted potential gradient variations was incorrect in the circumstances detailed above. That is, when the ion plume is executing motions relatively far away

from the field mill the predicted and actual potential gradient values will be in antiphase. Consequently, if this type of situation is maintained throughout a field run then the overall cross-correlation between the values will be negative. This is referred to as effect 'c'.

Secondly, a more complex situation arises if the negative ion plume moves much nearer the field mill. The potential gradient will, in all probability, be reversed, but, because of the failure of the mills to descriminate between positive and negative values, the actual negative potential gradient will be recorded as positive. Therefore, in this case the larger, but usually less common, peaks would be in phase with their predicted counterparts. However, as before the smaller, but invariably more numerous, peaks will be in antiphase. This state of affairs will lead to either a small positive or negative cross-correlation depending on which factor is dominant. This is referred to as the effect 'b'.

8.2.3.3 Concluding notes

The 'bivane method' of investigating ion plumes has been reasonably well established despite considerable instrumental problems and difficulties with data analysis. Cross-correlation techniques proved rather disappointing but careful visual examination of the results indicated that, with relatively few exceptions, the agreement between predicted and actual potential gradient values was good. The physical complexity of operating the experiments in the field was such that only a small number of runs could be attempted. Conse-

quently the coverage of various meteorological conditions was nothing like as comprehensive as in the case of the Series I experiments. Nevertheless, it was possible to discern, as anticipated, that the bivane data model was more reliable at moderate wind speeds and with the ion source well above the ground.

The results of these experiments also indicated that there was little difference between the behaviour of positive and negative ions, although investigation of negative ion plumes was, to some extent, frustrated by the lack of sign discrimination on the field mills.

A photographic technique was devised to re-examine the validity of the bivane approach in an attempt to discover the reason for the occasional disagreements between the predicted and actual potential gradient values. The details of this method and the results obtained are now discussed.

8.2.4 Smoke plume photography

Suppose a smoke plume were generated by a suitable source placed as close as possible to the ion generator. Then, ignoring electrostatic effects, the smoke and ion plumes should be coincident. Further, the position of the smoke, and hence the ion, plume could be determined directly by photography and the computed configurations obtained from the bivane could be compared with these photographic results. In this way the reality of the bivane data model could be critically assessed. It would also be possible, if time permitted, to compute the expected potential gradient from the photographs, and departures from the actual values indicating the

magnitude of the electrostatic effects present. However, the success of such experiments depended entirely on two factors. Firstly, the smoke must be electrically uncharged, and secondly, the ions and smoke particles must not interact. In the first case field mills placed downwind of a smoke candle indicated that the smoke was, fortunately, electrically neutral. The magnitude, if any, of an ion-smoke interaction was not investigated.

The experimental technique, briefly described in Sec. 4.7., was an extension of the method used in the previous investigations with the bivane. Two 8 mm cine cameras were placed at suitable distances upwind and crosswind of the smoke candle. These cameras, which were mounted on sturdy tripods, could be remotely controlled and were connected into the recording system by a specially designed interface system. In order that accurate synchronisation could be maintained between the photographic and recording systems, small lamps were situated near the cameras and within their field of view. These lamps were arranged to light during that part of the recording cyle in which bivane data was being sampled.

Initially, it was hoped to ignite the smoke candles electrically. It became apparent, however, that the mast, already overloaded, would not support any additional wiring and thus an alternative method of igniting the smoke generators had to be found. In practice the only method appeared to be that of attaching time fuses to the candles and lighting these with the mast retracted. Once the fuses were burning the mast was pumped to its maximum height and the top guy ropes secured. Clearly, this was a somewhat tedious procedure and the diffi-

culties were increased by the fact that once the fuses were lit no further control could be exercised over the time of ignition.

The type of smoke candle used burned for approximately 4 min. and produced a dense white smoke. Despite the relatively high opacity of this smoke, on some occasions the contrast between plume and sky was rather poor. This led to difficulties when trying to discern the position of the plume on the cine films. In an attempt to alleviate this more powerful smoke generators were tested but these appeared to produce a much hotter smoke and considerable convective activity was observed. Unfortunately, this precluded their use in this project.

Despite all these difficulties quite useful results were obtained and these are now discussed briefly.

In these experiments the correlation between the predicted and actual potential gradient values were examined as before. Although the duration of the runs was now much shorter, only 4 min., the cross-correlation coefficients were similar in value to those obtained from the previous 24-min. recordings. However, this correlation was not the primary concern here, the main interest being centred on the relation between the plume configurations obtained photographically and those computed with the bivane data model. Experiments were performed with the ion and smoke sources at two heights, namely 9 m and 2.3 m. In the case of the higher sources, however, the plume-sky contrast was so poor that very little could be learnt from the cine film record. Thus the conclusions listed below derive

mainly from results obtained with the sources at 2.3 m. These experiments were performed on a clear day in March 1973 with near-neutral conditions and a wind speed of about 4 ms^{-1} . The general conclusions are as follows:

(a) The bivane data model appeared to exaggerate the vertical motions. This might conceivably explain the occasional large peaks found in the predicted potential gradient records which apparently bore little relation to the actual values. Presumably, it is the presence of the ground which is inhibiting these vertical motions. (See Sec. 2.6.)

(b) The discrete nature of the model resulted in, as had already been suspected, quite important features present in the actual plume being omitted entirely in the computed version.

(c) It was clear that vertical and crosswind diffusion must have had a considerable effect on the charge distribution even at distances of a few tens of metres from the source.

(d) As expected, the bivane data model was more accurate at short distances downwind of the source.

Although the above are fairly harsh criticisms of the bivane data model it should be pointed out that, at times, there was little discrepancy between the actual and computed plume configurations, and thus the effects causing the departures from the predictions were not by any means always operative.

It should, of course, be noted that the above comments are based on the detailed analysis of only a few runs and therefore any conclusions are inevitably tentative. Nevertheless, in a first attempt at understanding the dynamics of ion plumes the 'bivane method' would seem a simple and quite effective approach.

8.3
Experiments with the Ion Collector

The use of an ion collector was considered at the inception of this project but reasonably priced solid state amplifiers of the type required were not then available. During the later stages of the work such items did appear on the market and an ion collector was constructed. The collector, which is described in Sec. 4.5., did not work as well as had been hoped. Whilst the performance was quite satisfactory on the less sensitive range, a considerable amount of noise was present on the output signal on the higher gain setting. Some efforts were made to cure this problem, but as the noise appeared to originate from brush interference in the impeller motor, little could be done without completely rebuilding the instrument.

In the field the device was placed directly downwind of the ion source. The mean wind direction was obtained from a light wind vane mounted close to the ion source as before. A special metal gantry of variable height was constructed to support the ion collector. The collector-source distance was altered by moving the gantry and collector as a single unit. OGDEN (1967) has pointed out that such structures may disturb the ion distribu-

tion because of electrode effects. The alternative proposition, i.e. to construct the gantry out of an insulating material, seemed equally unsatisfactory as quite possibly non-conducting materials would become electrically charged and thus also disturb the ion distribution.

The ion collector output was taken to a small mains-driven chart recorder. The mains supply was obtained from the Group's portable generator, considerable care being needed when siting the latter. The exhaust gases from the generator engine could be quite highly ionized, and to avoid the possibility of any interference with the experiments, the AC generator was placed well downwind of both ion source and collector.

The ion concentration, at least near the source, fluctuated considerably with time at any particular point. The character of these fluctuations was, of course, much the same as those of smoke concentration that would be measured near a smoke source and is a direct indication of the turbulent nature of the wind. However, if mean values of the ion concentration are taken over periods of several minutes, then quite definite trends can be discerned in the recorded data. These results are shown in Fig. 8.5. and were obtained on a day when there was little vertical motion and the ambient ion concentration at various heights and distances downwind of the ion source. Unfortunately, insufficient data was available to draw concentration isopleths but, by carefully inspecting the results, the following somewhat tentative conclusions can be drawn.

Firstly, particularly very near the ion source, it is evident that the ion plume width is much greater than that of a smoke

plume in similar conditions. This is taken as direct evidence of the electrostatic repulsion effect described in Sec. 3.5.

Secondly, the mean values at 5 m downwind suggest that the axis of the ion plume is tilted downward. In this case the effect is attributed to image forces.

Thirdly, the ion source produces considerably more negative than positive ions, some indication of this having already been seen in the field mill records. It is estimated that when the ion generator was connected so as to produce negative ions its output was about twice that obtained when set to generate positive ions.

8.4 Experiments at longer distances from the ion source

This work was intended to be a preliminary study. The main objective was to establish, at least approximately, the characteristics of the electric field several hundred metres downwind of the ion source. In practice, a number of difficulties arose in the execution of these long-range experiments. Equipment had to be checked frequently to ensure it was working satisfactorily and as a result a great deal of time was spent walking between the various items of apparatus. Also at large distances downwind of the ion source the correct placing of a field mill presented problems. It was necessary to observe the wind vane, placed near the ion generator, with powerful binoculars and considerable skill was needed to keep the image steady for a sufficient time. It is recommended that any future experiments along these lines be carried out by at least two persons, and that an efficient means of communication be provided between them.

SPOT MEAN VALUES OF ION CONCENTRATION DIRECTLY DOWNWIND OF THE ION SOURCE

(RESULTS OBTAINED WITH THE ION COLLECTOR)

DATE 8.11.72 *TIME* 1200-1500 *WIND SPEED* 4 ms^{-1}

(a) ion source producing positive ions

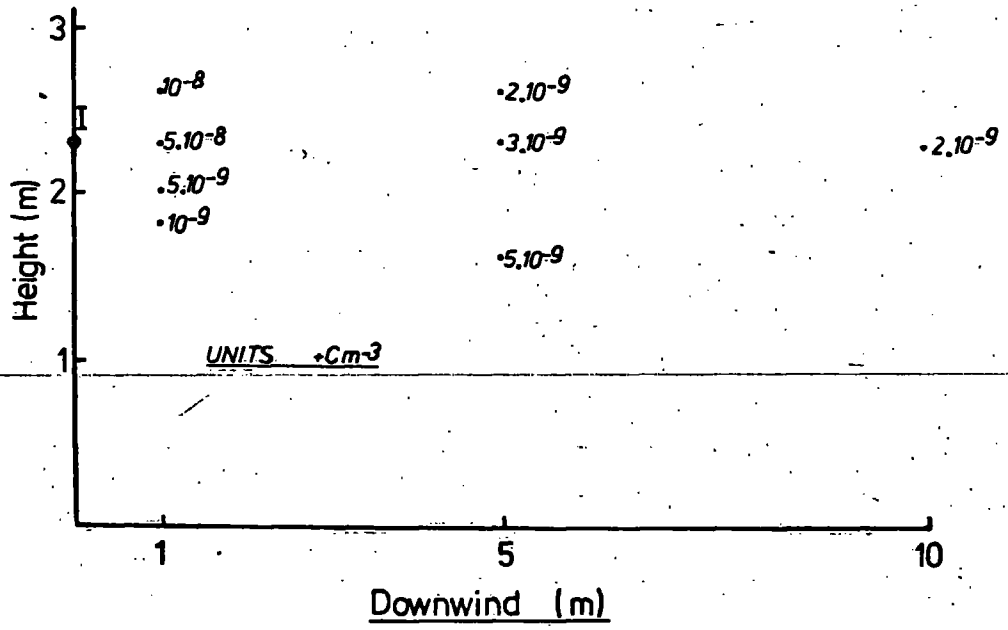

I = ION SOURCE

(b) ion source producing negative ions

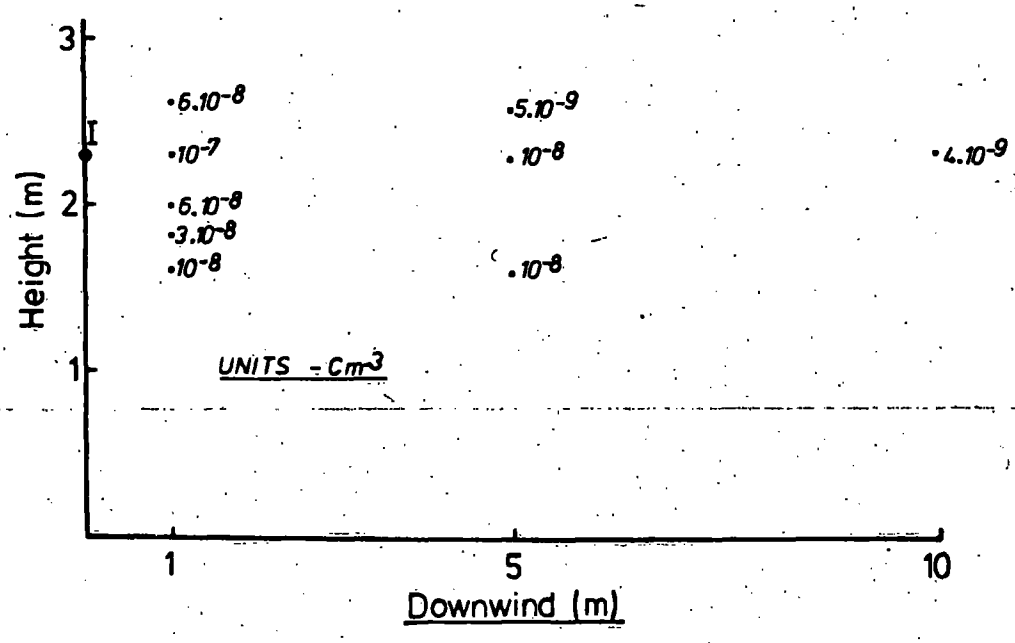

POTENTIAL GRADIENT VARIATIONS RECORDED 140m DOWNWIND OF THE ION SOURCE

(ion source was pulsed 45s on, 45s off)

ion source height 5m 23.3.73

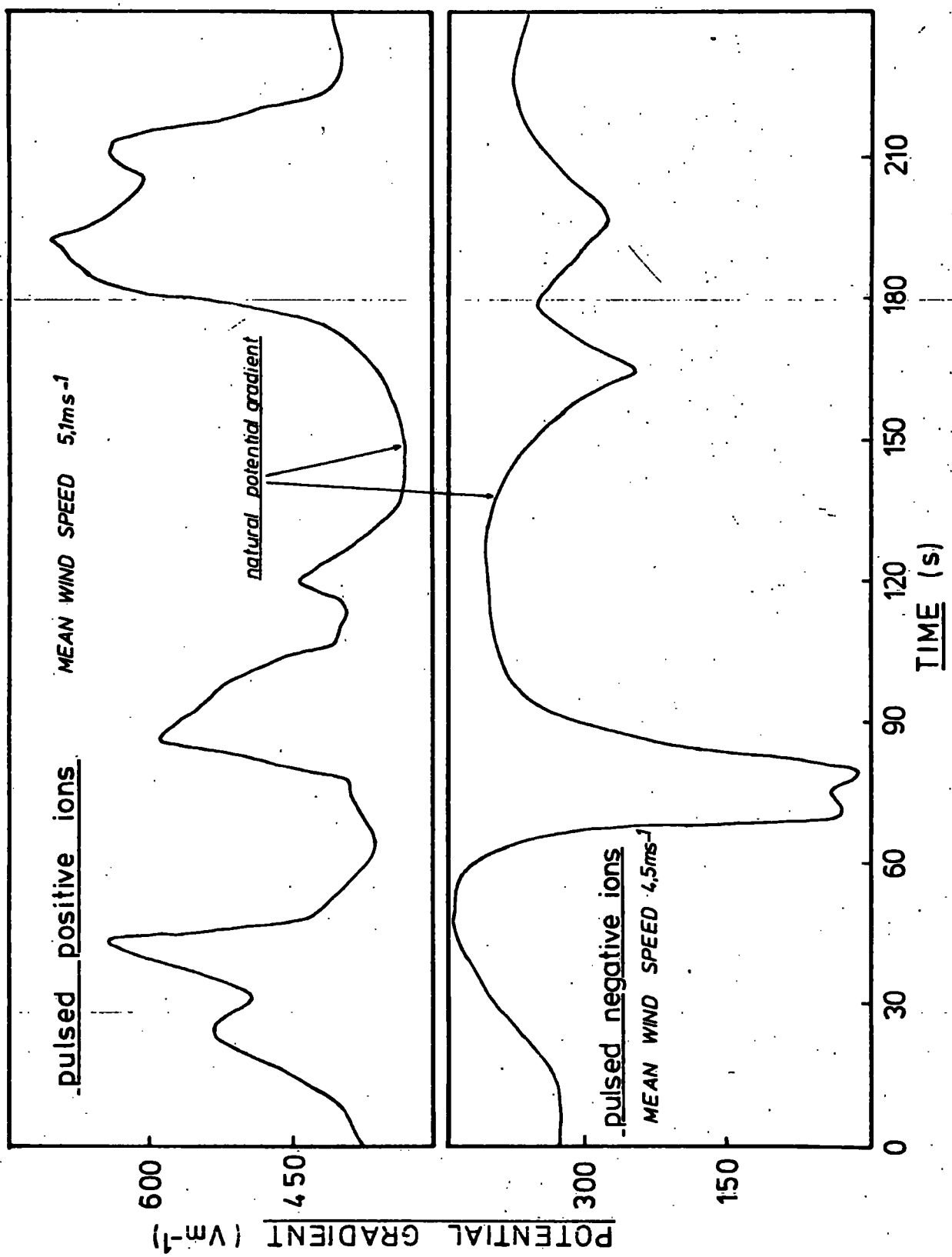

It would be reasonable to expect the character of the potential gradient to be different, in several ways, from that nearer the source. Firstly, because of the longer distance of travel the ion plume will be more diffuse and hence the potential gradient fluctuations will be smaller. Secondly, at these longer distances any small scale variations in concentration will be 'smeared out' by diffusion and therefore variations of potential gradient will tend to be slower. In fact, it was thought that at three or four hundred metres from the source the artificially produced variations would not be much larger than those occurring naturally. It was known that pollutants, even in low concentrations, could markedly affect the potential gradient and, as a precaution, initial trials were carried out at a site where pollution levels were known to be low. The site chosen was a large flat-topped hill about 1 km north of Lanehead, County Durham. Previous workers, particularly SHARPLESS (1968), had already established that pollution effects were minimal at a station in the village and thus at the site itself one could be certain that the air was clean.

In the initial work quantities of negative and positive charge were released (separately) 300 m upwind of a field mill. On the occasion chosen the wind speed was very low being about 1 ms^{-1}. Several peaks (or troughs) having amplitudes between 60 and 200 Vm^{-1} were detected downwind of the source, the larger variations being associated with the negative ions. Also at this distance the general time scale of the potential gradient variations was much longer, as expected.

It was already known that the ion source produced negative ions more copiously than positive ions but negative ions were

thought to be more numerous for an additional reason. At large distances from the source the ion concentration levels are, of course, relatively low. Small concentrations of positive ions would serve to slightly enhance the natural potential gradient, whereas similar concentrations of negative ions would diminish the prevailing value. If the negative ion concentration were not large enough to reverse the natural potential gradient then a negative ion cloud would be driven upward by electrostatic forces. Nearer the ion source where negative ion concentration is larger the potential gradient will be reversed and thus the ion cloud will move downward under the action of image forces. For these reasons we may expect the negative ions to remain airborne for longer periods.

Further experiments were planned at the Lanehead site but were abandoned for the following reason. In order to save time and effort in placing the field mill and ion source the Land Rover was often used as a means of transport. Most moorland regions, and this site was no exception, often possess extensive boggy areas. Experiments were discontinued when the Land Rover was inadvertently driven into such a waterlogged area, considerable difficulty being encountered in freeing the vehicle. In view of this a less ambitious project was attempted at the Maiden Castle site.

In these experiments a slightly different approach was adopted as trouble had already been experienced with polluted air. The method consisted of cyclically switching the ion generator on and off thereby producing 'packets' of ions which travelled downwind. Potential gradients measured downwind of such a pulsed source should therefore possess a markedly periodic

character and it was hoped this would enable the artificially produced field variations to be readily distinguished.

Some results were obtained 140 m downwind of the ion source, a typical section of the records being shown in Fig. 8.6. The 'pulsed' nature of the measured potential gradient is evident in the diagram and, at this distance downwind, the size of the variations is quite substantial.

It was hoped initially to estimate a value for the ionic recombination rate from the long range potential gradient measurements. However, as a result of the experimental difficulties referred to earlier, very little data was actually obtained and therefore estimates of the recombination rate were not feasible. Further, it was felt that rather more extensive experiments, both in terms of distance and equipment, would be necessary to obtain reliable information on this quantity. Nevertheless, the results given above are interesting because they clearly indicate that a significant fraction of the ions generated, particularly if negative, can persist in the lower atmosphere for at least 5 min.

Chapter 9: CONCLUSIONS AND SUGGESTIONS FOR FURTHER WORK

9.1 Summary of Important Results

The experimental results have, broadly speaking, substantiated the ideas about the behaviour of ion plumes developed theoretically in Chs. 2 and 3. The central feature of these ideas was that with the strength of ion source being used in this project, ion movement and dispersion would largely be determined by the pattern of the local air motion. However, two important exceptions to this statement were deduced theoretically and later established experimentally. Firstly in very light winds the electrostatic repulsion effect (see Sec. 3.5.) operating between the ions comprising the plume caused a larger crosswind and vertical spreading than did the effects of turbulence. Secondly, image charge effects, also discussed in Sec. 3.5., resulted in downward forces being exerted on the ion plume, particularly when it was near the ground.

Later experiments with the bidirectional vane enabled the shape of the ion plume to be deduced theoretically. In this way it was possible to compare the values of potential gradient obtained by measurement with those arrived at by computation. The plume model used in this reconstruction took no account of electrostatic forces, or indeed of crosswind and vertical diffusion, but nevertheless on most occasions the agreement between predicted and measured potential gradient values was good. These results also suggested that the plume behaviour was determined by atmospheric motion and turbulence except in low wind speeds or with low source heights.

It would be unwise to quote any hard and fast rules about when or when not small ion behaviour reflects the true character of atmospheric turbulence. With wind speeds of 4 ms^{-1} or greater and ion plume heights in excess of 10 m the effects of electrostatic forces are small. Of course, it must be remembered that these figures apply to an ion source of 0.3μA output and these results should be amended accordingly when sources of different strengths are under consideration (see Sec. 3.5.).

9.2 Implication of the Results

The importance of these results is evident. In all but light winds and at the lowest levels the ion plume behaviour is determined by the characteristics of the local air motion. Consequently, there would seem to be no reason why small ions could not be used as a tracer in small-scale atmospheric diffusion experiments. The advantages of such a choice would be as follows. Ions are cheap and easy to produce and have minimal physiological effects. The detection of ions and measurement of ion concentration, either indirectly by electric field methods or by the more direct approach using ion collectors, does not require elaborate techniques. The response time of many conventional detectors to changes in concentration whether it be sulphur dioxide or some other pollutant is often relatively slow and the alternative of an entirely electrical detection system offers the attractive possibility of designing rapid response instruments.

Whilst the behaviour of ions within a hundred metres or so of the source has been fairly well established, it should be

pointed out that further downwind, recombination and other effects may be of major importance in determining the fate of the ion plume. Thus it should be emphasised that the results of this project only indicate that the use of ions for short range (i.e. up to 100 m) diffusion studies would be feasible. Before longer range investigations using the method can be attempted, further research into ion plumes is necessary. At larger distances downwind particular care should be taken to determine the nature of the ambient variations, both of electric field and ion concentration.

9.3 Difficulties with the Present System

Apart from one or two minor exceptions, the equipment detailed in Chs. 4 and 5, functioned very satisfactorily in the field. One of the main problems was caused by the sheer complexity of the system. On arrival at a site considerable time was required to set out the field mills, attach the instruments and ion source to the mast and connect up the sampling and recording systems. Once operational conditions were established, provided no special circumstances arose, the equipment could be relied upon to operate automatically. Nevertheless, it was thought prudent to make frequent checks to ensure that each item of equipment was working correctly. This was done as often as possible so that if a fault did arise minimum recording time was lost. The more advanced experiments using the bivane and later the cine cameras were even more complicated and were, at times, almost too much to cope with single-handed.

Turning now to the instruments themselves, several refinements and alterations can be suggested in the light of operational experience. Firstly, the omission of sign discrimination on the field mills should have been remedied at an early stage. Some technical difficulties do exist here but it is not thought they are insuperable. In particular, the bias plate would need to be supplied with a highly stable, yet adjustable, DC voltage. With portable equipment, carrying batteries of limited power, care would be required in the design of such a voltage supply system. Secondly, a higher speed sampling system would have been advantageous, particularly when taking bivane readings. This would have greatly facilitated the development of a more accurate bivane data model. Naturally, the response time of the field mills and other instruments should be decreased in order to take full advantage of the higher speed sampling.

Considerable difficulty was experienced in accurately aligning the bivane, see Sec. 4.6. The procedure described in that section to effect this alignment was both tedious and time consuming and a better method should be devised. It is felt that the only really satisfactory system would be to rigidly attach the bivane and other instruments to a fixed mast. Apart from any improvements in accuracy a large amount of time would be saved when setting out equipment for field work.

Recently considerable advances have been made in integrated circuit techniques and as a consequence the entire electronics system could well be redesigned to take advantage of these innovations. Two points are particularly worth noting. Firstly, very high input *impedance* amplifiers are now available

and these would serve ideally as field mill amplifiers. This is an attractive possibility because the construction of large numbers of mills (e.g. for use in arrays) having standard performance would now be feasible. Secondly, the appearance of high precision voltage to frequency and frequency to voltage convertors could replace the existing transistor systems. The use of VHF radio links to replace the long cables between field mills and the central recording system would also be of great assistance. (The reader's attention is drawn to the fact that a Post Office Licence must be obtained before radio techniques are used.)

9.4 Suggestions for Future Work

9.4.1 Experimental Work

A number of points raised by the current investigation require elucidation. These are now discussed.

The fate of the ions at large distances downwind of the source is not clear but it appears to depend in a sensitive manner on the ambient small and large ion densities and also on the prevailing nucleus concentration. A logical extension of this project would therefore be to place small and large ion collectors, together with nucleus counters, downwind of the ion source. In this way it should be possible to establish the behaviour of the ion plume reasonably conclusively.

A method involving the use of a ground level collector plate might be used to assess the effect of image forces. Ions arriving at the ground, by whatever cause, constitute a current

and, provided the ambient ionization were low, the magnitude of this current could be related to the effects of image forces. The ion concentration and electric field would also have to be measured simultaneously but this would not pose any difficulties. Some arrangement would need to be made for displacement current compensation and, with the large and rapidly changing electric fields that would inevitably be present, this might present something of a problem. KASEMIR (1955) has developed a method of compensation which might be suitable.

Measurements of the electric field at ground level have already provided very valuable information concerning the behaviour of ion plumes. Whilst the technique could be extended by employing more field mills at ground level it might be more productive, certainly more interesting, to consider the possibility of total vector measurements using elevated field mills. By measuring the three field components of the electric field a great deal more information could be obtained, particularly about plume movements in the vertical plane. Some theoretical calculations, results of which are given in Sec. 6.4.2., indicate that near the ion plume very large horizontal electric fields would be present. From the technical standpoint considerable difficulties would arise in the design and operation of elevated three component field mills; nevertheless, it is not thought these problems are insurmountable. IMIANITOV (1949) has reported a design for a device apparently capable of measuring the three components of the electric field.

In the later stages of this project, a technique involving the comparison of computed ion plume configurations with those

obtained directly by cine photography of a smoke plume was developed. Lack of time did not permit this method to be properly exploited. The indications are that the photographic approach could be a very useful adjunct to the understanding of ion plume behaviour.

9.4.2 Theoretical Work

There appear to be three areas where further theoretical effort could usefully be directed.

The treatments of both image and repulsion forces, presented in Ch. 3, are, to say the least, somewhat simplified and it is felt that considerable refinement would be most desirable. A rigorous analytical approach to the problem would be very complex mathematically and possibly numerical techniques involving the use of a digital computer might be a more feasible alternative. In particular, the interaction of electrostatic and turbulent effects has only been considered very superficially and further theoretical work should be aimed in this direction.

On a more practical level the bivane data model, although capable of yielding good results, did possess a number of faults. The effects of certain of these could be minimised by a more sophisticated experimental arrangement whereas the remaining defects require modification of the computer model for their elimination. As previously mentioned, a higher sampling rate should greatly increase the accuracy of the bivane data model as it would correspondingly decrease the separation of the computed plume elements (see Sec. 3.4.).

On the theoretical side incorporation of the effects of electrostatic forces and those of turbulent diffusion would considerably enhance the realism of the model. In practice, considerable restriction might be placed on the researcher by the limitations of the computer. No doubt, the speed of computers will be further improved and the inclusion of these suggested modifications would ultimately present little difficulty. One might also be able to allow for certain more subtle features of atmospheric turbulence. For instance, the bivane data model derives its results from 'Eulerian', i.e. fixed point measurements, whereas, of course, the ion plume travelling downwind is essentially in a 'Lagrangian' environment. Possibly, this feature may be catered for by the inclusion of the Lagrangian-Eulerian time scale ratio in a later model, see PASQUILL (1961).

Finally, it should be remarked that as employing ions as a tracer does appear to be a potentially useful method of studying short-range diffusion, such an approach may stimulate further theoretical investigations into turbulence by revealing factors hitherto unsuspected from experiments using more conventional techniques.

REFERENCES

ACKERMANN, B. The application of variance spectrum analysis to cloud measurements
TECH. NOTE NO. 34.
DEPT. OF GEOPHYSICAL SCIENCES, UNIVERSITY OF CHICAGO

ASPINALL, W.P. 1969 Ph.D. THESIS
UNIVERSITY OF DURHAM

BENDAT, J.S. and PIERSOL, A.G. 1966 Measurement and analysis of Random Data
WILEY

BENT, R.B. 1964 Ph.D. THESIS
UNIVERSITY OF DURHAM

BEST, A.C. 1935 Transfer of heat and momentum in the lowest layers of the atmosphere
Met. Office Geophysical Memoirs No. 65

BLACKMANN, R.B. and TUKEY, J.W. 1958 The measurement of power spectra
DOVER PUBLICATIONS

BLEANEY, B. I. and BLEANEY, B. 1965 Electricity and Magnetism 764 p.
C.U.P.

BRUNT, D. 1939 Physical and Dynamical Meteorology
C.U.P.

CARSLAW, H.S. and JAEGER, J.C. 1959 Conduction of heat in solids 510 p.
OXFORD, CLARENDON PRESS

CHALMERS, J.A. 1963 Taking the mystery out of Gauss's theorem
Contemp. Physics 4, 456-8

CHALMERS, J.A. 1967 Atmospheric Electricity 515 p.
PERGAMON

CRAMER, H.E., GILL, G.C. and RECORD, F.A.	1954	Research into atmospheric turbulence and associated diffusion of aerosols and gases near the Earth's surface MIT. Report under contract AF19 (604 - 145
CRAMER, H.E., GILL, G.C. and RECORD, F.A.	1957	Heated thermocouple anemometers and light bivanes Exploring the Atmosphere's First Mil edited by H. LETTAU and B. DAVIDSON 1, 233 - 242 PERGAMON
CROZIER, W.D.	1963	Electrode effect during night-time low wind conditions J. Geophys. Res. 68, 3451-8
DAVIDSON, B. and HALITSKY, J.	1958	A method of estimating the field of concentration from tower bivane data J. Air. Poll. Contr. Ass. 7, 316 - 3
DAYARATNA	1969	Ph.D. THESIS UNIVERSITY OF DURHAM
DEACON, E.G.	1955	The turbulent transfer of momentum in the lower layers of the atmospher Tech. Paper No. 4. Melbourne CSIRO Div. Met. Phys.
DE'SA, O. and MOLYNEUX, L.	1962	Electronic Engineering, 34, 468 - 46 A transistor voltage to frequency convertor
EBERT, H	1901	Aspirations Apparat zur Bestimmung des Ionen Gehaltes der Atmosphäre Phys. Z, 2, 662-6
EBERT, H	1904	Über die Ursache des normalen atmosphärischen Potentialgefälles und der negativen Erdladung Phys. Z., 5, 135-40
ELSTER, J and GEITEL, H.	1899	Über die Existenz elektrischer Ionen in der Atmosphäre Terr. Magn. Atmos. Elect. 4, 213-34

HOPPEL, W.A. and GATHMAN, S.G.	1972	Experimental determination of the eddy diffusion coefficient over the open ocean from Atmospheric Electric Measurements J. Phys. Oceanog. Vol. 2, No. 3, 248-254
IMIANITOV, I.M.	1949	Measuring the horizontal component of the atmospheric-electric field IZV. AKAD, NAUK. SSSR. Ser. Geog. Geofiz 13, 320-40
KAWANO, M	1957	The coefficient of eddy diffusivity estimated by the method of Atmospheric Electricity J. Met. Soc. Japan Series II 35, No. 6, 29-32
KELVIN, LORD	1860	Electricity Atmospheric Nichol's Cyclopaedia 2nd Ed., Paper on Elec. and Magn. 192-208
LANGEVIN, P.	1905	Sur les ions de l'atmosphère C.R. Acad. Sci. Paris, 140, 232-4
LARGE, M.I. and PIERCE, E.T.	1957	The dependence of point discharge currents on wind as examined by a new experimental approach J. Atmos. Terr. Phys. 10, 251-7
LEMONNIER, L.G.	1752	Observations sur l'électricité de l'air Mem. Acad. Sci. 2, 233
LOEB, L.B.	1968	Electric coronas - their basic principle mechanisms 694 p. UNIVERSITY OF CALIFORNIA PRESS
LUMLEY, J.L. and PANOFSKY, H.A.	1964	The structure of atmospheric turbulence 239 p. WILEY
LUMLEY, J.L. and TENNEKES, H.	1972	A first course in turbulence 300 p. MIT PRESS

MAPLESON, W.W. and WHITLOCK, W.S.	1955	Apparatus for accurate and continuou measurement of the Earth's electric field J. Atmos. Terr. Phys. 7, 61-72
MAUND, J.E.	1958	Ph.D. THESIS UNIVERSITY OF DURHAM
MÜHLEISEN, R.	1953	Die luftelektrischer Elemente in Grossstadtbereich Z. Geophys. 29, 142-60
OGDEN, T.L.	1967	Ph.D. THESIS UNIVERSITY OF DURHAM
PASQUILL, F.	1962	Atmospheric Diffusion 297 p. Van NOSTRAND
PRIESTLEY, C.H.B.	1959	Turbulent transfer in the lower atmo phere 130 p. UNIVERSITY OF CHICAGO PRESS
PROJECT PRAIRIE GRASS	1956	Detailed description of the techniqu used can be found in: CRAMER, H.E., GILL, G.C. and VAUGHAN, H.C. (1958) The study of the diffusion of gases or aerosols in the lower atmosphere MIT. Dept. of Meteorology, Final Rep under contract AF 19 (604) - 1058
RACTLIFFE, J.F.	1962	Elements of Mathematical Statistics 202 p. O.U.P.
RICHARDSON, L.F.	1925	Turbulence and vertical temperature differences near trees Phil. Mag. 49, 81-90
ROBERTS, O.F.T.	1923	The theoretical scattering of smoke i a turbulent atmosphere PROC. ROY. SOC. (LONDON) A 104, 640-6

SCHMIDT, W. 1918 Wirkungen des Luftaustauches aus des Klina und der taglichen Gang der Lufttemperature in der Höhe

Sitzber. Akad, Wisserisch. Wien 127, 1942-1957

SCRASE, F.J. 1930 Some characteristics of eddy motion in the atmosphere

Met. Office Geophys. Memoirs No. 52

SHARPLESS, G.T. 1968 Ph.D. THESIS

UNIVERSITY OF DURHAM

SUTTON, O.G. 1953 Micrometeorology 333 p.

McGRAW-HILL

TAYLOR, G.I. 1935 Statistical theory of turbulence Parts 1-4

Proc. Roy. Soc. A 151, 421-478

THOMPSON, R 1971 Numerical Calculation of turbulent diffusion

Q.J. ROY. MET. SOC. 97, 93-98

TORRESON, O.W. 1939 Condensation nuclei in the atmosphere in Peru, and their relation to atmospheric-electrical and meteorological observations

Terr. Magn. Atmos. Elect. 44, 59-74

WHITLOCK, W.S. and CHALMERS, J.A. 1956 Short period variations in the atmospheric electric potential gradient

Q.J. ROY. MET. SOC. 82, 325-36

WILSON, C.T.R. 1900 On the leakage of electricity through dust free air

Proc. Camb. Phil. Soc. 11, 32

WRIGHT, H.L. 1936 The size of atmospheric nuclei, some deductions from measurements of the number of charged and uncharged nuclei at Kew observatory

PROC. ROY. SOC. (LONDON) 48, 675-689